Fakultät für Physik und Astronomie

Ruprecht-Karls-Universität Heidelberg

Diplomarbeit

im Studiengang Physik

vorgelegt von

Julian Niklas Heeck

geboren in Telgte

2011

Phänomenologie einer geeichten

$L_\mu - L_\tau$-Symmetrie

Die Diplomarbeit wurde von Julian Niklas Heeck

ausgeführt am

Max-Planck-Institut für Kernphysik

unter der Betreuung von

Herrn Dr. Werner Rodejohann

Department of Physics and Astronomy

University of Heidelberg

Diploma thesis

in Physics

submitted by

Julian Niklas Heeck

born in Telgte

2011

Phenomenology of a Gauged $L_\mu - L_\tau$ Symmetry

This diploma thesis was carried out by Julian Niklas Heeck

at the

Max-Planck-Institut für Kernphysik

under the supervision of

Dr. Werner Rodejohann

Phänomenologie einer geeichten $L_\mu - L_\tau$-Symmetrie
Die anomaliefreie (zufällige) $L_\mu - L_\tau$-Symmetrie des Standardmodells lässt sich zu einer lokalen Eichsymmetrie erheben, was zu einem zusätzlichen neutralen Vektorboson Z' mit generationsabhängiger Kopplung an Leptonen führt. Teilchen der ersten Generation werden nur durch Mischung des Z' mit dem Z-Boson beeinflusst, sei es durch eine nichtdiagonale Z–Z' Massenmatrix oder kinetische Mischung mit dem Generator der Hyperladung. Wir benutzen aktuelle Messdaten, von elektroschwachen Präzisionsmessungen bis hin zur Kosmologie, um den erlaubten Parameterbereich für ein nahezu masseloses Vektorboson (Fünfte Kraft) einzuschränken, und gehen insbesondere auf die Auswirkungen auf Neutrinophysik ein, z.B. zusätzliche CP-Verletzung. Die Verbesserung der Grenzen durch zukünftige Long-Baseline-Experimente wird diskutiert und verglichen. Des Weiteren wird der Fall eines schweren Z' in der Nähe der elektroschwachen Skala diskutiert. Wir erörtern den Zusammenhang zwischen den Mischungswinkeln der Neutrinooszillationen und der spontanen Brechung der $L_\mu - L_\tau$-Symmetrie und zeigen, dass mindestens zwei neue komplexe Skalarfelder nötig sind um in unterster Ordnung der Störungstheorie eine mit den Messdaten kompatible Massenmatrix zu erhalten. Die Auswirkungen der simpelsten Higgs-Sektoren werden im Detail diskutiert.

Phenomenology of a Gauged $L_\mu - L_\tau$ Symmetry
Promoting the anomaly-free (accidental) $L_\mu - L_\tau$ symmetry of the Standard Model to a local gauge symmetry introduces an additional neutral vector boson with generation-dependent couplings. First-generation particles are affected only through mass mixing with the Z boson and kinetic mixing with the hypercharge generator. We discuss current constraints on the model parameters for the ultralight case (fifth force) from electroweak precision data to cosmology, and in particular the effects on neutrino phenomenology, like additional CP violation. The sensitivity of future long-baseline experiments to the parameters is discussed and compared. We also mention the bounds on a higher breaking scale corresponding to a gauge boson with mass in the electroweak range. The connection between the spontaneous breaking of $L_\mu - L_\tau$ and the neutrino mixing matrix is examined; we argue that at least two additional complex scalar fields are necessary for a valid mass matrix at tree-level. The implications of the simplest scalar sectors are investigated in detail.

Contents

Chapter 1

Introduction

1.1 The Standard Model and Beyond

In the course of the last century, the theoretical description of observed phenomena has developed a marvellous accuracy. From atomic spectra to high-energy colliders, science managed to push the shortest observable distance to astounding limits, most recently in the Large Hadron Collider (LHC), probing energies up to 14 TeV (corresponding to distances down to 10^{-5} fm). The theoretical description of such high energy processes is combined into the Standard Model (SM) of particle physics, one of the most successful physical theories to date.

The SM is based on the gauge group $SU(3)_C \times SU(2)_L \times U(1)_Y$ with three sets of "families" (differing only in their mass), consisting of an electrically charged lepton, an uncharged lepton and two charged quarks in the representations of Tab. 1.1. The electric charge Q of a particle is connected to its weak isospin T_3 and hypercharge Y via $Q \equiv T_3 + Y/2$. The left-handed lepton doublets $(\nu_\ell, \ell)_L^T$ will often be denoted as L_ℓ and are not to be confused with the corresponding lepton quantum number. It should be obvious from context if we are talking about a field or a quantum number.

To explain the lepton and gauge-boson masses in a renormalisable way, the Higgs mechanism is invoked, adding one scalar $SU(2)_L$ doublet field with a non-zero expectation value, thereby breaking the gauge group down to $SU(3)_C \times U(1)_{\mathrm{EM}}$. This generates masses for the $W^\pm$ and Z bosons and the charged fermions and furthermore introduces one physical, electrically neutral, scalar field to the particle spectrum of the theory, the Higgs particle. Since this particle is yet to be discovered at the collider experiments Tevatron and LHC, there is much discussion about its properties (e.g. is it an elementary particle or a composite object?).

This one elusive particle aside, the SM has proven to be amazingly successful in describing high-energy physics; collider experiments like LEP measured the masses and couplings of the gauge bosons to high accuracy and atomic physics is sensitive to loop-order effects. In recent years astrophysics and cosmology became an important testing ground for the SM as well, posing at least three challenges:

- to explain the acceleration of the Universe (dark energy),
- to explain the rotational speed of galaxies as well as gravitational lensing of galaxy clusters (dark matter),
- to explain the solar and atmospheric neutrino flux (neutrino oscillations).

$L_e = \begin{pmatrix} \nu \\ e \end{pmatrix}_L \sim (1, 2, -1)$	$\overline{e_R} \sim (1, 1, +2)$	$H_{\text{SM}} \sim (1, 2, +1)$
$Q_L^u = \begin{pmatrix} u \\ d \end{pmatrix}_L \sim (3, 2, +\frac{1}{3})$	$\overline{u_R} \sim (\overline{3}, 1, -\frac{4}{3})$	$\overline{d_R} \sim (\overline{3}, 1, +\frac{2}{3})$

Table 1.1: $SU(3)_C \times SU(2)_L \times U(1)_Y \equiv G_{\text{SM}}$ representations of left-handed fermions and the Standard Model Higgs (only first generation shown).

There are, of course, additional fields of Beyond the Standard Model (BSM) physics, e.g. description of inflation, explaining the matter-antimatter asymmetry of the early Universe, solving the hierarchy problem, and in general combining particle physics with the theory of gravity. However, since this thesis does not cover any of the above topics, except for neutrino oscillations, we will not go into any detail, but only review neutrino physics. We will then go on to introduce extra neutral gauge bosons in different scenarios, as they are the main focus of this work. In the second to last section of this introduction, we give a short review of anomalies in Quantum Field Theory (QFT), since they constitute an important part of model building in BSM physics. The last section constitutes the motivation for this thesis, as well as a brief review of previous work on the model.

Seeing as we cover a lot of different topics and experiments in this thesis, it will prove convenient to postpone some of the introductions until the relevant chapters and sections, so as to allow for a more linear flow of reading.

1.2 Neutrino Oscillations

As mentioned above, the neutrino enters into the SM only via its left-handed coupling to the weak gauge bosons. Since it lacks a right-handed partner to form a gauge invariant coupling to the Higgs ($Y_\nu \bar{L} H \nu_R$), it stays massless after Electroweak Symmetry Breaking (EWSB). This is in accord with direct mass measurements of beta-decay experiments, which however only probe masses $\gtrsim 1\,\text{eV}$. As neutrino detection experiments (both solar and atmospheric) have measured an oscillating flavour flux of neutrinos, it is pretty clear by now that neutrinos do have a mass,[1] and that the mass eigenstates are heavily mixed superpositions of the flavour eigenstates, contrary to the quark sector, where the mixing matrix is close to the identity matrix.

While it is in principle easy to introduce right-handed fermions as partners for the neutrinos (they have to be in the trivial representation of the gauge group and therefore do not couple directly to gauge bosons), the corresponding Yukawa couplings $Y_\nu \sim m_\nu / v_{\text{SM}}$ are many orders of magnitude smaller than the couplings of the other fermions. This gave rise to a lot of theories trying to explain this smallness in a natural way, the most prominent one being the seesaw mechanism (treated in Sec. 5.1). A similarly large number of models try to explain the observed mixing pattern by impos-

[1] Alternative explanations of the measured fluxes with massless neutrinos (e.g. non-standard neutrino interactions) have been ruled out, see Sec. 1.3.

ing additional (usually global) symmetries, both continuous and discrete. The mixing angles and squared mass differences are already quite well-measured by solar (Sudbury Neutrino Observatory) and atmospheric experiments (Super Kamiokande), and will be further improved in current and upcoming long-baseline experiments (MINOS, T2K, NOνA).

Unfortunately, neutrino oscillations do not provide any insight on the nature of the neutrinos, Dirac or Majorana, which is instead probed via neutrinoless double beta decay observations (or the lack thereof), for example in the recently started GERDA experiment.

We will now shortly review the phenomenon of neutrino oscillations in the simplified case of two flavours, ν_e and ν_μ:

Since the creation and detection of neutrinos always occurs via weak processes, let us assume a muon neutrino ν_μ is created at time $t = 0$ and an electron neutrino ν_e detected at $t = T$. In the two-flavour case, the mass basis $\{|\nu_1\rangle, |\nu_2\rangle\}$ and the flavour basis are simply connected by a rotation matrix, so we can write

$$|\nu_e\rangle = |\nu_1\rangle \cos\theta + |\nu_2\rangle \sin\theta\,, \qquad |\nu_\mu\rangle = -|\nu_1\rangle \sin\theta + |\nu_2\rangle \cos\theta\,. \tag{1.1}$$

The time evolution of the mass/energy eigenstates $|\nu_j\rangle$ is described by the operation

$$|\nu_j, t\rangle = \exp[-iHt]\,|\nu_j, 0\rangle = \exp[-iE_j t]\,|\nu_j, 0\rangle \approx \exp[-i(E + m_j^2/2E)t]\,|\nu_j, 0\rangle\,, \tag{1.2}$$

where we approximated $E_i = \sqrt{|\boldsymbol{p}|^2 + m_i^2} \approx E + m_i^2/2E$ since the neutrinos are highly relativistic. Differentiation leads to the "Schrödinger-like" equation[2] for the propagation of the mass eigenstates

$$i\frac{\mathrm{d}}{\mathrm{d}t}\,|\nu_j, p, t\rangle \approx \left(|\boldsymbol{p}| + \frac{m_j^2}{2|\boldsymbol{p}|}\right)|\nu_j, p, t\rangle\,, \tag{1.3}$$

where the first term on the right-hand side is irrelevant for neutrino oscillations since it does not depend on j. The oscillation probability is therefore

$$\begin{aligned} P_{\mu\to e}(T) &= |\,\langle\nu_e|\nu(T)\rangle\,|^2 \\ &= \left|-\langle\nu_e|\nu_1\rangle \sin\theta\, e^{-im_1^2 T/2E} + \langle\nu_e|\nu_2\rangle \cos\theta\, e^{-im_2^2 T/2E}\right|^2 \\ &= \sin^2 2\theta \sin^2\left(\frac{\Delta m_{21}^2 L}{4E}\right), \end{aligned} \tag{1.4}$$

where we used the travelling distance $L \approx T$ and $\Delta m_{21}^2 \equiv m_2^2 - m_1^2$. Measuring the energy and flux of a specific flavour at different distances gives the amplitude $\sin^2 2\theta$ and the phase Δm_{21}^2 of the neutrino oscillation. The three-flavour case is slightly more complicated; instead of one mixing angle, we now have three angles plus one phase (more if neutrinos are Majorana particles, but this is irrelevant for neutrino oscillations). One

[2] Expanding in $m \ll |\boldsymbol{p}|$, as opposed to $|\boldsymbol{p}| \ll m$ like in the Schrödinger equation for non-relativistic quantum mechanics.

θ_{12}	$\arcsin\sqrt{0.318} \pm 0.02\,(3\%)$
θ_{13}	0 ± 0.2
θ_{23}	$\arcsin\sqrt{0.500} \pm 0.07\,(9\%)$
δ_{CP}	$\in [0, 2\pi]$
Δm^2_{21} $[10^{-5}\,\mathrm{eV}^2]$	$7.59 \pm 0.23\,(3\%)$
$\lvert\Delta m^2_{31}\rvert$ $[10^{-3}\,\mathrm{eV}^2]$	$2.40 \pm 0.12\,(5\%)$

Table 1.2: Neutrino oscillation parameters, their standard deviation and the relative uncertainty, taken from Ref. [1].

possible parameterisation for the Pontecorvo-Maki-Nakagawa-Sakata mixing matrix (PMNS matrix) is given by the three consecutive rotations $U = U(\theta_{23})U(\theta_{13}, \delta_{\mathrm{CP}})U(\theta_{12})$:

$$U = \begin{pmatrix} c_{12}c_{13} & s_{12}c_{13} & s_{13}e^{-i\delta_{\mathrm{CP}}} \\ -c_{23}s_{12} - s_{23}s_{13}c_{12}e^{i\delta_{\mathrm{CP}}} & c_{23}c_{12} - s_{23}s_{13}s_{12}e^{i\delta_{\mathrm{CP}}} & s_{23}c_{13} \\ s_{23}s_{12} - c_{23}s_{13}c_{12}e^{i\delta_{\mathrm{CP}}} & -s_{23}c_{12} - c_{23}s_{13}s_{12}e^{i\delta_{\mathrm{CP}}} & c_{23}c_{13} \end{pmatrix}, \tag{1.5}$$

with the notation $c_{ij} \equiv \cos\theta_{ij}$, $s_{ij} \equiv \sin\theta_{ij}$; current values are summarised in Tab. 1.2. It is important to note that only the two mass parameters Δm^2_{21} and $|\Delta m^2_{31}|$ are known, shedding no light on the absolute mass scale or the hierarchy (sign of Δm^2_{31}).

An important starting point for model building in recent years is the so-called "Tri-Bimaximal Mixing" (TBM) [2], defined via $\theta_{13} = 0$, $\sin^2\theta_{23} = 1/2$ and $\sin^2\theta_{12} = 1/3$ or[3]

$$U_{\mathrm{TBM}} = \begin{pmatrix} \sqrt{2/3} & 1/\sqrt{3} & 0 \\ -1/\sqrt{6} & 1/\sqrt{3} & -1/\sqrt{2} \\ -1/\sqrt{6} & 1/\sqrt{3} & 1/\sqrt{2} \end{pmatrix}, \tag{1.6}$$

which is compatible with data and can be obtained by imposing discrete flavour-symmetries on the neutrinos (e.g. the wildly popular group A_4) [3]. A slight generalisation that only predicts $\theta_{13} = 0$ and $\theta_{23} = \pi/4$ but leaves the solar mixing angle θ_{12} free is the μ-τ-symmetric model, based on a neutrino mass matrix of the form

$$\mathcal{M}_\nu^{\mu\leftrightarrow\tau} = \begin{pmatrix} x & y & y \\ \cdot & z & w \\ \cdot & \cdot & z \end{pmatrix}, \tag{1.7}$$

obeying the symmetry $\mu \leftrightarrow \tau$ (or $\nu_2 \leftrightarrow \nu_3$). For real parameters this form predicts the third mixing angle to be

$$\sin^2 2\theta_{12} = \frac{8y^2}{(x - w - z)^2 + 8y^2}, \tag{1.8}$$

as long as the denominator does not vanish. Tri-bimaximal mixing is obtained for the choice $x + y = w + z$.

[3] To obtain this common form of the TBM matrix from Eq. (1.5), one needs to choose the negative sign $\theta_{23} = -\pi/4$. The difference to $\theta_{23} = +\pi/4$ is of course unphysical, it is just a matter of convention.

An important generalisation of the oscillation formula (1.3) describes the evolution of neutrinos in matter (Mikheyev-Smirnov-Wolfenstein (MSW) effect [4]). Since the interaction channels of ν_e are different than those of $\nu_{\mu,\tau}$ (ν_e has an additional charged-current interaction because matter contains electrons but not muons or tauons), the effective potential for the neutrinos becomes non-universal, which affects neutrino oscillations. In flavour basis, the propagation equation takes the form

$$i\frac{\mathrm{d}}{\mathrm{d}t}\boldsymbol{\nu} = \frac{1}{2E}\left[UM_\nu^2U^\dagger + \begin{pmatrix} A(x) & 0 & 0 \\ 0 & 0 & 0 \\ 0 & 0 & 0 \end{pmatrix}\right]\boldsymbol{\nu}\,, \tag{1.9}$$

where U is the PMNS matrix (1.5) and the neutrino mass matrix M_ν is diagonal. $A(x)$ parameterises the charged-current interactions and is explicitly given by $A(x) = 2\sqrt{2}G_F n_e(x)E$, with the electron density n_e of the matter. Solving this evolution equation is obviously pretty complicated, so we will once again only look at the two-flavour scenario, where the result is a position dependent mixing angle

$$\tan 2\theta \to \tan 2\theta_m(x) \equiv \frac{\tan 2\theta}{1 - A(x)/\Delta m_{21}^2 \cos 2\theta}\,, \tag{1.10}$$

so even a small mixing angle θ can induce large oscillations when the neutrino goes through a resonance $n_e \approx \cos 2\theta \Delta m_{21}^2/2\sqrt{2}G_F E$. This effect is crucial for understanding the solar neutrino flux, since solar neutrinos travel an extensive length through the Sun (which has a highly decreasing electron density towards the outer regions), so the resonant behaviour can generate an appreciable number of $\nu_e \to \nu_\mu$ conversions.

1.3 Non-Standard Neutrino Interactions

An alternative approach to neutrino oscillations, with massless neutrinos, is the introduction of additional interactions of neutrinos with other SM particles. Even though current data highly favour the standard oscillation picture discussed in Sec. 1.2, this does not mean Non-Standard neutrino Interactions (NSI) are excluded, as they can be introduced in addition to mass mixing. Since it is not strictly necessary to specify the actual new neutrino interactions, NSI are a convenient way to generically probe physics beyond the Standard Model in the neutrino sector. In a model-independent approach one considers the effect of (non-renormalisable) $d = 6$ operators like

$$\mathcal{L}_{\mathrm{NSI}}^{\mathrm{eff}} = -2\sqrt{2}G_F\varepsilon_{\alpha\beta}^{fP}\left[\bar{f}\gamma^\mu Pf\right]\left[\bar{\nu}_\alpha\gamma_\mu P_L\nu_\beta\right]\,, \tag{1.11}$$

where P denotes a chiral projection operator ($P_L = \frac{1}{2}(1-\gamma_5)$ or $P_R = \frac{1}{2}(1+\gamma_5)$) and $f = e, u, d$ labels the particles of normal matter. Similar operators can be constructed for "charged-current NSI", which do not influence the neutrino oscillations but rather the production and detection processes. Even though they are generally more constrained than the neutral-current NSI, they should not be neglected, as pointed out in Ref. [5]. However, since the model of this thesis does not induce these kinds of operators, we will not delve into the specifics but rather discuss the neutral-current NSI given in

Eq. (1.11). This corresponds to the so-called "matter NSI", since it changes the usual MSW potential for neutrino interaction (in flavour basis) to:

$$i\frac{\mathrm{d}}{\mathrm{d}t}\boldsymbol{\nu} = \frac{1}{2E}\left[UM_\nu^2U^\dagger + A\begin{pmatrix}1+\varepsilon_{ee} & \varepsilon_{e\mu} & \varepsilon_{e\tau}\\ \varepsilon_{e\mu}^* & \varepsilon_{\mu\mu} & \varepsilon_{\mu\tau}\\ \varepsilon_{e\tau}^* & \varepsilon_{\mu\tau}^* & \varepsilon_{\tau\tau}\end{pmatrix}\right]\boldsymbol{\nu}\,. \tag{1.12}$$

Here we have the usual $A = 2\sqrt{2}G_F n_e E$ and the effective NSI parameters $\varepsilon_{\alpha\beta}$ are connected to Eq. (1.11) via $\varepsilon_{\alpha\beta} \equiv \sum_{f,P}\frac{n_f}{n_e}\varepsilon_{\alpha\beta}^{fP}$, introducing a dependence on the density n_f of fermion f.

Important examples are the effective NSI parameter for neutrinos going through Earth-like matter $\varepsilon_{\alpha\beta}^{\oplus}$ (roughly same number of electrons, protons and neutrons) and solar matter $\varepsilon_{\alpha\beta}^{\odot}$ (mostly electrons and protons):

$$\varepsilon_{\alpha\beta}^{\oplus} \approx \sum_P\left[\varepsilon_{\alpha\beta}^{eP} + 3\varepsilon_{\alpha\beta}^{uP} + 3\varepsilon_{\alpha\beta}^{dP}\right], \qquad \varepsilon_{\alpha\beta}^{\odot} \approx \sum_P\left[\varepsilon_{\alpha\beta}^{eP} + 2\varepsilon_{\alpha\beta}^{uP} + \varepsilon_{\alpha\beta}^{dP}\right], \tag{1.13}$$

since these are the relevant quantities for neutrino-oscillation data. Current limits at 90% Confidence Level (C.L.) are given in Ref. [6], we only quote

$$|\varepsilon_{\alpha\beta}^{\oplus}| < \begin{pmatrix}4.2 & 0.33 & 3.0\\ \cdot & 0.068 & 0.33\\ \cdot & \cdot & 21\end{pmatrix}, \qquad |\varepsilon_{\alpha\beta}^{\odot}| < \begin{pmatrix}2.5 & 0.21 & 1.7\\ \cdot & 0.046 & 0.21\\ \cdot & \cdot & 9.0\end{pmatrix}. \tag{1.14}$$

Some subtleties concerning the extraction of these bounds from fits will be discussed when we actually use the limits in Sec. 4.2.1.

We close by mentioning that, of course, Eq. (1.12) does not inhibit an exact solution, but since current data fits constrain most ε to be less than $0.1-0.01$, it proves convenient to expand the solution in ε (or solve (1.12) numerically). This can be enlightening to some degree, even though the analytic approximate expressions are very involved; we will discuss that route in Sec. 3.3.2.

1.4 Extra Neutral Gauge Bosons

Our goal in this section is a review of the different BSM motivations for additional neutral spin-1 particles. Only some of them are relevant to the thesis at hand, but all are interesting in their own right.

1.4.1 Grand Unified Theories

Motivated by the success of the unification of weak and electromagnetic interactions by the gauge group $SU(2)_L \times U(1)_Y$, broken to $U(1)_{\mathrm{EM}}$ at the scale $v_{\mathrm{SM}} \sim 250\,\mathrm{GeV}$, the natural extension would be an overlying gauge group G, that is broken down to the SM gauge group G_{SM} at some scale $\Lambda_{\mathrm{GUT}} \gg v_{\mathrm{SM}}$; typical examples for G are the simple Lie groups $SU(N)$ and $SO(N)$, direct products of them, or, motivated by string theory, exceptional groups like E_6. Such an overlying simple group also implies

a unification of the gauge couplings, i.e. the running couplings of the SM should all meet at the scale Λ_{GUT}. This is not observed experimentally if we use the SM particle spectrum in the renormalisation group equations to calculate the coupling constants at collider energies. Supersymmetric extensions of the SM however are pretty close to achieving this unification, typically around $\Lambda_{\mathrm{GUT}} \sim 10^{13\ldots17}\mathrm{GeV}$. Further nice features provided by some Grand Unified Theories (GUTs) are a spontaneous rather than an explicit breaking of parity (left-right symmetric models) and/or the accommodation of one particle generation into one irreducible representation (for example one family plus a right-handed neutrino fit into the spinor representation 16 of $SO(10)$, as we will show below), motivating the number of particles per family.

Every GUT adds at least extra gauge bosons and scalar particles to the theory, in some cases additional fermions are also necessary to cancel anomalies (see Sec. 1.5); the concrete particle spectrum, of course, depends on the specific breaking pattern. Non-observation of the new gauge bosons sets strong lower bounds on their masses, but indirect effects are even more constraining; a common prediction of GUTs is for example the decay of the proton, yet to be observed, which excludes a lot of models (e.g. the Georgi-Glashow model, based on the group $SU(5)$). Since the breaking of a larger gauge group than $SU(5)$ (meaning higher rank than 4) to the SM leads to additional $U(1)'$ factors, i.e. neutral gauge bosons, it is common to search for Z-like particles at colliders (specific GUTs differ in the coupling of the Z' to fermions). As of now, non-observation of the corresponding resonances at colliders as well as indirect effects due to Z–Z' mixing[4] constrain the mass and the mixing angle severely [7, 8]. It is important to note that the coupling constant g' is fixed by unification and kept constant in the analysis; leaving only the mass of the Z' and the Z–Z'-mixing angle as free parameters (once the breaking pattern of a GUT is chosen).

We will now give a rough sketch of a GUT, trying to motivate how the extra $U(1)'$ turns up in the process. The prototypical example of a group that breaks down to $G_{\mathrm{SM}} \times U(1)'$ is the simple Lie group $SO(10)$,[5] since it has rank 5, i.e. one more diagonal generator than G_{SM}; it has dimension $10(10-1)/2 = 45$ and thus introduces $45 - 8\,(\text{gluons}) - 3\,(W^{\pm}, Z) - 1\,(\text{photon}) = 33$ new gauge bosons. There are several different ways to break the symmetry to an intermediate symmetry group [9, 10, 11], most prominently $SO(10) \to SU(5) \times U(1)'$ and $SO(10) \to SU(3)_C \times SU(2)_L \times SU(2)_R \times U(1)_{B-L}$ (left-right symmetric model). The former is problematic since it often suffers a similarly fast proton decay as the Georgi-Glashow model; we will discuss it anyway.

Before we describe the breaking pattern, we discuss the fermion representation; to that effect we list some important $SO(10)$ and $SU(5)$ representations and how they transform under a specific subgroup in Tab. 1.3. Fermions come in 3 generations of the $SO(10)$ spinor representation 16, which can be decomposed in $SU(5)$ representations as $10 + \overline{5} + 1$, the singlet 1 accommodating the right-handed neutrino. The $SU(5)$ 10 and $\overline{5}$ transform under G_{SM} as $(3, 2, 1/3) + (\overline{3}, 1, -4/3) + (1, 1, 2)$ and $(\overline{3}, 1, 2/3) + (1, \overline{2}, -1)$ respectively, which correctly describes one generation of Standard Model particles (see

[4] Mixing is induced by off-diagonal mass terms like $\delta M^2 Z^\mu Z'_\mu$ or kinetic mixing $Z^{\mu\nu} Z'_{\mu\nu}$ (see Sec. 2.2).
[5] Sometimes called $Spin(10)$ theory since the Lie algebra involved is actually that of $Spin(10)$, the double cover of $SO(10)$, a detail which is not important for us.

$SO(10)$ representation	$SU(5) \times U(1)'$ decomposition
45	$(24,0) + (10,-4) + (\overline{10},4) + (1,0)$
16	$(10,1) + (\overline{5},-3) + (1,5)$
10	$(5,-2) + (\overline{5},2)$
$SU(5)$ representation	$SU(3) \times SU(2) \times U(1)$ decomposition
24	$(8,1,0) + (1,3,0) + (1,1,0) + (3,2,-\frac{5}{6}) + (\overline{3},2,\frac{5}{6})$
10	$(3,2,\frac{1}{3}) + (\overline{3},1,-\frac{4}{3}) + (1,1,2)$
$\overline{5}$	$(\overline{3},1,2/3) + (1,\overline{2},-1)$

Table 1.3: Representations of $SO(10)$ [10] and $SU(5)$ and their transformation properties under the respective subgroups $SU(5) \times U(1)$ and $SU(3) \times SU(2) \times U(1)$.

Tab. 1.1). Namely, the 10 contains $\{(u,d)_L,\ \overline{u_R},\ \overline{e_R}\}$ and the $\overline{5}$ contains $\{\overline{d_R},\ (\nu,e)_L\}$. The transformation of leptons and quarks into each other via $SO(10)$ gauge bosons causes proton decay for example, the non-observation of which sets a lower bound to the corresponding gauge boson masses, typically $M_X > 10^{10\ldots16}$GeV.

The simplest way to break the $SO(10)$ uses a Higgs field ϕ in the adjoint representation 45, i.e. an antisymmetric 10×10 matrix. As can be seen in Tab. 1.3, this adjoint includes an $SU(5) \times U(1)'$ singlet $(1,0)$, which means if this field acquires a Vacuum Expectation Value (VEV) of order Λ_{GUT}, the vacuum will no longer be $SO(10)$ invariant, but only $SU(5) \times U(1)'$ invariant. This describes a possible first step in the GUT breaking. To break down the $SU(5)$ to the Standard Model, one can use the $SU(5)$ adjoint 24 (like in the Georgi-Glashow model) since this contains a G_{SM} singlet $(1,1,0)$, so a VEV would break the $SU(5)$ to G_{SM}. How do we get the $SU(5)$ adjoint 24? Conveniently, it is already part of the ϕ field, since the 45 contains a part $(24,0)$, which can acquire a VEV. Since none of the VEVs up to this point carried a $U(1)'$ charge, we are left with the symmetry group $G_{\mathrm{SM}} \times U(1)'$.

To complete the breakdown, we need to introduce more scalar fields, for example a field Φ in the spinor representation 16, which contains an $SU(5)$ singlet part $(1,5)$ that is however charged under $U(1)'$ and can therefore be used to break this last additional symmetry and give the corresponding neutral vector boson Z' a mass (the $U(1)'$ is denoted in the literature as $U(1)_\chi$ and the neutral gauge boson correspondingly as Z_χ). Due to this breaking over intermediate scales, this mass M_{Z_χ} need not be at the GUT scale Λ_{GUT}, but can in principle be around the electroweak scale and thus observable at current experiments. Accordingly, the most important bounds stem from LEP and Tevatron, excluding the mass range below roughly one TeV (concrete values for the different Z' models can be found in Refs. [7, 8, 12]).

The final symmetry breaking to $SU(3)_C \times U(1)_{\mathrm{EM}}$ can be accomplished with a $\overline{16}$, since it includes an $SU(2)_L$ doublet, just like the standard Higgs mechanism in the electroweak theory of Glashow, Weinberg and Salam.

It should be clear that GUTs based on groups with even higher rank can induce additional $U(1)'$ factors; for example, the exceptional group E_6 can be broken into $SO(10) \times U(1)''$, with possible breakdown to $G_{\mathrm{SM}} \times U(1)' \times U(1)''$.

1.4.2 Hidden Photons/Paraphotons

While GUT models provide a motivation for TeV-scale Z' bosons, there has also been extensive research on lighter or even massless gauge bosons, based simply on the gauge group $G_{\text{SM}} \times U(1)'$. Sometimes, models of this type (with an ultralight gauge boson or scalar) are dubbed "Fifth Force" (besides the known four: gravitation, electromagnetism, weak and strong force) and for small mediator masses M one typically encounters spherically symmetric potentials of the Yukawa form

$$V(r) \sim \frac{g'^2}{4\pi} \frac{e^{-Mr}}{r} , \tag{1.15}$$

and ascribes them a range $r = 1/M$, motivated by dimensional considerations (derivation of the Yukawa form in Sec. 3.2). Experiments constrain the coupling to first-generation particles g' and the range M; on astronomical scales, tests of the equivalence principle (to be discussed in Sec. 3.4) yield constraints up to $g'^2/4\pi < 10^{-49}$.

Even for shorter ranges, one typically needs rather small coupling constants (at least to first-generation particles), otherwise they would have been observed in high-precision atomic physics or at colliders. To explain such small coupling somewhat naturally, many models proposed an interaction with SM particles only through kinetic mixing [13], i.e. operators like

$$\mathcal{L} \supset \frac{\sin\chi}{2} F^{\mu\nu}_{\text{EM}} F'_{\mu\nu} , \tag{1.16}$$

which induce a coupling $\sim \sin\chi$ of otherwise sterile particles to photons, as long as they are charged under the new gauge group $U(1)'$ ("millicharged particles"). Of course, this also generates Z' interactions with particles uncharged under $U(1)'$ (e.g. SM particles). The smallness of the Z' coupling (to be consistent with data) is then explained by a small mixing angle χ rather than a small coupling constant g'. The $d = 4$ operator (1.16) is allowed because for abelian symmetries, the field-strength tensor $F^{\mu\nu} \equiv \partial^\mu A^\nu - \partial^\nu A^\mu$ is already a gauge invariant quantity, making also the product (1.16) a gauge singlet, as long as both factors stem from a $U(1)$. Kinetic mixing is therefore only possible between γ and Z' (or the hypercharge generator instead of γ, if we work in the high-energy regime), but not between for example gluons and Z'. We will discuss kinetic mixing (and the mass mixing, mentioned in Sec. 1.4.1) extensively in Sec. 2.2.

Such "hidden" $U(1)$ gauge factors arise for example in the low-energy limit of some string-theory models [14, 15, 16] and have been used for quite some time in dark-matter model building [17, 18]. The basic idea is to charge the dark matter only under $U(1)'$, while all SM particles remain uncharged, allowing only for weak interactions between these sectors via kinetic mixing (i.e. the Z' as a mediator to the dark sector) or, in some models, via Higgs exchange (if an additional, $U(1)'$-charged scalar is introduced, for example to break the $U(1)'$ at some possibly low scale).

Other models do not include matter charged under the new $U(1)'$, but break it (often in the most economic way, i.e. via a Stückelberg mechanism (App. C)) and subsequently induce photon-paraphoton oscillations (in complete analogy to neutrino oscillations). These models can be tested with precision measurements of electromagnetism [19] or

with so-called "light shining through a wall" experiments [20, 21], constraining the kinetic mixing angle and the mass of the paraphoton. The usual framework consists of the electromagnetic gauge group $U(1)_{\mathrm{EM}}$ and one additional $U(1)'$:

$$\mathcal{L} \supset -\frac{1}{4}F_1^{\mu\nu}F_{1\mu\nu} - \frac{1}{4}F_2^{\mu\nu}F_{2\mu\nu} + \frac{1}{2}m^2 A_2^\mu A_{2\mu} + j^\mu_{\mathrm{EM}}\left(eA_{1\mu} + e_2 A_{2\mu}\right) \tag{1.17}$$

or some variation of this. The coupling of the paraphoton A_2 to the electromagnetic current can also be generated by kinetic mixing ($e_2 \sim e\chi$). The crucial point is the creation of the two mass eigenstates A_1 and A_2 by a charged source, which leads to photon-paraphoton oscillations in direct analogy to neutrino oscillations. Since the linear combination $eA_2 - e_2 A_1$ does not couple to j_{EM}, photons can oscillate into the sterile component, pass through an opaque barrier and oscillate back, hence the name "light shining through a wall".

1.4.3 Leptophotons

All models up to this point were assumed to be lepton universal. While universality is a very accurate symmetry in the SM (for example the leptonic Z decay branching ratios are universal to 0.1% [22]), there have been numerous models without this feature. Family non-universal long-range forces (mediated by "leptophotons") have also been considered, mainly ones that couple to first-generation particles, since they would be the easiest to observe in current experiments. For this thesis, the most relevant exception to this is a series of papers by Okun [19, 23] and others [24, 25, 26], who discussed unbroken $U(1)_\mu$, $U(1)_\tau$ and $U(1)_{\mu-\tau}$ gauge symmetries and their effect on electrodynamics and the early Universe. Since we now know that lepton family number is violated by neutrino oscillations, it is necessary to break the $U(1)'$ symmetry and therefore give the gauge boson a mass. However, depending on the breaking mechanism, this mass can be arbitrarily small, giving rise to a long-range interaction.

Even though long-range forces between e.g. electrons are highly constrained by experiments testing the equivalence principle (stating, in our context, that the force between two bodies (on large scales) depends only on their electric charge and mass, not on other quantum numbers), they can still have an impact in neutrino physics. This is due to the shear number of e.g. electrons in the Sun ($N_e^\odot \sim 10^{57}$), which can compensate even the small coupling $g'^2/4\pi \sim 10^{-50}$, and the fact that the leptonic potential in neutrino oscillations is to be compared to $\Delta m^2/E_\nu$, which can be small in itself (e.g. high energy atmospheric neutrinos). Neutrino physics therefore provides an interesting testing ground for family-non-universal forces. While this is formally similar to the NSI description of BSM interactions, it is to be distinguished simply because it is not confined to matter, i.e. the long-range forces also change the vacuum oscillations of neutrinos.

This connection between family-non-universal, leptophilic forces and neutrino oscillation has been derived by Joshipura et al. [27, 28] for the spontaneously broken $U(1)_{e-\mu,\tau}$, which is the main motivation for the topic of this thesis.

The neutrino sector is also interesting in such lepton-non-universal models since they predict a specific structure of the neutrino mass matrix and hence the PMNS mixing

matrix. For example a gauged $L_e - L_\mu$ symmetry gives rise to the Majorana mass matrix

$$\mathcal{M}_{\text{Majorana}} = \begin{pmatrix} 0 & a & 0 \\ a & 0 & 0 \\ 0 & 0 & b \end{pmatrix} , \tag{1.18}$$

which of course gets additional entries if we break the $U(1)_{L_e - L_\mu}$ symmetry (which we have to do to be in accord with the measured mixing angles).

A phenomenologically very interesting mass structure comes from the $L_\mu - L_\tau$ symmetry [29], because here the Majorana mass matrix (with $a \approx b$, i.e. quasidegenerate neutrinos)

$$\mathcal{M}_{\text{Majorana}} = \begin{pmatrix} a & 0 & 0 \\ 0 & 0 & b \\ 0 & b & 0 \end{pmatrix} , \tag{1.19}$$

implies a maximal mixing angle $\theta_{23} = \pi/4$ in the atmospheric sector, in agreement with data (see Tab. 1.2). To also get a viable solar angle, one needs to introduce perturbations to this mass matrix, i.e. break the $L_\mu - L_\tau$ symmetry. The fact that the associated massive gauge boson Z' does not couple to normal matter but only to $\mu, \nu_\mu, \tau, \nu_\tau$ seems to forbid an analogous discussion of a long-range force; we will show however that the most general theory based on the gauge group $G_{\text{SM}} \times U(1)_{L_\mu - L_\tau}$ does actually predict a force between matter and neutrinos that can be tested with neutrino oscillation experiments.

We will consider both the case of an ultralight $Z'_{\mu-\tau}$ (long-range force, Ch. 3) and that of a boson with a mass around the electroweak scale (Ch. 4), making it accessible to current colliders. Some specific models of the spontaneous breakdown of $U(1)_{L_\mu - L_\tau}$ through additional scalars will also be discussed (Ch. 5).

1.5 Anomalies

The main interest in gauged $L_\alpha - L_\beta$ symmetries ($\alpha, \beta \in e, \mu, \tau$) originally stemmed from the fact that they are anomaly-free without the need to introduce new particles to the Standard Model. We will show this explicitly for the $L_\mu - L_\tau$ symmetry in Sec. 2.1, but the argument is exactly the same for $L_e - L_{\mu,\tau}$.

This section serves as a very short introduction to anomalies, it is not meant to be self-contained, but more extensive pedagogic treatments can be found in most textbooks on Quantum Field Theory (QFT), e.g. Refs. [30, 31, 32].

Anomalies describe the breakdown of a classical symmetry through quantum effects. We will only focus on anomalies associated with local symmetries, for these can render a theory inconsistent, owing to the link between gauge invariance and renormalisability, as worked out by Gross and Jackiw [33]. There are different ways to locate and calculate anomalies; we will, for simplicity, take the perturbative route, calculating directly the problematic Feynman diagrams.

As a toy model, let us consider a left-handed, massless Dirac field Ψ, charged under

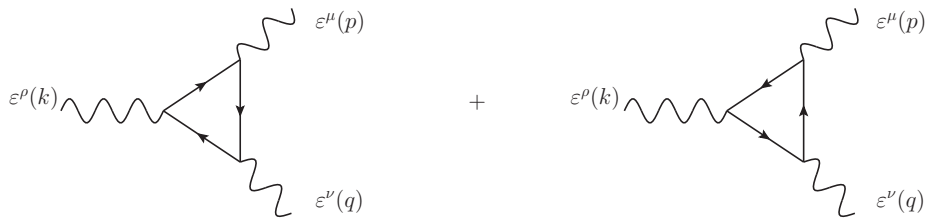

Figure 1.1: Three-point vertex diagrams, all momenta are outgoing.

a $U(1)$ gauge group, so the Lagrange density takes the form:

$$\mathcal{L} = -\frac{1}{4}F^{\mu\nu}F_{\mu\nu} + i\overline{\Psi}\gamma^\mu\left(\partial_\mu - igA_\mu\right)P_L\Psi\,. \tag{1.20}$$

This Lagrangian is classically invariant under the global transformation $\Psi \to e^{-ig\theta}\Psi$ which implies the conserved current $j^\mu_L(x) = \overline{\Psi}(x)\gamma^\mu P_L\Psi(x)$ according to Noether's theorem, which in turn implies gauge invariance of the scattering amplitudes. In momentum space this can be understood in the following way: If we write the scattering amplitude $\mathcal{T}$ for a process with an outgoing "photon" with momentum k^μ and polarisation λ as $\mathcal{T} = \varepsilon^\mu_\lambda(\boldsymbol{k})\mathcal{M}_\mu$, then gauge invariance (and therefore renormalisability) demands $k^\mu\mathcal{M}_\mu = 0$, because a gauge transformation shifts $\varepsilon^\mu_\lambda - \varepsilon'^\mu_\lambda \sim k^\mu$.

In the theory at hand, this critical relation is violated in the three-point vertex function, i.e. in the triangle diagrams of Fig. 1.1, denoted as $i\boldsymbol{V}^{\mu\nu\rho}(p,q,k)$.

A long calculation [30] results in

$$p_\mu \boldsymbol{V}^{\mu\nu\rho} = -\frac{ig^3}{8\pi^2}(1-c)\varepsilon^{\nu\rho\alpha\beta}q_\alpha k_\beta + \mathcal{O}(g^5)\,, \tag{1.21}$$

$$q_\nu \boldsymbol{V}^{\mu\nu\rho} = -\frac{ig^3}{8\pi^2}(1-c)\varepsilon^{\rho\mu\alpha\beta}k_\alpha p_\beta + \mathcal{O}(g^5)\,, \tag{1.22}$$

$$k_\rho \boldsymbol{V}^{\mu\nu\rho} = -\frac{ig^3}{8\pi^2}(2c)\varepsilon^{\mu\nu\alpha\beta}p_\alpha q_\beta + \mathcal{O}(g^5)\,, \tag{1.23}$$

where c is a numerical constant that is related to the regulator of the occurring loop-integral. As can be seen, at least one of these expressions is non-zero, therefore the theory is no longer gauge invariant (or, more importantly, renormalisable) at one-loop level.

However, if we introduce N left-handed fields Ψ_i (charge Q_i), we have to sum over the different fermions in the loop, effectively changing

$$g^3 \to \sum_{i=1}^{N}(gQ_i)^3\,. \tag{1.24}$$

If this expression equals zero, gauge invariance will be restored.[6]

[6] A different approach to anomalies, via the functional measure of Feynman path integrals, shows that this is true to all orders of perturbation theory, i.e. Eq. (1.24) is a necessary and sufficient condition

This result generalises relatively easily to the case of a general (non-abelian) gauge group with left-handed fermions in the (possibly reducible) representation R. Aside from the polarisation and momentum, the "photons" in Fig. 1.1 now carry group indices a, b, c (since they belong to the adjoint representation of the gauge group). Denoting the generating group matrices for representation R as T_R^a, the gauge-invariance condition (1.24) turns into

$$\mathrm{tr}\left[\{T_R^a, T_R^b\}T_R^c\right] = 0\,, \tag{1.25}$$

where the curly brackets stand for the anticommutator $\{A, B\} \equiv AB + BA$.

The coupling to gravity introduces yet another condition [34]. The diagram with two gravitons and one gauge boson will be proportional to $\mathrm{tr}[T_R^a]$, which therefore needs to vanish as well. Since the generators of non-abelian groups are traceless, this only constrains the abelian $U(1)$ factors: the $U(1)$ charges Y_i of all fermions need to satisfy

$$\sum_i Y_i = 0\,, \tag{1.26}$$

otherwise either gauge invariance or general covariance of the theory breaks down.

The above statements remain true if we consider massive fermions, as long as the mass terms are allowed by the gauge symmetry [31].

1.6 Motivation and Outline

This section shall provide a brief review of the previous research concerning the $L_\mu - L_\tau$ symmetry, followed by the motivation and outline for this thesis.

We already mentioned the work of Okun [19, 23] and others [24, 25, 26], who discussed leptonic photons (i.e. unbroken symmetries) and their constraints from cosmology. They also find that the symmetry $L_\alpha - L_\beta$ can be consistently gauged (no anomalies within the SM) and is therefore of interest, the $L_\mu - L_\tau$ symmetry being the least constrained one. While neutrino oscillations forbid exact $L_\alpha - L_\beta$ symmetries, the derived constraints can still be adapted for the fifth-force limit of the broken symmetry (see Sec. 3.4.2).

More recent discussions on gauged $L_\alpha - L_\beta$ symmetries are based mainly on $L_e - L_{\mu,\tau}$, since the corresponding gauge boson couples to electrons and is therefore easier to constrain. We mention the work of Joshipura et al. on some phenomenological aspects of a heavy $Z'_{L_e - L_{\mu,\tau}}$ [35] and more importantly on the effects of a corresponding long-range force on neutrino oscillations [27, 28, 36], due to the potential generated by electrons in the Sun. In this way, Joshipura et al. improve the bounds on the strength of this new force compared to constraints from the equivalence principle.

Renewed interest in the overlooked $L_\mu - L_\tau$ symmetry arose to explain the anomalous magnetic moment of the muon, most prominently by Ma et al. [37, 38] and Baek et al. [39, 40]. The deviation of the experimental and theoretical value for $(g-2)_\mu$ can be explained by a $U(1)_{L_\mu - L_\tau}$ gauge boson because this contributes at one-loop level and is otherwise hardly constrained. Ma et al. also construct a Higgs sector that

for gauge invariance; no new anomalies are introduced in higher loop order.

imposes nearly bimaximal mixing of neutrinos, but is by now highly disfavoured since it generates a large value of $\sin\theta_{13} \approx 0.22$. In Ref. [38], the authors discuss mass-mixing between Z and $Z'_{L_\mu - L_\tau}$, used to explain the difference of the measured Weinberg angle $\sin^2\theta_W$ at NuTeV [41] compared to other measurements (in other words, NuTeV measured a different neutrino coupling than expected from the SM). Baek et al. examine the signatures of $Z'_{L_\mu - L_\tau}$ in muon collisions [39] and the possibility to use it as a mediator to the dark matter sector, using its leptophilic nature to explain the PAMELA anomaly [40] (excess of positrons in cosmic rays compared to antiprotons [42]). All of these papers (and Ref. [43] as well) discuss signatures of the extra neutral gauge boson at the LHC.

Further motivation comes from the neutrino sector; as mentioned in Sec. 1.2, the structure of the PMNS mixing matrix seems to suggest an underlying symmetry principle. As shown in Ref. [29], from the nine continuous global abelian symmetries based on lepton number, the three combinations $L_\mu - L_\tau$, $L_e - L_\mu - L_\tau$ and L_e generate a bimaximal mixing matrix at zeroth order (while e.g. $L_e - L_{\mu,\tau}$ do not lead to successful mixing matrices unless highly perturbed). Since $L_\mu - L_\tau$ can be promoted to a local symmetry[7] and is furthermore barely constrained, it is the most interesting possibility to consider. In this way, we make a connection between the gauge sector and the flavour sector.

In this thesis, we will try to elucidate the connection between neutrinos and the gauge sector of the theory. In order to do so, we will discuss the most general Lagrangian for our Z', including all the mixing terms that have been ignored in most previous work (Ch. 2), and emphasise the effects that arise in neutrino interactions, how they can be observed in current and future neutrino experiments, and how they differ from the NSI effects usually discussed. Since the ability to accommodate a light Z' is quite unique to this model, our main focus will be on a discussion of an ultralight Z', affecting neutrino oscillations solely through mixing and its flavour structure, a possibility that has not been discussed before. Chapter 3 is devoted to a discussion of current constraints on this fifth force, sensitivity of future long-baseline experiments to its effects, and how it might just be able to explain a recently measured neutrino-antineutrino anomaly at the MINOS experiment (Sec. 3.6).

Still in a low mass range compared to other Z' models, we then discuss the phenomenology of a Z' mass below and around the electroweak scale (Ch. 4). We once again discuss the impact of mixing effects on neutrino interactions and proceed to identify the parameter values currently allowed, locating an actually favoured region using a global fit to electroweak precision data. This improves previous analyses which mainly focussed on the anomalous magnetic moment of the muon. Since collider phenomenology is already well considered, we comment only briefly on it and try to improve some of the analysis.

Since previous research only discusses the extended scalar sector of the theory in passing, we devote Ch. 5 to a detailed discussion of specific models. We investigate several symmetry breaking sectors and their imprint on the neutrino mass matrix. The

[7] A short calculation shows that it is not possible to cancel the anomalies in $L_e - L_\mu - L_\tau$ and L_e just by some right-handed neutrinos like in the $(B - L)$ case.

various scalar potentials are examined and we discuss the resulting mixing among the scalars, their impact on the Higgs search at the LHC and the generation of lepton flavour violating decays.

Since we cover a lot of different areas of physics, it proves convenient to sprinkle in introductions and conclusions in each chapter, as to improve reading fluency. An overall conclusion and outlook will be given in Ch. 6.

In the Appendix we summarise some of the conventions we use, concerning units etc. (App. A), and give a brief introduction to the statistical tools we need throughout this thesis (App. B). In App. C, we review the Stückelberg mechanism and a possible application in our model. App. D is a collection of lengthy formulae from a perturbative treatment of the three-flavour oscillation probabilities. In App. E, we explore a different charge assignment to the right-handed neutrinos N_i compared to the main text. Finally, we list the different types of two-Higgs-doublet models discussed in the literature (App. F), and the electroweak precision observables we use in the χ^2-fit for the heavy Z' (App. G).

Chapter 2

Theoretical Framework

In this chapter, we will define our model in the most general way practicable, starting from the Lagrange density; we include all renormalisable mixing terms and derive the proper mass eigenstates of the gauge bosons. Our first section deals with the anomaly freedom of the gauge group, to verify the validity of the theory.

2.1 Anomaly Cancellation in $G_{\mathrm{SM}} \times U(1)_{L_\mu - L_\tau}$

In the following, we will show that the gauge group G_{SM} of the Standard Model can be extended to $G_{\mathrm{SM}} \times U(1)_{L_\mu - L_\tau}$, without the need to introduce further particles to cancel anomalies. For the sake of shortness, we will use the notation $U(1)_{L_\mu - L_\tau} \equiv U(1)'$ often throughout the thesis.

We use the hypercharge convention $Q = T_3 + \frac{Y}{2}$, yielding the particle representations given in Tab. 1.1. In addition, we assign the $U(1)_{L_\mu - L_\tau}$ charge $+1$ to μ_L, ν_μ and $\overline{\tau_R}$, and -1 to τ_L, ν_τ and $\overline{\mu_R}$, while all other particles remain uncharged (see Tab. 2.1). This will be denoted by an additional bracket in the representation, for example, $\overline{\mu_R} \sim (1,1,+2)(-1)$ means that $\overline{\mu_R}$ transforms as a singlet under $SU(3)$ (colour) and $SU(2)$ (isospin), while the $U(1)_Y$ hypercharge transformation takes the form $\overline{\mu_R} \to \exp\left(i(+2)\theta(x)\right)\overline{\mu_R}$. The (now gauged) $U(1)'$ transformation is represented as $\overline{\mu_R} \to \exp\left(i(-1)\theta'(x)\right)\overline{\mu_R}$.

The anomaly-freedom of the Standard Model is shown in Ref. [31], we will therefore only focus on the additional triangle diagrams with the $U(1)'$ gauge boson (shown in

$L_e \sim (1,2,-1)(0)$	$L_\mu \sim (1,2,-1)(+1)$	$L_\tau \sim (1,2,-1)(-1)$
$\overline{e_R} \sim (1,1,+2)(0)$	$\overline{\mu_R} \sim (1,1,+2)(-1)$	$\overline{\tau_R} \sim (1,1,+2)(+1)$

Table 2.1: $G_{\mathrm{SM}} \times U(1)_{L_\mu - L_\tau}$ representations of left-handed leptons.

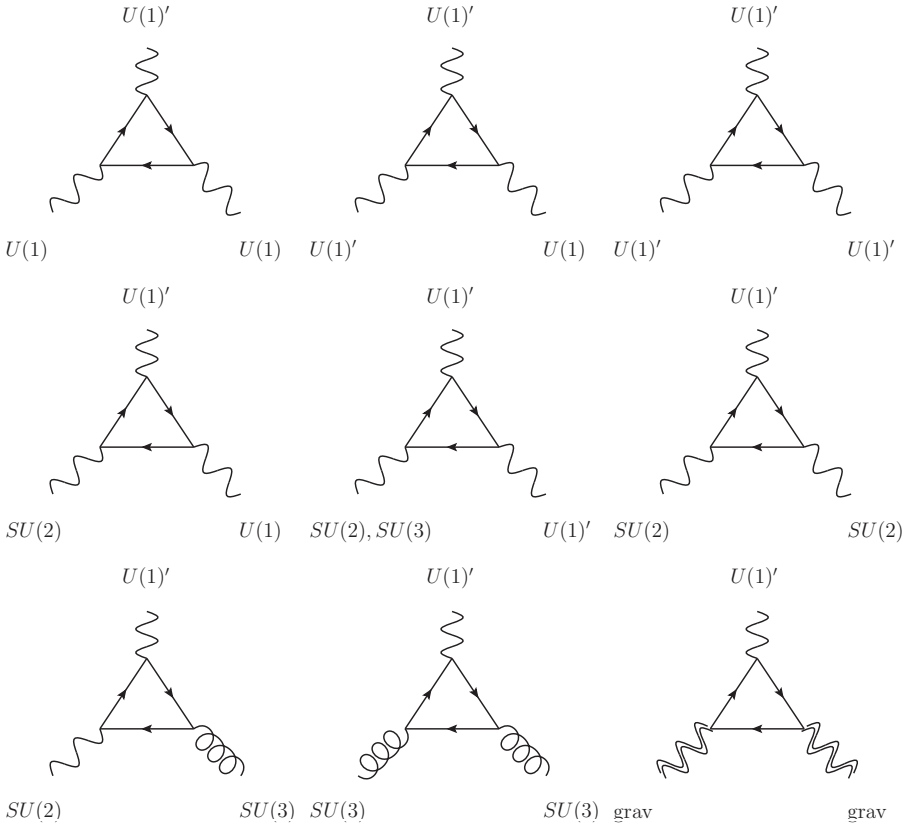

Figure 2.1: Additional triangle diagrams involving the $U(1)_{L_\mu - L_\tau}$ gauge boson Z'.

Fig. 2.1). To deal with them, we need expressions like:

$$\begin{aligned}
\mathrm{tr}(Y'Y^2) &= \sum_\ell Y'(\ell)Y^2(\ell) \\
&= \left[Y'(\mu_L)Y^2(\mu_L) + Y'(\nu_\mu)Y^2(\nu_\mu) + Y'(\overline{\mu_R})Y^2(\overline{\mu_R})\right] \\
&\quad + \left[Y'(\tau_L)Y^2(\tau_L) + Y'(\nu_\tau)Y^2(\nu_\tau) + Y'(\overline{\tau_R})Y^2(\overline{\tau_R})\right] \\
&= \left[(+1)\cdot 2\cdot(-1)^2 + (-1)\cdot(+2)^2\right] + \left[(-1)\cdot 2\cdot(-1)^2 + (+1)\cdot(+2)^2\right] \\
&= 0\,.
\end{aligned} \tag{2.1}$$

Analogous calculations give the equations:

$$\begin{aligned}
\mathrm{tr}(Y'Y^2) &= \left[(+1)\cdot 2\cdot(-1)^2 + (-1)\cdot(+2)^2\right] + \left[(-1)\cdot 2\cdot(-1)^2 + (+1)\cdot(+2)^2\right] = 0\,, \\
\mathrm{tr}(Y'^2Y) &= \left[(+1)^2\cdot 2\cdot(-1) + (-1)^2\cdot(+2)\right] + \left[(-1)^2\cdot 2\cdot(-1) + (+1)^2\cdot(+2)\right] = 0\,, \\
\mathrm{tr}(Y'^3) &= \left[(+1)^3\cdot 2 + (-1)^3\right] + \left[(-1)^3\cdot 2 + (+1)^3\right] = 0\,, \\
\mathrm{tr}(Y'Y) &= \left[(+1)\cdot 2\cdot(-1) + (-1)\cdot(+2)\right] + \left[(-1)\cdot 2\cdot(-1) + (+1)\cdot(+2)\right] = 0\,, \\
\mathrm{tr}(Y') &= \left[(+1)\cdot 2 + (-1)\right] + \left[(-1)\cdot 2 + (+1)\right] = 0\,.
\end{aligned} \tag{2.2}$$

The first row of triangles in Fig. 2.1 vanishes by the first three of the equations (2.2); the anomalies involving one $SU(2)$ gauge boson cancel because $\text{tr}(\sigma^a) = 0$. The one with two $SU(2)$ gauge bosons simplifies via $\text{tr}(\sigma^a \sigma^b) \sim \text{tr}(\delta^{ab})$ to $\text{tr}(Y')$, and therefore vanishes. The anomalies involving $SU(3)$ cancel trivially, because the quarks carry no $U(1)'$ charge. Finally, the anomaly involving the gravitons is proportional to $\text{tr}(Y')$ and hence equals zero by the last equation of (2.2).

Since we introduced a generation-dependent symmetry, the anomalies do not cancel among just one generation (except, of course, the first generation). To explain neutrino oscillations, we may want to introduce additional fermions to the theory. By choosing them to be singlets $\sim (1,1,0)(0)$, we do not introduce new anomalies. It is also possible to charge them under $U(1)'$ (still singlets of the Standard Model), as long as their Y' charges fulfil

$$\sum_i {Y'_i}^3 = 0 = \sum_i Y'_i \,, \tag{2.3}$$

e.g. two right-handed neutrinos in $(1,1,0)(-a)$ and $(1,1,0)(+a)$, respectively. The only nontrivial possibility for three right-handed neutrinos is $N_{R,1} \sim (1,1,0)(-a)$, $N_{R,2} \sim (1,1,0)(+a)$ and $N_{R,3} \sim (1,1,0)(0)$. This case, with $a \equiv 1$, has been discussed for the global $U(1)_{L_\mu - L_\tau}$ in Ref. [29]. For four right-handed neutrinos the anomalies have to cancel pairwise, i.e. $Y'_1 = -Y'_2$ and $Y'_3 = -Y'_4$.

2.2 The Lagrangian for $G_{\text{SM}} \times U(1)_{L_\mu - L_\tau}$

The general Lagrange density after breaking the $SU(3)_C \times SU(2)_L \times U(1)_Y \times U(1)'$ symmetry to $SU(3)_C \times U(1)_{\text{EM}}$ can be written as [44]

$$\mathcal{L} = \mathcal{L}_{\text{SM}} + \mathcal{L}_{Z'} + \mathcal{L}_{\text{mix}} \,, \tag{2.4}$$

where the relevant part of the Standard Model Lagrangian is

$$\mathcal{L}_{\text{SM}} = -\frac{1}{4}\hat{B}_{\mu\nu}\hat{B}^{\mu\nu} - \frac{1}{4}\hat{W}^a_{\mu\nu}\hat{W}^{a\mu\nu} + \frac{1}{2}\hat{M}_Z^2 \hat{Z}_\mu \hat{Z}^\mu - \frac{\hat{e}}{\hat{c}_W} j_B^\mu \hat{B}_\mu - \frac{\hat{e}}{\hat{s}_W} j_W^{a\mu} \hat{W}^a_\mu \,, \tag{2.5}$$

and the hats merely denote that the fields are not mass eigenstates. The Z' part is in our case given by

$$\mathcal{L}_{Z'} = -\frac{1}{4}\hat{Z}'_{\mu\nu}\hat{Z}'^{\mu\nu} + \frac{1}{2}\hat{M}_Z'^2 \hat{Z}'_\mu \hat{Z}'^\mu - \hat{g}' j'^\mu Z'_\mu \,, \tag{2.6}$$

$$j'^\mu = \bar{\mu}\gamma^\mu \mu + \bar{\nu}_\mu \gamma^\mu P_L \nu_\mu - \bar{\tau}\gamma^\mu \tau - \bar{\nu}_\tau \gamma^\mu P_L \nu_\tau \,, \tag{2.7}$$

with the projection operator $P_L \equiv \frac{1}{2}(1 - \gamma_5)$. The kinetic- and mass-mixing terms are parameterised as

$$\mathcal{L}_{\text{mix}} = -\frac{\sin\chi}{2} \hat{Z}'^{\mu\nu} \hat{B}_{\mu\nu} + \delta \hat{M}^2 \hat{Z}'_\mu \hat{Z}^\mu \,, \tag{2.8}$$

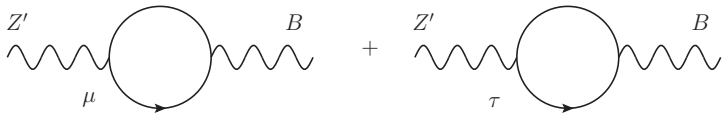

Figure 2.2: Loop-induced kinetic mixing via Z'_μ and B_μ.

with the kinetic-mixing angle χ (we choose kinetic mixing with the hypercharge, see App. A).

Even if χ is zero at some energy, vacuum polarisation diagrams with muons and tauons in the loop can generate such an interaction due to mass splittings (Fig. 2.2). At very low energies we have roughly (for massless Z') [13]

$$\chi \sim \frac{1}{6\pi^2}\frac{\hat{e}}{\hat{c}_W}\hat{g}' \ln\left(\frac{m_\tau}{m_\mu}\right) \approx \hat{g}' \times 10^{-2}\,. \tag{2.9}$$

A similar effect arises with the introduction of $U(1)'$-charged scalars (which we need to break the symmetry anyhow), depending on their quantum numbers.

The off-diagonal mass element $\delta\hat{M}^2$ can be generated by the VEV of a scalar, charged under both $U(1)'$ and $SU(2)_L \times U(1)_Y$. We do not specify the Higgs sector of the model yet, even though it can introduce further interesting couplings,[1] like $|H'|^2|H_{\mathrm{SM}}|^2$. The difficulties in defining a proper Higgs sector for the ultralight Z' will be discussed in Sec. 3.8; numerous examples for the heavy Z' will be given in Ch. 5. To stay as model independent as possible, we will work for the most part with Eq. (2.8) as effective parameters, ignoring their origin.

We will now derive the proper mass eigenstates, following Refs. [44, 45]. From Eq. (2.4) we obtain the mass matrix

$$\frac{1}{2}\begin{pmatrix}\hat{A} & \hat{Z} & \hat{Z}'\end{pmatrix}\begin{pmatrix}0 & 0 & 0\\ 0 & \hat{M}_Z^2 & \delta\hat{M}^2\\ 0 & \delta\hat{M}^2 & \hat{M}_{Z'}^2\end{pmatrix}\begin{pmatrix}\hat{A}\\ \hat{Z}\\ \hat{Z}'\end{pmatrix} \equiv \frac{1}{2}\begin{pmatrix}\hat{A} & \hat{Z} & \hat{Z}'\end{pmatrix}\mathcal{M}^2\begin{pmatrix}\hat{A}\\ \hat{Z}\\ \hat{Z}'\end{pmatrix}\,. \tag{2.10}$$

For convenience we will first apply the Weinberg rotation

$$\begin{pmatrix}\hat{A}\\ \hat{Z}\\ \hat{Z}'\end{pmatrix} = U\begin{pmatrix}\hat{B}\\ \hat{W}^3\\ \hat{Z}'\end{pmatrix} = \begin{pmatrix}\cos\theta & \sin\theta & 0\\ -\sin\theta & \cos\theta & 0\\ 0 & 0 & 1\end{pmatrix}\begin{pmatrix}\hat{B}\\ \hat{W}^3\\ \hat{Z}'\end{pmatrix}\,, \tag{2.11}$$

and then perform a non-unitary transformation to diagonalise the kinetic term:

$$\begin{pmatrix}\hat{B}\\ \hat{W}^3\\ \hat{Z}'\end{pmatrix} = R\begin{pmatrix}B\\ W^3\\ Z'\end{pmatrix} = \begin{pmatrix}1 & 0 & -\tan\chi\\ 0 & 1 & 0\\ 0 & 0 & 1/\cos\chi\end{pmatrix}\begin{pmatrix}B\\ W^3\\ Z'\end{pmatrix}\,. \tag{2.12}$$

[1] In some Higgs models, there will be additional terms in our leptonic $U(1)'$-current as well, which can lead to flavour-changing interactions (see Sec. 5.1.3). Since such terms are strongly constrained, we will omit them for now.

The kinetic terms are now properly normalised:

$$\begin{aligned}
&-\frac{1}{4}\hat{B}_{\mu\nu}\hat{B}^{\mu\nu} - \frac{1}{4}\hat{Z}'_{\mu\nu}\hat{Z}'^{\mu\nu} - \frac{\sin\chi}{2}\hat{Z}'^{\mu\nu}\hat{B}_{\mu\nu} \\
&= -\frac{1}{4}\begin{pmatrix}\hat{B}^{\mu\nu} & \hat{Z}'^{\mu\nu}\end{pmatrix}\begin{pmatrix}1 & \sin\chi \\ \sin\chi & 1\end{pmatrix}\begin{pmatrix}\hat{B}_{\mu\nu} \\ \hat{Z}'_{\mu\nu}\end{pmatrix} \\
&= -\frac{1}{4}\begin{pmatrix}B^{\mu\nu} & Z'^{\mu\nu}\end{pmatrix}\begin{pmatrix}1 & 0 \\ -\tan\chi & 1/\cos\chi\end{pmatrix}\begin{pmatrix}1 & \sin\chi \\ \sin\chi & 1\end{pmatrix}\begin{pmatrix}1 & -\tan\chi \\ 0 & 1/\cos\chi\end{pmatrix}\begin{pmatrix}B_{\mu\nu} \\ Z'_{\mu\nu}\end{pmatrix} \\
&= -\frac{1}{4}\begin{pmatrix}B^{\mu\nu} & Z'^{\mu\nu}\end{pmatrix}\begin{pmatrix}1 & 0 \\ 0 & 1\end{pmatrix}\begin{pmatrix}B_{\mu\nu} \\ Z'_{\mu\nu}\end{pmatrix},
\end{aligned} \tag{2.13}$$

and we can perform further unitary transformations without changing this kinetic structure. It is convenient to undo the Weinberg rotation via

$$\begin{pmatrix}B \\ W^3 \\ Z'\end{pmatrix} = U^\dagger \begin{pmatrix}\tilde{A} \\ \tilde{Z} \\ \tilde{Z}'\end{pmatrix}, \tag{2.14}$$

so that the mass matrix in the $(\tilde{A}, \tilde{Z}, \tilde{Z}')$ basis takes the form

$$\mathcal{M}^2_{\tilde{A},\tilde{Z},\tilde{Z}'} = \left(URU^\dagger\right)^\dagger \mathcal{M}^2 URU^\dagger = \begin{pmatrix}0 & 0 & 0 \\ 0 & a & b \\ 0 & b & c\end{pmatrix}, \tag{2.15}$$

where a, b and c are defined as:

$$\begin{aligned}
&a \equiv \hat{M}_Z^2\,, \qquad b \equiv \hat{s}_W \tan\chi \hat{M}_Z^2 + \frac{\delta\hat{M}^2}{\cos\chi}\,, \\
&c \equiv \frac{1}{\cos^2\chi}\left(\hat{M}_Z^2\hat{s}_W^2\sin^2\chi + 2\hat{s}_W\sin\chi\delta\hat{M}^2 + \hat{M}_{Z'}^2\right).
\end{aligned} \tag{2.16}$$

The mass matrix $\mathcal{M}^2_{\tilde{A},\tilde{Z},\tilde{Z}'}$ can be diagonalised by an orthogonal matrix U_ξ:

$$\begin{pmatrix}\tilde{A} \\ \tilde{Z} \\ \tilde{Z}'\end{pmatrix} = U_\xi \begin{pmatrix}A \\ Z_1 \\ Z_2\end{pmatrix} = \begin{pmatrix}1 & 0 & 0 \\ 0 & \cos\xi & -\sin\xi \\ 0 & \sin\xi & \cos\xi\end{pmatrix}\begin{pmatrix}A \\ Z_1 \\ Z_2\end{pmatrix}. \tag{2.17}$$

The fields A, Z_1 and Z_2 obtain the masses zero and

$$M^2_{1,2} = \frac{a+c}{2} \pm \sqrt{b^2 + \left(\frac{a-c}{2}\right)^2}\,, \tag{2.18}$$

respectively, and the new mixing angle is given by

$$\tan 2\xi = \frac{2b}{a-c}\,. \tag{2.19}$$

The mixing angle also satisfies the equations

$$\tan^2\xi = \frac{M_1^2 - a}{a - M_2^2}\,, \qquad \sin^2\xi = \frac{M_1^2 - a}{M_1^2 - M_2^2}\,, \tag{2.20}$$

the last one uses $\sin^2 = \tan^2/(1+\tan^2)$. To summarise: The gauge eigenstates $\hat{A}$, $\hat{Z}$ and $\hat{Z}'$ are related to the mass eigenstates via

$$\begin{pmatrix}\hat{A}\\ \hat{Z}\\ \hat{Z}'\end{pmatrix} = \begin{pmatrix}1 & -\hat{c}_W \sin\xi\tan\chi & -\hat{c}_W\cos\xi\tan\chi\\ 0 & \cos\xi + \hat{s}_W\sin\xi\tan\chi & \hat{s}_W\cos\xi\tan\chi - \sin\xi\\ 0 & \frac{\sin\xi}{\cos\chi} & \frac{\cos\xi}{\cos\chi}\end{pmatrix}\begin{pmatrix}A\\ Z_1\\ Z_2\end{pmatrix}\,, \tag{2.21}$$

or, inverted:

$$\begin{pmatrix}A\\ Z_1\\ Z_2\end{pmatrix} = \begin{pmatrix}1 & 0 & \hat{c}_W\sin\chi\\ 0 & \cos\xi & -\hat{s}_W\cos\xi\sin\chi + \sin\xi\cos\chi\\ 0 & -\sin\xi & \cos\xi\cos\chi + \hat{s}_W\sin\xi\sin\chi\end{pmatrix}\begin{pmatrix}\hat{A}\\ \hat{Z}\\ \hat{Z}'\end{pmatrix}\,. \tag{2.22}$$

Decoupling corresponds to $\chi = 0 = \xi$, so we expect these two mixing angles to be small to be in accord with electroweak data.

2.2.1 Definition of the Weinberg Angle

To make a connection between theory and experiment, we should express the parameters of the Lagrangian by measurable quantities. Since the coupling of the photon to j_{EM} does not change, we identify $\hat{e} = e = \sqrt{4\pi\alpha}$. Defining the SM weak mixing angle by the NOV scheme (Novikov-Okun-Vysotsky [46, 22]), i.e. via

$$s_W^2 c_W^2 \equiv \frac{\pi\alpha(M_1)}{\sqrt{2}G_F M_1^2}\,, \tag{2.23}$$

we obtain the corresponding expression for the case with mixing

$$\hat{s}_W^2 \hat{c}_W^2 \equiv \frac{\pi\alpha(\hat{M}_Z)}{\sqrt{2}G_F \hat{M}_Z^2}\,, \tag{2.24}$$

since G_F stems from muon decay measurements and therefore only contains the unchanged W boson mass. Eq. (2.20) then gives

$$\frac{1}{\hat{s}_W\hat{c}_W} = \frac{1}{s_W c_W}\frac{\hat{M}_Z}{M_1} = \frac{1}{s_W c_W}\sqrt{1 + \sin^2\xi\left(\frac{M_2^2}{M_1^2} - 1\right)}\,, \tag{2.25}$$

which can be approximated to

$$\hat{s}_W^2 \approx s_W^2 - s_W^2 \frac{1 - s_W^2}{1 - 2s_W^2} \sin^2 \xi \left(\frac{M_2^2}{M_1^2} - 1 \right) . \tag{2.26}$$

The coupling strengths of $W^\pm$ and Z_{SM} are therefore almost unaffected by the mixture (since the effect goes with ξ^2); the main effect is the additional coupling to j' (which is linear in the mixing angles), i.e. a different coupling to electron, muon and tauon (and their neutrinos). Since the photon stays massless, we do not end up with a coupling $j'_\mu A^\mu$, which would effectively charge neutrinos.

Chapter 3

An Ultralight Z' – The Fifth-Force Limit

Our main focus in this chapter is the limit of an ultralight Z', affiliated with a long-range interaction. This family-non-universal force can affect neutrino oscillations through mixing effects, even though it is highly constrained by astrophysical experiments. We will derive the current constraints and discuss the possibilities for a detection at future neutrino oscillation experiments. Special emphasis will be put on the distinction between this long-range potential and the conventional non-standard neutrino interactions.

3.1 Approximations

The expressions for the mass eigenstates and couplings (2.16) can be simplified when dealing with an ultralight Z'. Making b small results in

$$M_1^2 = a + \frac{b^2}{a-c} + \mathcal{O}(b^4), \qquad M_2^2 = c - \frac{b^2}{a-c} + \mathcal{O}(b^4)\,, \tag{3.1}$$

so setting $a \approx M_{Z_0}^2$ and making c and b small, compared to $\hat{M}_Z^2$, will give a light Z' and a small mixing angle

$$\xi \approx \frac{b}{a-c} \approx \frac{1}{\cos\chi}\left(\hat{s}_W \sin\chi + \frac{\delta\hat{M}^2}{\hat{M}_Z^2}\right) \approx \hat{s}_W\chi + \frac{\delta\hat{M}^2}{\hat{M}_Z^2}\,. \tag{3.2}$$

The last approximation follows from the observation that a small b results in $\tan\chi \ll 1$ and $\delta\hat{M}^2 \ll \hat{M}_Z^2$. Gauge and mass eigenstates are connected via Eq. (2.21):

$$\begin{aligned} \hat{A} &\approx A - c_W\chi Z_2\,, \\ \hat{Z}' &\approx Z_2 + \xi Z_1\,, \\ \hat{Z} &\approx Z_1 - (\xi - s_W\chi)Z_2\,. \end{aligned} \tag{3.3}$$

In this approximation, the mass eigenstates have interaction terms

$$\begin{aligned} \mathcal{L}_A &= -e j_{\mathrm{EM}} A\,, \\ \mathcal{L}_{Z_1} &= -\left(\frac{e}{s_W c_W}(j_3 - s_W^2 j_{\mathrm{EM}}) + g'\xi j'\right) Z_1\,, \\ \mathcal{L}_{Z_2} &= -\left(g' j' - (\xi - s_W\chi)\frac{e}{s_W c_W}(j_3 - s_W^2 j_{\mathrm{EM}}) - e c_W \chi j_{\mathrm{EM}}\right) Z_2\,. \end{aligned} \tag{3.4}$$

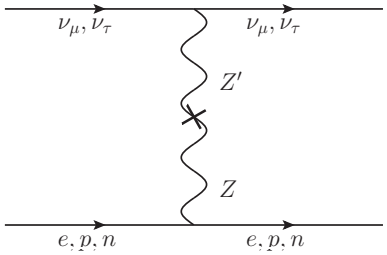

Figure 3.1: Long-range $\nu_{\mu,\tau}$–(e, p, n) interaction through Z–Z' mixing.

We choose to eliminate $\delta\hat{M}^2$ in favour of ξ and χ by means of Eq. (3.2). In the case $\delta\hat{M}^2 = 0$, we need further terms in the approximation of ξ. It turns out that only terms containing $\hat{M}_{Z'}/\hat{M}_Z$ contribute to the $j_{\mathrm{NC}}Z_2$ coupling, the lowest one being $s_W\chi\hat{M}^2_{Z'}/\hat{M}^2_Z$. Since $\hat{M}^2_{Z'}/\hat{M}^2_Z$ is very small for the ultralight Z' discussed below, this coupling will be too small to generate any observable effect (as will be seen later). We will therefore only consider the case $\delta\hat{M}^2 \neq 0$ in the following.

3.2 Potential from the Sun

If we take the mass of the Z' to be $M_2 < 1/\mathrm{A.U.} \sim 10^{-18}\,\mathrm{eV}$, we obtain a static potential at Earth generated by the Sun. This has been studied by Joshipura et al. [27, 36] for the gauge bosons of the $U(1)_{L_e-L_{\mu,\tau}}$ symmetries. Since in our case the Z' does not couple directly to protons, neutrons or electrons, the only effect comes from the mixing, i.e. the j_3 and j_{EM} currents (see Fig. 3.1). The Sun is electrically neutral, so we have $j^0_{\mathrm{EM}} = 0$ and

$$j^0_3 = -\frac{1}{2}\bar{e}_L\gamma^0 e_L + \frac{1}{2}\bar{p}_L\gamma^0 p_L - \frac{1}{2}\bar{n}_L\gamma^0 n_L = -\frac{1}{4}\left(n_e - n_p + n_n\right) = -\frac{n_n}{4}\,, \tag{3.5}$$

where we used $P_L = \frac{1}{2} - \frac{1}{2}\gamma_5$, and the fact that the axial (γ_5) terms will result in a spin operator in the non-relativistic limit and we assume the Sun is not polarised (see Ref. [47]). The equation of motion for Z^0_2 follows from the Euler-Lagrange equation

$$\partial_\nu \frac{\delta}{\delta(\partial_\nu Z_{2\mu})}\left(-\frac{1}{4}Z_{2\alpha\beta}Z_2^{\alpha\beta}\right) - \frac{\delta}{\delta Z_{2\mu}}\left(\frac{1}{2}M_2^2 Z_{2\alpha}Z_2^\alpha + \mathcal{L}_{Z_2}\right) = 0\,, \tag{3.6}$$

which can be equated with (3.4):

$$\left(\partial^2 + M_2^2\right)\, Z^0_2 = (\xi - s_W\chi)\frac{e}{s_W c_W}\frac{n_n}{4}\,. \tag{3.7}$$

For a static potential outside of the Sun, the neutron density can be written as $n_n(\boldsymbol{x}) = N_n\delta^{(3)}(\boldsymbol{x})$, with the total number of neutrons N_n:

$$\left(\Delta - M_2^2\right)\, Z^0_2 = -(\xi - s_W\chi)\frac{e}{s_W c_W}\frac{1}{4}N_n\delta^{(3)}(\boldsymbol{x})\,, \tag{3.8}$$

with the well-known solution

$$V(r) = Z_2^0 = (\xi - s_W\chi)\frac{e}{s_W c_W}\frac{1}{4}N_n \times \frac{e^{-rM_2}}{4\pi r}\,. \tag{3.9}$$

For simplicity, we take the limit $M_2 \to 0$ and calculate the potential for ν_μ ($Y' = +1$) and ν_τ ($Y' = -1$) on Earth:[1]

$$V_{\mu,\tau} = \pm\, g'(\xi - s_W\chi)\frac{e}{4s_W c_W}\frac{N_n}{4\pi R_{A.U.}} + \mathcal{O}(\xi^2, \chi^2, \xi\chi)\,. \tag{3.10}$$

The total number of neutrons in the Sun is approximately $N_n \approx N_e/4 \approx 1.5\times10^{56}$, and the distance between Sun and Earth is $R_{A.U.} \approx 7.6\times10^{26}\,\mathrm{GeV}^{-1}$, yielding the potential

$$V_{\mu,\tau} = \pm\, 2.82\times10^{-14}\,\mathrm{eV}\left(\frac{\alpha}{10^{-50}}\right), \qquad \alpha \equiv g'(\xi - s_W\chi)\,. \tag{3.11}$$

Since this potential should be of order of, or lower than, the typical matter potential ($A \sim 10^{-13}\mathrm{eV}$), we expect the typical order of magnitude $\alpha \sim 10^{-50}$. As with most additional long-range forces, we enter a game of very small numbers at every corner.

The Earth also generates a comparable potential; approximating a static potential at the surface, we calculate the ratio

$$\frac{V_\mathrm{Earth}}{V_\mathrm{Sun}} = \frac{N_{n,\mathrm{Earth}}}{N_{n,\mathrm{Sun}}}\frac{R_{A.U.}}{R_\mathrm{surface}} \approx \frac{1.8\times10^{51}}{1.5\times10^{56}}\frac{1.5\times10^{8}}{6380} \approx 0.28\,, \tag{3.12}$$

where the total number of neutrons has been calculated with the chemical decomposition of the Earth from Ref. [48], but can also be estimated by half the nucleon number of the Earth $\sim M_\oplus/m_\mathrm{nuc.}$. The Moon can be ignored since

$$\frac{V_\mathrm{Moon}}{V_\mathrm{Sun}} = \frac{N_{n,\mathrm{Moon}}}{N_{n,\mathrm{Sun}}}\frac{R_{A.U.}}{R_{\mathrm{Earth-Moon}}} \approx \frac{2.3\times10^{49}}{1.5\times10^{56}}\frac{1.5\times10^{8}}{3.8\times10^{5}} \approx 6\times10^{-5}\,. \tag{3.13}$$

Our full potential at the surface of the Earth is therefore:[2]

$$V_{\mu,\tau} = \pm\, 3.60\times10^{-14}\,\mathrm{eV}\left(\frac{\alpha}{10^{-50}}\right). \tag{3.14}$$

We could also reintroduce the factor $\exp(-rM_2)$, or take our force to be only of Earth-radius range ($M_2 \sim 1/R_\oplus$). All of this merely changes the prefactor in V, i.e. the scale of α. In the following, we will make our calculations with the potential (3.14); in particular, we approximate a constant potential. Additional effects from the proper position dependence are discussed in Sec. 3.7, but are only important for atmospheric neutrino oscillations.

[1] In the following we assume that the mixing angles are somewhat smaller than g', so we can drop the $\mathcal{O}(\xi^2, \chi^2, \xi\chi)$ terms against $\mathcal{O}(g'\chi, g'\xi)$. In the actual neutrino oscillations the terms without g' will be flavour independent and therefore drop out.

[2] The potential in the $L_e - L_{\mu,\tau}$ models is generated by the electrons in the Sun, which leads to $V_{e\mu,\tau} \approx 1.3\times10^{-11}\,\mathrm{eV}(\alpha_{e\mu,\tau}/10^{-50})$, where $\alpha_{e\mu,\tau} = g^2_{e\mu,\tau}/4\pi$. The constraints from solar-neutrino and KamLAND data are $\alpha_{e\mu} < 3.4\times10^{-53}$ and $\alpha_{e\tau} < 2.5\times10^{-53}$ at 3σ [28].

Range	V_{new}/V	$\alpha_{\text{new}}/\alpha$
Earth radius	0.22	4.57
Earth-Sun distance	1	1
galactic distances	46.88	2.13×10^{-2}
	187.50	5.33×10^{-3}

Table 3.1: Ranges for our fifth force and corresponding rescaling of α.

By taking $M_2 < 1/R_{\text{gal}} \sim 10^{-27}\,\text{eV}$, R_{gal} denoting the distance between the Sun and the core of the Milky Way Galaxy (with $100 - 400$ billion stars), we obtain a potential

$$\frac{V_{\text{gal}}}{V_{\text{Sun}}} = \frac{(1-4)\times 10^{11}}{1.6\times 10^{9}} \approx 60 - 240\,, \tag{3.15}$$

which would dominate over our other potentials. In Tab. 3.1, we list the different possibilities and how α needs to be rescaled. For example, an obtained bound $\alpha < 10^{-50}$ translates for a galactic long-range force to $\alpha_{\text{gal}} \lesssim 10^{-52}$.

3.3 Effect on Neutrino Oscillations

Since the potential $V(\alpha)$ only affects ν_μ and ν_τ, the propagation equation for the flavour eigenstates changes to

$$i\frac{\mathrm{d}}{\mathrm{d}t}\boldsymbol{\nu} = \frac{1}{2E}UM_\nu^2U^\dagger\boldsymbol{\nu} + \begin{pmatrix} 0 & 0 & 0 \\ 0 & V_\mu & 0 \\ 0 & 0 & V_\tau \end{pmatrix}\boldsymbol{\nu} \equiv H_{\text{F}}\boldsymbol{\nu}\,, \tag{3.16}$$

with the usual PMNS mixing matrix

$$U = \begin{pmatrix} c_{12}c_{13} & s_{12}c_{13} & s_{13}e^{-i\delta} \\ -c_{23}s_{12} - s_{23}s_{13}c_{12}e^{i\delta} & c_{23}c_{12} - s_{23}s_{13}s_{12}e^{i\delta} & s_{23}c_{13} \\ s_{23}s_{12} - c_{23}s_{13}c_{12}e^{i\delta} & -s_{23}c_{12} - c_{23}s_{13}s_{12}e^{i\delta} & c_{23}c_{13} \end{pmatrix}\,, \tag{3.17}$$

where $c_{ij} = \cos\theta_{ij}$, $s_{ij} = \sin\theta_{ij}$, and $V_\mu = -V_\tau \equiv V$. Since H_{F} is constant, Eq. 3.16 has the simple solution $\boldsymbol{\nu}(t) = \exp(-iH_{\text{F}}t)\boldsymbol{\nu}_0$. In case matter effects are important, we obtain

$$i\frac{\mathrm{d}}{\mathrm{d}t}\boldsymbol{\nu} = \frac{1}{2E}\left[UM_\nu^2U^\dagger + \begin{pmatrix} A(x) & 0 & 0 \\ 0 & 2EV & 0 \\ 0 & 0 & -2EV \end{pmatrix}\right]\boldsymbol{\nu}\,, \tag{3.18}$$

with $A(x) = 2\sqrt{2}G_F n_e(x)E$. For antineutrinos, the signs of A and V change. Eq. (3.18) illustrates that V has to be compared to $\sim \Delta m^2/E$, which means the effect will be most notable for high-energy neutrinos, as already mentioned in the introduction.

3.3.1 Two-Flavour Solution

The analytic solution of Eq. (3.18) is rather messy, so we will first consider ν_μ–ν_τ oscillations in the two-flavour framework (V mainly changes the ν_μ–ν_τ sector). Since V should be small, as to not dominate the oscillation, we should write our evolution equation (3.18) in the mass eigenstates $\boldsymbol{\nu}_M$, with a small perturbation in the parameter V:

$$i\frac{\mathrm{d}}{\mathrm{d}t}\boldsymbol{\nu}_M = \frac{1}{2E}\begin{pmatrix} m_2^2 & 0 \\ 0 & m_3^2 \end{pmatrix}\boldsymbol{\nu}_M + V\cdot U^\dagger \begin{pmatrix} 1 & 0 \\ 0 & -1 \end{pmatrix} U\boldsymbol{\nu}_M\,, \tag{3.19}$$

where

$$U = \begin{pmatrix} \cos\theta & \sin\theta \\ -\sin\theta & \cos\theta \end{pmatrix}\,, \qquad \theta = \theta_{\mathrm{atm}}\,, \tag{3.20}$$

and we define $\Delta m^2 \equiv m_3^2 - m_2^2$ as well as $\eta \equiv \frac{2EV}{\Delta m^2}$. So our Hamiltonian is given by

$$H_V = \frac{1}{2E}\begin{pmatrix} m_2^2 + 2EV\cos 2\theta & 2EV\sin 2\theta \\ 2EV\sin 2\theta & m_3^2 - 2EV\cos 2\theta \end{pmatrix} = \frac{1}{2E}U_V\begin{pmatrix} m_{2,V}^2 & 0 \\ 0 & m_{3,V}^2 \end{pmatrix}U_V^\dagger\,, \tag{3.21}$$

with a new rotation matrix

$$U_V = \begin{pmatrix} \cos\phi & \sin\phi \\ -\sin\phi & \cos\phi \end{pmatrix}\,, \qquad \tan 2\phi = \frac{2\eta\sin 2\theta}{1-2\eta\cos 2\theta}\,, \tag{3.22}$$

mass eigenvalues

$$m_{2,3,V}^2 = \frac{m_2^2 + m_3^2}{2} \mp \frac{\Delta m^2}{2}\sqrt{1 - 4\eta\cos 2\theta + 4\eta^2}\,, \tag{3.23}$$

and mass eigenstates

$$\boldsymbol{\nu}_{M,V} = U_V^\dagger\,\boldsymbol{\nu}_M = U_V^\dagger U^\dagger\,\boldsymbol{\nu}_{\mathrm{flavour}}\,. \tag{3.24}$$

In the presence of V, the mixing angle between flavour and mass eigenstates becomes $\theta_V \equiv \theta + \phi$ and Δm^2 changes to $\Delta m_V^2 \equiv m_{3,V}^2 - m_{2,V}^2$. As can be seen from Eq. (3.22) and Eq. (3.23), this corresponds for small η to

$$\begin{aligned} \theta \to \theta_V &= \theta + \eta\sin 2\theta + \mathcal{O}(\eta^2\cos 2\theta)\,, \\ \Delta m^2 \to \Delta m_V^2 &= \Delta m^2\left(1 - 2\eta\cos 2\theta + 2\eta^2\sin^2 2\theta\right) + \mathcal{O}(\eta^3\cos 2\theta)\,, \end{aligned} \tag{3.25}$$

so we effectively generate energy-dependent θ and Δm^2. It is worth noting once more, that V (and therefore η) changes sign for antineutrinos, resulting in a different oscillation behaviour of neutrinos and antineutrinos in the presence of our potential. For the maximal-mixing scenario $\theta \approx \pi/4$ (favoured by data, see Tab. 1.2), the shift in the mass parameter is equal for neutrinos and antineutrinos, while for $\sin^2 2\theta \neq 1$, we

have in principle a different parameter Δm^2 for ν and $\overline{\Delta m^2}$ for $\overline{\nu}$. This will be further discussed in Ch. 3.6, which contains a fit of our model to the data of the long-baseline experiment MINOS [49, 50], where exactly this effect ($\Delta m^2 \neq \overline{\Delta m^2}$) is observed [51], albeit with very low statistics.

We end up with an oscillation probability $P(\nu_\mu \to \nu_\tau) \equiv P_{\mu\tau}$ of the form

$$\begin{aligned} P_{\mu\tau} &= \sin^2(2\theta_V)\sin^2\left(\frac{\Delta m_V^2}{4}\frac{L}{E}\right) \\ &= \sin^2\left(2\theta + \arctan\left(\frac{2\eta\sin 2\theta}{1-2\eta\cos 2\theta}\right)\right) \times \sin^2\left(a\sqrt{1-4\eta\cos 2\theta+4\eta^2}\right) \\ &\approx \sin^2(2\theta)\sin^2(a) \times \Big\{1 + 4(1-a\cot a)\cos 2\theta\,\eta \\ &\quad - 4\left[1 - a\cot a + \cos^2 2\theta\left(5a\cot a - 4 - a^2\frac{\cos 2a}{\sin^2 a}\right)\right]\eta^2\Big\}, \end{aligned} \tag{3.26}$$

with $a \equiv \frac{\Delta m^2}{4}\frac{L}{E}$. This simplifies for $\sin^2 2\theta \approx 1$ to

$$P_{\mu\tau} = \sin^2(2\theta)\sin^2(a) \times \left\{1 - 4\,(1 - a\cot a)\,\eta^2 + \mathcal{O}(\eta^4)\right\}. \tag{3.27}$$

For maximal mixing the first correction due to V is of order V^2 and therefore identical for ν and $\overline{\nu}$. For non-maximal mixing we have $P(\nu_\mu \to \nu_\tau) \neq P(\overline{\nu}_\mu \to \overline{\nu}_\tau)$, i.e. CP violation (similar to the usual MSW effect, but here also in vacuum).

The maximum of $P_{\mu\tau}$ occurs at $a = \pi/2$, where $a\cot a \to 0$, so the value of the maximum is lowered by a factor

$$(1-4\eta^2)\big|_{a=\pi/2} = \left(1 - \frac{4L^2V^2}{\pi^2}\right), \tag{3.28}$$

while the position of the maximum itself depends only very weakly on V. We see that the effect of V will be enhanced for longer baselines.

$P_{\mu\tau}$ is no longer symmetric around $\theta = \pi/4$ for a non-zero η, but rather obeys the extended symmetry

$$P_{\mu\tau}(\theta = \pi/4 - \sigma, \alpha) = P_{\mu\tau}(\theta = \pi/4 + \sigma, -\alpha). \tag{3.29}$$

We mention the following degeneracies of the exact two-flavour oscillation probability:

$$\begin{aligned} P_{\mu\tau}(\theta, \Delta m^2, \alpha) &= P_{\mu\tau}(\theta, -\Delta m^2, -\alpha) \\ &= P_{\mu\tau}(\theta + \pi/2, \Delta m^2, -\alpha) \\ &= P_{\mu\tau}(\theta + \pi/2, -\Delta m^2, \alpha), \end{aligned} \tag{3.30}$$

and analogous equations for the antineutrino transition probability, defined via

$$P_{\bar{\mu}\bar{\tau}}(\theta, \Delta m^2, \alpha) \equiv P_{\mu\tau}(\theta, \Delta m^2, -\alpha). \tag{3.31}$$

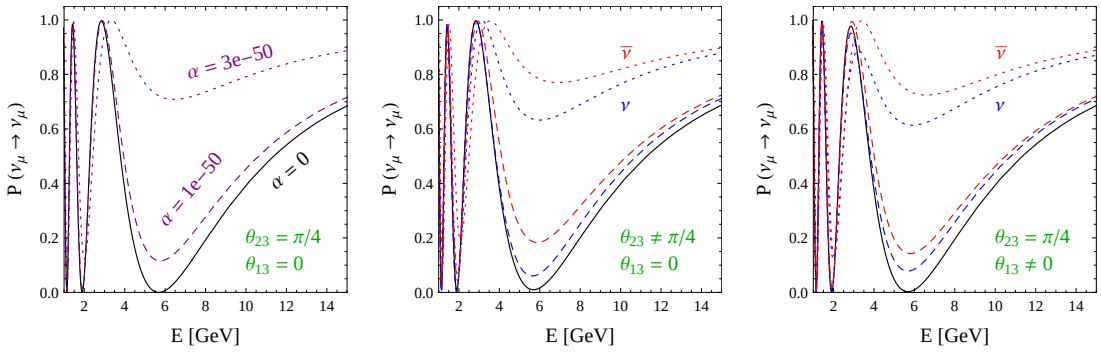

Figure 3.2: Survival probability $P(\nu_\mu \to \nu_\mu)$ as a function of the neutrino energy E for $L = 3000\,\text{km}$ and different values of α (left). For non-maximal mixing (here $\theta_{23} = \pi/4 - 0.05$) the probabilities for neutrino $P(\nu_\mu \to \nu_\mu)$ and antineutrino $P(\overline{\nu}_\mu \to \overline{\nu}_\mu)$ split up (middle), which also happens for non-vanishing θ_{13} (here: $\theta_{13} = 0.15$) (right).

3.3.2 Three-Flavour Effects

We will show the survival probability $P(\nu_\mu \to \nu_\mu)$, using the full solution of Eq. (3.18) (with vanishing matter density and oscillation parameters from Tab. 1.2). Fig. 3.2 illustrates the effect of α on the oscillation, the changes are most significant around the oscillation minimum and enhance the survival probability. As we have already seen in the exact two-flavour solution, a non-maximal atmospheric mixing angle θ_{23} destroys the symmetry $P_{\mu\mu} = P_{\bar{\mu}\bar{\mu}}$, so neutrinos and antineutrinos oscillate differently. This is pictured in Fig. 3.2 (middle), where we set $\theta_{23} = \pi/4 - 0.05$; shifting θ_{23} in the opposite direction just changes $\nu \leftrightarrow \overline{\nu}$, due to Eq. (3.29), which is still a good symmetry for $\sin\theta_{13} \ll 1$.

Interestingly (a true three-flavour effect), a similar splitting also occurs for non-vanishing θ_{13} (Fig. 3.2 (right)), with the main difference that this also lowers the maximum of $P_{\mu\mu}$ compared to $P_{\bar{\mu}\bar{\mu}}$. For small θ_{13}, the degeneracies from Eq. (3.30) are still good symmetries, which means without knowledge of the mass hierarchy (the sign of Δm^2_{31}), we can say nothing about the sign of α. We will comment on a possible resolution at future long-baseline neutrino experiments in Sec. 3.5.7.

For completeness, we show analytic expressions of $P_{\alpha\beta}$ (including a constant matter potential) from an expansion to second order in the small quantities[3] V, Δm^2_{21} and θ_{13} in App. D (approximations that were not made in Fig. 3.2). These expressions can be used to verify that $P_{e\beta}$ is only affected in order V^3 by the potential, while $P_{\mu\mu}$ and $P_{\mu\tau}$ have linear contributions of the form $(s^2_{23} - c^2_{23})V$, which reinstates the symmetry (3.29) for the three-flavour framework. This once again shows how the $P(\nu) = P(\overline{\nu})$ symmetry is linked to maximal ν_μ–ν_τ mixing. The breaking of this symmetry due to $\theta_{13} \neq 0$ is not described by the perturbative expressions of App. D, because the effect goes with $s^2_{13}\,V$.

Let this suffice as a discussion of the modified neutrino oscillations under the influence of the potential V.

[3]The actual expansion parameters are $\Delta m^2_{21}/\Delta m^2_{31}$, $\sin\theta_{13}$ and $2EV/A_{\text{matter}} \approx \alpha/(3 \times 10^{-50})$, all assumed to be of the same order.

3.4 Current Bounds on the Coupling Constant and Mixing Angles

This section gives a review over the restrictions placed on the mixing angles ξ and χ and the coupling constant g', by various experiments from particle physics to cosmology.

3.4.1 Equivalence Principle

The model with an ultralight Z' violates the equivalence principle because it adds a lepton-number-dependent long-range force to gravitation. The bounds on such forces are very strict [52], but not directly applicable here, since they are based on lunar ranging and torsion balance experiments, which are only sensitive to the electron and baryon content of matter. That means the only effect comes once again from Z–Z' mixing. As shown above, the Z_2 potential generated by a massive body depends on the number of neutrons N:

$$V = \frac{e(\xi - s_W\chi)}{4 s_W c_W} N \frac{e^{-rM_2}}{4\pi r} \,. \tag{3.32}$$

The gravitational potential between two bodies with masses m_1 and m_2, and neutron content N_1 and N_2, is therefore changed to

$$V_{\text{grav}} = -G_N \frac{m_1 m_2}{r} \left(1 - \left(\frac{e(\xi - s_W\chi)}{4 s_W c_W} \right)^2 \frac{N_1}{m_1} \frac{N_2}{m_2} \frac{1}{4\pi G_N} e^{-rM_2} \right) . \tag{3.33}$$

The constraints for a neutron-dependent fifth force are shown in Fig. 3.3 (taken from Ref. [52], see references therein for a description of the experiments), where

$$|\tilde{\alpha}| \equiv \frac{1}{4\pi G_N u^2} \left(\frac{e(\xi - s_W\chi)}{4 s_W c_W} \right)^2 , \qquad \lambda \equiv \frac{1}{M_2} \,. \tag{3.34}$$

For an Earth-Sun-distance range we take the conservative bound $|\tilde{\alpha}| < 10^{-11}$, corresponding to

$$(\xi - s_W\chi) < 5 \times 10^{-24} \,, \tag{3.35}$$

whereas an Earth-radius range Z' only yields $|\tilde{\alpha}| < 5 \times 10^{-9}$, corresponding to $(\xi - s_W\chi) < 10^{-22}$.

3.4.2 Big Bang Nucleosynthesis

Additional relativistic degrees of freedom, like new light neutrinos or our Z' boson, can potentially affect the physics of the early Universe, e.g. the successful Big Bang Nucleosynthesis (BBN) [55]. We will briefly review relevant BBN processes: At a temperature $T_D \sim 1\,\text{MeV}$, the neutrinos decoupled from the primordial plasma, because their interaction rate $\Gamma^{\nu}_{\text{int}} \sim G_F^2 T^5$ (describing processes like $n \to p\, e\, \overline{\nu}_e$, $\nu_e\, n \to p\, e$ and $e^+\, n \to p\, \overline{\nu}_e$) became smaller than the expansion rate of the Universe $H \sim \sqrt{g^*} T^2 / M_{\text{Pl}}$.

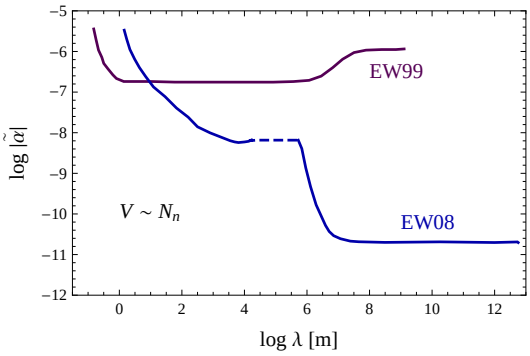

Figure 3.3: Bounds on a neutron-dependent long-range force (from Fig. 5 of Ref. [52], based on Refs. [53, 54], see references therein for details on the experiments). The region above the curves is excluded at 95% C.L. The definition of the parameters is given in Eq. (3.34).

Shortly thereafter, the neutron-proton ratio froze out, slowly decreasing through neutron decay; this process stopped with the formation of nuclei, most importantly ^{4}He (since it has the highest binding energy). In the approximation that all neutrons went into ^{4}He, the abundance parameter Y (mass ratio of ^{4}He) equates to

$$Y = \frac{\frac{n_n}{2} \times (2m_n + 2m_p)}{n_n m_n + n_p m_p} \approx \frac{2n_n/n_p}{1 + n_n/n_p} \,. \tag{3.36}$$

The ratio n_n/n_p depends on the freeze-out temperature, which in turn is a function of g^*, the number of relativistic degrees of freedom at freeze-out ($T_{\text{freeze}} \sim (g^*)^{1/6}$MeV). Consequently, the measured value of Y can constrain g^*. The Standard Model predicts $g^*(T_D) = 10.75$; deviations Δg^* from that value are often expressed via the number of additional neutrinos ΔN_ν that these d.o.f. correspond to ($\Delta g^* = (7/4) \times \Delta N_\nu$).

Current measurements [56] give $Y = 0.2565 \pm 0.0010\,(\text{stat.}) \pm 0.0050\,(\text{syst.})$. The resulting effective number of neutrino species depends on the baryon-photon ratio and the neutron lifetime, which apparently has huge systematic problems. The values with 2σ errors are shown below for a neutron lifetime $\tau_n = 885.4 \pm 0.9\,$s, and $\tau_n = 878.5 \pm 0.8\,$s, respectively [56]:

$$\Delta N_\nu = 0.68^{+0.80}_{-0.70} \,, \qquad\qquad \Delta N_\nu = 0.80^{+0.80}_{-0.70} \,. \tag{3.37}$$

How does the Z' affect the above discussion? The processes that lead to an equilibrium between the Z' and the neutrinos are shown in Fig. 3.4 and result in an interaction rate $\Gamma \sim g'^4 T$. So, for high temperatures, these processes are slow compared to the expansion rate of the Universe, i.e. the behaviour is opposite to that of the weak interactions. If the Z' bosons were in equilibrium at the temperature T_D, they would contribute $\Delta N_\nu = 3 \times (4/7) \approx 1.7$ to Y (treating the Z' as massive). Since this value is more than two standard deviations away from the best-fit values, we require the Z' equilibrium to set in at lower temperatures, i.e. $T_{Z'} < 1\,$MeV. This translates into the constraint [24]

$$\frac{g'^2}{4\pi} < 1.7 \times 10^{-11} \,, \tag{3.38}$$

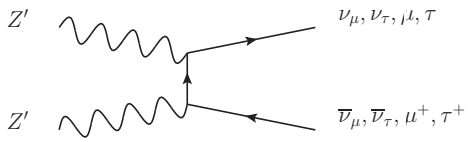

Figure 3.4: Equilibrium processes involving the Z'.

or, in a more useful form, $g' < 1.5 \times 10^{-5}$.

However, there are processes at higher temperatures that are still sensitive to such small values; let us assume a coupling between $10^{-18} < g'^2/4\pi < 10^{-11}$ (derivation of the lower bound below). The upper bound states that the process $\nu\nu \to Z'Z'$ is much slower than the Hubble expansion, so equilibrium sets in some time after the neutrinos decouple, hence the process is irrelevant. At temperatures $T \sim m_\mu$[4] however, the process $\gamma\mu \to Z'\mu$ has an interaction rate $\Gamma \sim e^2 g'^2 T^3/m_\mu^2$ and induces equilibrium of muons, photons and Z'. After the muon annihilation below $T \sim m_\mu$, the Z' freeze out and contribute to the expansion rate via g^*, but in an entropy suppressed way (entropy density $s \sim g^* T^3$, energy density $\sim g^* T^4$):

$$\Delta N_\nu = 3 \times \frac{4}{7} \times \left(\frac{g^*(1\,\mathrm{MeV})}{g^*(m_\mu)} \right)^{4/3} \approx 0.9\,. \tag{3.39}$$

This value is well within the currently allowed range, so there is for now no reason to exclude this range $10^{-18} < g'^2/4\pi < 10^{-11}$. If we were to do so (should the experimental accuracy improve), we should demand that the Z' bosons are not in equilibrium at $T \sim m_\mu$, yielding the constraint [26]

$$\frac{g'^2}{4\pi} < 4 \times 10^{-18}\,, \tag{3.40}$$

or $g' < 7.1 \times 10^{-9}$.

Nothing interesting happens at $T \sim m_\tau$, because the g'^2 limit scales as $\sqrt{g^*(m_\tau)}\, m_\tau$ and is therefore weaker than 3.40. Stated in a different way, there is no possibility for the Z' boson to be in equilibrium at m_τ and not at m_μ.

The results are summarised in Tab. 3.2, we will take Eq. (3.38) as a bound on g'. A similar limit can be obtained from the additional Z' luminosity in the supernova 1987a [25].

$g'^2/4\pi$	$0 \ldots 4 \times 10^{-18}$	$4 \times 10^{-18} \ldots 1.7 \times 10^{-11}$	$1.7 \times 10^{-11} \ldots 1$
ΔN_ν	0	0.9	1.7

Table 3.2: Number of additional neutrinos at BBN, induced by the ultralight Z' boson for different values of the coupling constant g'.

[4] While we actually do not have direct information about the processes at these temperatures, we can extrapolate using the degrees of freedom of the SM plus Z'.

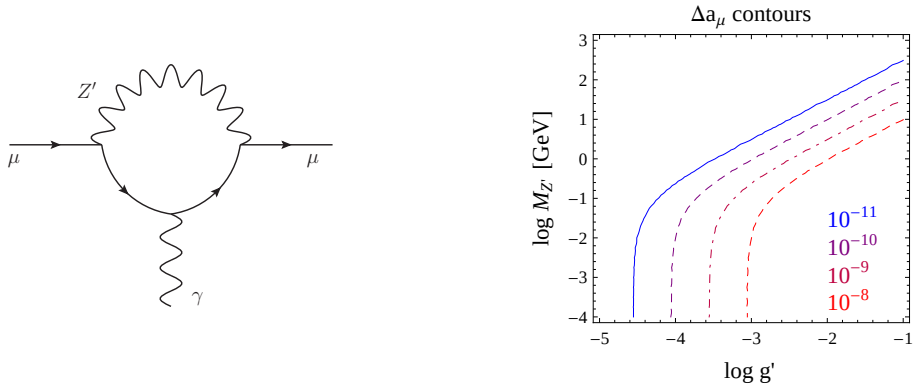

Figure 3.5: Contribution of the Z' boson to the magnetic moment of the muon (left); corresponding contours of Δa_μ in the $M_{Z'}$–g' plane (right). The allowed parameter space is left of the $\Delta a_\mu \sim 10^{-9}$ contour.

3.4.3 Anomalous Magnetic Moment of the Muon

Since the Z' boson couples to the muon, it contributes to the muon's anomalous magnetic moment, $a_\mu = (g_\mu - 2)/2$, via loop-diagrams like Fig. 3.5 (left). This corresponds quantitatively to [38]

$$\begin{aligned} \Delta a_\mu &= \frac{g'^2}{4\pi}\frac{1}{2\pi}\int_0^1 \mathrm{d}x\ \frac{2m_\mu^2 x^2(1-x)}{m_\mu^2 x^2 + M_{Z'}^2(1-x)} \\ &= \frac{g'^2}{4\pi}\frac{1}{2\pi}\begin{cases} 1 & \text{for } M_{Z'} \ll m_\mu\,, \\ 2m_\mu^2/3M_{Z'}^2 & \text{for } M_{Z'} \gg m_\mu\,, \end{cases} \end{aligned} \tag{3.41}$$

the mass range around m_μ is shown in Fig. 3.5 (right). For the ultralight Z', this translates into a constraint on the coupling g'. The current experimental value of a_μ differs by 3.2σ from the Standard Model prediction, although there is some uncertainty in the hadronic contributions [57, 22]. We can use g' to explain this difference by setting $\Delta a_\mu = a_\mu^{\mathrm{exp}} - a_\mu^{\mathrm{SM}} \lesssim 255 \times 10^{-11}$ ($\Rightarrow g' \lesssim 4.49 \times 10^{-4}$). As we have seen in Sec. 3.4.2, BBN requires a significantly smaller g', so the Z' will essentially not contribute to the magnetic moment of the muon.

3.4.4 Effect on Electromagnetic Interactions

The Z–Z' mixing also changes the electromagnetic behaviour, as can be seen from the Lagrangian in Eq. (3.4), slightly rewritten and shown only for muons, electrons and

protons:

$$\begin{aligned}\mathcal{L}_{Z_2} = &-\left\{\left[g' + ec_W\chi - (\xi - s_W\chi)\frac{e}{s_W c_W}\cdot\left(s_W^2 - \frac{1}{4}\right)\right]\overline{\mu}\gamma_\beta\mu\right.\\ &+\left[ec_W\chi - (\xi - s_W\chi)\frac{e}{s_W c_W}\cdot\left(s_W^2 - \frac{1}{4}\right)\right]\overline{e}\gamma_\beta e\\ &-\left[ec_W\chi - (\xi - s_W\chi)\frac{e}{s_W c_W}\cdot\left(s_W^2 - \frac{1}{4}\right)\right]\overline{p}\gamma_\beta p\\ &\left.+\,(\xi - s_W\chi)\frac{e}{s_W c_W}\left[-\frac{1}{4}\overline{e}\gamma_\beta\gamma_5 e - \frac{1}{4}\overline{\mu}\gamma_\beta\gamma_5\mu + \frac{1}{4}\overline{p}\gamma_\beta\gamma_5 p\right]\right\} Z_2^\beta + \dots .\end{aligned} \tag{3.42}$$

Ignoring, for simplicity, any spin dependence (i.e. the axial currents), and interference with the photon, we obtain in the non-relativistic limit[5] an electron-proton potential (in direct analogy to the derivation in Sec. 3.2)

$$V_{\mathrm{H}}(r) = -\frac{e^2}{4\pi r} - \frac{e^2}{4\pi r}\tilde{Q}_P^2 \times e^{-rM_2}\,. \tag{3.43}$$

We introduced the "charge" $\tilde{Q}_P \equiv -(\xi - s_W\,\chi)(1/4 - s_W^2)/(s_W\,c_W) - c_W\chi$ for convenience. On atomic scales, the factor e^{-rM_2} can be omitted, resulting in an effective change of the fine-structure constant, albeit only in second order of the mixing angles. Since the equivalence principle sets already very strong bounds on the mixing angles, we can safely ignore the $\tilde{Q}_P^2$ terms, i.e. the fine-structure constant yields inferior constraints.

A bound state of μ^+ and e^- (muonium) on the other hand has the potential

$$V_{\mathrm{muonium}}(r) = -\frac{e^2}{4\pi}\left(1 + \left[\tilde{Q}_P^2 - \frac{g'}{e}\,\tilde{Q}_P\right]\times e^{-rM_2}\right)\frac{1}{r} \approx -\frac{e^2}{4\pi}\left(1 - \frac{g'}{e}\,\tilde{Q}_P\right)\frac{1}{r}\,, \tag{3.44}$$

which means muonium should have a different fine-structure constant than non-muonic atoms, i.e. muons would seem to have a different electric charge than electrons and protons. We interpret the ratio of the potentials as the ratio of the muon/proton charge:[6]

$$\frac{e_{\mu^+}}{e_{e^+,p}} = \frac{V_{\mathrm{muonium}}}{V_{\mathrm{H}}} = \frac{\frac{e^2}{4\pi}\left(1 + \tilde{Q}_P^2 - \frac{g'}{e}\tilde{Q}_P\right)}{\frac{e^2}{4\pi}\left(1 + \tilde{Q}_P^2\right)} \approx 1 - \frac{g'}{e}\tilde{Q}_P\,, \tag{3.45}$$

which has been measured via the muonium hyperfine-structure [58] to be 1 with an accuracy of 10^{-9}, corresponding to a limit

$$g'\left(\chi + \frac{(1 - 4s_W^2)}{3s_W}\xi\right) < 3.5\times 10^{-10}\,. \tag{3.46}$$

[5] In the non-relativistic limit, the vector current $\overline{\psi}\gamma^\mu\psi$ has a vanishing spatial part, while the axial current $\overline{\psi}\gamma^\mu\gamma_5\psi$ has a vanishing time-like part (the $\mu = 0$ component). Therefore, the coupling $j_V j_A$ vanishes, while $j_A j_A$ does not. It describes a spin-dependent potential which goes with $\tilde{Q}_P^2$ and is thus highly suppressed.

[6] Since the equality of proton charge $|e_p|$ and electron charge $|e_e|$ is measured to a high accuracy ($\sim 10^{-21}$ [22]), from experiments on the neutrality of matter, we do not distinguish between them.

The contribution of ξ is reduced by $(1-4s_W^2)/3s_W \approx 0.05$ compared to χ. It is obvious from this limit that we need the mixing angles to be non-zero to influence electromagnetic interactions. Only the proposed "true muonium" (a bound state of μ^- and μ^+) [59] could give constraints depending only on g'.

We mention that there are experiments probing modified electromagnetic potentials of the form

$$V(r) = -\frac{e^2}{4\pi r}\left(1+\beta e^{-r/\lambda}\right) \tag{3.47}$$

over a wide range of λ (Ref. [60, 61]), but with very weak constraints for the ultralight Z' discussed here ($\lambda = 1/M_2$).[7]

3.4.5 Connection to Paraphotons

For convenience, we repeat the relevant part about paraphotons from Sec. 1.4.2:

The usual framework for paraphotons consists of the electromagnetic gauge group $U(1)_{\mathrm{EM}}$ and one additional $U(1)'$:

$$\mathcal{L} \supset -\frac{1}{4}F_1^{\mu\nu}F_{1\mu\nu} - \frac{1}{4}F_2^{\mu\nu}F_{2\mu\nu} + \frac{1}{2}m^2 A_2^\mu A_{2\mu} + j_{\mathrm{EM}}^\mu\left(eA_{1\mu} + e_2 A_{2\mu}\right) \tag{3.48}$$

or some variation of this. The coupling of the paraphoton A_2 to the electromagnetic current can also be generated by kinetic mixing $e_2 \sim e\chi$. The crucial point is the creation of the two mass eigenstates A_1 and A_2 by a charged source, which leads to photon-paraphoton oscillations in direct analogy to neutrino oscillations. Since the linear combination $eA_2 - e_2 A_1$ does not couple to j_{EM}, the oscillation can lead to so-called "light shining through a wall" (LSW) effects [21], i.e. photons oscillate into the sterile component, pass through an opaque barrier and oscillate back.

Our ansatz however was a mixing with the hypercharge, not the electric charge. This generates a coupling to the neutral current, so even though there will also be a "sterile" linear combination of γ and Z_2 (the Z_1 decouples at a short distance due to its high mass), it will not be sterile with respect to the weak current. This should either forbid "light shining through a wall" or at least modify it significantly. While this may be interesting in its own right, we will not go into details and simply omit constraints from these kinds of experiments, as even their strongest limits are weaker than those from the equivalence principle.

3.4.6 Atmospheric Neutrino Oscillations

The strongest limit on our potential $V(\alpha)$ stems from Atmospheric Neutrino Oscillations (AνO). The aforementioned $L_e - L_{\mu,\tau}$ model [27] (based on the potential generated by electrons inside the Sun) uses the two-neutrino framework to fit their coupling strength $\alpha_{e\,\mu,\tau} = g^2_{e\,\mu,\tau}/4\pi$ to Super-K data (from only 3 years of operation). In the

[7] For a boson of Earth-radius range ($M'_Z \sim 10^{-14}\,\mathrm{eV}$), there exists the limit $\beta < 10^{-2}$ from the magnetic field of the Earth [61], corresponding to $(3s_W\chi + (1-4s_W^2)\xi) < 0.2$.

notation

$$i\frac{\mathrm{d}}{\mathrm{d}t}\begin{pmatrix}\nu_\mu\\ \nu_\tau\end{pmatrix} = \begin{pmatrix}-\frac{\Delta m^2_{23}}{4E_\nu}\cos 2\theta_{23} & \frac{\Delta m^2_{23}}{4E_\nu}\sin 2\theta_{23}\\ \frac{\Delta m^2_{23}}{4E_\nu}\sin 2\theta_{23} & \frac{\Delta m^2_{23}}{4E_\nu}\cos 2\theta_{23} - V_{e\tau}\end{pmatrix}\begin{pmatrix}\nu_\mu\\ \nu_\tau\end{pmatrix}, \tag{3.49}$$

with $V_{e\tau} = 3.3\times10^{-11}\,\mathrm{eV}\left(\frac{\alpha_{e\tau}}{3.3\times10^{-50}}\right)$, they obtain an upper bound of $\alpha_{e\tau} < 6.4\times10^{-52}$ at 90% C.L. for a force of Earth-Sun distance. This is equivalent to:

$$V_{e\tau} < 6.4\times10^{-13}\,\mathrm{eV}\,. \tag{3.50}$$

In the two-neutrino framework, we can write

$$i\frac{\mathrm{d}}{\mathrm{d}t}\begin{pmatrix}\nu_\mu\\ \nu_\tau\end{pmatrix} = \begin{pmatrix}-\frac{\Delta m^2_{23}}{4E_\nu}\cos 2\theta_{23} + \frac{V_{e\tau}}{2} & \frac{\Delta m^2_{23}}{4E_\nu}\sin 2\theta_{23}\\ \frac{\Delta m^2_{23}}{4E_\nu}\sin 2\theta_{23} & \frac{\Delta m^2_{23}}{4E_\nu}\cos 2\theta_{23} - \frac{V_{e\tau}}{2}\end{pmatrix}\begin{pmatrix}\nu_\mu\\ \nu_\tau\end{pmatrix} - \frac{V_{e\tau}}{2}\begin{pmatrix}\nu_\mu\\ \nu_\tau\end{pmatrix},$$

where the last term does not contribute to the oscillation, and hence can be dropped. We therefore have the correspondence to our $L_\mu - L_\tau$ model via $V \mathrel{\widehat{=}} \frac{V_{e\tau}}{2}$, leading to the bound $V < 3.2\times10^{-13}\,\mathrm{eV}$, or, expressed as a bound on α:

$$\alpha = g'(\xi - s_W\chi) < 8.9\times10^{-50}\,. \tag{3.51}$$

The improved bounds [28] on $\alpha_{e\,\mu,\tau}$ from an analysis with solar neutrino and KamLAND data can not be translated that freely, since the above argument fails in the three-neutrino framework and would require a full three-flavour fit to all data, which is outside the realm of this work.

We will however improve the bound (3.51) in Sec. 3.7, where we perform an analogous analysis on a more recent dataset.

3.4.7 Non-Standard Neutrino Interactions

Comparing the form of our potential $V(\alpha)$ in flavour basis to the NSI matter potential Eq. (1.12), we find a correspondence

$$\varepsilon_{\mu\mu} = -\varepsilon_{\tau\tau} \mathrel{\widehat{=}} \frac{V(\alpha)}{\sqrt{2}G_F n_e(\boldsymbol{x})}\,, \tag{3.52}$$

all other NSI parameters being zero. Can we relate the constraints on $\varepsilon_{\mu\mu}$ to α? Unfortunately, we have to take the position dependence of the electron density $n_e(\boldsymbol{x})$ into account. For long-baseline experiments (discussed below), neutrinos travel through the crust of the Earth with a basically constant n_e, which would make it possible to use Eq. (3.52) directly. But since the limits on the NSI parameters we are concerned with stem predominantly from atmospheric neutrinos, which travel through all the different layers of the Earth, we cannot use Eq. (3.52). Moreover, since the NSI potential and $V(\alpha)$ (even if we take its true position dependence into account) have a different position dependence, it might not be possible to extract a limit on α from NSI at all.

We postpone the discussion of the NSI limits until Sec. 3.7, where we examine the

$(\xi - s_W\chi) < 5 \times 10^{-24}$	EP (95% C.L.)
$g' < 1.5 \times 10^{-5}$	BBN (equilibrium below T_D)
$g' \lesssim 4.5 \times 10^{-4}$	Muon magnetic moment
$g'\left(3s_W\chi + (1 - 4s_W^2)\xi\right) \lesssim 5.1 \times 10^{-10}$	Muon fine structure
$\alpha = g'(\xi - s_W\chi) < 8.9 \times 10^{-50}$	AνO (90% C.L.)
$\xi \leq 0.036$	Z boson mass (3σ)
$g'\xi < 1.1 \times 10^{-3}$	Z–τ coupling (3σ)

Table 3.3: Current constraints on a $U(1)_{L_\mu - L_\tau}$ gauge boson of Earth-Sun-distance range.

position dependence of $V(\alpha)$ and perform a χ^2-fit to atmospheric neutrino data.

3.4.8 Electroweak Precision Data

The Z–Z' mixing is in principle constrained through precision data from LEP and other collider experiments, but far less than through EP, BBN and AνO. For example, the mass mixing with Z changes the so-called ρ parameter, $\rho \equiv M_W^2/M_Z^2 c_W^2$, from its SM value 1. However, since its precision is of order 10^{-3} [22], it cannot compete with the EP bounds. Similar conclusions hold for the modified coupling of Z to fermions. For completeness, we list the dominant constraints from electroweak precision data in Tab. 3.3.

All constraints are summarised in Tab. 3.3, most of which derived under the assumption $\xi \ll 1$, $\chi \ll 1$, $\delta M^2 \ll M_Z^2$ and $M_{Z'}^2 \ll M_Z^2$. The, by far, most dominant bound is given by the atmospheric neutrino oscillations in addition to the equivalence principle. For $\chi \equiv 0$, the bounds simplify to $g' < 7.1 \times 10^{-9}$ (BBN), $g'\xi < 8.9 \times 10^{-50}$ (AνO) and $\xi < 5 \times 10^{-24}$ (EP), the allowed parameter space is shown in Fig. 3.6.

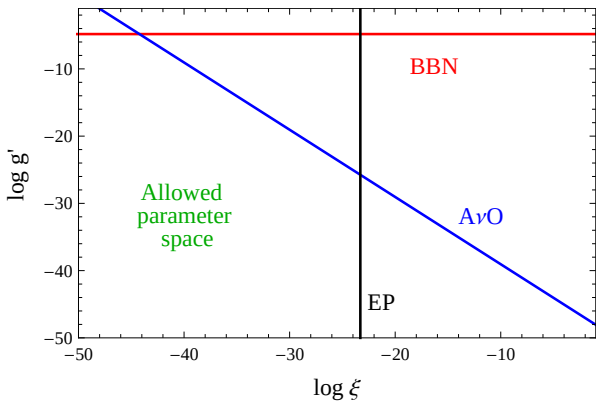

Figure 3.6: Constraints on g' and ξ for the case $\chi \equiv 0$. BBN limit from decoupling at $T = m_\mu$.

3.5 Simulation with GLoBES

GLoBES [62, 63] ("General Long-Baseline Experiment Simulator") is, as the name suggests, a software package (C library) to simulate long-baseline experiments, i.e. simulate the oscillation of neutrinos in different settings. It uses the Abstract Experiment Definition Language (AEDL) to specify the details of a concrete experiment, such as

- length of baseline and matter profile (Earth matter density profile from Refs. [64, 65]),
- running time of the experiment and detector mass,
- energy of the neutrinos, resolution functions, smearing algorithms, cuts and bin definition,
- cross sections and neutrino fluxes,
- efficiencies, background and oscillation channel definition.

Since GLoBES is designed to simulate neutrino point sources, we differentiate between four kinds of experiments at our disposal:

- Superbeam experiments
  Low-energy, high-intensity muon neutrino beam created in accelerator facilities such as CERN or FermiLab. Measurement of ν_e-appearance signals and/or ν_μ disappearance.
- Neutrino factory (Nufact)
  Neutrino beam created through muon decay in storage rings. The beam consists of ν_μ and $\overline{\nu}_e$ (in the ν-run), so a magnetised detector is necessary to distinguish the μ^- from $\nu_\mu \rightsquigarrow \mu^-$ and the μ^+ from the oscillated $\overline{\nu}_e \to \overline{\nu}_\mu \rightsquigarrow \mu^+$ (both through charged-current interactions in the detector).
- Reactor experiments
  Detecting neutrinos from radioactive decay in a nuclear power reactor. Looking for disappearance of the created electron neutrinos.
- Beta beams
  Electron neutrinos are created in an accelerator through the decay of different isotopes (e.g. ^{18}Ne for ν_e and ^{6}He for $\overline{\nu}_e$). The specification of the experiment strongly depend on the relativistic acceleration factor γ of these isotopes.

With the creation and detection of the neutrinos defined in the AEDL file, GLoBES calculates the neutrino evolution using the full three-neutrino framework, i.e. it calculates the S-matrix for given oscillation parameters θ_{12}, θ_{13}, θ_{23}, Δm^2_{21}, Δm^2_{31} and δ_{CP}, including the specified matter effects. From this, we get rates and $\Delta\chi^2$-values, allowing us to analyse the sensitivity of an experiment to one parameter, or combination of parameters (we can also perform a simultaneous analysis of different experiments). One of the main features of GLoBES is the projection of $\Delta\chi^2$ to any parameter subspace by local minimisation.

Experiment	Baseline	Running time [yrs]	Beam energy [GeV]	Detector mass
T2K	295 km	5 ν (+5 $\overline{\nu}$)	$0.2 - 2$	22.5 kt
T2HK	295 km	4 ν + 4 $\overline{\nu}$	$0.4 - 1.2$	500 kt
SPL	130 km	2 ν + 8 $\overline{\nu}$	$0.01 - 1.01$	500 kt
NOνA	812 km	3 ν + 3 $\overline{\nu}$	$0.5 - 3.5$	15 kt
Nufact	3000 km	4 ν + 4 $\overline{\nu}$	$4 - 50$	50 kt

Table 3.4: Future long-baseline experiments (T2K already started taking data).

We refer to App. B for an introduction to the necessary statistical tools (χ^2 analysis in real and simulated experiments). Since all the data is simulated, we need to specify some *true parameter values*, against which we can minimise. The values used by us (and their errors) are given in Tab. 1.2, the average matter density will be kept fixed. The experiments are summarised in Tab. 3.4, and further described below; the obtained sensitivities of the experiments to the non-standard parameter α are tabulated at the end of this chapter, in Tab. 3.5.

3.5.1 The Setting

We simulate the effect of α on the neutrino oscillations at different types of long-baseline experiments. Since α mainly affects the ν_μ and ν_τ oscillations, we expect a correlation with the atmospheric observables θ_{23} and Δm^2_{31}. We will therefore concentrate on superbeam and neutrino factory experiments.

We use the pre-defined AEDL files provided by GLoBES [62, 63] (in version 3.0) and calculate the S-matrix following from our neutrino evolution equation (3.18) numerically as described in Ref. [63]. The values for the parameters are given in Tab. 1.2 and stem from the February 2010 update of Ref. [1] (including ν_e-appearance data from MINOS). The errors on θ_{12} and θ_{23} correspond to 1σ errors, translated via

$$\delta\theta \approx \frac{\mathrm{d}\theta}{\mathrm{d}\sin^2\theta}\delta(\sin^2\theta) = \frac{1}{2\sin\theta\cos\theta}\delta(\sin^2\theta)\,. \tag{3.53}$$

Although the analysis in Ref. [1] favours a non-zero θ_{13} (best-fit value and 1σ errors: $\sin^2\theta_{13} = 0.013^{+0.013}_{-0.009}$), we will take $\theta_{13} = 0$ as the *true value* with the 2σ error $\sin^2\theta_{13} \leq 0.039$ as the error in our computation. For simplicity, we choose symmetric error bars, i.e. we approximate the experimental error via e.g. $\sin^2\theta_{23} = 0.50^{+0.07}_{-0.06} \to 0.50 \pm 0.07$.

For the most part, we will examine the normal hierarchy (NH) case, inverted hierarchy (IH) will be briefly discussed in Sec. 3.5.7. In the following subsections, we show some projections on χ^2 hyperplanes where all other oscillation parameters are minimised over (matter density kept fixed). The projections show the $\Delta\chi^2 = 2.3$, 6.18 and 11.83 confidence levels[8] (corresponding to 1, 2 and 3σ or 68.27%, 95.45% and 99.73% C.L.), following the commonly used condition for 2 parameters [22] (see App. B). The best-fit value in all cases corresponds to $\alpha = 0$ (our *true parameter value*). The graph χ^2 vs. α also shows the 1, 2 and 3σ ranges for 1 parameter ($\Delta\chi^2 = 1.0$, 4.0 and 9.0).

[8] Since our *true parameter values* are defined at $\chi^2 = 0$, we have $\Delta\chi^2 \equiv \chi^2$ in the following.

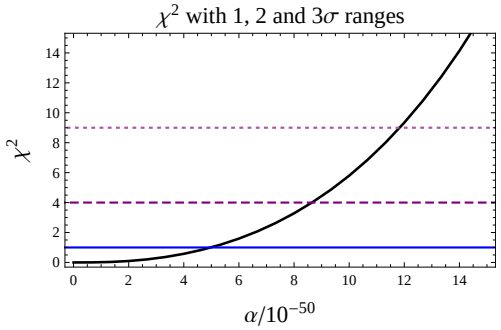

Figure 3.7: α dependence of χ^2 for the 5 year ν-run at T2K.

3.5.2 T2K

The T2K (Tokai to Kamioka) experiment [66, 67] uses the water Čerenkov detector of the Super-Kamiokande experiment in Kamioka, Japan, to measure a muon neutrino beam produced, using a high intensity proton accelerator, at J-PARC in Tokai village, Japan. Two of the main goals are to measure the ν_e-appearance signal and in turn θ_{13}, as well as precision measurements of the oscillation parameters Δm^2_{31} (to 10%) and θ_{23} (to 1%) via ν_μ disappearance.

The ν_e appearance is described by (see perturbative expression in App. D)

$$P_{\mu e}(\alpha = 0 = A) \approx \sin^2(2\theta_{13}) s^2_{23} \sin^2\left(\frac{\Delta m^2_{31} L}{4E}\right) + c^2_{23} \sin^2(2\theta_{12}) \left(\frac{\Delta m^2_{21} L}{4E}\right)^2 + 4 c_{12} s_{12} c^2_{13} s_{13} c_{23} s_{23} \left(\frac{\Delta m^2_{21} L}{4E}\right) \left[\cos\delta \sin\left(\frac{\Delta m^2_{31} L}{2E}\right) - 2 \sin\delta \sin^2\left(\frac{\Delta m^2_{31} L}{4E}\right)\right], \tag{3.54}$$

so the probability is proportional to $\sin^2 2\theta_{13}$, for not too small θ_{13} (for θ_{13} below $\sim 10^{-2}$ the third term will be important too).

The neutrino beam is generated at J-PARC by the collision of protons with a target, subsequently producing pions which decay dominantly (99.988%) via $\pi^+ \to \mu^+ \nu_\mu$, thus creating an almost pure ν_μ beam with a peak energy $0.5 - 0.7\,\text{GeV}$. The (2.5 degree off-axis[9]) detection at Super-Kamiokande (22.5 kt fiducial mass) measures the Čerenkov light cone produced by muons (electrons) after quasi-elastic (charged-current) neutrino-nucleon scattering of the ν_μ (ν_e) with the water in the detector. The sharpness of the light cone is used to distinguish between electrons and muons.

The simulation uses the two AEDL files `0709-t2k.glb` and `0709-t2k-anti.glb` (not distributed with GLoBES, but available on their website) to describe the 5 year ν-run and the 5 year $\overline{\nu}$-run, respectively, using the sources[10] [68, 69, 70, 71, 72].

For the 5 year ν-run we obtain the α dependence of χ^2 in Fig. 3.7, from which we

[9] A detector slightly off-axis to the beam is desirable, because it allows for an almost monochromatic neutrino flux. The neutrino energy is approximately connected to the pion energy via $E_\nu \sim E_\pi/(1 + \theta^2 E^2_\pi/m^2_\pi)$, so any angle $\theta \neq 0$ will drive the dependence $\mathrm{d}E_\nu/\mathrm{d}E_\pi$ to zero for large E_π.

[10] Since there is no accurate, public information on the Super-Kamiokande performance with a $\overline{\nu}$ beam, the simulated $\overline{\nu}$-run should be viewed as an approximation based on extrapolated data.

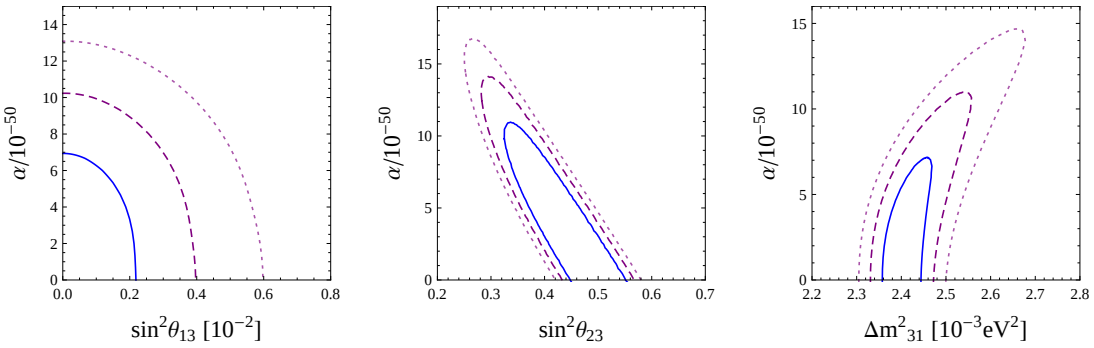

Figure 3.8: Correlation between α and θ_{13} (left), α and θ_{23} (middle) and α and Δm^2_{31} (right), for the 5 year ν-run at T2K. Shown are the 1, 2 and 3σ contours corresponding to $\Delta\chi^2 = 2.3$, 6.18 and 11.83.

read off a sensitivity of $\alpha < 11.8 \times 10^{-50}$ at 99.73%. The nontrivial correlations with other oscillation parameters are shown in Fig 3.8 (the contours denote $\Delta\chi^2 = 2.3$, 6.18 and 11.83).

As expected, we find a correlation with the parameters θ_{23}, Δm^2_{31} and θ_{13}. Including a 5 year $\overline{\nu}$-run we increase the sensitivity significantly (Fig. 3.9), but wash out the strong correlations; the reason being the different behaviour of ν_μ and $\overline{\nu}_\mu$ under the potential $V(\alpha)$. We obtain a sensitivity of $\alpha < 4.3 \times 10^{-50}$ at 99.73% C.L.

3.5.3 T2HK

The T2HK superbeam experiment is an upgrade of the T2K experiment (Phase II, improved beam power and larger detector (Hyper-Kamiokande)), the differences are given in Tab. 3.4. From now on we will only show the results of a combined $\nu+\overline{\nu}$ analysis. The GLoBES simulation uses the AEDL file `T2HK.glb` (distributed with GLoBES) to describe the experiment [73, 66, 74] with a running time of 4 years ν and 4 years $\overline{\nu}$.

We obtain a sensitivity of $\alpha < 1.7 \times 10^{-50}$ at 99.73% C.L., an improvement by a factor of 2.5 over the T2K sensitivity. The correlations with the other parameters look qualitatively like those of T2K.

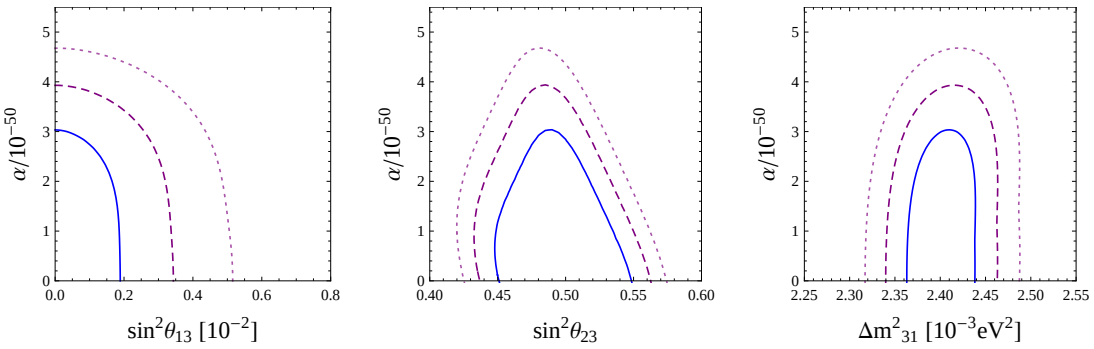

Figure 3.9: Correlations for the full T2K running time (5 year ν plus 5 years $\overline{\nu}$).

3.5.4 NOνA

The NOνA [75] (NuMI Off-axis ν_e Appearance) experiment (begin data taking $\sim$ 2013), uses a 15 kt liquid scintillator near Ash River, Minnesota to detect an off-axis muon neutrino beam created at Fermilab (810 km baseline). The ν_μ beam is created through collisions of protons with a graphite target, resulting in pions and kaons which subsequently decay into muons and neutrinos. To improve the knowledge about the beam, there will also be a small near detector, about 1 km from the target. Part of the NOνA project is an upgrade of the existing NuMI (Neutrino at Main Inject) beam to 700 kW. The main goals of NOνA are a measurement of ν_e appearance and therefore θ_{13}, precision measurements in the $\nu_\mu \to \nu_\mu$ channel to determine θ_{23}, and a determination of the sign of Δm^2_{31}, i.e. the mass hierarchy.

The GLoBES simulation uses the AEDL file `0709-NOvA.glb` (not distributed with GLoBES, but available on their website) to describe the experiment [76, 77] with a running time of 3 years ν and 3 years $\overline{\nu}$.

We obtain an overall sensitivity of $\alpha < 1.9 \times 10^{-50}$ at 99.73% C.L. Since the correlations with the other parameters look very similar to T2K (of course with rescaled axes), we omit from showing them here. Since both T2K and NOνA are designed to probe the atmospheric neutrino parameters and hence have a similar L/E value, one would expect a similar sensitivity to α (similar detector mass and running time). However, as mentioned in Sec. 3.3.1, the effect of α is dominantly of the form $\eta \sim VE/\Delta m^2$, so the doubled neutrino energy of NOνA compared to T2K means an enhancement of α by roughly a factor of 2. This can also be understood by means of the longer baseline, see Eq. 3.28.

3.5.5 SPL

The SPL [70] (Super Proton Linac) experiment is proposed to use a 500 kt water Čerenkov detector in the Fréjus tunnel, 130 km away from CERN, to study a neutrino beam created by decays of pions, muons and kaons, produced after hitting a Hg target with protons accelerated in a linear collider. The beam is almost pure ν_μ, the contamination with ν_e is $\sim 0.7\%$ ($\sim 6\%$ in the $\overline{\nu}$ run) [70]. SPL will measure θ_{13} through the $\nu_\mu \to \nu_e$ appearance channel. The GLoBES simulation uses the AEDL file `SPL.glb` (distributed with GLoBES) to describe the experiment [78, 79] with a running time of 2 years ν and 8 years $\overline{\nu}$.

We obtain a sensitivity (Fig. 3.10) of $\alpha < 7.5 \times 10^{-50}$ at 99.73% C.L.

3.5.6 Neutrino Factory

In a neutrino factory [80] (Nufact), muons are accelerated to energies $\mathcal{O}(10)$ GeV and injected into a storage ring with long straight sections, where the muons decay via $\mu^- \to e^- \overline{\nu}_e \nu_\mu$ (ν-run) or $\mu^+ \to e^+ \nu_e \overline{\nu}_\mu$ ($\overline{\nu}$-run). The well-known beam ($\nu_\mu, \overline{\nu}_e$ or $\overline{\nu}_\mu, \nu_e$ depending on beam polarity) allows for very precise measurements of e.g. $\nu_e \to \nu_\mu$ (golden channel) and/or $\nu_e \to \nu_\tau$ (silver channel).[11]

[11] The silver channel is possible because the neutrinos in a Nufact can have energies above the threshold of 3.5 GeV for the production of tauons in charged-current interactions [72].

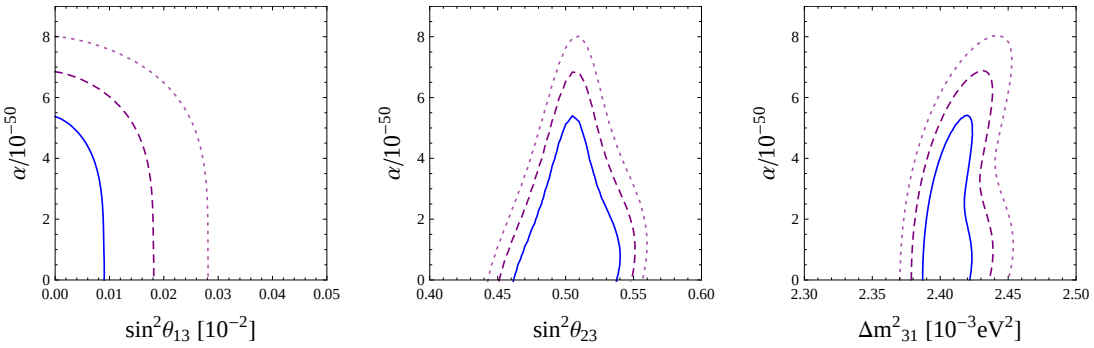

Figure 3.10: Correlations for the full running time at SPL (2 year ν plus 8 years $\overline{\nu}$).

We use the parameters listed in Tab. 3.4 with the AEDL file `NFstandard.glb` (distributed with GLoBES) to describe the experiment [73]. In particular, we do not use the silver channel here, only ${}^{(}\overline{\nu}_{\mu}$ appearance and disappearance (using a 50 kt magnetised iron neutrino detector).

For a standard neutrino factory we obtain a sensitivity (Fig. 3.11) of

$$\alpha < 5.3 \times 10^{-51} \tag{3.55}$$

at 99.73% C.L., due to the high energy of the neutrinos (and the very long baseline). We also have a small correlation with δ_{CP} (albeit practically insignificant).

Neutrino Factory with Silver Channel We will now consider an improved Nufact with an additional 5 kt emulsion cloud chamber for the detection of tauons. The rest of the setup will be similar to the standard neutrino factory discussed above (baseline, energy), except for the treatment of the disappearance channels. In the standard Nufact, the charge identification is used to reduce the background from the appearance neutrinos, whereas here the appearance and disappearance rates are treated as indistinguishable for the disappearance channel, meaning we throw away the information whether the measured charged lepton was a muon or an antimuon. This can actually improve the analysis, since it allows the use of low-energy events with higher efficiency [81]; the efficiencies and thresholds used are similar to MINOS [49]. Therefore we cannot compare

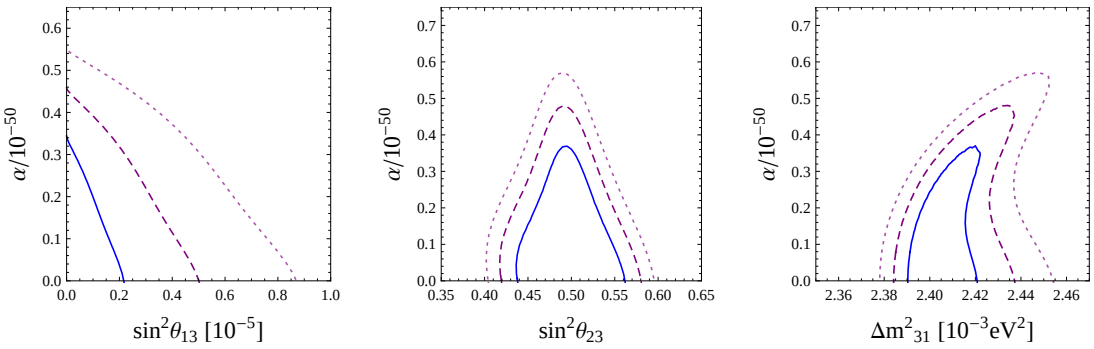

Figure 3.11: Correlations for a Nufact with a running time of 4 year ν and 4 year $\overline{\nu}$.

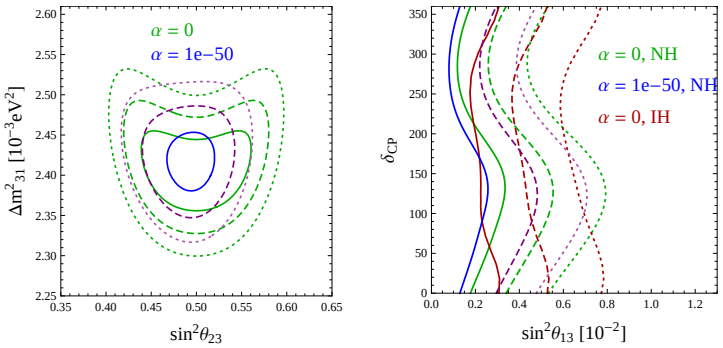

Figure 3.12: Effect of a non-zero α on the Δm^2_{31}–θ_{23} and θ_{13}–δ_{CP} correlations for NOνA.

this simulation with the standard neutrino factory, but must use a setting with the same systematics.

The comparison is done with the AEDL files `NFvar.glb` and `NF_GoldSilver.glb` (distributed with GLoBES), the latter including the silver channel [82]. We simulated 4 years of ν-running (gold channel) plus 4 years of $\overline{\nu}$-running (gold and silver channel).[12] The results are virtually indistinguishable, the difference between the χ^2 is of order of 0.1, so we conclude that an additional ν_τ-appearance channel will not improve the sensitivity to α. A similar conclusion has been reached for the determination of NSI parameters in Ref. [83].

3.5.7 Effect on Other Correlations

Having discussed the correlations of α with the other parameters, we will state the effects of $\alpha \neq 0$ on other correlations. In particular, we will examine the resolution of the mass hierarchy and the sign of α.

NOνA To look at the effect of a non-zero α on the sensitivity of other oscillation parameters, we show the θ_{23}–Δm^2_{31} plane for $\alpha = 0$ and $\alpha = 1 \times 10^{-50}$, calculated for the NO$\nu$A experiment, as well as an analogous fit in the θ_{13}–δ_{CP} plane (Fig. 3.12). As expected from all the α correlations discussed above, a non-zero α tightens the allowed θ_{23} range, but slightly enlarges that of Δm^2_{31}. The effect of $\alpha < 0$ differs only marginally.

The different correlations in the θ_{13}–δ_{CP} plane for normal and inverted hierarchy allow in principle to resolve the two cases (if $\theta_{13} \neq 0$), except for a small parameter space [84]. α shifts the contours towards $\theta_{13} = 0$, irrespective of its sign or the assumed hierarchy (we only show the $(\alpha > 0)$-NH case as to not clutter the plot). As a result, while NOνA can in principle resolve the mass hierarchy, it is not helpful for measuring the sign of α.

Neutrino Factory The described effects in the θ_{23}–Δm^2_{31} plane of NOνA are merely enhanced for a Nufact. More interesting is the correlation of θ_{13} and δ_{CP} (Fig. 3.13), since it introduces a distinction between $\pm\alpha$. In case of normal hierarchy, a positive α

[12] Since the neutrino-nucleon cross section is smaller for $\overline{\nu}_\tau$ (at these energies $\sigma(\nu N)/\sigma(\overline{\nu} N) \approx 3 - 2$), we only consider the silver channel in the $\overline{\nu}$-run (stored μ^+).

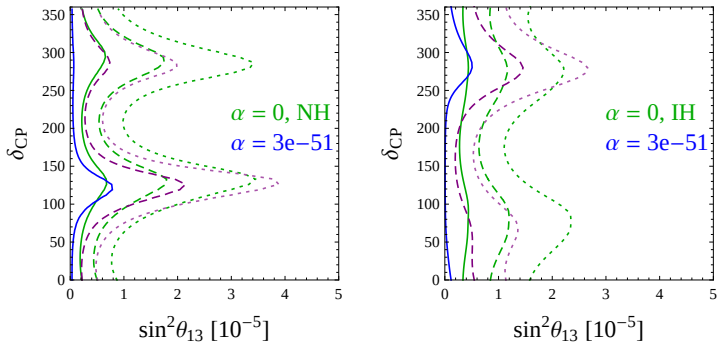

Figure 3.13: Effect of a non-zero α on the θ_{13}–δ_{CP} correlation for Nufact, shown for normal (left) and inverted hierarchy (right).

favours a δ_{CP} around 120°, while a negative α selects just the other one, around 280°. For inverted hierarchy it is just the other way around; this could be used to determine $\mathrm{sgn}(\alpha)$, assuming the mass hierarchy is known, e.g. from NOνA.

The reason for this behaviour is an interplay with the usual matter effect, since at these baselines it is significant and leads to CP violation in correlation with δ_{CP}.

3.5.8 Discovery Limits

As mentioned in App. B, there is a second interesting quantity concerning the opportunities of a simulated experiment to certain model parameters, beside the sensitivity to it. This so-called discovery potential gives the concrete value a parameter needs to have in order to exclude another value at a certain confidence level. For the parameter α this means we vary the *true value* α_{true} and find the value at which

$$\chi^2(\alpha = 0)\big|_{\alpha_{\mathrm{true}}} - \chi^2(\alpha = \alpha_{\mathrm{true}})\big|_{\alpha_{\mathrm{true}}} = \Delta\chi^2\,, \tag{3.56}$$

where, of course, $\chi^2(\alpha = \alpha_{\mathrm{true}}) = 0$ by definition and we will choose $\Delta\chi^2 = 9.0$ to exclude the value $\alpha = 0$ at 99.73% C.L. (3σ).

While this seems easy enough, we will illustrate the problem we encounter at the example of NOνA. Setting $\alpha_{\mathrm{true}} = 2\times10^{-50}$, we obtain the simulated $\chi^2(\alpha)$ of Fig. 3.14 (left). The second (local) minimum around $\alpha = 0$ favours a non-maximal mixing, $\theta_{23} \neq \pi/4$. Increasing α_{true} to lift this second minimum over the 99.73% C.L. barrier requires true values that are already excluded by atmospheric neutrino oscillations, hence it makes no sense to define a discovery potential for α in this way.

Even though the above discussion suggests that α cannot be "discovered" at LBL experiments, this would be an oversimplification. Assuming we have non-maximal mixing in the atmospheric sector, a non-zero α gives rise to CP violation that could be easily discovered by comparing neutrino and antineutrino rates (e.g. in the MINOS experiment 3.6). If we actually have maximal mixing, then $\chi^2(\alpha = 0)$ gets pushed to high values as the error on θ_{23} tightens, making it possible to define a proper discovery limit. To illustrate this point, we assume an improved error of $\theta_{23} = \pi/4 \pm 0.02$ and show that NOνA could then discover an $\alpha = 2\times10^{-50}$, 3σ away from the standard

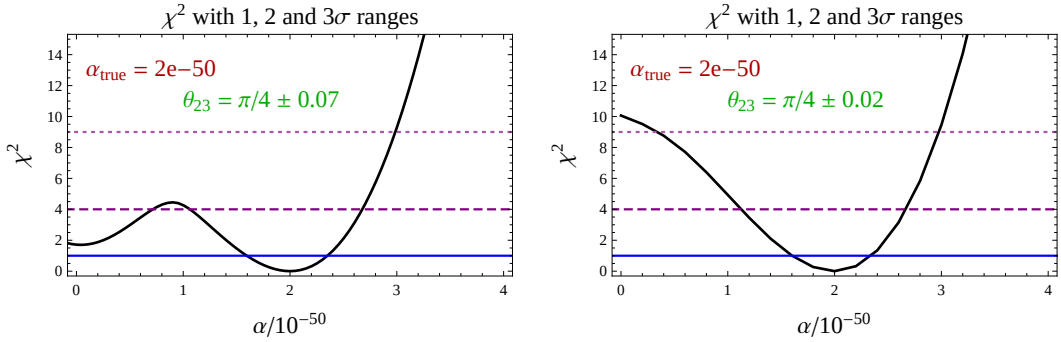

Figure 3.14: $\chi^2(\alpha)$ for $\alpha_{\text{true}} = 2 \times 10^{-50}$ at NOνA. The assumed standard deviation of θ_{23} is 0.07 (left) and 0.02 (right), the latter allowing to set a discovery limit of $\alpha = 2 \times 10^{-50}$.

oscillation value $\alpha = 0$ (see Fig. 3.14 (right)).

3.6 MINOS Anomaly

In this section, we will show how the model under consideration can explain the different neutrino oscillation behaviour of ν and $\bar{\nu}$, as measured by the MINOS experiment [51]. It serves as a short version of the paper we wrote on the subject [85], but contains an improved discussion of the possible shortcomings.

3.6.1 Introduction

The MINOS (Main Injector Neutrino Oscillation Search) experiment is a two detector long-baseline experiment which uses the NuMI beam line from Fermilab. The far detector is set up 735 km from the source, resulting in an $L/E \sim 500\,\text{km/GeV}$, sensitive to atmospheric neutrino oscillations (Δm^2_{32} and $\sin^2 2\theta_{23}$). With 7×10^{20} Protons On Target (POT) for the neutrino run and 1.7×10^{20} POT for the antineutrino run, they obtain the best-fit values

$$\begin{aligned} \Delta m^2 &= \left(2.35^{+0.11}_{-0.08}\right) \times 10^{-3}\,\text{eV}^2\,, & \sin^2 2\theta &> 0.91\,, \\ \overline{\Delta m^2} &= \left(3.36^{+0.45}_{-0.40}\right) \times 10^{-3}\,\text{eV}^2\,, & \sin^2 2\overline{\theta} &= 0.86 \pm 0.11\,, \end{aligned} \tag{3.57}$$

in a respective fit of the oscillation probability to the data. The apparent difference of the neutrino and antineutrino parameters has motivated several explanation attempts, in the form of CPT violation [86, 87, 88], NSIs [89, 90, 91], gauged $B - L$ plus sterile neutrinos [92] and, of course, via gauged $L_\mu - L_\tau$ [85]. Most of these explanations are problematic in a certain way [93], we will however mainly comment on our model.

3.6.2 Fitting our Model

As shown in the previous sections, the introduction of the potential $V_{\mu\tau}$ leads to a different oscillation behaviour for electron, muon and tauon neutrinos. Since the potential changes sign for the corresponding antineutrinos, it also changes the oscillation of ν_ℓ and $\bar{\nu}_\ell$, which could explain the MINOS results (3.57).

Using the exact two-flavour results derived in Sec. 3.3.1, we obtain the survival probabilities for neutrinos and antineutrinos

$$P \equiv P(\nu_\mu \to \nu_\mu) = 1 - \sin^2 2\theta_V \, \sin^2 \frac{\Delta m_V^2}{4\,E} L \,, \tag{3.58}$$

$$\overline{P} = P(\overline{\nu}_\mu \to \overline{\nu}_\mu) = P(\nu_\mu \to \nu_\mu)(\alpha \leftrightarrow -\alpha) \,, \tag{3.59}$$

with the energy-dependent parameters

$$\sin^2 2\theta_V = \frac{\sin^2 2\theta}{1 - 4\,\eta\,\cos 2\theta + 4\,\eta^2} \,, \tag{3.60}$$

$$\Delta m_V^2 = \Delta m^2 \sqrt{1 - 4\,\eta\,\cos 2\theta + 4\,\eta^2} = \Delta m^2 \sqrt{\sin^2 2\theta / \sin^2 2\theta_V} \,. \tag{3.61}$$

The parameter $\eta \equiv \frac{2\,E\,V}{\Delta m^2}$ contains our potential and therefore changes sign for antineutrinos. Since η only contributes in the form $\eta \cos 2\theta$, a non-maximal mixing angle θ is necessary to induce different ν and $\bar{\nu}$ behaviour. Since we introduce only one additional parameter α, we predict a connection between the oscillation parameters for ν and $\bar{\nu}$, e.g. from (3.60) $\Delta m^2 \sin 2\theta = \overline{\Delta m^2} \sin 2\overline{\theta}$, which could distinguish our model from other solutions.

Using the expressions (3.58, 3.59), we have performed a χ^2-fit to the MINOS data (given in bins of energy E_i) on the ratio of observed events divided by the expectation for no oscillations. This data was taken, as in Ref. [89], from the slides of the talk referred to in our Ref. [51]. In case of asymmetric errors, the largest one was used and inserted in the χ^2-function

$$\chi^2(\theta, \Delta m^2, \alpha) = \sum_i \left(\frac{P(\theta, \Delta m^2, \alpha, E_i) - R_i}{\sigma_i^2} \right)^2 + \sum_i \left(\frac{\overline{P}(\theta, \Delta m^2, \alpha, E_i) - \overline{R}_i}{\overline{\sigma}_i^2} \right)^2 , \tag{3.62}$$

where P ($\overline{P}$) is the survival probability $P(\nu_\mu \to \nu_\mu)$ from Eq. (3.58) (from Eq. (3.59)), R_i ($\overline{R}_i$) the ratio of observed events relative to the no-oscillation expectation, and σ_i ($\overline{\sigma}_i$) the error for the neutrino (antineutrino) data set.

We have checked our analysis by setting $\alpha = 0$ and have obtained the best-fit values $\Delta m^2 = 2.28 \times 10^{-3}\,\mathrm{eV}^2$, $\sin^2 2\theta = 0.94$ for the neutrino data set, and $\overline{\Delta m^2} = 3.38 \times 10^{-3}$ eV^2, $\sin^2 2\overline{\theta} = 0.81$ for the antineutrinos, in good agreement with the MINOS results. A fit to the total data set yields $\Delta m^2 = (2.38^{+0.20}_{-0.17}) \times 10^{-3}$ eV^2 and $\sin^2 2\theta = 0.89^{+0.08}_{-0.07}$, with $\chi^2_{\mathrm{min}}/N_{\mathrm{dof}} = 49.43/51 \simeq 0.97$.

The result of our fit including α is

$$\begin{aligned} \sin^2 2\theta &= 0.83 \pm 0.08 \,, \\ \Delta m^2 &= (-2.48 \pm 0.19) \times 10^{-3}\,\mathrm{eV}^2 \,, \\ \alpha &= \left(1.52^{+1.17}_{-1.14}\right) \times 10^{-50} \,, \end{aligned} \tag{3.63}$$

with $\chi^2_{\mathrm{min}}/N_{\mathrm{dof}} = 47.77/50 \simeq 0.96$. Recall the degeneracies for the two-flavour oscillation listed in Eq. (3.30). In Fig. 3.15 we show the experimental data together with the

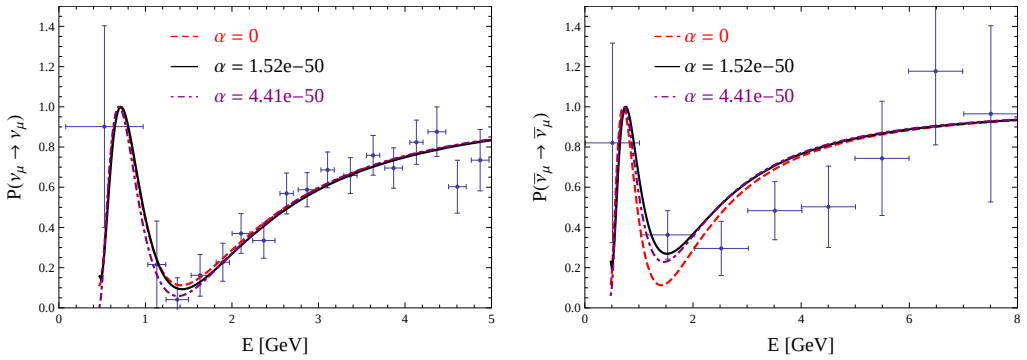

Figure 3.15: The oscillation probabilities for the best-fit values from Eq. (3.63) for neutrinos and antineutrinos, superimposed on the MINOS data. Also plotted are the cases $\alpha = 0$ and the value for the second (local) minimum of $\chi^2(\alpha)$.

results of our fit.

One can see that the non-zero value of α puts in particular the data points at the oscillation minimum in better agreement with the curves. From the plot of the χ^2-function in Fig. 3.16 one sees that there is a second (local) minimum, corresponding to $\sin^2 2\theta = 0.98$, $\Delta m^2 = 2.36 \times 10^{-3}\,\text{eV}^2$ and $\alpha = 4.41 \times 10^{-50}$, with $\chi^2_{\text{min}}/N_{\text{dof}} = 48.73/50 \simeq 0.97$. The curves for this point are also plotted in Fig. 3.15. The second minimum also explains the "rabbit head looking" shape of the contours in α–Δm^2 and α–$\sin^2 2\theta$ space shown in Fig. 3.17.

The goodness-of-fit is not particularly worse for the absence of new physics, which has been noted also in Ref. [89].

Setting the true parameter values of α, θ and Δm^2 (and their errors) to our best-fit values from Eq. (3.63), we can see how the "precision" on α can be improved by future LBL experiments, using GLoBES (see Sec. 3.5 for details). From the plots of χ^2 in Fig. 3.18 one sees that NOνA would give $\alpha = (1.52 \pm 0.27) \times 10^{-50}$, T2K would yield $\alpha = (1.52 \pm 0.46) \times 10^{-50}$ and Nufact would determine very precisely $\alpha = \left(1.52^{+0.11}_{-0.21}\right) \times 10^{-50}$.

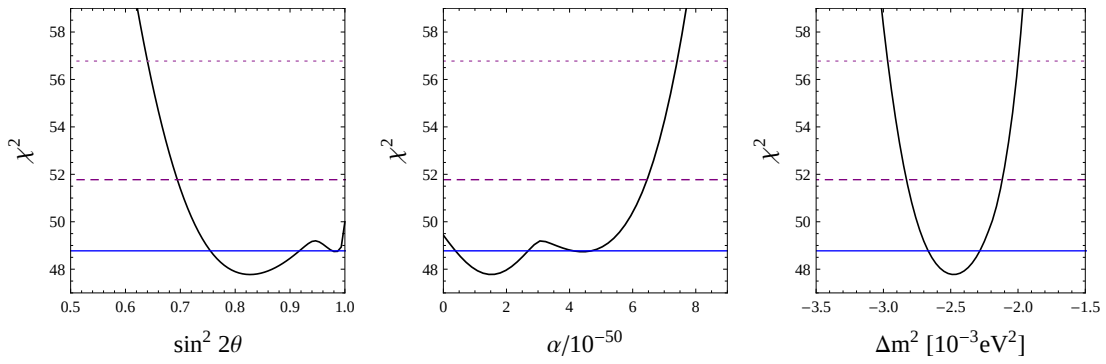

Figure 3.16: χ^2 from Eq. (3.62) as a function of the fit parameters. The horizontal lines define the 1, 2 and 3σ ranges, for one parameter defined as $\Delta\chi = 1$, 4 and 9.

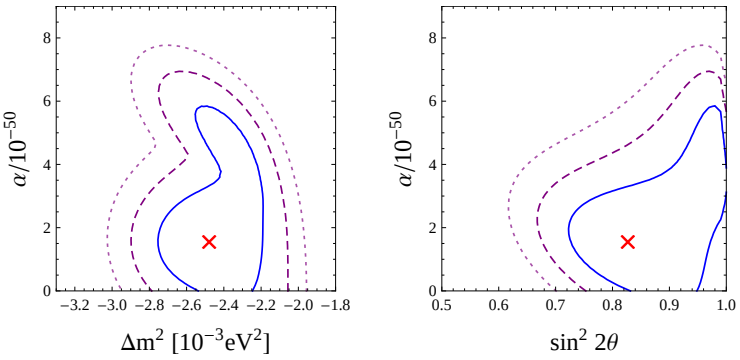

Figure 3.17: The $1, 2$ and 3σ contours in the α–Δm^2 plane when marginalised over θ (left) and in the α–$\sin^2 2\theta$ plane when marginalised over Δm^2 (right). The cross marks the best-fit point.

3.6.3 Discussion

The best-fit value for α is not in conflict with any of the constraints discussed in Sec. 3.4, but it would be in conflict with NSI constraints if we took the correspondence (3.52), namely

$$\varepsilon_{\mu\mu} = -\varepsilon_{\tau\tau} \mathrel{\widehat{=}} \frac{V(\alpha)}{\sqrt{2} G_F n_e(\boldsymbol{x})}\,, \tag{3.64}$$

seriously. This is because our best-fit α results in a potential $V \approx 5.5 \times 10^{-14}\,\mathrm{eV}$, together with the approximately constant matter density along the path of flight we obtain $\varepsilon_{\mu\mu} \approx 0.5$, or half of that, depending on how we treat the $\varepsilon_{\mu\mu} = -\varepsilon_{\tau\tau}$ condition. Either way, this is an order of magnitude above the current limit and therefore excluded.

However, one has to take into account where the NSI bound actually comes from; bounds based on ν–e scattering [94], which changes in the presence of NSI due to changed couplings, are not applicable, since in our case the coupling (be it g' or ξ) is too small to be observable in single particle scattering. Therefore the bounds from neutrino oscillation experiments have to be used; for the NSI parameters under consideration here these stem from atmospheric neutrinos (measured for example at Super-Kamiokande).

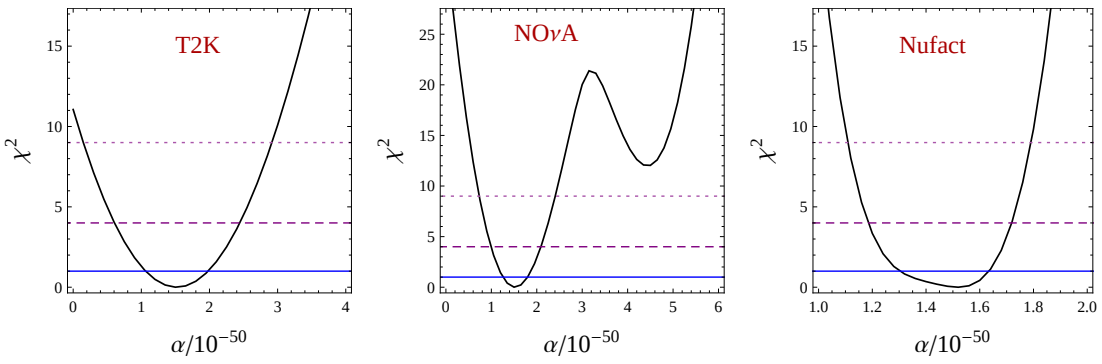

Figure 3.18: The sensitivity on α which can be obtained by T2K (left), NOνA (middle) and a neutrino factory (right) if $\alpha_{\mathrm{true}} = \left(1.52^{+1.17}_{-1.14}\right) \times 10^{-50}$.

The analysis of atmospheric neutrino data is based on zenith-angle distributions, i.e. the direction where the neutrinos come from (and hence the amount of matter they travel through). In this case, it is important to take the radial dependence of the NSI potential into account, since it changes from the core to the crust of the Earth in a different way than our potential $V(\alpha)$. The entire next section is devoted to the examination of the position dependence, and how one can relate the NSI bound to α. The result will be that, while it is not possible to relate them directly, a slightly better estimate of their connection weakens the bound given above. Fitting our model for a potential with Earth-radius range to atmospheric neutrino data yields constraints that, while excluding the MINOS best-fit value, still allow values within one standard deviation, i.e. $\alpha = \alpha_{\text{best}} - 1\sigma$ saturates the Super-K constraint derived below.

The other solutions for the MINOS anomaly, mentioned in the introduction, suffer worse problems [93]; for example, the NSI solution via the off-diagonal element $\varepsilon_{\mu\tau}$ suggests values ~ 0.1, while a gauge-invariant approach to NSI gives limits of order 10^{-4} from charged-lepton decays.

The implications of breaking the CPT symmetry to explain MINOS, as put forward in Refs. [86, 87, 88], are of course much more severe on a conceptional level than in actual constraints.

Independent of whether or not our model can actually explain the MINOS anomaly, it must be emphasised that with the low statistics accumulated until now by the MINOS collaboration, neither of the BSM physics models mentioned in the introduction improves the fit significantly. Only time will show if the MINOS anomaly survives and how it can be explained theoretically.

3.7 Effects of a Position-Dependent Potential

In the previous sections, we approximated the Z' potential as constant, which allowed us to solve at least the simplest two-flavour neutrino oscillation probabilities exactly. The solution of the differential equation

$$i\frac{\mathrm{d}}{\mathrm{d}t}\boldsymbol{\nu}_M = \frac{1}{2E}\begin{pmatrix} m_2^2 & 0 \\ 0 & m_3^2 \end{pmatrix}\boldsymbol{\nu}_M + V(\boldsymbol{x}(t)) \cdot U^\dagger \begin{pmatrix} 1 & 0 \\ 0 & -1 \end{pmatrix} U\boldsymbol{\nu}_M \tag{3.65}$$

can only be obtained numerically. In this section, we will comment on the effects arising from a proper treatment of $V(r)$ and verify that, for the LBL experiments discussed so far, a constant potential is indeed a very good approximation. This is however not the case for AνO, since the through-going neutrinos see the high potential inside the Earth. Since the effect will be most important for a force of Earth-radius range (contributions from the Sun would smoothen the potential considerably), we will consider $M_2 \sim 1/R_\oplus$ and denote α as $\alpha^\oplus$. To compare the values from the previous sections, one needs to rescale α according to Tab. 3.1.

The proper potential generated by the neutrons of the Earth is given by

$$V(\boldsymbol{x}) \sim \int n(\boldsymbol{x}') \frac{e^{-|\boldsymbol{x}-\boldsymbol{x}'|M_2}}{|\boldsymbol{x}-\boldsymbol{x}'|} \,\mathrm{d}^3x', \tag{3.66}$$

which can be evaluated, assuming a rotationally symmetric neutron distribution $n_n(r)$ and letting once again $M_2 \to 0$, to

$$V(r \le R_\oplus) = \frac{\alpha^\oplus e}{4 s_W c_W} \int_r^{R_\oplus} \frac{\mathrm{d}r'}{r'^2} \left(\int_0^{r'} \mathrm{d}s \; n_n(s) s^2 \right) + V(R_\oplus) \tag{3.67}$$

inside the Earth and $V(r > R_\oplus) = V(R_\oplus)\, R_\oplus / r$ outside, where it coincides with our previous potential (rescaled to Earth-radius range). It is easy to verify that (3.67) satisfies the Poisson equation $\Delta V(\boldsymbol{x}) = -\frac{\alpha^\oplus e}{4 s_W c_W} n_n(\boldsymbol{x})$ (3.8) in spherical coordinates

$$\frac{1}{r^2} \frac{\partial}{\partial r} \left(r^2 \frac{\partial V(r)}{\partial r} \right) = -\frac{\alpha^\oplus e}{4 s_W c_W} n_n(r), \tag{3.68}$$

and has integration constants chosen to make $V(r)$ continuous and vanishing as $r \to \infty$. The neutron density $n_n(r)$ is proportional to the matter density $\rho(r) \approx 2 m_n n_n(r)$ and is therefore highly discontinuous if we follow the Preliminary Reference Earth Model (PREM) [64]. Due to the two integrations, the potential will however be smooth and differentiable, albeit a little difficult to actually calculate. We will therefore at first analyse the simplified model of a constant neutron density, where the integrations (3.67) are easily executed:

$$V_r(r) = \alpha^\oplus N_n \frac{e}{4 s_W c_W} \frac{1}{4\pi} \begin{cases} 1/r, & r > R_\oplus, \\ (3 - r^2/R_\oplus^2)/2R_\oplus, & r \le R_\oplus, \end{cases} \tag{3.69}$$

with the radius of Earth $R_\oplus$ and the total number of neutrons N_n. We show this simplified version together with the full potential based on the PREM matter density in Fig. 3.19; the difference is rather small and only important near the core, i.e. for neutrinos that travel through the whole Earth. This will be analysed later for atmospheric neutrinos. Also shown is the form of the PREM matter density, which is proportional to the usual NSI potential $V_{\mathrm{NSI}}(r) = \sqrt{2} G_F n_e(r) \varepsilon_{\alpha\beta} \sim \rho_{\mathrm{PREM}}(r)$.

The path of flight $r(t)$ for a neutrino depends on the baseline; for example, in a parameterisation $t \in [0, L]$:

$$r(t) = \sqrt{(t - L/2)^2 + R_\oplus^2 - L^2/4}. \tag{3.70}$$

With this $V_r(r(t))$ we can solve Eq. (3.65) numerically, but first we look at the potential itself. For $L \ll R_\oplus$, we can expand in $L/R_\oplus$ and find $V_r(r(t)) = V_r(R_\oplus)(1 + \mathcal{O}(L^2/R_\oplus^2))$, i.e. the corrections due to the position dependence of the potential are quadratic in $L/R_\oplus$ and hence very small for the future long-baseline experiments discussed in Sec. 3.5. The biggest difference occurs, of course, at $t = L/2$, yielding the relative cor-

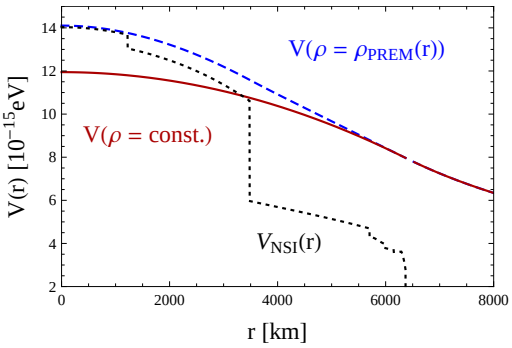

Figure 3.19: Proper radial dependence of the potential $V_r(r)$ for a constant neutron density inside the Earth (red) and using the full PREM density (blue). The potential scales with $\alpha^{\oplus}/10^{-50}$. The dotted black curve gives a conveniently rescaled NSI matter potential $V_{\mathrm{NSI}}(r) \sim \rho_{\mathrm{PREM}}(r)$.

rection $(V_r - V)/V = L^2/8R_{\oplus}^2$, which is even small for the Nufact distances $L \sim 3000\,\mathrm{km}$ (of order of a few percent). It is therefore not surprising that the oscillation probability $P_{\mu\tau}$ undergoes only minor changes.

We plot $P_{\mu\tau}(E)$ for the cases $V \equiv 0$ (standard neutrino oscillation), $V \sim \alpha^{\oplus}/R_{\oplus}$ (constant potential as discussed in the previous sections) and $V = V_r(r, L)$, with the oscillation parameters Δm^2 and θ_{23} from Tab. 1.2, $\alpha^{\oplus} = 15 \times 10^{-50}$ and $L = 3000\,\mathrm{km}$ (Fig. 3.20 (left)). The difference between $V = \text{const.}$ and $V = V(r)$ is very small, hence the large value chosen for $\alpha^{\oplus}$. Since the difference $\Delta P(E, \alpha^{\oplus}) \equiv P_{\mu\tau}(V = \text{const.}) - P_{\mu\tau}(V = V(r))$ is largest at the maximum of $P_{\mu\tau}(E)$, we show it explicitly as a function of $\alpha^{\oplus}$, for energies around the maximum $E \sim 6\,\mathrm{GeV}$ (Fig. 3.20 (right)).

3.7.1 Approximate Solution

Even though we do not have an exact solution for Eq. (3.65) like in the $V = \text{const.}$ case, we can nevertheless find an approximate solution for some limiting cases, like the LBL limit $L \ll R_{\oplus}$. To obtain it, we note that the reason why we cannot just write the

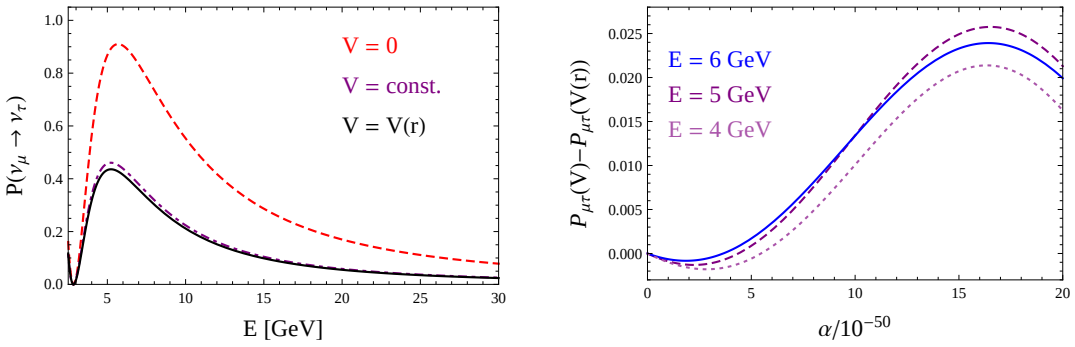

Figure 3.20: Left panel: Oscillation probability $P_{\mu\tau}(E)$ for standard neutrino oscillations ($\alpha^{\oplus} = 0 = V$) (red), for a constant potential ($V \sim \alpha^{\oplus}/R_{\oplus}$) (purple) and with the proper, position-dependent potential $V = V_r(r)$ (black). Right panel: Difference $P_{\mu\tau}(V = \text{const.}) - P_{\mu\tau}(V = V(r))$ as a function of $\alpha^{\oplus}$ for energy values around the maximum.

solution as

$$\boldsymbol{\nu}_M(t) = \exp\left[-i\int_0^t \mathrm{d}t'\, H_V(t')\right]\, \boldsymbol{\nu}_0\,, \tag{3.71}$$

with the Hamiltonian

$$H_V(t) = \frac{1}{2E}\begin{pmatrix} m_2^2 & 0 \\ 0 & m_3^2 \end{pmatrix} + V_r(\boldsymbol{x}(t)) \cdot U^\dagger \begin{pmatrix} 1 & 0 \\ 0 & -1 \end{pmatrix} U\,, \tag{3.72}$$

is the fact that $H_V(t_1)$ does not commute with $H_V(t_2)$, i.e. we need to introduce a time-ordering into Eq. (3.71). This can be done using the so-called Magnus expansion[13] of the exact solution [95], i.e. we can write

$$\boldsymbol{\nu}_M(t) = \exp\left[-i\sum_{k=0}^{\infty}\Omega_k(t)\right]\, \boldsymbol{\nu}_0\,, \tag{3.73}$$

with the first three terms

$$\begin{aligned} \Omega_1(t) &= \int_0^t \mathrm{d}t_1\, H_V(t_1)\,, \qquad \Omega_2(t) = \frac{(-i)}{2!}\int_0^t \mathrm{d}t_1 \int_0^{t_1} \mathrm{d}t_2\, \left[H_V(t_1), H_V(t_2)\right]\,, \\ \Omega_3(t) &= \frac{(-i)^2}{3!}\int_0^t \mathrm{d}t_1 \int_0^{t_1} \mathrm{d}t_2 \int_0^{t_2} \mathrm{d}t_3\, \left\{\left[H_V(t_1), \left[H_V(t_2), H_V(t_3)\right]\right] + (t_3 \leftrightarrow t_1)\right\}\,. \end{aligned} \tag{3.74}$$

An explicit calculation of the first arising commutator gives

$$\left[H_V(t_1), H_V(t_2)\right] \sim \frac{\Delta m^2}{2E}\sin 2\theta \begin{pmatrix} 0 & -1 \\ 1 & 0 \end{pmatrix} \left[V_r(t_1) - V_r(t_2)\right]\,, \tag{3.75}$$

with a vanishing integral at $t = L$, so $\Omega_2(L) = 0$ (this does no longer hold using a non-constant matter density). Assuming only a minor correction due to Ω_3, we conclude that Eq. (3.71) is a good approximation for the exact solution. Since V_r is the only position-dependent quantity in Eq. (3.71), we can simply replace $V \cdot t \to \int \mathrm{d}t\, V_r(r(t))$ in the exact two-flavour solution derived in Sec. 3.3.1. For a LBL measurement of $P(\nu_\mu \to \nu_\tau)$, this simply corresponds to the replacement of $V = \text{const.}$ with the mean potential

$$\langle V_r \rangle = \frac{1}{L}\int_0^L \mathrm{d}t\, V_r(r(t)) = V(R_\oplus)\left(1 + \frac{L^2}{12R_\oplus^2}\right)\,. \tag{3.76}$$

[13] In contrast to other expansion schemes, the Magnus expansion provides a unitary time-evolution operator even for the truncated series $\exp\left[-i\sum_{k=0}^{N}\Omega_k(t)\right]$, because the Ω_k are hermitian.

The dominant effect of the position dependent potential can, for LBL experiments, be approximated by replacing $\alpha^\oplus \to \alpha^\oplus \times (1 + L^2/12R_\oplus^2)$, which is once again only a percent correction.

Note that the Magnus expansion is not an expansion in the small quantity V (or $\alpha^\oplus$ to take a proper perturbation parameter), which is the approach of the NSI expansion in App. D. From Eq. 3.75 we see however, that all higher terms $\Omega_{j>1}$ vanish not only for $V \equiv 0$, but more generally for $V = \text{const.}$, hence this expansion provides interesting information about the position dependence of V. A discussion of Ω_3 will show the accuracy of the approximation; we calculate

$$\Omega_3(L) = \frac{V(R_\oplus)^2 \Delta m^2 L^5 \sin 2\theta}{720\, E R_\oplus^2} \begin{pmatrix} -\left(1 + \frac{2L^2}{21R_\oplus^2}\right)\sin 2\theta & \cos 2\theta - \frac{21}{84}\frac{\Delta m^2}{V(R_\oplus)E} + \frac{8}{84}\frac{L^2}{R_\oplus^2}\cos 2\theta \\ \cdot & + \left(1 + \frac{2L^2}{21R_\oplus^2}\right)\sin 2\theta \end{pmatrix},$$

which is to be compared to

$$\Omega_1(L) = V(R_\oplus) L \begin{pmatrix} \left(1 + \frac{L^2}{12R_\oplus^2}\right)\cos 2\theta & \left(1 + \frac{L^2}{12R_\oplus^2}\right)\sin 2\theta \\ \cdot & -\left(1 + \frac{L^2}{12R_\oplus^2}\right)\cos 2\theta + \frac{\Delta m^2}{2V(R_\oplus)E} \end{pmatrix}.$$

We extract the condition for $\Omega_1 \gg \Omega_3$ from the overall prefactor (this is of course arbitrary to some degree)

$$V(R_\oplus) L \gg \frac{V(R_\oplus)^2 \Delta m^2 L^5 \sin 2\theta}{720\, E R_\oplus^2}, \tag{3.77}$$

which translates into

$$V(R_\oplus) \ll 720 \frac{E R_\oplus^2}{\Delta m^2 L^4} \overset{L \to 2R_\oplus}{\longrightarrow} 45 \frac{E}{\Delta m^2 R_\oplus^2} \approx 1.8 \times 10^{-14}\,\text{eV}\, \frac{E}{1\,\text{GeV}}. \tag{3.78}$$

It is important to note that the mean-potential approximation is very good in the LBL limit, due to the L^4 factor, but for atmospheric neutrino oscillations we have to consider "baselines" up to $L = 2R_\oplus$, which enlarges Ω_3. In this case one needs to include the higher corrections $\Omega_{j>1}$ or solve Eq. (3.65) numerically.

3.7.2 Comparison with Non-Standard Neutrino Interactions

Having discussed the radial dependence of $V(\alpha^\oplus)$, we can finally discuss NSI constraints. As already mentioned in Sec. 3.4.7, the difficulty in comparing our potential to NSI lies in the different position dependence, even though they share the same flavour structure and energy dependence. From Fig. 3.19, we see that our potential increases at most by a factor of 1.8 from the surface to the core of the Earth, the NSI potential by a factor $4 - 5$. From our above discussion it seems plausible as a first approximation to compare the mean potentials $\langle V \rangle = \frac{1}{L}\int_0^L \mathrm{d}t\, V(r(t))$ along some baseline L, rather than just the plain potential at the surface. The effects enhance with the amount of matter

the neutrinos travel through, so the strongest bounds should hold for $L \approx 2R_\oplus$. An NSI constraint [6] $\varepsilon_{\mu\mu} < 0.068$ corresponds to a mean potential $\langle V_{\text{NSI}} \rangle < 2.2 \times 10^{-14}\,\text{eV}$ and leads to the bound $\alpha^\oplus_{\text{PREM}} < 1.9 \times 10^{-50}$ for the potential of range $R_\oplus$ discussed in this section.[14] This might be off by a factor of 2, depending on how one treats the $V_{\mu\mu} = -V_{\tau\tau}$ condition our model imposes and which NSI bound one applies (this ambiguity will be discussed in Sec. 4.2.1). In any case, these bounds are not to be taken too literally, since they are only derived for the longest baseline and in the approximation $\Omega_1 \gg \Omega_{j>1}$. Taking all baselines into account is basically equivalent to a direct fit to atmospheric neutrino data; this will be the subject of the next subsection, where we derive constraints of roughly the same order.

To reiterate: The different radial dependence of $V(\alpha^\oplus)$ and V_{NSI} forbids a direct comparison of the limits. An estimation gives bounds similar to the ones we will derive below (in general slightly tighter).

3.7.3 Atmospheric Neutrino Oscillations

The radial dependence of $V(r)$ is most important for AνO, which will be discussed in this section. Since it is not clear if the limits from NSI are valid for our model (different position dependence, only in lowest order (3.71) directly comparable), we will perform our own χ^2-fit (following the analysis of Ref. [27]), based on data from Super-Kamiokande I,II and III [96] (1489.2+798.6+518.1 days of exposure), namely ν_μ appearance for different energies and zenith-angles. These data are given in 10 bins for the cosine of the zenith angle ($\cos\theta_\text{z} = -0.9, \ldots, +0.9$), which corresponds to baselines

$$L = \sqrt{(R_\oplus + h)^2 - R_\oplus^2 (1 - \cos^2\theta_\text{z})} - R_\oplus \cos\theta_\text{z}\,, \tag{3.79}$$

where $h \approx 15\,\text{km}$ denotes the height where the atmospheric neutrinos originate. Since the oscillation probability $P_{\mu\mu}(E, L(\cos\theta_\text{z}))$ oscillates very fast over one $\cos\theta_\text{z}$ bin,[15] we take the average:

$$P^i_{\mu\mu}(E) \equiv \langle P_{\mu\mu}(E, \cos\theta^i_\text{z}) \rangle \equiv \frac{1}{0.2} \int\limits_{\cos\theta^i_\text{z} - 0.1}^{\cos\theta^i_\text{z} + 0.1} \text{d}\cos\theta_\text{z}\; P_{\mu\mu}\left(E, L(\cos\theta_\text{z})\right)\,. \tag{3.80}$$

The corresponding number of muon neutrinos $(\nu_\mu + \overline{\nu}_\mu)$ per bin, with energies from E_1 to E_2, is then given by

$$(\nu_\mu + \overline{\nu}_\mu)^i = \int\limits_{E_1}^{E_2} \text{d}E\;\left[P^i_{\mu\mu}(E)\,\Phi_\mu(E, \cos\theta^i_\text{z})\,\sigma_\nu(E) + P^i_{\overline{\mu}\overline{\mu}}(E)\,\Phi_{\overline{\mu}}(E, \cos\theta^i_\text{z})\,\sigma_{\overline{\nu}}(E)\right]\,, \tag{3.81}$$

[14] Going back to the constant potential for the Earth-Sun distance, this translates into $\alpha^\odot < 0.62 \times 10^{-50}$.

[15] The fast oscillations mainly occur in the first couple of the $\cos\theta_\text{z}$ bins, corresponding to large baselines L.

with the atmospheric neutrino flux Φ (we use the Honda-flux 2006 given in Ref. [97] in $(E, \cos\theta_z^i)$ bins). σ_ν denotes the total cross section for neutrino-nucleon scattering, roughly $\sigma_\nu \sim E$, $\sigma_\nu/\sigma_{\overline{\nu}} \approx 0.5$ [47] (we use values from Ref. [98] for σ_ν, which corrects small deviations from the linear energy dependence for sub-GeV energies). The value $(\nu_\mu + \overline{\nu}_\mu)^i$, of course, depends on the oscillation parameters (for two flavours: θ and Δm^2); to make contact with experiment, we calculate the ratio

$$r^i(\theta, \Delta m^2, E_1, E_2) \equiv \frac{(\nu_\mu + \overline{\nu}_\mu)^i(\theta, \Delta m^2)}{(\nu_\mu + \overline{\nu}_\mu)^i(0, 0)}\,, \tag{3.82}$$

which is to be compared to the measured number of events divided by the expected number without neutrino oscillations (given by a Monte Carlo simulation in Ref. [96]). In this way the overall normalisation and detector efficiencies hopefully cancel out.

As data samples we take the two multi-GeV datasets `Multi-GeV 1-ring` μ`-like (FC+PC stop)`[16] with energies $1 - 2.5\,\mathrm{GeV}$ and $> 2.5\,\mathrm{GeV}$, respectively,[17] and one sub-GeV dataset `Sub-GeV 1-ring` μ`-like 1-decay` with the energy range $0.63 - 1\,\mathrm{GeV}$. All of them are divided into 10 $\cos\theta_z^i$ bins, so we have 30 datapoints to fit our function (3.82).

The χ^2-function we use for each dataset is simply

$$\chi^2(\theta, \Delta m^2, E_1, E_2) = \sum_{i=1}^{10} \frac{\left(r^i(\theta, \Delta m^2, E_1, E_2) - \frac{\mathrm{data}^i(E_1,E_2)}{\mathrm{data}^i_{\mathrm{MC}}(E_1,E_2)}\right)^2}{\left(\mathrm{data}^i_{\mathrm{error}}(E_1, E_2)\right)^2}\,, \tag{3.83}$$

so the total χ^2 is just the sum over the different energy regions:

$$\begin{aligned}\chi^2(\theta, \Delta m^2) = {} & \chi^2(\theta, \Delta m^2, 0.63\,\mathrm{GeV}, 1\,\mathrm{GeV}) \\ & + \chi^2(\theta, \Delta m^2, 1\,\mathrm{GeV}, 2.5\,\mathrm{GeV}) \\ & + \chi^2(\theta, \Delta m^2, 2.5\,\mathrm{GeV}, 100\,\mathrm{GeV})\,.\end{aligned} \tag{3.84}$$

After a lot of numerical calculations, we obtain the best-fit values for θ and Δm^2

$$\sin^2 2\theta = 0.98_{-0.03}\,, \qquad \Delta m^2 = \left(3.75^{+0.83}_{-0.66}\right) \times 10^{-3}\,\mathrm{eV}^2\,, \tag{3.85}$$

with confidence levels shown in Fig. 3.21 (left). The value (and range) for Δm^2 is way off from the Super-K best-fit, $\Delta m^2 = (2.1^{+0.45}_{-0.10}) \times 10^{-3}\,\mathrm{eV}^2$ [96], which is based on a far more sophisticated analysis. Our result is however reminiscent of that of Ref. [27], on which our analysis is dominantly based (the authors present a best-fit value of $\Delta m^2 = 3.9 \times 10^{-3}\,\mathrm{eV}^2$, based on multi-GeV SK-I datasets). Therefore it seems to be a systematic error in the applied method, most likely due to detector effects.

Performing the same analysis including our potential $V(r)$ (using PREM), we obtain

[16] Fully Contained (FC) events lie in the inner detector, while particles produced in Partially Contained (PC) events reach the outer detector and are further classified into stopping and through-going events.

[17] To calculate the integral (3.81) for the latter, we choose an upper bound of 100 GeV. Since the flux drops like $E^{-2.7}$, the actual upper bound is not that important.

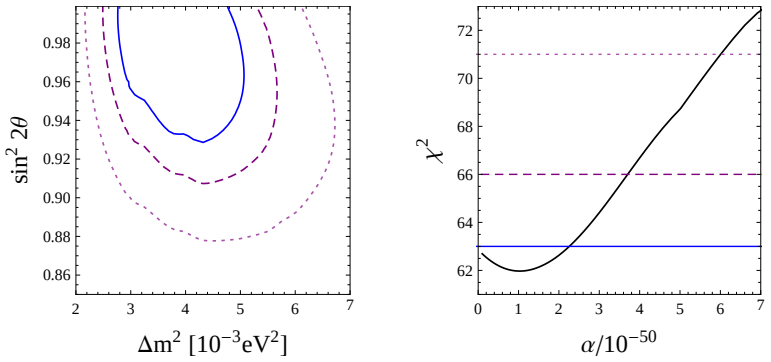

Figure 3.21: Left panel: Two-flavour fit to data from SK-I, II and III, with best-fit values $\sin^2 2\theta = 0.98$, $\Delta m^2 = 3.75 \times 10^{-3}\,\mathrm{eV}^2$ (contours at 68.27, 90 and 99% C.L.). Right panel: $\chi^2(\alpha)$, marginalised over θ and Δm^2 (68.27, 95.45 and 99.73% C.L.).

$\chi^2(\theta, \Delta m^2, \alpha^\oplus)$. The best-fit values shift to

$$\sin^2 2\theta = 0.95^{+0.04}_{-0.03}\,, \quad \Delta m^2 = \left(4.44^{+0.48}_{-1.26}\right) \times 10^{-3}\,\mathrm{eV}^2\,, \quad \alpha^\oplus = 1.03 \times 10^{-50}\,, \tag{3.86}$$

with a slight improvement of the overall fit by one unit.

Marginalising over θ and Δm^2, we can set a 90% C.L. limit[18] $\alpha^\oplus < 3.1 \times 10^{-50}$, see Fig. 3.21 (right). The $\chi^2(\theta, \Delta m^2, \alpha^\oplus)$ contours in the θ–Δm^2 plane move towards non-maximal mixing for increasing $\alpha^\oplus$.

Since we only discussed the potential with range $R_\oplus$ in this section, let us make a few comments concerning the MINOS experiment (Sec. 3.6). Rescaling the MINOS best-fit value to Earth-radius range, we obtain

$$\alpha^\oplus_{\mathrm{MINOS}} = \left(6.94^{+5.35}_{-5.21}\right) \times 10^{-50}\,. \tag{3.87}$$

For LBL experiments like MINOS, the position dependence is insignificant, so we can directly compare (3.87) to our new 90% C.L. Super-K bound $\alpha^\oplus < 3.1 \times 10^{-50}$. The best-fit value is obviously excluded (to a high degree actually, looking at Fig. 3.21), but at least the one sigma intervals overlap.

With this section we improved the constraint on $\alpha^\oplus$ obtained in Sec. 3.4.6 by a factor of 13, by accounting properly for the position dependence of $V(r)$, using a larger dataset and the most recent calculations for fluxes and cross sections.

3.8 Possible Higgs Sector

Having discussed the fifth-force Z' in a rather effective approach, our penultimate section deals with the final part missing in our theory, the scalar particles that break the $U(1)'$. It is not easy to construct a Higgs sector for the ultralight Z'; some of the problems mentioned below should apply to the $U(1)_{L_e - L_\mu, L_\tau}$ models in Refs. [36, 27] as well.

[18] This is to be compared to the (rescaled to Earth-radius range) constraint of Sec. 3.4.6: $\alpha^\oplus < 4.57 \times 8.9 \times 10^{-50} \approx 40 \times 10^{-50}$ at 90% C.L.

As mentioned above, we need $\delta\hat{M}^2 \neq 0$ to affect neutrino oscillations at all (which is far more interesting than the alternative); if we restrain from generating $\delta\hat{M}^2$ via loops this makes it necessary to have a scalar field in a nontrivial representation of $SU(2)_L$, i.e. a doublet ϕ, a triplet Δ, or a field with even more components. The mass of the Z' will be given by $\hat{M}_{Z'} \sim g'v$, where v denotes the vacuum expectation value of the electrically neutral component of our $U(1)_{L_\mu - L_\tau}$-charged Higgs field. Since we do not want to make g' too small, we should choose $v \ll v_{\mathrm{SM}}$. Counting degrees of freedom makes clear that we will end up with at least one additional neutral scalar besides the SM Higgs.[19] To reiterate, we will try to build a Higgs sector which accommodates:

- Ultralight Z',
- Small, but non-zero $\delta\hat{M}^2$ (for a measureable effect on oscillations),
- Neutrino masses $\sim 0.1\,\mathrm{eV}$ and proper mixing.

The calculation of the neutrino mass matrices for the different Higgs sectors is given in Sec. 5.1, albeit for $L_\mu - L_\tau$ breaking around the electroweak scale; the formulae are still valid here. While the three points above are already hard to combine, the biggest problem turns out to be a light physical scalar field coupling to Z, since it contributes to the (invisible) Z width and is thus highly constrained by LEP measurements.

Let us consider the triplet Higgs at first, since its VEV is already constrained to be $\langle\Delta\rangle \sim v_T \lesssim 1\,\mathrm{GeV}$ from its contribution to the ρ parameter (Sec. 5.1.4). The neutrino masses scale like $\mathcal{M}_\nu \sim Y v_T$, so we should keep $v_T > 10^{-2}\,\mathrm{eV}$. A fifth force with the range $R_{\mathrm{A.U.}}$, $M_{Z'} < 10^{-18}\,\mathrm{eV}$, then implies $g' \lesssim 10^{-16}$. The parameter α can be simplified to $\alpha \sim g_Z M_{Z'}^2/M_Z^2 \sim 10^{-58}$ – too small to be observable in neutrino oscillations, at least if we stick to $R_{\mathrm{A.U.}}$ range. Now to the crux of this model, the scalar sector. Even though we need more than one triplet for valid neutrino mixing angles, we will focus on one extra scalar field in the representation $\Delta \sim (1, 3, +2)(Y')$.

Since there cannot be any "trilinear" terms in the scalar potential, i.e. the term

$$V \supset \mu H_{\mathrm{SM}}^T i\sigma_2 \Delta^\dagger H_{\mathrm{SM}} \tag{3.88}$$

is not $U(1)_{L_\mu - L_\tau}$ gauge invariant, the only mass scales in the potential are the quadratic "mass-terms" (not necessarily positive), which are connected to the VEVs. The physical spectrum contains a light neutral scalar h_T with mass $m_{h_T}^2 = \lambda v_T^2$ (λ is just a combination of Yukawa couplings) and a coupling to the Z boson

$$\mathcal{L} \sim \frac{e}{s_W c_W} M_{Z'} Z'_\mu Z^\mu h_T\,. \tag{3.89}$$

Since $M_{Z'}, m_{h_T} \ll M_Z$, this opens up a decay channel $Z \to Z' h_T$ with a contribution to $\Gamma_{\mathrm{inv}}(Z)$ about 100-times higher than allowed, without any adjustable parameters. This problem is well known from Majoron models (spontaneously broken global lepton number) and usually cured by introducing the μ term (3.88). One could therefore try

[19] A notable exception is the Stückelberg model (see App. C), where no physical scalars occur and $M_{Z'}$ can be arbitrarily small. However, this model cannot accommodate a viable neutrino mass matrix.

to induce this term by introducing a scalar field S with the same Y' as Δ, and replace $\mu \to \langle S \rangle \equiv v_S$. Since μ will also contribute to $M_{Z'}$ we should make it small, i.e. $\mu \sim v_T$, resulting in a similar model as in Ref. [99], the crucial difference being the additional scalar $\mathrm{Re}\, S$. It turns out that the mass matrix for $\mathrm{Re}\, S$ and the real part of the neutral component of Δ, $\mathrm{Re}\, H_0$, looks like

$$\mathcal{M}^2_{\mathrm{Re}\, H_0, \mathrm{Re}\, S} \approx \frac{\lambda}{2} v^2_{\mathrm{SM}} \begin{pmatrix} v_S/v_T & -1 \\ -1 & v_T/v_S \end{pmatrix}, \tag{3.90}$$

resulting once again in a massless (or, at most, $m_h \sim v_T \ll M_Z$) physical scalar h that allows the decay $Z \to Z'h$. Triplet models are therefore quite though to realise and demand a large number of additional fields (also needed for a realistic neutrino mass matrix, as we will see in Sec. 5.1.4).

Similar complications arise in the doublet models, in this case because the term

$$V \supset m^2_{12} H^\dagger_{\mathrm{SM}} \phi\,, \tag{3.91}$$

which could push the scalar masses above M_Z, even for a light VEV $v_D = \langle \phi \rangle$, is not gauge invariant. Here, however, we can simply allow a higher VEV, and therefore scalar masses above M_Z, thus prohibiting the direct decay. So, we will take $v_D \sim 100\,\mathrm{GeV}$, resulting in $g' \lesssim 10^{-29}$ for $R_{\mathrm{A.U.}}$ range and α is once again $\sim 10^{-58}$. Earth-radius range $M_{Z'} \sim 10^{-14}\,\mathrm{eV}$ implies $g' \sim 10^{-25}$ and $\alpha \sim 10^{-50}$, in principle observable in neutrino oscillations (note that a force of shorter range is less restricted by experiments testing the equivalence principle). The Higgs sector with all masses and interactions is derived in Sec. 5.1.3; the potentially dangerous decay $Z \to Z'Z'Z'$ via virtual scalars now gives $\Gamma \sim 10^{-2}\,\mathrm{MeV}$, well within the errors of $\Gamma_{\mathrm{inv}}(Z)$.

Unfortunately, this $U(1)'$ breaking around the electroweak scale has no longer "naturally" small neutrino masses, like in the triplet model (even though in the model at hand we really should not bring up the topic of naturalness). This can be cured by the seesaw mechanism to a certain degree, but we end up with a $L_\mu - L_\tau$ symmetry breaking around the electroweak scale and therefore with perturbations of the $L_\mu - L_\tau$-symmetric neutrino matrix of the same order as the actual entries. The doublet model can therefore not explain the observed neutrino mixing angles in a natural way. We will see how this can be cured, by the addition of one singlet, in Sec. 5.5, which allows the doublet VEV to be as low as needed. In any case, the effective VEV of all $U(1)'$ charged scalars, $v^2_{\mathrm{eff}} = \sum_i Y'^2_i \langle \phi_i \rangle^2$, has to be around the electroweak scale in the simplest models, which would naturally generate a Z' mass of similar order.

Let this suffice as an overview over the possible problems one encounters when constructing a Higgs sector for such an ultralight gauge boson (we will see that some of the problems are also present for the heavy Z'). We conclude this section by stating, that neutrino oscillation experiments are not only sensitive to the coupling constant g' and the mixing parameters ξ and χ, but, for specific, mixing-inducing Higgs sectors, also to the mass of the Z', since $\alpha \sim g_Z M^2_{Z'}/M^2_Z$ for the simplest doublet/triplet models; inserting numbers we find that current experiments are sensitive to forces of $R_\oplus$ range, a lower mass induces not enough mixing for observable effects.

Experiment	Sensitivity to $\alpha/10^{-50}$ at 99.73% C.L.
T2K (ν-run)	11.8
T2K (full)	4.3
T2HK	1.7
SPL	7.5
NOνA	1.9
Combined Superbeams	1.4
Nufact	0.53

Table 3.5: Sensitivity of the different long-baseline experiments to α. Also given is the result of an analysis of all Superbeams combined.

3.9 Conclusion

In this chapter, we discussed the effects of an ultralight Z', coupling to first-generation particles only through mixing with the Standard Model Z boson. The most dominant bounds come from equivalence-principle experiments, strongly constraining long-range neutron-dependent forces and therefore our mixing angles, and Big Bang nucleosynthesis, limiting the allowed number of additional relativistic particles, which translates into a bound for the gauge coupling g'. Since the BBN constraint is more severe than the one from the anomalous magnetic moment of the muon, it is not possible to explain the measured deviation by the contribution of the ultralight Z'. Neutrino oscillations are influenced by the mixing-induced neutron potential generated by the Earth and/or the Sun in a similar vein as the usual MSW or NSI potentials, but not confined to matter, due to the long-range nature. This modifies oscillations mainly in the μ–τ sector, and gives strong constraints on the involved parameters (coupling constant times mixing angles). The most interesting new effect is an additional source of CP violation, resulting in different transition probabilities for neutrinos and antineutrinos. The size of the CP violation is not only linked to the potential $V_{L_\mu - L_\tau}$, but also to the neutrino mixing angles; it vanishes for tri-bimaximal mixing. We determined the necessary value for the potential to explain the MINOS anomaly; while the best-fit value is incompatible with atmospheric neutrino oscillations measured at Super-Kamiokande, allowed values could still improve the MINOS fit. Due to the implications of our model in the μ–τ sector, we have the opportunity to explore this model in future long-baseline neutrino oscillation experiments. A neutrino factory would have the strongest sensitivity, while in the near future the NOνA experiment could be twice as sensitive as T2K, due to the longer baseline (Tab. 3.5).

Chapter 4

The Physics of a Heavy Z'

Following the elaborate discussion of the ultralight Z', this chapter will provide an overview over a Z' boson with a mass in the electroweak range ($10 - 1000\,\mathrm{GeV}$). We will illustrate the indirect effects on precision observables and the direct detection possibilities at current colliders. Furthermore, we discuss the effect on neutrino oscillations, since this model gives an explicit realisation of NSI parameters. Eventually, we perform a χ^2-fit to a large amount of electroweak precision observables to find the allowed regions for $M_{Z'}/g'$ and $g' \sin\xi$.

4.1 Decay Width

Since we will need it later on, we will quickly derive the decay width of a massive vector boson, coupled to leptons via the interaction terms

$$\mathcal{L} \supset -g\overline{\psi}\gamma^\mu(g_V - g_A\gamma_5)\psi X_\mu\,. \tag{4.1}$$

The tree-level decay amplitude for $X(p,\lambda) \to \psi(k,s), \bar{\psi}(q,s')$ is then given by

$$i\mathcal{M} = \bar{\varepsilon}^\mu_\lambda(p)\bar{u}_s(k)\gamma_\mu(-ig)(g_V - g_A\gamma_5)v_{s'}(q)\,, \tag{4.2}$$

resulting in a spin-averaged squared amplitude

$$\begin{aligned}\langle|\mathcal{M}|^2\rangle &= \frac{1}{3}g^2\left(\sum_{\lambda=0,\pm1}\bar{\varepsilon}^\mu_\lambda\varepsilon^\nu_\lambda\right)\mathrm{tr}\left[(\not{k}+m)\gamma_\mu(g_V - g_A\gamma_5)(\not{q}-m)\gamma_\nu(g_V - g_A\gamma_5)\right]\\ &= \frac{4}{3}g^2M_X^2\left[g_V^2\left(1+\frac{2m^2}{M_X^2}\right)+g_A^2\left(1-\frac{4m^2}{M_X^2}\right)\right]\,,\end{aligned} \tag{4.3}$$

where the last line was equated in the centre of mass system. The total decay rate follows from an integration over the phase space:

$$\Gamma(X\to\psi\bar{\psi}) = \frac{g^2}{12\pi}M_X\sqrt{1-\frac{4m^2}{M_X^2}}\left[g_V^2\left(1+\frac{2m^2}{M_X^2}\right)+g_A^2\left(1-\frac{4m^2}{M_X^2}\right)\right]\,. \tag{4.4}$$

An unmixed $U(1)_{L_\mu - L_\tau}$ (no decays into quarks or electrons) has only vector couplings:

$$\begin{aligned}\Gamma(Z' \to \bar{\mu}\mu, \bar{\tau}\tau) &= \frac{g'^2}{12\pi} M_{Z'} \sqrt{1 - \frac{4m_{\mu,\tau}^2}{M_{Z'}^2}} \left(1 + \frac{2m_{\mu,\tau}^2}{M_{Z'}^2}\right), \\ \Gamma(Z' \to \bar{\nu}_\mu \nu_\mu, \bar{\nu}_\tau \nu_\tau) &\approx \frac{1}{2} \frac{g'^2}{12\pi} M_{Z'}\,,\end{aligned} \tag{4.5}$$

where the neutrino masses have been ignored.

4.2 Constraints on a Heavy Z'

We will now derive the constraints on a heavy Z' with mass $10\,\text{GeV} \lesssim M_{Z'} \lesssim 1\,\text{TeV}$. Taking M_2, g', ξ and χ as free parameters, we will derive bounds from the ρ parameter, the anomalous magnetic moment of the muon Δa_μ, NSI, and collider experiments. We will concentrate on the region $M_2 < M_{Z_{\text{SM}}}$, i.e. we try to construct a gauge boson lighter than Z (as opposed to the TeV Z' bosons most other models look for).

Electroweak Constraints Measurements around the Z pole examined the mass eigenstate Z_1 and its couplings to fermions. We recall the formulae from Sec. 2.2, in particular the change of the current-Vector interactions in the presence of mixing

$$\begin{aligned}&e j_{\text{EM}} A + \frac{e}{2 s_W c_W} j_{\text{NC}} Z + g' j' Z' \to \\ &\begin{pmatrix} e j_{\text{EM}} & \frac{e}{2\hat{s}_W \hat{c}_W} j_{\text{NC}} & g' j' \end{pmatrix} \begin{pmatrix} 1 & -\hat{c}_W \sin\xi \tan\chi & -\hat{c}_W \cos\xi \tan\chi \\ 0 & \cos\xi + \hat{s}_W \sin\xi \tan\chi & \hat{s}_W \cos\xi \tan\chi - \sin\xi \\ 0 & \frac{\sin\xi}{\cos\chi} & \frac{\cos\xi}{\cos\chi} \end{pmatrix} \begin{pmatrix} A \\ Z_1 \\ Z_2 \end{pmatrix},\end{aligned} \tag{4.6}$$

with the Weinberg angle from Eq. (2.25)

$$\frac{1}{\hat{s}_W \hat{c}_W} = \frac{1}{s_W c_W} \frac{\hat{M}_Z}{M_1} = \frac{1}{s_W c_W} \sqrt{1 + \sin^2\xi \left(\frac{M_2^2}{M_1^2} - 1\right)}. \tag{4.7}$$

Therefore the strength of the Z_1 coupling to fermions changes through mixing to (using already that the mixing angles χ and ξ need to be small to satisfy the constraints)

$$\frac{e}{2 s_W c_W} \to \frac{e}{2 s_W c_W} \left[1 + \frac{\xi^2}{2}\left(\frac{M_2^2}{M_1^2} - 1\right) + s_W \xi \chi\right] \equiv \frac{e}{2 s_W c_W} \left[1 + \frac{\alpha_{\text{EM}} T}{2}\right], \tag{4.8}$$

so the ρ parameter changes to

$$\rho \approx 1 + \alpha_{\text{EM}} T \approx 1 + 2 s_W \xi \chi - \xi^2 \left(1 - \frac{M_2^2}{M_1^2}\right). \tag{4.9}$$

The current value from a fit of the Standard Model parameters to experimental data is $\rho = 1.0008^{+0.0017}_{-0.0007}$ [22], the 3σ contours are shown in Fig. 4.1 (left). Since χ and ξ contribute with different signs, a non-zero χ weakens the bound. The vector and axial

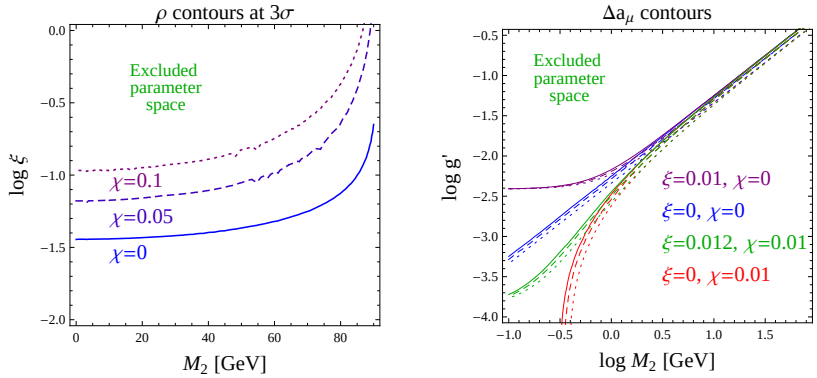

Figure 4.1: Left panel: ρ parameter contours (3σ) for values of the kinetic-mixing angle $\chi = 0$, 0.05 and 0.1. Right panel: Δa_μ contours for different values of ξ and χ. The solid, dashed and dotted lines represent the $\Delta a_\mu = 2 \times 10^{-9}$, 2.55×10^{-9} and 3×10^{-9} contours, respectively.

couplings of Z to the tauon change with g' to

$$g_V^\tau \to 2s_W^2 - \frac{1}{2} - 2\frac{s_W c_W}{e} g'\xi, \qquad g_A^\tau \to -\frac{1}{2}, \tag{4.10}$$

so the asymmetry parameter $A^\tau \equiv 2g_V^\tau g_A^\tau / ((g_V^\tau)^2 + (g_A^\tau)^2)$ becomes approximately

$$A^\tau \to A^\tau + A^\tau \frac{4 s_W c_W}{1 - 4s_W^2} \frac{g'\xi}{e} \equiv A^\tau + \Delta A^\tau(g'\xi)\,. \tag{4.11}$$

This quantity is measured to be $A^\tau = 0.143 \pm 0.004$ [22], while the SM expectation is $A^\tau = 0.1495$. The measured A^τ and A^μ are of the same order, while a non-zero $g'\xi$ shifts them in different directions, we will therefore require $\Delta A^\tau(g'\xi)$ to be within the measured error, i.e. $\Delta A^\tau(g'\xi) < 0.004$. At 3σ, this restricts $g'\xi$ to values

$$g'\xi < 1.1 \times 10^{-3}\,. \tag{4.12}$$

This limit is stronger than e.g. the coupling of Z to ν_μ or the ratio of the decay widths $\Gamma(Z \to \mu^+\mu^-)/\Gamma(Z \to e^+e^-)$, where

$$\Gamma(Z \to \ell\bar{\ell}) = \frac{\alpha_{\rm EM} M_Z}{12 s_W^2 c_W^2} \left((g_V^\ell)^2 + (g_A^\ell)^2 \right) \tag{4.13}$$

at tree-level, ignoring lepton masses (see Eq. (4.4) for the full expression and derivation).

Anomalous Magnetic Moment of the Muon As already mentioned in Sec. 3.4.3, in the unmixed case ($\xi = \chi = 0$), and for $M_{Z'} \gg m_\mu$, we have the Z' contribution to the anomalous magnetic moment of the muon:

$$\Delta a_\mu = \frac{g'^2}{4\pi} \frac{1}{3\pi} \frac{m_\mu^2}{M_2^2}\,, \tag{4.14}$$

so a constraint $\Delta a_\mu \lesssim 255 \times 10^{-11}$ corresponds to $g'/M_2[\text{GeV}] \lesssim 5.2 \times 10^{-3}$. From the inequality $M_2 \lesssim M_{Z'}$, and the expression $M_{Z'} = g'\sqrt{\sum_i Y_i'^2 v_i^2}$, we conclude

$$192\,\text{GeV} \lesssim \sqrt{\sum Y_i'^2 v_i^2}\,. \tag{4.15}$$

We should be more thorough though and include all the Z–Z' mixing terms. A chiral Z-like boson yields a one-loop contribution to the magnetic moment [100, 101]

$$a_\mu(Z-\text{like}) = -\frac{m_\mu^2 g^2}{8\pi^2 M_Z^2}\frac{2}{3}\left((C_L - C_R)^2 - C_L C_R\right)\,, \tag{4.16}$$

where $C_{L,R}$ denotes the coupling to $\mu_{L,R}$; a vector boson ($C_L = C_R$) gives a positive δa_μ. The Standard Model Z boson ($C_R = s_W^2, C_L = s_W^2 - 1/2$, and $g = e/s_W c_W$) contributes at one-loop:[1]

$$a_\mu^{\text{SM}}(Z) = -\frac{G_F m_\mu^2}{8\sqrt{2}\pi^2}\frac{1}{3}\left(5 - \left(1 - 4s_W^2\right)^2\right) \approx -1.94 \times 10^{-9}\,. \tag{4.17}$$

To calculate the real change of a_μ with Z', we subtract the Standard Model contribution $a_\mu^{\text{SM}}(Z)$ and add $a_\mu(Z_1) + a_\mu(Z_2)$ with the changed couplings and masses. Actually we should also consider the scalar interactions, but they turn out to be negligible in the Higgs sector we pursue in Ch. 5 (the one-singlet-one-doublet model, see discussion in Sec. 5.5). The couplings change to:

$$\begin{aligned}
gC_L(Z_1) &\to \frac{e}{\hat{s}_W\hat{c}_W}\left(-\frac{1}{2} + \hat{s}_W^2\right)(\cos\xi + \hat{s}_W \sin\xi\tan\chi) + g'\frac{\sin\xi}{\cos\chi} + e\hat{c}_W \sin\xi\tan\chi,\\
gC_R(Z_1) &\to \frac{e}{\hat{s}_W\hat{c}_W}\left(\hat{s}_W^2\right)(\cos\xi + \hat{s}_W \sin\xi\tan\chi) + g'\frac{\sin\xi}{\cos\chi} + e\hat{c}_W \sin\xi\tan\chi,\\
gC_L(Z_2) &\to g'\frac{\cos\xi}{\cos\chi} + \frac{e}{\hat{s}_W\hat{c}_W}\left(-\frac{1}{2} + \hat{s}_W^2\right)(\hat{s}_W\cos\xi\tan\chi - \sin\xi) + e\hat{c}_W\cos\xi\tan\chi,\\
gC_R(Z_2) &\to g'\frac{\cos\xi}{\cos\chi} + \frac{e}{\hat{s}_W\hat{c}_W}\left(\hat{s}_W^2\right)(\hat{s}_W\cos\xi\tan\chi - \sin\xi) + e\hat{c}_W\cos\xi\tan\chi\,.
\end{aligned} \tag{4.18}$$

We want to explain the measured Δa_μ and therefore set

$$(a_\mu(Z_1) - a_\mu^{\text{SM}}(Z)) + a_\mu(Z_2) \lesssim 255 \times 10^{-11}\,. \tag{4.19}$$

The Δa_μ bound is shown in Fig. 4.1 (right), the mixing angles are only important for small coupling g' and mass M_2. Diagrams similar to Fig. 3.5, but with Z instead of γ, lead to non-universal Z–ℓ couplings; the limits from LEP measurements are however weaker than those from Δa_μ [37].

[1] The $W^\pm$ bosons give the positive contribution $a_\mu^{\text{SM}}(W^\pm) = +\frac{G_F m_\mu^2}{8\sqrt{2}\pi^2}\,\frac{10}{3}$, making a_μ^{EW} positive.

4.2.1 Z'-Induced NSI

Non-standard neutrino interactions have been introduced in Sec. 1.3, here we will show how a heavy, non-universal gauge boson Z' induces NSI parameters $\varepsilon_{\alpha\beta}$. Limits on these parameters can be obtained by fitting atmospheric and solar neutrino oscillation data, as well as neutrino scattering experiments [94], but most of the limits are obtained assuming only one non-zero $\varepsilon^{fP}_{\alpha\beta}$ at a time [6, 5]. We will therefore use a limit from a two-neutrino fit to atmospheric and K2K data [102] (a very thorough analysis based only on Super-Kamiokande (I+II) data but with weaker constraints can be found in [103]). The used fit parameters in this case are $\varepsilon \equiv \varepsilon^{dL}_{\mu\tau} + \varepsilon^{dR}_{\mu\tau}$ and $\varepsilon' \equiv \varepsilon^{dL}_{\mu\mu} + \varepsilon^{dR}_{\mu\mu} - \varepsilon^{dL}_{\tau\tau} - \varepsilon^{dR}_{\tau\tau}$. Unfortunately, it is common to only consider the d-quark NSI as the neutrino travels through Earth, while we need a combined constraint on $\varepsilon^{e,d,u}$, because they are all connected in our model (see below). We will therefore translate the 90% C.L. bound[2]

$$|\varepsilon'| = |\varepsilon^{dV}_{\mu\mu} - \varepsilon^{dV}_{\tau\tau}| < \delta\varepsilon' = 0.029\,, \tag{4.20}$$

with $\varepsilon^V = \varepsilon^L + \varepsilon^R$, into the approximated Earth-like matter NSI constraint

$$|\varepsilon^{\oplus}_{\mu\mu} - \varepsilon^{\oplus}_{\tau\tau}| \equiv |(\varepsilon^{eV}_{\mu\mu} + 3\varepsilon^{uV}_{\mu\mu} + 3\varepsilon^{dV}_{\mu\mu}) - (\varepsilon^{eV}_{\tau\tau} + 3\varepsilon^{uV}_{\tau\tau} + 3\varepsilon^{dV}_{\tau\tau})| < 3\,\delta\varepsilon'\,, \tag{4.21}$$

basically just replacing $3\varepsilon^{dV}_{\mu\mu} \to \sum_f \frac{n_f}{n_e}\varepsilon^{fV}_{\mu\mu}$ in Earth-like matter.

We will now discuss NSI in the context of the gauged $U(1)_{L_\mu - L_\tau}$; in the case of a heavy Z' we can integrate it out to obtain an NSI operator. Using the full Z_2 Lagrangian from Eq. (2.21), we get

$$\begin{aligned}\mathcal{L}^{\text{eff}}_{Z_2} = \frac{-1}{M_2^2}\Bigg(& g'\frac{\cos\xi}{\cos\chi}j' - e\hat{c}_W\cos\xi\tan\chi j_{\text{EM}} \\ &+ \frac{e}{\hat{s}_W\hat{c}_W}(\hat{s}_W\cos\xi\tan\chi - \sin\xi)(j_3 - \hat{s}^2_W j_{\text{EM}})\Bigg)^2\,.\end{aligned} \tag{4.22}$$

The terms proportional to g'^2 do not involve e, u or d, and are therefore irrelevant for NSI. The terms without g' will be generation independent and can be ignored in neutrino oscillations. We are left with the terms linear in g' (generating the NSI parameters $\varepsilon_{\mu\mu}$ and $\varepsilon_{\tau\tau} = -\varepsilon_{\mu\mu}$) and read off the relation

$$2\sqrt{2}G_F\varepsilon^{fP}_{\mu\mu} = \frac{2}{M_2^2}\,g'\,\frac{\cos\xi}{\cos\chi}\,F^{fP}\,, \tag{4.23}$$

with $F^{fP} = \frac{e}{\hat{s}_W\hat{c}_W}(\hat{s}_W\cos\xi\tan\chi - \sin\xi)(T^f_3 - \hat{s}^2_W Q^f) - e\hat{c}_W\cos\xi\tan\chi Q^f$. Just like in the fifth-force case, the effect goes with g' times mixing angles and therefore vanishes in an unmixed scenario.

To get some numbers, we take $\chi \equiv 0$ and calculate the effective, Earth-like matter

[2] Since the NSI limits are obtained by fitting ε and ε' simultaneously, the limit on ε' alone should actually be a little bit stronger. This is because the fit favours a non-zero ε, so the χ^2 is larger if we do not marginalise over ε, but set it to zero. The effect is however rather small and does not justify a reanalysis.

NSI parameter to lowest order in ξ:

$$\begin{aligned}\varepsilon^{\oplus}_{\mu\mu} &= \varepsilon^{eV}_{\mu\mu} + 3\varepsilon^{uV}_{\mu\mu} + 3\varepsilon^{dV}_{\mu\mu} \\ &= \frac{1}{2}\frac{1}{\sqrt{2}G_F}\frac{e}{s_W c_W}\frac{g'}{M_2^2}\cos\xi\sin\xi \\ &\approx 217\, g'\cos\xi\sin\xi\left(\frac{10\,\mathrm{GeV}}{M_2}\right)^2 .\end{aligned} \tag{4.24}$$

This expression is constrained to be $< 3\delta\varepsilon'/2 \approx 0.044$ (since $\varepsilon^{\oplus}_{\tau\tau} = -\varepsilon^{\oplus}_{\mu\mu}$):

$$g'\cos\xi\sin\xi\left(\frac{10\,\mathrm{GeV}}{M_2}\right)^2 < 2.00\times 10^{-4} . \tag{4.25}$$

A full analysis should also take the modified Z couplings into account, i.e. integrate out Z_1, keep only the linear g' coupling and compare to Eq. (1.11). This gives the NSI parameters

$$\varepsilon^{fP}_{\mu\mu} = \frac{g'}{\sqrt{2}G_F\cos\chi}\left(\frac{\sin\xi}{M_1^2}F_1^{fP} + \frac{\cos\xi}{M_2^2}F_2^{fP}\right) \tag{4.26}$$

with the couplings

$$\begin{aligned}F_1^{fP} &= \frac{e}{\hat{s}_W\hat{c}_W}(\hat{s}_W\sin\xi\tan\chi + \cos\xi)(T_3^f - \hat{s}_W^2 Q^f) - e\hat{c}_W\sin\xi\tan\chi\, Q^f , \\ F_2^{fP} &= \frac{e}{\hat{s}_W\hat{c}_W}(\hat{s}_W\cos\xi\tan\chi - \sin\xi)(T_3^f - \hat{s}_W^2 Q^f) - e\hat{c}_W\cos\xi\tan\chi\, Q^f .\end{aligned} \tag{4.27}$$

The summation over f and P for the effective Earth parameter $\varepsilon^{\oplus}_{\mu\mu}$ only leaves the T_3^e term because the Earth is neutral and the up- and down-quark belong to the same doublet, i.e. $T_3^u + T_3^d = 0$. The expression simplifies to

$$\varepsilon^{\oplus}_{\mu\mu} = \frac{-g'}{2\sqrt{2}G_F\cos\chi}\frac{e}{\hat{s}_W\hat{c}_W}\left[\cos\xi\sin\xi\left(\frac{1}{M_1^2} - \frac{1}{M_2^2}\right) + \hat{s}_W\tan\chi\left(\frac{\sin^2\xi}{M_1^2} + \frac{\cos^2\xi}{M_2^2}\right)\right] , \tag{4.28}$$

which is dominated by the $1/M_2^2$ terms; expanding in small mixing angles gives $\varepsilon^{\oplus}_{\mu\mu} \sim (\delta\hat{M}^2 + s_W\hat{M}^2_{Z'}\chi)/\hat{M}^2_Z$ (totally analogous to the α parameter in the fifth force case). The constraint from the NSI parameter $\varepsilon^{\oplus}_{\mu\mu}$ is shown in Fig. 4.2 (left) for different values of χ and ξ. A non-zero χ weakens the bound since it contributes with an opposite sign to the $1/M_2^2$ term. We show the mass range starting at $M_2 = 1\,\mathrm{GeV}$, one has to be careful though since for such low masses it might not be valid to integrate out the Z' to obtain the NSI parameter.

Also shown in Fig. 4.2 (right) is the NSI constraint for $\chi = 0$ together with the bound from Δa_μ (only weakly dependent on ξ). To explain the anomalous magnetic moment of the muon, one needs to choose parameter values around the green band. The qualitative behaviour of the contours is obvious from Eq. (4.14) and Eq. (4.24), which give $\Delta a_\mu \sim g'^2/M_2^2$ and $\varepsilon^{\oplus}_{\mu\mu} \sim \xi g'/M_2^2$, resulting in the different slopes in the

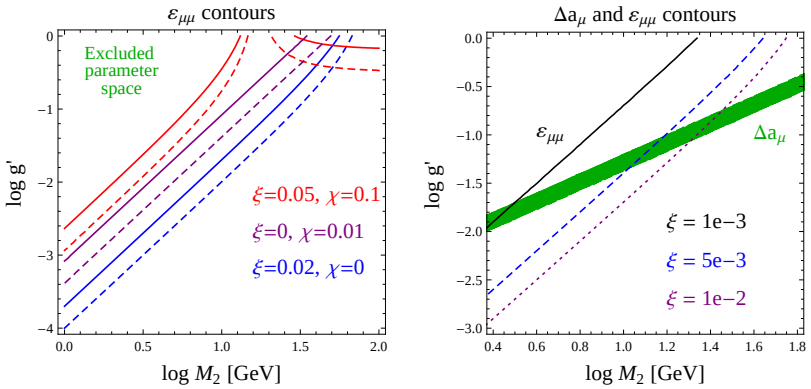

Figure 4.2: Left panel: Constraint from the NSI parameter $|\varepsilon^{\oplus}_{\mu\mu}|$ for different values of χ and ξ. The dashed line corresponds to the 90% C.L. bound, the solid line is twice that value, so the allowed parameter space is below the curves. Right panel: Some $|\varepsilon^{\oplus}_{\mu\mu}|$ contours (90% C.L.) for $\chi = 0$; the green band shows the parameter space that resolves Δa_μ.

double-logarithmic plot. This explicit realisation of NSI parameters does not suffer from charged-lepton flavour-violating (LFV) decays, which typically give stronger constraints on NSI if one takes into account one-loop effects [94]. The absence of LFV is rooted in the diagonal structure of the NSI parameters $\varepsilon_{\alpha\beta}$ in flavour space, as imposed by our symmetry. Consequently, LFV will enter into our model via the symmetry breaking sector. This will be discussed in Ch. 5 for a number of specific Higgs models. The LFV bounds typically constrain Yukawa couplings and do not change our above discussion of the NSI.

4.2.2 Collider Searches

For $m_\tau \ll M_2 < M_{Z^0}$, the decay width of the Z' is approximately (see Sec. 4.1)

$$\Gamma(Z' \to \bar{\mu}\mu, \bar{\tau}\tau, \bar{\nu}_\mu\nu_\mu, \bar{\nu}_\tau\nu_\tau) \approx \frac{3g'^2}{12\pi} M_{Z'} = \frac{3g'^3}{12\pi} v_{\text{eff}} \,, \tag{4.29}$$

where we ignored the decay channels into other particles, such as quarks, since they would be proportional to mixing angles; the decay into or via Higgs particles will be ignored since we assume the scalars to be heavy, we will come back to that later on in the discussion of the Higgs sector. For $v_{\text{eff}} = 192\,\text{GeV}$ this equates to $\Gamma(Z') \approx g'^3\, 15.3\,\text{GeV}$.

Since current colliders work with first-generation particles in their beams, the cross sections for $\sigma(\bar{p}p, e^+e^- \to Z') \times \text{BR}(Z' \to \mu^+\mu^-)$ will be proportional to $(g_{\text{EW,EM}}\xi)^2 g'^2$, instead of $g^4_{Z'}$ as in generation-independent Z' models. Collider bounds can be satisfied by making the cross section small ($g'\xi$ small) or the width of Z' small so to make it fit into a gap between data points (g' small for fixed VEV). The most promising process for non-zero mixing would be the s-channel resonance $e^+e^- \to Z'^* \to \mu^+\mu^-, \tau^+\tau^-$, because these interactions are the lowest order in the mixing angle $\sin\xi$.

Collider data for the process $e^-e^+ \to \mu^-\mu^+$, in the range $\sqrt{s} = 14 - 207\,\text{GeV}$, from Petra [104], Tristan [105] and LEP [106, 107, 108], is shown in Fig. 4.3; also shown are the SM prediction, and some examples for the case of non-zero mixing. Even for

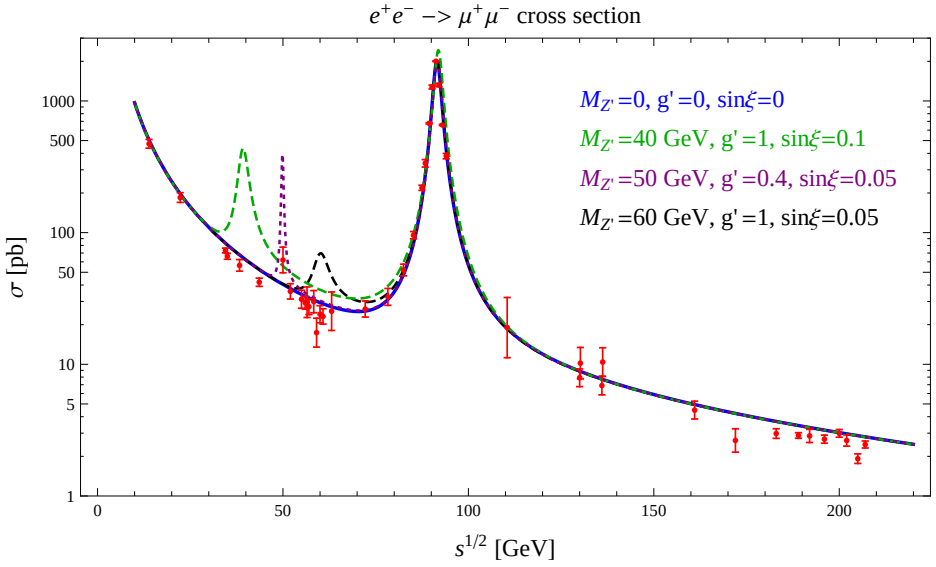

Figure 4.3: Total cross section $\sigma(e^+e^- \to \mu^+\mu^-)$ for different values of $\hat{M}_{Z'}$, g' and $\sin\xi$. Data points from Petra, Tristan and LEP.

small mixing $\sin\xi$, as to not influence the Z_{SM} pole too much, we can have sizable cross sections from Z'. We will however not take the possibility of a very narrow Z' seriously, i.e. we do not attempt to perform a χ^2-analysis on the data.

In higher order, but still at tree-level, processes like

$$e^+e^- \to Z^*, \gamma^* \to \mu\mu^* \to \mu\mu Z'^* \to \mu^+\mu^-\mu^+\mu^-,\ \mu^+\mu^-\tau^+\tau^- \tag{4.30}$$

can constrain the Z' even in the unmixed case $\xi = \chi = 0$. The Feynman diagram of this process is shown in Fig. 4.4 (omitting the possible neutrino final states). An analysis of these final states around the Z pole has been performed by the ALEPH collaboration at LEP [109]. The authors calculated the Standard Model prediction of 20.0 ± 0.6 4μ and 12.9 ± 0.4 $2\mu 2\tau$ events, against the measured 20 and 15, respectively.

$\sqrt{s}$ [GeV]	88.361	89.419	90.218	91.234	92.078	93.020	93.928
L [pb^{-1}]	1.34	10.15	1.42	52.68	1.45	10.49	1.52
σ_{SM} [pb]	0.0433	0.0819	0.149	0.239	0.158	0.0771	0.0442

Table 4.1: ALEPH data [109] and our calculated cross sections for $e^+e^- \to \mu^+\mu^-\mu^+\mu^-$ via the Standard Model particles Z and γ.

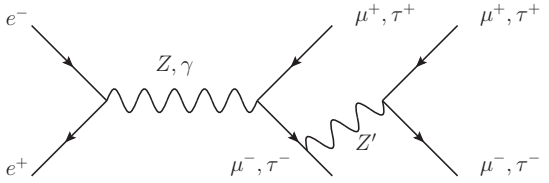

Figure 4.4: Electron-positron scattering process with an unmixed Z'.

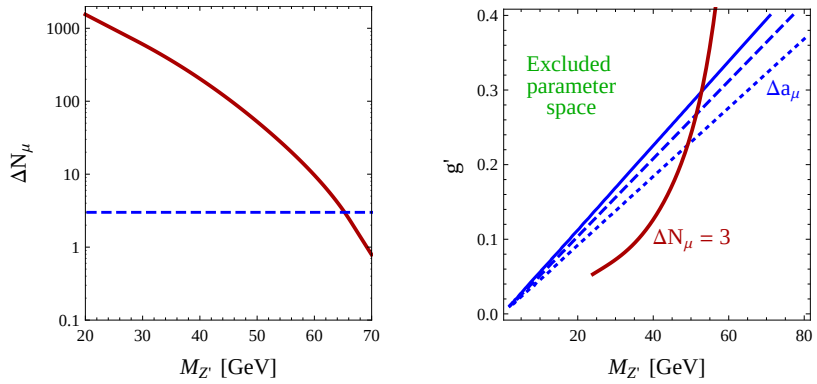

Figure 4.5: Left panel: Number of additional 4μ events in e^+e^- collisions in the presence of Z' (with $g' = 1$, $\xi = \chi = 0$). The dashed blue line marks the 95% C.L. limit $\Delta N_\mu = 3$. Right panel: Corresponding $\Delta N_\mu = 3$ exclusion limit in the $M_{Z'}$–g' plane together with the Δa_μ contours.

Since the 4μ final state gives the strongest bounds, we will only consider this process, following the analysis of Ma et al. [37]. The integrated luminosities at the energies around the Z pole are given in Tab. 4.1, together with our calculated Standard Model cross section for this process. We excluded diagrams involving the Higgs boson since the contribution to the cross section is several orders of magnitude smaller than that of the Z and γ (small Yukawa couplings compared to gauge couplings and no Higgs resonance since $m_H \gtrsim 114\,\text{GeV} > \sqrt{s}$). The calculation of the tree-level cross sections has been performed with the program CompHEP [110, 111], which uses Monte Carlo integration[3] for the 4-particle phase space; we implemented the cuts for the transverse momentum of the final muons $p_T > 3\,\text{GeV}$, necessary for muon identification. Since this calculation is less sophisticated than the one performed by ALEPH and we furthermore do not have the proper cuts and detector efficiencies ε_i at all 7 energies, we will approximate the additional number of muon events through Z' via

$$\Delta N_\mu = \sum_i \varepsilon_i \times \sigma_{Z'}(s_i) \times L(s_i) \approx \frac{20.0}{\sum_j \sigma_{\text{SM}}(s_j) \times L(s_j)} \sum_i \sigma_{Z'}(s_i) \times L(s_i)\,. \quad (4.31)$$

Here, $\sigma_{Z'} \equiv \sigma_{\text{SM}+Z'} - \sigma_{\text{SM}}$ denotes the effect of Z' on the cross section, including interference terms. The ALEPH collaboration also gave the distribution of the invariant mass of $\mu^+\mu^-$ and e^+e^- final-state pairs and found no events with mass $> 24\,\text{GeV}$, in agreement with the Monte Carlo simulation. The additional Z' contribution with $24\,\text{GeV} < M_{Z'} < \sqrt{s}$ will generate events in this invariant-mass range differing from zero. According to the Poisson distribution, we will set the 95% C.L. at 3 additional events. The range below 24 GeV will not be considered here.

We used the values $\xi = \chi = 0$ and, in Fig. 4.5 (left), $g' = 1$ for a plot against the Z' mass, resulting in a limit $M_{Z'} > 65\,\text{GeV}$. The corresponding contour in the $M_{Z'}$–g' plane is shown in Fig. 4.5 (right), together with the limits from the anomalous magnetic moment Δa_μ.

[3]The MC integration causes a statistical error on the cross section that was kept below 1% through enlargement of samplings and iterations.

This should improve the analysis of Ref. [37], which was based only on the dominant Feynman-diagram $ee \to Z^* \to \mu\mu Z'$ with the subsequent decay $Z' \to \mu\mu$ in the narrow width approximation. The results including interference and full width differ only slightly, showing how good the cross section is described by the process $ee \to Z^* \to \mu\mu Z'$. Since the narrow width approximation is based on $\Gamma \sim g'^2 M_{Z'} \ll M_{Z'}$ our calculation should improve the behaviour at large g', which is unfortunately the already excluded region.

In any case, the constraints from this process are not that much stronger than those from Δa_μ; however, taking the viewpoint that the Z' should explain the anomalous Δa_μ (i.e. the parameter space is reduced to the dashed blue line in Fig. 4.5 (right)), we extract the constraint $M_{Z'} \gtrsim 51\,\text{GeV}$.

An analysis with a larger data sample would be very interesting since it offers for $M_{Z'} \leq \sqrt{s}$ the possibility to find the Breit-Wigner resonance peak in the invariant mass distribution of any $\mu^-\mu^+$ pair. The discovery limits at future linear colliders (e^+e^- at $\sqrt{s} = 500, 1000\,\text{GeV}$) and the LHC have been derived in Ref. [37], following again the narrow-width approach. Since our more elaborate analyses will only marginally change these results, we will restrain from a reevaluation. The four muon final state is particularly interesting at the LHC, since it also constitutes the so-called "gold plated channel" for Higgs discovery $h \to ZZ \to 4\mu$, and will therefore be carefully analysed [112].

4.3 Z' Above 100 GeV

We will now briefly discuss the constraints for $M_2 > M_1$, i.e. the light mass eigenstate is now the mainly Z_{SM} one. The ρ parameter is in that case ≥ 1, we show the $1 - 3\sigma$ contours in Fig. 4.6 (right), together with direct detection constraints from Tevatron.

To explain Δa_μ, while still in the perturbative range $g' \sim 1$, we need $\hat{M}_{Z'} \approx 190\,\text{GeV}$. Tauon coupling then constrains the mixing to $\delta\hat{M} < 3\,\text{GeV}$ for $\chi = 0$, or $\chi < 2 \times 10^{-3}$ for $\delta\hat{M} = 0$.

This scenario is also constrained by direct detection measurements, e.g. at the Fermilab Tevatron collider. With first-generation particles in the initial state, we should look at least for final muon or tauon states, to make the combined Z' coupling as big as possible. Since tauons are harder to identify at hadron colliders, the dimuon final state is the better choice. Such a dimuon final state has been analysed by the DØ collaboration at Tevatron (very detailed in Ref. [113] on $L = 0.17\,\text{fb}^{-1}$ of integrated luminosity and shortly thereafter for $L = 0.25\,\text{fb}^{-1}$ (still preliminary [114])) and more recently by the CDF collaboration [115, 116] (on $4.6\,\text{fb}^{-1}$ of data). The limits are given on the cross section $\sigma^\mu \equiv \sigma(p\bar{p} \to Z') \times \text{BR}(Z' \to \mu\bar{\mu})$ against the invariant mass of the final muon pair, corresponding to the mass of the Z' in the s-channel process $p\bar{p} \to Z'^* X \to \mu\bar{\mu}X$. To arrive at the theoretical expression, we use the approximations from Ref. [8], namely a narrow width Z' resonance, approximated structure functions for the quarks and, most importantly, subdominant mixing effects, i.e. we only include the mixing via the Z' coupling to quarks (since otherwise the Z' decouples completely).

This leads to the cross section

$$\sigma^\mu \equiv \sigma(p\bar{p} \to Z') \times \mathrm{BR}(Z' \to \mu\bar{\mu}) \approx \frac{1}{s}\, c_{Z'}\, C \exp\left(-AM_{Z'}/\sqrt{s}\right) , \tag{4.32}$$

where $c_{Z'}$ contains the information about the Z' couplings:

$$c_{Z'} = \frac{4\pi^2}{3}\frac{\Gamma_{Z'}}{M_{Z'}}\mathrm{BR}(Z' \to \mu\bar{\mu})\left(\mathrm{BR}(Z' \to u\bar{u}) + \frac{1}{C_{ud}}\mathrm{BR}(Z' \to d\bar{d})\right) . \tag{4.33}$$

The other parameters are for proton-antiproton collisions given by $A = 20, C = 300$ and $C_{ud} = 25$ [8].

The total number of produced muon pairs by this process is $N_\mu = \sigma^\mu L$, typical cross sections and luminosities result in $\mathcal{O}(1-10)$ relevant signals. We will for simplicity only consider $\chi = 0$, so the coupling of Z_2 to quarks leads to the decay rates

$$\Gamma(Z' \to q\bar{q}) \approx N_c \left(\frac{e\sin\xi}{2s_W c_W}\right)^2 \frac{M_{Z'}}{12\pi}\left(g_V^2(q) + g_A^2(q)\right) , \tag{4.34}$$

where $g_{V,A}$ are the usual Z_{SM} couplings:

$$g_V(u) = \frac{1}{2} - \frac{4}{3}s_W^2, \qquad g_A(u) = \frac{1}{2}, \tag{4.35}$$

$$g_V(d) = -\frac{1}{2} + \frac{2}{3}s_W^2, \qquad g_A(d) = -\frac{1}{2}, \tag{4.36}$$

and $N_c = 3$ counts the different colours of the quarks. For small mixing, the Z' boson decays mainly in μ, τ, ν_μ and ν_τ, so we approximate $\Gamma_{Z'} \approx g'^2 M_{Z'}/4\pi$ and $\mathrm{BR}(Z' \to \mu\mu) = 1/3$. We will also approximate the leading order QCD corrections via $K \approx 1 + \frac{\alpha_s}{2\pi}\frac{4}{3}(1 + \frac{4}{3}\pi^2) \approx 1.3$. This leads to

$$\sigma^\mu \approx \frac{100\pi}{3}K\left(\frac{e\sin\xi}{2s_W c_W}\right)^2\left(g_V^2(u) + g_A^2(u) + \frac{g_V^2(d)}{25} + \frac{g_A^2(d)}{25}\right)\frac{e^{-20M_{Z'}/\sqrt{s}}}{s} . \tag{4.37}$$

Surprisingly, the coupling constants g' cancel each other, because mixing introduces a branching ratio $\mathrm{BR}(Z' \to q\bar{q}) \sim \sin^2\xi/g'^2$, instead of just a number. This leaves us with a formula only dependent on $M_{Z'}$ and $\sin\xi$.[4] The above mentioned DØ results from $p\bar{p}$ collisions at an energy $\sqrt{s} = 1.96\,\mathrm{TeV}$ are shown in Fig. 4.6 (left), the corresponding 95% C.L. exclusion contour in the $M_{Z'}$–$\sin\xi$ plane in Fig. 4.6 (right). The limits are not particularly strong.

The more recent analysis by the CDF collaboration is also shown in Fig. 4.6, yielding, of course, stronger bounds. At $M_{Z'} \approx 200\,\mathrm{GeV}$ we get $\sin\xi \lesssim 0.03$, corresponding roughly to $\delta\hat{M} \lesssim 30\,\mathrm{GeV}$. In any way, the precision results obtained from measurements around the Z pole will give stronger limits than direct detection because of better statistics, as can be seen in Fig. 4.6 (right). The approximations we used for the cross section become more accurate for higher $M_{Z'}$, where however the constraints weaken.

[4] Due to all the other approximations, it does not really matter if we take $\hat{M}_{Z'}$ or M_2, the difference is negligible for $\sin\xi \lesssim 0.1$.

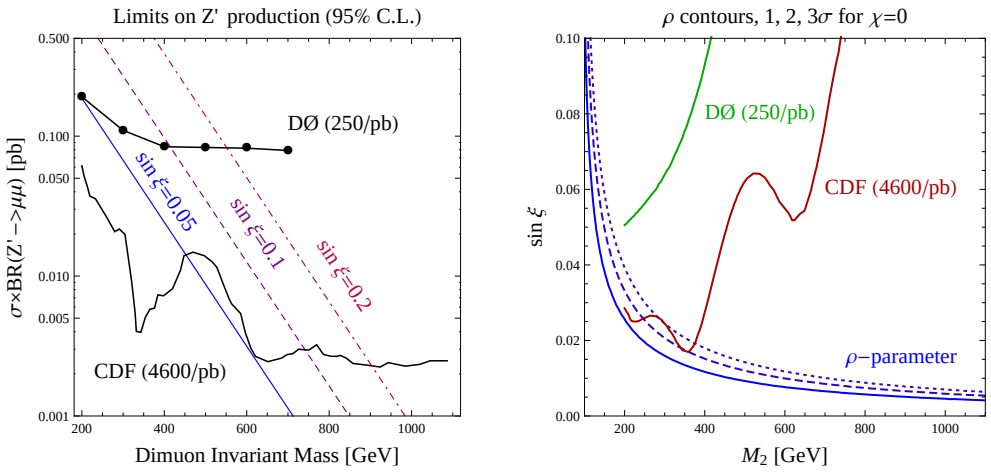

Figure 4.6: Left panel: 95% C.L. limits for $\sigma \times \mathrm{BR}(Z' \to \mu\mu)$ from DØ and CDF, for different values of the mixing angle ξ (with $\chi = 0$). Right panel: The corresponding 95% C.L. exclusion limit in the $M_{Z'}$–$\sin\xi$ plane, together with the stronger indirect $1 - 3\sigma$ constraints from the ρ parameter. The region above the curves is excluded.

The range $M_{Z_{\mathrm{SM}}} < M_{Z'} < 200\,\mathrm{GeV}$ has been probed by LEP II, the corresponding $e^+e^- \to \mu^+\mu^-$ cross section is already shown in Fig. 4.3. Just like in the $M_{Z'} < M_{Z_{\mathrm{SM}}}$ case, we will not analyse this data, since it would only yield the obvious narrow-width peaks in the gaps between data points.

4.4 A Fit to Electroweak Precision Data

Using a recent version (April 2010) of the Fortran program GAPP (Global Analysis of Particle Properties) [117, 118], kindly provided by Jens Erler, we can fit the $U(1)_{L_\mu - L_\tau}$ model, with a mass around the electroweak scale, to a vast amount of electroweak precision data (listed in App. G), including radiative corrections of the Standard Model. For simplicity, we set the kinetic-mixing angle to zero and leave the Higgs sector unspecified. The implemented analysis assumes $M_{Z'} > M_Z$, so the interpretation of the results is tricky; in particular we performed all fits with the fixed coupling constant $g' \equiv 1$, and extrapolated the bounds using the scaling $M_{Z'} \to M_{Z'}/g'$ and $\sin\xi \to g' \sin\xi$ (which is the usual approach [7]). The reasoning is as follows and only valid for $\sin\xi \ll g'$: We have already seen in the NSI discussion in Sec. 4.2.1, how integrating out the Z_2 gives effective interactions $\mathcal{L}^{\mathrm{eff}}_{Z_2} = -g'^2/M_2^2\, j'^\mu j'_\mu + \mathcal{O}(g'\xi, \xi^2)$, while the Z_1 coupling to j_{NC} gets an additional term $\sim g' \sin\xi j'$ (Eq. (4.6)). We keep this term, but not the Z_2 term of order $g'\xi$, since it is further suppressed by $1/M_2^2$ and we assumed $M_1 < M_2$. Since these are the two lowest order processes one has to take into account for measurements around the Z_1 pole, it is indeed valid to restrict the analysis to $g' = 1$, and rescale afterwards. We checked this scaling law explicitly for several values of g' in the range $0.1 - 3$.

As fit parameters, we used the conventional set of masses (Z, Higgs, top-, bottom- and charm-quark) and couplings (strong coupling constant α_s and the radiative con-

	SM	SM+Z'
M_Z [GeV]	91.1877	91.1877
m_t [GeV]	164.0	164.0
m_b [GeV]	4.199	4.200
m_c [GeV]	1.270	1.278
α_s	0.1183	0.1185
$\Delta\alpha^{(3)}_{\text{had}}(1.8\,\text{GeV})$	5.75×10^{-3}	5.72×10^{-3}
m_H [GeV]	114.4	114.4
$M_{Z'}/g'$ [GeV]	–	219.6
$g' \sin(\xi)$	–	-2.5×10^{-4}
$\chi^2_{\text{min}}/N_{\text{dof}}$	43.8/44	36.4/42

Table 4.2: Fit parameters and their best-fit values in an analysis with/without Z'. The masses denote pole masses.

tribution of the lightest three quarks to the QED coupling constant $\Delta\alpha^{(3)}_{\text{had}}$ [5]), listed in Tab. 4.2. We also enforced the direct 95% C.L. exclusion limit $m_H > 114.4\,\text{GeV}$ given by LEP; since a Higgs mass $\sim 90\,\text{GeV}$ is favoured by an unconstrained fit, m_H lies at its lower bound. The results of our SM fit differ only slightly from those given by the PDG [22] (well within a standard deviation), which are also based on GAPP and give a $\chi^2_{\text{min}}/N_{\text{dof}} = 43.0/44$, not imposing the lower Higgs bound.[6] Except for $M_{Z'}$ and $\sin\xi$, we will not bother calculating the errors on the best-fit values, since they are not of interest here.

The best-fit values for the SM parameters hardly change with the addition of the Z'. As can be seen, the χ^2 reduces by 7.4 units with the addition of the two effective parameters $M_{Z'}/g'$ and $g' \sin\xi$, a significant improvement. Marginalising over $\sin\xi$ we can visualise the narrowness of the χ^2-minimum (Fig. 4.7).

In Fig. 4.8 we show the contours $\Delta\chi^2 = 2.30$, 4.61 and 9.21, corresponding to 68.27%, 90% and 99% C.L. for 2 parameters. The best-fit value at $g' \sin\xi = -2.5 \times 10^{-4}$ and $M_{Z'}/g' = 219.6\,\text{GeV}$ is shown as well.

As can be seen, there is a preferred area for a Z' around $M_{Z'}/g' = 200 - 300\,\text{GeV}$,

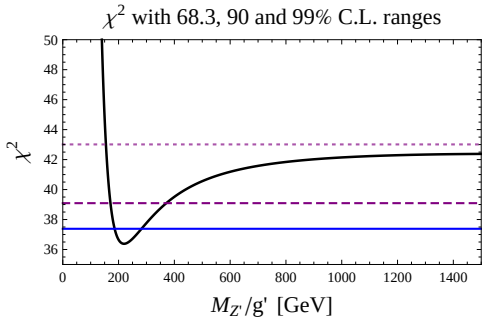

Figure 4.7: χ^2 as a function of $M_{Z'}/g'$, marginalised over $\sin\xi$.

[5] Contributing to the on-shell coupling via $\alpha(M_Z) = \alpha/[1 - \Delta\alpha(M_Z)]$.
[6] Without the lower Higgs bound, we obtain $\chi^2_{\text{min}}/N_{\text{dof}} = 43.0/44$ for the Standard Model fit as well.

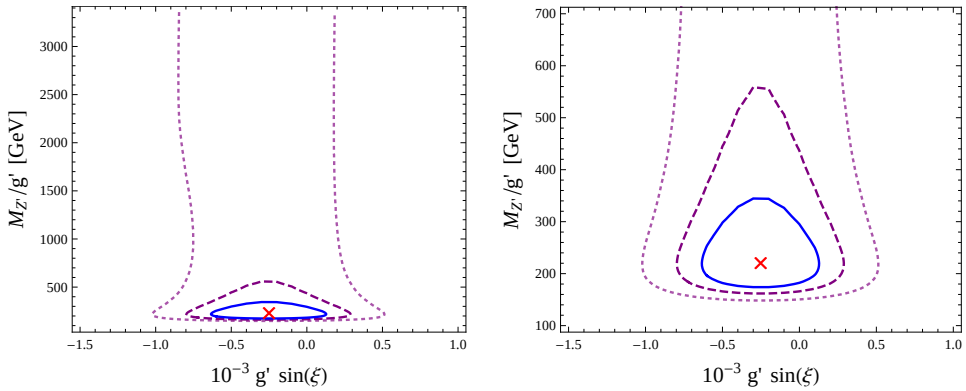

Figure 4.8: χ^2 contours (68.27%, 90% and 99% C.L.) in the $M_{Z'}$–$\sin\xi$ plane.

mainly constrained by Δa_μ.

The reason for the difference between the best-fit value $M_{Z'}/g' \approx 220\,\text{GeV}$ obtained here and the one based only on Δa_μ in Sec. 4.2 ($M_{Z'}/g' \approx 190\,\text{GeV}$) is just the proper treatment of the error on Δa_μ (about 25%) in GAPP, while we ignored it previously. Consequently, our previous value lies well within the 1σ range of the GAPP result. It is interesting to note that the best-fit values suggest the possibility that the $U(1)'$ and the $SU(2)_L \times U(1)_Y$ breaking coincide, implying an additional symmetry in the Higgs sector. However, since $M_{Z'}/g'$ is in general not a single VEV, but rather $M_{Z'}/g' = \sqrt{\sum Y_i'^2 v_i^2}$, this only works for one scalar with the charge $Y' = \pm 1$. Since the one-doublet and one-triplet models are excluded, a breaking scale $v_S = v_{\text{EW}}$ is only possible with one scalar singlet $S_{\pm 1}$, which however gives wrong neutrino oscillation angles (Sec. 5.1.2).

Performing a separate minimisation for each of the parameters (marginalising over the others), we derive the 90% C.L. bounds:

$$\begin{aligned} 160\,\text{GeV} \lesssim M_{Z'}/g' \lesssim 560\,\text{GeV}\,, \\ -0.0008 < g' \sin\xi < +0.0003\,. \end{aligned} \tag{4.38}$$

Keeping these values fixed we can calculate the induced NSI parameter $\varepsilon^{\oplus}_{\mu\mu}$, as a function of g'.[7] Since parts of the above analysis are based on $M_{Z'} \gg M_Z$ we restrict $g' \gtrsim 0.4$; over the 90% C.L. ranges this yields values for $\varepsilon^{\oplus}_{\mu\mu}$ roughly ~ 100-times smaller than the current upper limit, i.e. not observable in neutrino oscillations any time soon.

Ignoring the constraint $M_{Z'} \gg M_Z$, we need to take the direct-detection limit $M_{Z'} > 51\,\text{GeV}$ from ALEPH (Sec. 4.2.2) into account. The largest NSI value allowed by the conditions (4.38) is then a factor of 10 below the current limit.

Analysis Without Δa_μ To underline the importance of Δa_μ in the previous fit, we calculated the χ^2 without the Δa_μ terms. Not surprisingly, the mass constraint stems solely from Δa_μ. Since we only needed $M_{Z'} \gg m_\mu$ in the analysis for Δa_μ, our constraint (4.38) should be valid irrespective of $M_{Z'} > M_Z$, so g' can be arbitrarily small.

[7] While NSI based on neutrino oscillations were not part of the analysis, the different couplings of Z to muons and tauons (and their neutrinos) were, resulting in a similar constraint on $g' \sin\xi$.

4.5 Muon Collider

In this section we will briefly discuss the discovery potential of a future muon collider for our model. A muon collider would provide a nice framework to study the SM and its extensions, since it uses elementary particles in the initial state (as opposed to proton colliders which have to deal with large QCD backgrounds), and can reach high energies due to low bremsstrahlung effects (as opposed to an electron collider). It is under discussion as a Higgs factory [119], making use of the higher Yukawa coupling of the muon compared to the electron ($g_{H\mu\mu}/g_{Hee} \sim 200$), which allows sizable production of a Higgs particle in the s-channel, ideal for precision measurements of its mass and width.

A muon collider allows for the detection of an unmixed Z', since the processes $\mu\mu \to \mu\mu, \tau\tau$ include an s-channel contribution from Z', resulting in a Breit-Wigner resonance peak in the invariant mass of the final state (in complete analogy to the Z peak in e^+e^- collisions at LEP). If a fixed energy $\sqrt{s}$ is used (e.g. tuned to the Higgs mass, if by then discovered at the LHC) the cleanest observation would be in a final state $\mu^+\mu^- X$, so energy can be properly distributed to X when the invariant mass $M(\mu^+\mu^-)$ is clustered around M_Z and $M_{Z'}$. For sizable coupling g', this allows a unique direct detection for masses $M_{Z'} \leq \sqrt{s}$. A mass above $\sqrt{s}$ still gives indirect signals, visible, for example, in the a higher number of $\tau\tau$ final states compared to ee.

Detecting the $M_{Z'}$ peak and its width would then give insides into the symmetry breaking sector of the $U(1)'$, e.g. by scalar contributions to the invisible width. In a similar vein, a measurement around the SM Higgs resonance would provide an accurate measurement of its Yukawa couplings to fermions, making it possible to discriminate different extensions of the Higgs sector that change these couplings through mixing effects (such as 2HDM-Types, see App. F).

The fact that the heavy right-handed neutrinos can be charged (see Sec. 2.1) under the extended gauge group $G_{\text{SM}} \times U(1)'$ allows for the direct production via Z'. For low N_i masses, the process $\mu\bar{\mu} \to Z' \to N_i\bar{N}_i$, with subsequent N_i decay into light neutrinos and scalars, could be probed (very challenging). This is similar to the discussion in Ref. [120], where the mediator to the heavy neutrino sector is the neutral gauge boson of the $U(1)_{B-L}$. N_1, being the only true singlet of the extended gauge group, can not be produced in this manner.

4.6 Conclusion

In this chapter, we discussed the breaking of $U(1)_{L_\mu - L_\tau}$ in the range $10 - 1000$ GeV, most naturally connected to a Z' with mass of similar order. We visualised some indirect constraints on the heavy-Z' model, and mentioned direct detection possibilities at current colliders. A fit of the model parameters to electroweak data improves the usual Standard Model fit by 7.4 units, mainly due to the resolved magnetic-moment anomaly of the muon. The preferred model parameters $160\,\text{GeV} \lesssim M_{Z'}/g' \lesssim 560\,\text{GeV}$, together with the direct-detection limit $M_{Z'} > 51\,\text{GeV}$, can only result in small NSI effects, so the most promissing detection experiments are current colliders and of course improved

measurements/calculations of the muon's anomalous magnetic moment. We make the obvious observation that the nicest way to probe this model would be an expensive muon collider.

Chapter 5

The Scalar Sector

To complete our model, we will now investigate several symmetry-breaking sectors and their imprint on the neutrino mass matrix. We discuss the interactions of the various scalar particles arising from spontaneously breaking the $U(1)'$ symmetry. Even though we will construct the model for a heavy Z', many results can be applied to the fifth-force case as well, simply by choosing $g' \ll 1$, and maybe lowering the $U(1)'$-breaking VEVs.

In the following (and actually everywhere else), the terms singlet, doublet and triplet only denote the representations of (complex) dimension 1, 2 and 3 under the $SU(2)_L$; consequently, even "singlets" can still be charged under $SU(3)_C \times U(1)_Y \times U(1)'$. We will choose all scalars to be in the trivial representation of $SU(3)_C$. In order to construct an electrically neutral VEV, we choose hypercharges $Y = -2\,T_3$; for singlets this fixes $Y = 0$, whereas doublets can have $Y = \pm 1$.

5.1 Neutrino Masses

An unbroken $U(1)_{L_\mu - L_\tau}$ symmetry gives diagonal Dirac mass matrices and Majorana matrices of the form

$$\mathcal{M}_{\text{Majorana}} = \begin{pmatrix} a & 0 & 0 \\ 0 & 0 & b \\ 0 & b & 0 \end{pmatrix} , \tag{5.1}$$

sporting the discrete μ–τ symmetry (see Sec. 1.2 for the most general μ–τ-symmetric mass matrix), which implies vanishing θ_{13} and maximal mixing in the ν_μ–ν_τ sector ($\theta_{23} = \pi/4$). Either way, such neutrino matrices will not be in accord with oscillation experiments (especially with solar data); we will therefore break the $U(1)_{L_\mu - L_\tau}$ spontaneously via an extended Higgs sector. The next subsections are devoted to a brief discussion of the simplest extensions (additional scalar singlet, doublet and triplet) embedded in a seesaw mechanism.

5.1.1 Seesaw Mechanism and Neutrino Mixing Angles

As mentioned in Sec. 2.1, we can extend the fermion content of our theory, without introducing anomalies, by three right-handed neutrinos in the representations[1]

$$N_1 \sim (1,1,0)(0)\,, \qquad N_2 \sim (1,1,0)(+1)\,, \qquad N_3 \sim (1,1,0)(-1)\,. \tag{5.2}$$

The gauge invariant Yukawa couplings are (with $N_i^T\mathcal{C}^{-1}N_j = -N_i^T\mathcal{C}N_j = -\overline{N}_i^c N_j$)

$$\mathcal{L} \supset \frac{1}{2}N_i^T\mathcal{C}^{-1}(\mathcal{M}_R)_{ij}N_j + \lambda_e\overline{L}_e\tilde{H}_{\rm SM}N_1 + \lambda_\mu\overline{L}_\mu\tilde{H}_{\rm SM}N_2 + \lambda_\tau\overline{L}_\tau\tilde{H}_{\rm SM}N_3 + \text{h.c.}\,, \tag{5.3}$$

where $\mathcal{M}_R$ has the structure

$$\mathcal{M}_R = \begin{pmatrix} X & 0 & 0 \\ 0 & 0 & Y \\ 0 & Y & 0 \end{pmatrix}. \tag{5.4}$$

SM symmetry breaking ($H_{\rm SM} \to (0, \frac{1}{\sqrt{2}}(h_{\rm SM} + v_{\rm SM}))^T$) generates the bilinear terms

$$\mathcal{L} \supset -\begin{pmatrix} \overline{\nu}_e & \overline{\nu}_\mu & \overline{\nu}_\tau \end{pmatrix}\begin{pmatrix} m_{\nu_e} & 0 & 0 \\ 0 & m_{\nu_\mu} & 0 \\ 0 & 0 & m_{\nu_\tau} \end{pmatrix}\begin{pmatrix} N_1 \\ N_2 \\ N_3 \end{pmatrix} + \text{h.c.}\,, \tag{5.5}$$

where we introduced the Dirac mass matrix m_D with the entries $m_{\nu_i} \equiv \lambda_i v/\sqrt{2}$.

Combining the neutrinos into a vector $\omega_R^T \equiv \begin{pmatrix} \nu_e^c & \nu_\mu^c & \nu_\tau^c & N_1 & N_2 & N_3 \end{pmatrix}$, we obtain the full mass matrix

$$\mathcal{L} \supset -\frac{1}{2}\overline{\omega}_R^c\begin{pmatrix} 0_{3\text{x}3} & m_D \\ m_D^T & \mathcal{M}_R \end{pmatrix}\omega_R + \text{h.c.}\,, \tag{5.6}$$

which in the limit $X, Y \gg m_i$ results in a (symmetric) Majorana mass matrix for the light mass eigenstates $\mathcal{M}_\nu = -m_D\mathcal{M}_R^{-1}m_D^T$, in our case it takes of course the $L_\mu - L_\tau$-symmetric form

$$\mathcal{M}_\nu = -m_D\mathcal{M}_R^{-1}m_D^T = -\begin{pmatrix} \frac{m_{\nu_e}^2}{X} & 0 & 0 \\ \cdot & 0 & \frac{m_{\nu_\mu}m_{\nu_\tau}}{Y} \\ \cdot & \cdot & 0 \end{pmatrix}, \tag{5.7}$$

with the eigenvalues $\pm\frac{m_{\nu_\mu}m_{\nu_\tau}}{Y}$ and $-\frac{m_{\nu_e}^2}{X}$. This can also be understood by integrating out the heavy fields N_i; assuming a negligible kinetic energy, the equations of motion for the N_i (from $\frac{\partial\mathcal{L}}{\partial N_j} = 0$) can be algebraically solved to $\mathcal{M}_R\boldsymbol{N} \sim m_D^T\boldsymbol{\nu}$. This leads to the desired low-energy mass matrix when inserted back into the Lagrangian (5.5). The scale of the neutrino masses can therefore be made small by a high N_i-scale X, Y[2]

[1] The trivial possibility of right-handed neutrinos in the singlet representation of the whole gauge group $G_{\rm SM} \times U(1)'$ will be discussed briefly in App. E.

[2] In the context of grand unified theories possibly their breaking scale $\Lambda_{\rm GUT} \sim 10^{16}\,\text{GeV}$.

(hence the name seesaw), rather than by small Yukawa couplings. The mixing pattern of the neutrinos is however determined by our generation-dependent symmetry.

Due to the Majorana nature of the resulting mass eigenstates, the matrix $\mathcal{M}_\nu$ can be diagonalised via $U^T \mathcal{M}_\nu U = \mathrm{diag}(m_1, m_2, m_3)$; note the transposed unitary matrix U instead of a conjugated.

The phenomenology of texture zeros in neutrino mass matrices (like in Eq. (5.7)) has been discussed, for example, in Ref. [121], where a classification for the different structures is given. Most importantly, an analysis shows that $\mathcal{M}_\nu$ can have at most two texture zeros to be phenomenologically successful [122]. In the next sections, we will see that spontaneously breaking the $U(1)_{L_\mu - L_\tau}$ symmetry via scalar fields leads to additional entries in the mass matrix (5.7), but in the simplest cases still leaves some texture zeros. For example, introducing one scalar doublet, with charge $Y' = -1$, gives a low-energy neutrino mass matrix of the form

$$\mathcal{M}_\nu = \begin{pmatrix} A & C & 0 \\ \cdot & D & B \\ \cdot & \cdot & 0 \end{pmatrix}, \tag{5.8}$$

corresponding to the form B_4 of Frampton, Glashow and Marfatia [121]. The mass matrix can be analysed by evaluating $\mathcal{M}_\nu = U^* \mathrm{diag}(m_1, m_2, m_3) U^\dagger$ and solving the texture zeros $\mathcal{M}_\nu^{e\tau} = \mathcal{M}_\nu^{\tau\tau} = 0$ for $m_{1,2}$ as a function of the other parameters. For quasi-degenerate masses this leads to a valid structure, the most interesting relation one finds is

$$\Delta m^2_\odot / \Delta m^2_{\mathrm{atm}} \approx \frac{4 s_{13} (t_{23} + 1/t_{23}) \cos\delta_{\mathrm{CP}}}{\left| t_{12}(1 - t_{23}^4) \pm 2 s_{13} (t_{23} + 1/t_{23}) \cos\delta_{\mathrm{CP}} \right|}, \tag{5.9}$$

so a non-maximal θ_{23} and a non-zero θ_{13} are necessary for the mass splitting (one needs to choose the sign as to make the denominator minimal, depending on whether θ_{23} is larger or smaller than $\pi/4$). To get the desired $\Delta m^2_\odot / \Delta m^2_{\mathrm{atm}} \approx 0.03$, one typically needs $s_{13} \sim 10^{-2} - 10^{-3}$ (varying s_{23} around its 1σ interval). We also find the relations (for $\delta_{\mathrm{CP}} = 0$)

$$\begin{aligned} A/B &= -1/t_{23} + \mathcal{O}(s_{13}), \\ C/B &= \frac{s_{13}}{c_{23} s_{23}^2} + \mathcal{O}(s_{13}^2), \\ D/B &= t_{23} - 1/t_{23} + \mathcal{O}(s_{13}^2), \end{aligned} \tag{5.10}$$

demonstrating that we are indeed dealing with degenerate masses and the entries C and D are suppressed, i.e. a small $U(1)_{L_\mu - L_\tau}$ breaking suffices.

Since the one-doublet model is excluded by its large NSI parameters (Sec. 5.3), we will not go into any more details about the induced neutrino mixing angles. We merely mention that the allowed Higgs sectors, e.g. one singlet plus one doublet, contain enough parameters (and entries in $\mathcal{M}_\nu$) to create a successful neutrino phenomenology.

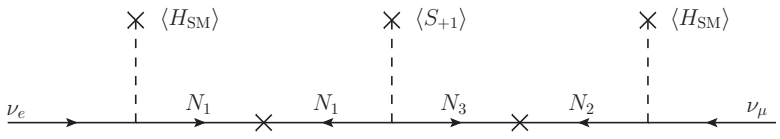

Figure 5.1: ν_e–ν_μ transition operator with a scalar singlet ($Y' = +1$).

5.1.2 Higgs Singlets

We will now introduce additional scalar singlets into our theory, which are charged under $U(1)_{L_\mu - L_\tau}$ and can be used to break the symmetry. The singlet $S_{Y'} \sim (1,1,0)(Y')$ can introduce additional $\mathcal{M}_R$ entries via Yukawa couplings

$$-p_{+1}\overline{N}_1^c N_3 S_{+1} - p_{-1}\overline{N}_1^c N_2 S_{-1} - p_{+2}\overline{N}_3^c N_3 S_{+2} - p_{-2}\overline{N}_2^c N_2 S_{-2} + \text{h.c.}\,, \tag{5.11}$$

which after breaking $S_{Y'} \to \frac{1}{\sqrt{2}}(v_s + h_s)$ generate the mass matrix

$$\mathcal{M}_R = \begin{pmatrix} X & \frac{v_s}{\sqrt{2}}p_{-1} & \frac{v_s}{\sqrt{2}}p_{+1} \\ \cdot & \frac{v_s}{\sqrt{2}}p_{-2} & Y \\ \cdot & \cdot & \frac{v_s}{\sqrt{2}}p_{+2} \end{pmatrix} \equiv \begin{pmatrix} X & s_{-1} & s_{+1} \\ \cdot & s_{-2} & Y \\ \cdot & \cdot & s_{+2} \end{pmatrix}. \tag{5.12}$$

Using the seesaw mechanism, we obtain the low-energy mass matrix

$$\begin{aligned} \mathcal{M}_\nu &= -\left[XY^2 - Xs_{-2}s_{+2} - 2Ys_{-1}s_{+1} + (s_{+1})^2 s_{-2} + (s_{-1})^2 s_{+2}\right]^{-1} \\ &\quad \times \begin{pmatrix} m_{\nu_e}^2(Y^2 - s_{-2}s_{+2}) & m_{\nu_e}m_{\nu_\mu}(s_{-1}s_{+2} - Ys_{+1}) & m_{\nu_e}m_{\nu_\tau}(s_{+1}s_{-2} - Ys_{-1}) \\ \cdot & -m_{\nu_\mu}^2(Xs_{+2} - s_{+1}^2) & m_{\nu_\mu}m_{\nu_\tau}(XY - s_{+1}s_{-1}) \\ \cdot & \cdot & -m_{\nu_\tau}^2(Xs_{-2} - s_{-1}^2) \end{pmatrix} \\ &\approx -\begin{pmatrix} \frac{m_{\nu_e}^2}{X} & 0 & 0 \\ \cdot & 0 & \frac{m_{\nu_\mu}m_{\nu_\tau}}{Y} \\ \cdot & \cdot & 0 \end{pmatrix} + \frac{1}{XY^2}\begin{pmatrix} m_{\nu_e}^2 s_{-2}s_{+2} & m_{\nu_e}m_{\nu_\mu}Ys_{+1} & m_{\nu_e}m_{\nu_\tau}Ys_{-1} \\ \cdot & m_{\nu_\mu}^2 Xs_{+2} & m_{\nu_\mu}m_{\nu_\tau}s_{+1}s_{-1} \\ \cdot & \cdot & m_{\nu_\tau}^2 Xs_{-2} \end{pmatrix}, \end{aligned} \tag{5.13}$$

where the last approximation is based on $X, Y \gg s_i$, viable for $U(1)'$ breaking around the EW scale. The result can be understood by means of Fig. 5.1, where the operator for the ν_e–ν_μ transition is depicted; the scale can be read off from the VEVs and fermion propagators to be

$$(\mathcal{M}_\nu)_{e\mu} \sim \langle H_{\text{SM}}\rangle \frac{1}{X} \langle S_{+1}\rangle \frac{1}{Y} \langle H_{\text{SM}}\rangle\,, \tag{5.14}$$

in accordance with Eq. (5.13).

Choosing a pair of singlets with $s_j = s_{-j}$ (e.g. via an additional discrete symmetry) one can reinstate the $\mu \leftrightarrow \tau$ symmetry even in the broken-$U(1)_{L_\mu - L_\tau}$ case.

To keep at most two texture zeros, we need at least two singlets in our theory. The breaking scale needs to be pretty high to make terms like $\frac{m^2}{X}\frac{s}{Y}$ not that much

smaller than $\frac{m^2}{X}$. The corrections should be of magnitude $\frac{s}{Y} \sim 10^{-2} - 10^{-3}$, so for $m \sim m_{\mu,\tau}$ this would set a lowest breaking scale of $s \sim 10^5\,\text{GeV}$. Another possibility is $X \sim 1\,\text{TeV}, m \sim m_e$, allowing the low scale $s \sim 100\,\text{GeV}$. In this case, the heavy neutrino sector could be probed at the LHC.

The connection to the Z' mass is (the same holds for doublets and triplets below)

$$M_{Z'} = g'\sqrt{\sum Y_i'^2 v_s^2} \sim g' s\,. \tag{5.15}$$

For the sake of completeness, we will now consider the case of just one singlet (w.l.o.g. S_{+1}), but without the approximation $s \ll X$. The low-energy neutrino mass matrix takes the simple form

$$\mathcal{M}_\nu(S_{+1}) = \frac{m_{\nu_e}^2}{X}\begin{pmatrix} 1 & -\varepsilon & 0 \\ \cdot & \varepsilon^2 & r \\ \cdot & \cdot & 0 \end{pmatrix}, \tag{5.16}$$

with $\varepsilon = \frac{m_{\nu_\mu}}{m_{\nu_e}}\frac{s_{+1}}{Y}$ and $r = \frac{m_{\nu_\mu} m_{\nu_\tau}}{m_{\nu_e}^2}\frac{X}{Y}$. While this has only two texture zeros, it gives wrong oscillation angles for all values of ε and r (typically too high θ_{13} for realistic θ_{12}). This is not in contradiction to the discussion of the B_4 structure (5.8) above, since here we have the B_4 form with an additional constraint $D = C^2$, which reduces the degrees of freedom.

This can be cured in the two-singlet model (S_{+1}+S_{-1}). The approximated low-energy mass matrix in this case is

$$\mathcal{M}_\nu(S_{+1} + S_{-1}) = -\frac{m_{\nu_e}^2}{X}\begin{pmatrix} 1 & -x & -y \\ \cdot & 0 & r - xy \\ \cdot & \cdot & 0 \end{pmatrix}, \tag{5.17}$$

with $x = \frac{m_{\nu_\mu} s_{+1}}{m_{\nu_e} Y}$, $y = \frac{m_{\nu_\tau} s_{-1}}{m_{\nu_e} Y}$ and $r = \frac{m_{\nu_\mu}}{m_{\nu_e}}\frac{m_{\nu_\tau}}{m_{\nu_e}}\frac{X}{Y}$. For $x \approx y \approx 1 - r \ll 1$, this matrix is diagonalised by tri-bimaximal mixing; to get the observed mass ratio $\Delta m^2_\odot / \Delta m^2_{\text{atm}}$, one needs values $r \approx 0.5 - 0.6$.

5.1.3 Higgs Doublets

Introducing $U(1)'$-charged Higgs doublets $\phi_{Y'} \sim (1, 2, +1)(Y')$ gives rise to the Yukawa terms

$$\mathcal{L} \supset -w_{\alpha\beta}\overline{L}_\alpha \phi_{Y'} \beta_R - u_{\alpha\beta}\overline{L}_\alpha \tilde{\phi}_{Y'} N_\beta + \text{h.c.}\,, \tag{5.18}$$

where the first term generates lepton flavour violation (LFV) in the charged lepton sector and will be ignored henceforth (the corresponding Yukawa couplings $w_{\alpha\beta}$ can be made small enough to stay within experimental bounds).

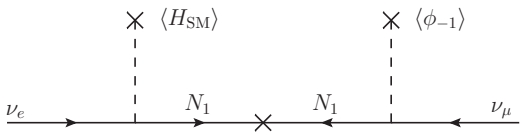

Figure 5.2: ν_e–ν_μ transition operator with a scalar doublet ($Y' = -1$).

Breaking $U(1)'$ via $\langle\phi\rangle = (0, \frac{v_d}{\sqrt{2}})^T$ brings forth new elements in the Dirac mass matrix

$$m_D = \begin{pmatrix} m_{\nu_e} & d_{+1} & d_{-1} \\ \tilde{d}_{-1} & m_{\nu_\mu} & d_{-2} \\ \tilde{d}_{+1} & d_{+2} & m_{\nu_\tau} \end{pmatrix}, \tag{5.19}$$

with $d_i = u_{\alpha\beta}\frac{v_d}{\sqrt{2}}$. This yields a light neutrino matrix (see Fig. 5.2 for a qualitative Feynman diagram)

$$\begin{aligned} \mathcal{M}_\nu = &- \begin{pmatrix} \frac{m_{\nu_e}^2}{X} & 0 & 0 \\ \cdot & 0 & \frac{m_{\nu_\mu} m_{\nu_\tau}}{Y} \\ \cdot & \cdot & 0 \end{pmatrix} \\ &- \begin{pmatrix} \frac{2d_{-1}d_{+1}}{Y} & \frac{m_{\nu_e}\tilde{d}_{-1}}{X} + \frac{m_{\nu_\mu}d_{-1}}{Y} + \frac{d_{+1}d_{-2}}{Y} & \frac{m_{\nu_e}\tilde{d}_{+1}}{X} + \frac{m_{\nu_\tau}d_{+1}}{Y} + \frac{d_{-1}d_{+2}}{Y} \\ \cdot & \frac{\tilde{d}_{-1}^2}{X} + \frac{2m_{\nu_\mu}d_{-2}}{Y} & \frac{\tilde{d}_{-1}\tilde{d}_{+1}}{X} + \frac{d_{+2}d_{-2}}{Y} \\ \cdot & \cdot & \frac{\tilde{d}_{+1}^2}{X} + \frac{2m_{\nu_\tau}d_{+2}}{Y} \end{pmatrix}. \end{aligned} \tag{5.20}$$

The requirement of at most two texture zeros can be fulfilled by one doublet with $Y' = \pm 1$. One can once again reinstate a μ–τ exchange symmetry by adding pairs of doublets with $d_j = d_{-j}$. The corrections are of order $\frac{d^2}{X}$ and $\frac{md}{X}$, that means the relative corrections are $\frac{d}{m}$ and $\frac{d^2}{m^2}$.

5.1.4 Triplet-Higgs Model

Instead of additional fermions N_i, we can also introduce a scalar triplet to the Lagrangian, allowing for a breaking of the $L_\mu - L_\tau$ symmetry and hence additional entries in $\mathcal{M}_\nu$. We consider

$$\Delta = \begin{pmatrix} H^+ & \sqrt{2}H^{++} \\ \sqrt{2}H^0 & -H^+ \end{pmatrix} \sim (1, 3, +2)(Y'), \tag{5.21}$$

where the H^i denote the electric charge eigenstates after EWSB. The allowed Yukawa couplings are

$$\begin{aligned} \mathcal{L} \supset &-\frac{1}{2} g_{\alpha\beta} L_\alpha^T \mathcal{C}^{-1} i\sigma_2 \Delta L_\beta + \text{h.c.} \\ = &-\frac{1}{2} g_{\alpha\beta} \left[\sqrt{2}\nu_\alpha \mathcal{C}^{-1} H^0 \nu_\beta - \nu_\alpha \mathcal{C}^{-1} H^+ \ell_\beta - \ell_\alpha \mathcal{C}^{-1} H^+ \nu_\beta - \sqrt{2}\ell_\alpha \mathcal{C}^{-1} H^{++} \ell_\beta \right] + \text{h.c.} \end{aligned} \tag{5.22}$$

The neutral part of Δ can now obtain a VEV $\langle H^0 \rangle = \frac{v_T}{\sqrt{2}}$ to break the $U(1)'$ and generate a Majorana mass matrix $v_T g_{\alpha\beta}$. The structure of the symmetric $g_{\alpha\beta}$ depends on the charge Y', as depicted below ($t_{Y'} \sim \langle H_0(Y') \rangle$):

$$\mathcal{M}_\nu = v_T g_{\alpha\beta} = \begin{pmatrix} t_0 & t_{-1} & t_{+1} \\ \cdot & t_{-2} & \tilde{t}_0 \\ \cdot & \cdot & t_{+2} \end{pmatrix} . \tag{5.23}$$

Since $\mathcal{M}_\nu$ can have at most two texture zeros, we need at least three triplets in our theory. Alternatively, we could introduce once again the three N_i and use the seesaw-I mechanism to create the $Y' = 0$ entries in $g_{\alpha\beta}$. So $3N_R + 2\Delta$ could also be a viable candidate.[3]

5.1.5 One Doublet Plus One Singlet

We take $S_{-1} \sim (1,1,0)(-1)$ and $\phi_{-1} \sim (1,2,+1)(-1)$ and, since the neutrino mass matrix is rather wide, we define $s \equiv s_{-1}$, $d \equiv d_{-1}$ and $\tilde{d} \equiv \tilde{d}_{-1}$ to fit it on one page. We choose $Y'(S) = -1$ to fill the zeros in the mass matrix (5.8). We obtain the low-energy Majorana mass matrix

$$\mathcal{M}_\nu = \frac{-1}{XY^2} \begin{pmatrix} (m_{\nu_e} Y - ds)^2 & Y(\tilde{d} m_{\nu_e} Y - d(\tilde{d} s - m_{\nu_\mu} X)) & s m_{\nu_\tau} (ds - m_{\nu_e} Y) \\ \cdot & \tilde{d}^2 Y^2 & Y m_{\nu_\tau} (m_{\nu_\mu} X - \tilde{d} s) \\ \cdot & \cdot & m_{\nu_\tau}^2 s^2 \end{pmatrix} . \tag{5.24}$$

We will not attempt to discuss the resulting neutrino phenomenology, because the one-doublet model alone already gives viable mixing angles; it should be clear that we can use s to improve the results even though its effect is suppressed by s/X compared to m and d.

Another possibility to fill the zeros is the field S_{-2}, leading to the fairly simple matrix

$$\mathcal{M}_\nu = - \begin{pmatrix} \frac{m_{\nu_e}^2}{X} - \frac{d_{-1}^2 s_{-2}}{Y^2} & \frac{\tilde{d}_{-1} m_{\nu_e}}{X} + \frac{d_{-1} m_{\nu_\mu}}{Y} & -\frac{d_{-1} m_{\nu_\tau} s_{-2}}{Y^2} \\ \cdot & \frac{\tilde{d}_{-1}^2}{X} & \frac{m_{\nu_\mu} m_{\nu_\tau}}{Y} \\ \cdot & \cdot & -\frac{m_{\nu_\tau}^2 s_{-2}}{Y^2} \end{pmatrix} . \tag{5.25}$$

5.2 Two Singlets

Having discussed the impact of the different scalar models on neutrino phenomenology, we will go on to examine the scalar sector in more detail. We start once again with singlets. Breaking the $L_\mu - L_\tau$ symmetry in the right-handed neutrino sector causes only minor changes in Standard Model particle interactions. We explicitly show the potential for two singlets, with $Y' = \pm 1$, in addition to the Standard Model doublet

[3] There are no additional Yukawa couplings of Δ to the N_i.

H_{SM}:

$$\begin{aligned} V = &-\mu_1|H_{\text{SM}}|^2 + \lambda_1|H_{\text{SM}}|^4 - \mu_2|S_1|^2 + \lambda_2|S_1|^4 - \mu_3|S_2|^2 + \lambda_3|S_2|^4 \\ &+ \delta_1|H_{\text{SM}}|^2|S_1|^2 + \delta_2|H_{\text{SM}}|^2|S_2|^2 + \left(\delta_3 S_1 S_2|H_{\text{SM}}|^2 + \text{h.c.}\right) \\ &+ \delta_4|S_1|^2|S_2|^2 + \left(\delta_5 S_1^2 S_2^2 + \text{h.c.}\right) + \left(M_{12}^2 S_1 S_2 + \text{h.c.}\right) . \end{aligned} \tag{5.26}$$

We will choose for simplicity all the parameters in V to be real to obtain a CP-conserving potential. The fields acquire the VEVs v_{SM}, v_1 and v_2, so we parameterise $H_{\text{SM}}^T = (H^+, (\text{Re}\, h + v_{\text{SM}} + i\text{Im}\, h)/\sqrt{2})$ and $S_j = (\text{Re}\, S_j + v_j + i\text{Im}\, S_j)/\sqrt{2}$.

In unitary gauge, the fields $H^\pm$ and $\text{Im}\, h$ are absorbed by $W^\pm$ and Z, the linear combination (Goldstone boson) $G \sim v_1 \text{Im}\, S_1 - v_2 \text{Im}\, S_2$ is absorbed by the Z' boson, leaving us with the degrees of freedom

$$H_{\text{SM}} \to \frac{1}{\sqrt{2}} \begin{pmatrix} 0 \\ \text{Re}\, h + v_{\text{SM}} \end{pmatrix} , \qquad S_j \to \frac{1}{\sqrt{2}} \left(\text{Re}\, S_j + i \frac{v_j}{v_S} A \right) . \tag{5.27}$$

We introduced the effective $U(1)'$ VEV $v_S = \sqrt{v_1^2 + v_2^2}$, and the CP-odd physical scalar $A = (v_2 \text{Im}\, S_1 + v_1 \text{Im}\, S_2)/v_S$, which has a mass

$$m_A^2 = -\frac{v_S^2}{2 v_1 v_2} \left(\delta_3 v_{\text{SM}}^2 + 2 M_{12}^2 + 4 \delta_5 v_1 v_2 \right) . \tag{5.28}$$

The contributing parameters in m_A can be understood by noticing that for $\delta_3 = \delta_5 = 0 = M_{12}^2$, the potential (5.26) has not only the local $U(1)_{L_\mu - L_\tau}$ symmetry, but the larger global $U(1) \times U(1)$, via $S_j \to e^{i\theta_j} S_j$. The spontaneous breakdown of these two abelian symmetries, by the VEVs v_1 and v_2, yields two massless Goldstone bosons, $\text{Im}\, S_1$ and $\text{Im}\, S_2$ (or G and A). In the presence of the parameters δ_3, δ_5 and M_{12}^2 however, there remains only one flat direction (G), so A becomes massive (pseudo-Goldstone).

Obviously, we need at least one of the parameters $\delta_3, \delta_5, M_{12}^2$ to be negative to give a positive m_A^2. There are surely bounds from the positivity constraint of the potential (5.26), on how negative these parameters can get, we will however not derive them (the parameter M_{12}^2 is not affected by this, since it is the coefficient of a quadratic coupling). The CP-even scalar fields mix according to the mass matrix (in the basis $(\text{Re}\, h, \text{Re}\, S_1, \text{Re}\, S_2)$)

$$\mathcal{M}_s^2 = \begin{pmatrix} 2\lambda_1 v_{\text{SM}}^2 & v_{\text{SM}}(\delta_1 v_1 + \delta_3 v_2) & v_{\text{SM}}(\delta_2 v_2 + \delta_3 v_1) \\ \cdot & 2\lambda_2 v_1^2 - \frac{1}{2}\frac{v_2}{v_1}\delta_3 v_{\text{SM}}^2 - \frac{v_2}{v_1} M_{12}^2 & M_{12}^2 + \frac{1}{2}\delta_3 v_{\text{SM}}^2 + (\delta_4 + 2\delta_5) v_1 v_2 \\ \cdot & \cdot & 2\lambda_3 v_2^2 - \frac{1}{2}\frac{v_1}{v_2}\delta_3 v_{\text{SM}}^2 - \frac{v_1}{v_2} M_{12}^2 \end{pmatrix} . \tag{5.29}$$

As can be seen, we have either a mixing in the CP-even sector (and therefore, if one of δ_1, δ_2 or δ_3 is non-zero, a coupling of our new scalar fields to first-generation fermions and $Z, W^\pm$), or a massless pseudoscalar A, which couples to Z', the N_i and, of course, the other scalars. As can already be seen from the potential (5.26), the Standard Model Higgs h decouples from the "new physics" for $\delta_1 = \delta_2 = \delta_3 = 0$. In contrast to the cxSM model (SM plus one complex scalar singlet, see Ref. [123] for a discussion),

h^3	h^4	S_i^3	S_i^4	A^4	$A^2S_i^2$	A^2h^2	$S_1^2S_2^2$	$A^2S_1S_2$
$h^2S_1S_2$	A^2h	A^2S_i	$S_1^2S_2$	$S_1S_2^2$	S_i^2h	h^2S_i	hS_1S_2	
Z^2h	Z^2h^2	W^+W^-h	$W^+W^-h^2$	$Z'AS_i$	Z'^2A^2	$Z'^2S_i^2$	Z'^2S_i	

Table 5.1: Interaction vertices involving scalars among themselves (first row), and with vector bosons (second row), not in mass basis yet.

the pseudoscalar A is in general unstable, because it can decay via Z' and S_i (see interaction terms below), and is therefore no candidate for dark matter. Let A be the lightest of the scalars in the following.

Since the potential in terms of the physical scalars is long and not particularly interesting, we merely list the occurring interaction vertices in Tab. 5.1. The scalars listed are not mass eigenstates and we denote, for simplicity, $\mathrm{Re}\, S_1 \equiv S_1$, $\mathrm{Re}\, S_2 \equiv S_2$, abusing the notation.

The gauge interactions are described by the Lagrangian

$$\begin{aligned}\mathcal{L} \supset\ & \frac{1}{2}\frac{e^2}{4s_W^2c_W^2}v_{\mathrm{SM}}^2Z^2\left(1+h/v_{\mathrm{SM}}\right)^2 + \frac{e^2}{4s_W^2}v_{\mathrm{SM}}^2W^+W^-\left(1+h/v_{\mathrm{SM}}\right)^2 + \frac{1}{2}g'^2(v_1^2+v_2^2)Z'^2 \\ & + g'Z'_\mu A\,\partial^\mu\left(\frac{v_2}{v_S}S_1 - \frac{v_1}{v_S}S_2\right) - g'Z'_\mu\left(\frac{v_2}{v_S}S_1 - \frac{v_1}{v_S}S_2\right)\partial^\mu A \\ & + \frac{1}{2}g'^2Z'^2\left(A^2+S_1^2+S_2^2\right) + g'^2Z'^2\left(v_1S_1+v_2S_2\right)\,.\end{aligned} \tag{5.30}$$

We calculate the decay $Z' \to AS_{1,2} \to AAA$ in the limit $m_A \equiv 0$, i.e. all mixing parameters to zero, and also, for simplicity, $M_{Z'} \ll m_{S_i}$. A long calculation gives

$$\Gamma(Z' \to AAA) \approx \frac{1}{2304}\,\frac{g'^5}{(2\pi)^3}\,\frac{|v_1^4 - v_2^4|}{(v_1^2+v_2^2)^{3/2}}\,, \tag{5.31}$$

highly suppressed compared to $\Gamma(Z' \to \bar{\nu}\nu)$. If instead $m_{S_i} < M_{Z'}$, the decay channel $Z' \to AS_i$ can be comparable:

$$\begin{aligned}\Gamma(Z' \to AS_1) &= \frac{1}{48\pi}\frac{v_2^2}{v_S^2}g'^2M_{Z'} + \mathcal{O}(m_{S_1}^2/M_{Z'}) \\ &\approx \frac{g'^3}{48\pi}\frac{v_2^2}{(v_1^2+v_2^2)^{1/2}} = \frac{1}{2}\frac{v_2^2}{v_S^2}\Gamma(Z' \to \bar{\nu}\nu)\,.\end{aligned} \tag{5.32}$$

For small mixing parameters $\delta_{1,2,3}$, one mass eigenstate will be mainly h, the Standard Model Higgs boson. If the mass of A is negligible, there will be the new decay channel $h \to AA$, approximately (where we set, for simplicity, $v_1 = v_2$)

$$\Gamma(h \to AA) \approx \frac{1}{128\pi}\frac{v_{\mathrm{SM}}^2}{m_h}\left(\delta_1+\delta_2-2\delta_3\right)^2 \approx 1.2\,\mathrm{GeV}\left(\frac{120\,\mathrm{GeV}}{m_h}\right)\left(\delta_1+\delta_2-2\delta_3\right)^2\,. \tag{5.33}$$

So A can contribute to, or even dominate, the invisible branching ratio of the Higgs,

especially for low m_h. In that case, the LEP limits on the Higgs mass are weakend, because they are based on the no longer dominant decay modes $h \to b\bar{b}, \tau^-\tau^+$; this would improve the current fit of the Standard Model to experimental data, since it favours a Higgs mass $\sim 90\,\text{GeV}$.

The decay $S_1 \to AA$, for $m_A \ll m_{S_1}$, can be calculated analogously:

$$\Gamma(S_1 \to AA) \approx \frac{1}{32\pi}\frac{1}{m_{S_1}}\frac{v_1^2}{v_S^2}\left(2\lambda_2 v_2^2 + (\delta_4 - 2\delta_5)v_1^2 - 4\delta_5 v_2^2\right)^2 \approx \frac{1}{128\pi}\frac{m_{S_1}^3}{v_1^2}\,, \tag{5.34}$$

where the last approximation uses $v_1 = v_2$ and $\delta_{4,5} \ll \lambda_2$.

We close by mentioning that this model is naturally free of LFV at tree-level (except in the neutrino sector), because the S_i do not couple to charged fermions. The model is difficult to test experimentally, probably the best way would be the measurement of the invisible branching ratio of h; but since $|M_{12}^2|$ can be arbitrarily large, the (S_i, A) sector might as well decouple completely. The Higgs sector of the two-singlet model therefore lacks predictability. In general, measurements around the Z' pole (e.g. at a muon collider) could be used to measure the invisible width of Z', probing for light A or S_i; it would however be impossible to distinguish the origin of the light scalars, i.e. the concrete Higgs sector.

The mixing of CP-even scalars, and their effect on the S, T and U parameters, is discussed in Ref. [124]. The authors show that the two-singlet extension (which is effectively what we have with the mass matrix (5.29)), has a large allowed parameter space, for scalar masses around $140 - 250\,\text{GeV}$. As far as a possible detection at the LHC goes, they conclude that at most one scalar ϕ_i can be detected in the channel $\phi_i \to ZZ^* \to 4\ell$, while some mixing angles actually render all the scalars unobservable at an integrated luminosity of $30\,\text{fb}^{-1}$ (thereby "hiding" the Higgs, as put forward in the Refs. [125, 124]).

5.3 One Doublet

In the one-doublet model (with $Y' = \pm 1$ to generate enough entries in the neutrino mass matrix) we have the parameters $\langle\phi_{\pm 1}\rangle \equiv v_D/\sqrt{2}$ and g', which lead to the mass parameters in our Lagrangian (2.4):

$$\hat{M}_Z^2 = \frac{e^2}{4s_W^2 c_W^2}(v_{\text{SM}}^2 + v_D^2)\,, \qquad \delta\hat{M}^2 = \frac{eg'}{2s_W c_W}v_D^2\,, \qquad \hat{M}_{Z'}^2 = g'^2 v_D^2\,. \tag{5.35}$$

This constitutes the simplest nontrivial model, in the sense that it reduces the number of free parameters from $(\hat{M}_{Z'}, \delta\hat{M}^2, g')$ to (v_D, g'). We will now show that it is already excluded by NSI measurements. For small mixing we can approximate Eq. (4.28) to

$$\varepsilon_{\mu\mu}^{\oplus} \approx \frac{g'}{\sqrt{2}G_F}\frac{e}{2s_W c_W}\,\xi\,\frac{1}{M_2^2}\,, \tag{5.36}$$

which can be further approximated, using the expressions for the mass $M_2 \approx \hat{M}_{Z'} = g' v_D$ and the mixing angle $\xi \approx \delta\hat{M}^2/M_1^2 = \frac{e}{2 s_W c_W} g' v_D^2 / M_1^2$, to

$$\varepsilon^{\oplus}_{\mu\mu} \approx \frac{1}{\sqrt{2} G_F} \left(\frac{e}{s_W c_W} \right)^2 \frac{1}{M_1^2} \approx 0.9 \,, \tag{5.37}$$

only weakly dependent on the Z' parameters. Since this is roughly a factor 20 higher than the current 90% C.L. bound, this excludes the one-doublet model, at least in the range of validity of our NSI parameters and approximations ($1\,\text{GeV} \lesssim M_2 \lesssim 90\,\text{GeV}$). Note that this does not exclude this model for the fifth-force case, since the NSI are not well defined in that limit.

5.4 One Triplet

The one-triplet model is ruled out by LEP measurements, as we will show now. The kinetic term of the triplet Δ takes the form

$$\mathcal{L} \supset \frac{1}{2} \text{tr} \left((D_\mu \Delta)^\dagger D^\mu \Delta \right) \tag{5.38}$$

where the covariant derivative acts on Δ in the way

$$D_\mu \Delta = \partial_\mu \Delta - i \frac{g_2}{2} W_\mu^a \left[\sigma^a, \Delta \right] - i g_1 B_\mu \Delta - i g' Y' Z'_\mu \Delta \,. \tag{5.39}$$

A tedious calculation results in

$$\begin{aligned}
&\frac{1}{2} \text{tr} \left((D_\mu \Delta)^\dagger D^\mu \Delta \right) = \\
&\quad |\partial_\mu H^{++} - i 2 e A_\mu H^{++} - i \frac{e}{s_W c_W} (c_W^2 - s_W^2) Z_\mu H^{++} - i g' Y' Z'_\mu H^{++} + i \frac{e}{s_W} W_\mu^+ H^+|^2 \\
&\quad + |\partial_\mu H^+ - i g' Y' Z'_\mu H^+ - i e A_\mu H^+ + i e \frac{s_W}{c_W} Z_\mu H^+ + i \frac{e}{s_W} W_\mu^- H^{++} - i \frac{e}{s_W} W_\mu^+ H^0|^2 \\
&\quad + |\partial_\mu H^0 - i g' Y' Z'_\mu H^0 + i \frac{e}{s_W c_W} Z_\mu H^0 - i \frac{e}{s_W} W_\mu^- H^+|^2 \,,
\end{aligned} \tag{5.40}$$

which gives rise to a vast amount of possible interactions. After H^0 acquires a VEV, this leads to the mass terms

$$M_W^2 = \frac{e^2}{2 s_W^2} v_T^2 \,, \quad M_Z^2 = \frac{e^2}{s_W^2 c_W^2} v_T^2 \,, \quad M_{Z'}^2 = g'^2 Y'^2 v_T^2 \,, \quad \delta M^2 = \frac{e}{s_W c_W} g' Y' v_T^2 \,. \tag{5.41}$$

Additional mass terms arise, of course, from the SM Higgs, for $g' = 0$ we get

$$M_W^2 = \frac{e^2}{2 s_W^2} \left(v_T^2 + \frac{v_{\text{SM}}^2}{2} \right) \,, \qquad M_Z^2 = \frac{e^2}{s_W^2 c_W^2} \left(v_T^2 + \frac{v_{\text{SM}}^2}{4} \right) \,, \tag{5.42}$$

changing the ρ parameter to[4]

$$\rho = \frac{M_W^2}{c_W^2 M_Z^2} = \frac{1 + 2\frac{v_T^2}{v_{\mathrm{SM}}^2}}{1 + 4\frac{v_T^2}{v_{\mathrm{SM}}^2}} \approx 1 - 2\frac{v_T^2}{v_{\mathrm{SM}}^2}\,. \tag{5.43}$$

Current EW fits give the constraint $v_T/v_{\mathrm{SM}} < 0.017$, so v_T can at most be in the GeV range.[5] Taking three triplets and assuming a common breaking scale v_T, the ρ parameter changes to $\rho \approx 1 - 6v_T^2/v_{\mathrm{SM}}^2$, yielding $v_T/v_{\mathrm{SM}} < 0.010$.

For completeness, we also show the scalar potential, for simplicity for only one triplet:

$$\begin{aligned} -\mathcal{L} \supset\; & -m^2|H_{\mathrm{SM}}|^2 + \lambda_1|H_{\mathrm{SM}}|^4 - \frac{1}{2}M^2\mathrm{tr}\left(\Delta^\dagger\Delta\right) + \frac{\lambda_2}{4}\left(\mathrm{tr}\left(\Delta^\dagger\Delta\right)\right)^2 + \frac{\lambda_3}{2}\det\left(\Delta^\dagger\Delta\right) \\ & + \lambda_4|H_{\mathrm{SM}}|^2\mathrm{tr}\left(\Delta^\dagger\Delta\right) + \lambda_5\left(H_{\mathrm{SM}}^\dagger\sigma_i H_{\mathrm{SM}}\right)\mathrm{tr}\left(\Delta^\dagger\sigma_i\Delta\right) \\ & + \left(\frac{1}{\sqrt{2}}\mu\, H_{\mathrm{SM}}^T i\sigma_2\Delta^\dagger H_{\mathrm{SM}} + \mathrm{h.c.}\right)\,, \end{aligned} \tag{5.44}$$

where the μ term is only gauge invariant for $Y'(\Delta) = 0$.

Going into unitary gauge, we find a Z' boson with mass $\sim g'v_T$, but also a light neutral scalar h_T with mass $\sim v_T$. The interaction term

$$\mathcal{L} \supset\; 2\frac{e}{s_W c_W} g' Y' Z' Z |H^0|^2 \tag{5.45}$$

gives rise to the decay channel $Z \to Z' h_T$, which is, in the approximation $M_{Z'}, m_{h_T} \ll M_Z$, of the order $\mathcal{O}(100\,\mathrm{MeV})$, in direct contradiction to the invisible decay width $\Gamma_{\mathrm{inv}}(Z)$, as measured at LEP (accurately described by $Z \to \bar{\nu}\nu$ to $\sim 1\,\mathrm{MeV}$).

In the usual seesaw-II mechanism, the μ term in Eq. (5.44) can be used to make the scalar fields heavy enough to forbid such decays. Since a $U(1)'$-charged Δ does not allow such a term, this excludes the one-triplet model.

A possible solution could be an additional Higgs singlet VEV, which can push the Z' mass higher than M_Z. Consequent decays $Z \to h_T Z' \to h_T \bar{\nu}\nu$ are then suppressed by the Z' propagator and could be small enough. We would need even more scalars to get successful neutrino phenomenology, which results in a complicated scalar potential and particle content. This shall not be discussed further.

5.5 One Doublet Plus One Singlet

The doublet models are interesting for the breaking scale we are considering, because they naturally generate neutrino mass entries of similar order to the Standard Model Higgs (in contrast to the entries from singlet scalars); we will therefore try to cure the problems of the one-doublet model.

[4] This is also valid for $g' \neq 0$, because the mass mixing between Z and Z' gives a contribution to ρ of order $(v_T/v_{\mathrm{SM}})^4$, i.e. cannot be used to weaken the constraint.

[5] To be precise: $v_T < 0.017 \cdot 246\,\mathrm{GeV} \approx 4.2\,\mathrm{GeV}$ at 95% C.L.

One extension that has already been considered for $U(1)_{L_\mu - L_\tau}$ is the two-doublet model (e.g. Ref. [37]), albeit with little discussion of its phenomenology. Taking two doublets $\phi_{1,2}$ with opposite $U(1)'$ charge reduces the Z–Z' mixing, because the off-diagonal mass element has the form $\delta M^2 \sim g_Z g'(v_1^2 - v_2^2)$. This can lead to a model that is free of Z–Z' mixing and features a μ–τ-symmetric neutrino mass matrix. Since this has already been considered and will furthermore result in a quite messy scalar potential (without invoking the exchange symmetry), we will not discuss it here.

Instead, we look at the simplest extension, one doublet plus one singlet (occasionally abbreviated as 1D1S later on), i.e. we basically only add $g'^2 v_S^2$ to $\hat{M}_{Z'}^2$. The NSI parameter (5.37) is no longer constant, but depends on the ratio v_S/v_D in the form

$$\varepsilon_{\mu\mu}^{\oplus} \sim \frac{1}{1 + v_S^2/v_D^2} \,. \tag{5.46}$$

This factor needs to be smaller than $\sim 1/20$ (for $\chi = 0$), leading to $v_S/v_D > 4.6$, independent of g'. The anomalous magnetic moment Δa_μ gives the constraint $\sqrt{v_S^2 + v_D^2} \gtrsim 192\,\text{GeV}$, so to generate sufficiently small NSI values and still explain Δa_μ we need (for $\chi = 0$) $v_S \gtrsim 190\,\text{GeV}$ and $v_D \lesssim 40\,\text{GeV}$. Slightly weaker constraints come from the ρ parameter (Z–Z' mixing is small for $g' v_D^2 \ll M_Z^2$), we will in the following use the limit $v_D \ll v_S$, to be on the safe side. This automatically makes the corresponding entries in the neutrino Dirac mass matrix small, whereas the diagonal entries,coming from v_{SM}, rely on small Yukawa couplings. As a matter of convenience we will denote the VEVs v_S, v_D and v_{SM} as s, d and v in the following.

5.5.1 Scalar Potential

The potential for the scalar fields

$$H = \begin{pmatrix} h^+ \\ h^0 \end{pmatrix} \sim (1,2,+1)(0)\,, \quad \phi = \begin{pmatrix} \phi^+ \\ \phi^0 \end{pmatrix} \sim (1,2,+1)(-1)\,, \quad S \sim (1,1,0)(-1)\,, \tag{5.47}$$

can be written as

$$\begin{aligned} V = &- \mu_1 |H|^2 + \lambda_1 |H|^4 - \mu_2 |\phi|^2 + \lambda_2 |\phi|^4 - \mu_3 |S|^2 + \lambda_3 |S|^4 \\ &+ \delta_1 |H|^2 |\phi|^2 + \delta_2 |H^\dagger \phi|^2 + \delta_3 |H|^2 |S|^2 + \delta_4 |\phi|^2 |S|^2 \\ &- \left(\sqrt{2} |\mu| e^{i\kappa} H^\dagger \phi \overline{S} + \text{h.c.} \right) . \end{aligned} \tag{5.48}$$

The positivity of the potential gives constraints on the coefficients, easily derived using Sylvester's criterion for positive-definite quadratic forms:

$$\begin{aligned} &0 < \lambda_1\,, \qquad\qquad 0 < 4\lambda_1\lambda_2 - (\delta_1 + \delta_2)^2\,, \\ &0 < 4\lambda_1\lambda_2\lambda_3 + (\delta_1 + \delta_2)\delta_3\delta_4 - \lambda_1\delta_4^2 - \lambda_2\delta_3^2 - \lambda_3(\delta_1 + \delta_2)^2\,. \end{aligned} \tag{5.49}$$

Additional constraints come from the positivity of the scalar masses, which are however more intricate and will not be explicitly derived here; neither will the bounds from perturbativity and unitarity, which, in principle, give upper bounds on the couplings.

Introducing the VEVs[6]

$$\mathrm{Re}\, S \to s/\sqrt{2}\,, \qquad \mathrm{Re}\,\phi^0 \to d/\sqrt{2}\,, \qquad \mathrm{Re}\, h^0 \to v/\sqrt{2}\,, \tag{5.50}$$

and minimising the potential, gives three equations for $\mu_{1,2,3}$, which we plug back into the potential. To calculate the masses we will go to unitary gauge, i.e. eliminate the unphysical degrees of freedom, as determined by the kinetic terms:

$$\begin{aligned}
\mathcal{L} \supset\ & (D_\mu H)^\dagger (D^\mu H) + (D_\mu \phi)^\dagger (D^\mu \phi) + (D_\mu S)^\dagger (D^\mu S) \\
=\ & |\partial_\mu h^0 - i\frac{e}{2 s_W c_W} Z_\mu h^0 - i\frac{e}{\sqrt{2} s_W} W_\mu^- h^+|^2 \\
& + |\partial_\mu h^+ - i\frac{e}{s_W c_W}(c_W^2 - s_W^2) Z_\mu h^+ - ie A_\mu h^+ - i\frac{e}{\sqrt{2} s_W} W_\mu^+ h^0|^2 \\
& + |\partial_\mu \phi^0 + ig' Z'_\mu \phi^0 - i\frac{e}{2 s_W c_W} Z_\mu \phi^0 - i\frac{e}{\sqrt{2} s_W} W_\mu^- \phi^+|^2 \\
& + |\partial_\mu \phi^+ + ig' Z'_\mu \phi^+ - i\frac{e}{s_W c_W}(c_W^2 - s_W^2) Z_\mu \phi^+ - ie A_\mu \phi^+ - i\frac{e}{\sqrt{2} s_W} W_\mu^+ \phi^0|^2 \\
& + |\partial_\mu S + ig' Z'_\mu S|^2\,.
\end{aligned} \tag{5.51}$$

Expanding the fields around the VEVs, we find the mass terms for the gauge bosons

$$\begin{aligned}
M_W^2 &= \frac{e^2}{4 s_W^2}(v^2 + d^2)\,, & M_Z^2 &= \frac{e^2}{4 s_W^2 c_W^2}(v^2 + d^2)\,, \\
M_{Z'}^2 &= g'^2 (d^2 + s^2)\,, & \delta M^2 &= -\frac{e}{2 s_W c_W} g' d^2\,,
\end{aligned} \tag{5.52}$$

and cross terms between gauge bosons and Goldstone bosons, namely:

$$\begin{aligned}
\mathcal{L} \supset & -\frac{e}{\sqrt{2} s_W c_W} Z_\mu \partial^\mu (d\,\mathrm{Im}\,\phi^0 + v\,\mathrm{Im}\, h^0) + \sqrt{2} g' Z'_\mu \partial^\mu (d\,\mathrm{Im}\,\phi^0 + s\,\mathrm{Im}\, S) \\
& - \frac{e}{2 s_W} i W_\mu^+ \partial^\mu (d\,\phi^- + v\, h^-) + \mathrm{h.c.}
\end{aligned} \tag{5.53}$$

We read off the Goldstone fields (not properly normalised)

$$G^- \sim d\,\phi^- + v\, h^-, \qquad G_Z \sim d\,\mathrm{Im}\,\phi^0 + v\,\mathrm{Im}\, h^0, \qquad G' \sim d\,\mathrm{Im}\,\phi^0 + s\,\mathrm{Im}\, S\,, \tag{5.54}$$

which are not orthogonal. Using the gauge freedom to fix $G^- = G_Z = G' = 0$ would result in physical scalars with unconventional kinetic terms; this can be avoided by first constructing a orthonormal basis from G_Z and G'. We define the physical field σ via $\sigma \sim G' \times G_Z$, then "rotate" G_Z to $\tilde{G}_Z \equiv \sigma \times G'$. These fields are connected to the

[6] While we choose all VEVs real and positive for simplicity, it must be stressed that this is not the most general case.

gauge eigenstates by a unitary transformation:

$$\begin{pmatrix} G' \\ \tilde{G}_Z \\ \sigma \end{pmatrix} = \begin{pmatrix} \cos\theta & \sin\theta & 0 \\ -\cos\beta\sin\theta & \cos\beta\cos\theta & \sin\beta \\ \sin\beta\sin\theta & -\sin\beta\cos\theta & \cos\beta \end{pmatrix} \begin{pmatrix} \mathrm{Im}\, S \\ \mathrm{Im}\,\phi^0 \\ \mathrm{Im}\, h^0 \end{pmatrix} \tag{5.55}$$

with the two angles

$$\tan\theta \equiv \frac{d}{s}\,, \qquad\qquad \tan\beta \equiv \frac{v}{sd}\sqrt{s^2+d^2} = \frac{v}{s\sin\theta}\,. \tag{5.56}$$

The expected scaling $d \ll s \sim v$ implies $\sin\theta, \cos\beta \ll 1$. The unitary gauge, $G' = \tilde{G}_Z = 0$, leaves the physical field σ, contributing to the potential through

$$\begin{pmatrix} \mathrm{Im}\, S \\ \mathrm{Im}\,\phi^0 \\ \mathrm{Im}\, h^0 \end{pmatrix} = \begin{pmatrix} \cos\theta & \sin\theta & 0 \\ -\cos\beta\sin\theta & \cos\beta\cos\theta & \sin\beta \\ \sin\beta\sin\theta & -\sin\beta\cos\theta & \cos\beta \end{pmatrix}^T \begin{pmatrix} 0 \\ 0 \\ \sigma \end{pmatrix} = \begin{pmatrix} \sin\beta\sin\theta\,\sigma \\ -\sin\beta\cos\theta\,\sigma \\ \cos\beta\,\sigma \end{pmatrix}\,. \tag{5.57}$$

The field σ consists mainly of $\mathrm{Im}\,\phi$, so the imaginary part of h^0 is not zero as in the SM, but suppressed by $\cos\beta$.

The charged Goldstone boson is easier to handle, we have

$$\begin{pmatrix} \phi^- \\ h^- \end{pmatrix} = \begin{pmatrix} \cos\beta^- & -\sin\beta^- \\ \sin\beta^- & \cos\beta^- \end{pmatrix} \begin{pmatrix} G^- \\ \sigma^- \end{pmatrix} \xrightarrow{G^- \to\, 0} \begin{pmatrix} -\sin\beta^-\,\sigma^- \\ \cos\beta^-\,\sigma^- \end{pmatrix}\,, \tag{5.58}$$

with the angle $\tan\beta^- \equiv v/d = \cos\theta\tan\beta \approx \tan\beta \gg 1$. The physical fields σ, $\sigma^\pm$, $\mathrm{Re}\, S \equiv S$, $\mathrm{Re}\,\phi^0 \equiv \phi$ and $\mathrm{Re}\, h^0 \equiv h$ (abuse of notation) are not mass eigenstates. Setting, for simplicity, the CP-violating angle κ in the potential (5.48) to zero, we can at least read off the masses for σ and $\sigma^\pm$:

$$m_\sigma^2 = \frac{|\mu| vs}{d} + \frac{|\mu| ds}{v} + \frac{|\mu| vd}{s}\,, \tag{5.59}$$

$$m_{\sigma^\pm}^2 = \frac{|\mu| vs}{d} + \frac{|\mu| ds}{v} - \frac{1}{2}\delta_2(d^2+v^2)\,. \tag{5.60}$$

In the approximation we will use extensively, $d \ll s \sim v$, only the first term contributes and $m_\sigma \approx m_{\sigma^+}$. The masses m_σ and $m_{\sigma^\pm}$ increase for decreasing d, reminiscent of an inverse seesaw mechanism; useful values for $|\mu|$ will be discussed below.

The CP-even scalars share the symmetric mass matrix (in (S, ϕ, h) basis)

$$\mathcal{M}^2_{\mathrm{CP-even}} = \begin{pmatrix} 2\lambda_3 s^2 + \frac{|\mu| vd}{s} & -|\mu| v + \delta_4 ds & -|\mu| d + \delta_3 vs \\ \cdot & 2\lambda_2 d^2 + \frac{|\mu| vs}{d} & -|\mu| s + (\delta_1+\delta_2) vd \\ \cdot & \cdot & 2\lambda_1 v^2 + \frac{|\mu| ds}{v} \end{pmatrix}\,, \tag{5.61}$$

with the approximate eigenvalues (labelled according to the predominant field in the

unmixed scenario)

$$m^2_{\tilde{h},\tilde{S}} \approx \lambda_1 v^2 + \lambda_3 s^2 \pm \sqrt{(\lambda_1 v^2 - \lambda_3 s^2)^2 + \delta_3^2 s^2 v^2}\,, \tag{5.62}$$

$$m^2_{\tilde{\phi}} \approx \frac{|\mu| v s}{d}\,. \tag{5.63}$$

For small $\cos\beta \approx d/v$, the fields σ, σ^+ and ϕ have degenerate masses. In contrast to other 2HDM (and our two-singlet model), we do not have a light pseudoscalar σ. In the next section, we will see that the charged scalar mass is bounded from below, $m_{\sigma^\pm} \gtrsim 80\,\text{GeV}$, so there are no decay modes of h into real $\sigma\sigma$, $\sigma^+\sigma^-$ or $\phi\phi$, unless h has a mass of at least 160 GeV. S could, in principle, have a mass low enough to allow $h \to SS$, depending on λ_3. Decay channels as signatures in collider experiments will be discussed below. We point out that without large mass splittings in the scalar sector, the quantum corrections to the ρ parameter, due to scalar loops, will be small [126].

Obviously, the μ term in the potential is crucial for the generation of large scalar masses, without it, we would end up with masses $\sim d$, either below M_Z (introducing new invisible decay channels for Z) or above it (introducing too large of a Z–Z'-mixing angle). The potential in the $(\sigma, \sigma^\pm, S, \phi, h)$ basis is ridiculously lengthy and will not be shown here. It involves the interaction terms given in Tab. 5.2; also shown are the interactions with the gauge bosons. Making $|\mu|$ and the δ_i small, e.g. $|\mu| \sim d$, results in small mixing; for simplicity, we will work in zeroth order and treat S, ϕ and h as mass eigenstates. The additional mass mixing could be of the same order as the mixing through β and β^-, consequently the combined mixing could be larger or smaller, depending on their relative sign in the coupling. Since we are only performing order of magnitude approximations in the scalar sector, we do not care about this.

Just as an aside, we mention that none of the scalars are stable. The scalars σ and σ^- couple directly to fermions (albeit weakly) and will decay through this channel. The scalars ϕ and S couple predominantly to the heavy neutrino sector, but can in any way decay via a $Z'Z'$. So, without invoking some additional discrete symmetries, this model provides no candidate for dark matter.

5.5.2 Yukawa Interactions and Lepton Flavour Violation

The gauge invariant Yukawa interactions of the two doublets H and ϕ and the singlet S to the leptons and right-handed neutrinos N_i can be written as:

$$\begin{aligned} -\mathcal{L} \supset\ & + \lambda_H^{ee} \overline{L}_e H e_R + \lambda_H^{\mu\mu} \overline{L}_\mu H \mu_R + \lambda_H^{\tau\tau} \overline{L}_\tau H \tau_R \\ & + \lambda_H^{e1} \overline{L}_e \tilde{H} N_1 + \lambda_H^{\mu 2} \overline{L}_\mu \tilde{H} N_2 + \lambda_H^{\tau 3} \overline{L}_\tau \tilde{H} N_3 \\ & + \lambda_\phi^{e\mu} \overline{L}_e \phi \mu_R + \lambda_\phi^{\tau e} \overline{L}_\tau \phi e_R \\ & + \lambda_\phi^{e3} \overline{L}_e \tilde{\phi} N_3 + \lambda_\phi^{\mu 1} \overline{L}_\mu \tilde{\phi} N_1 + \lambda_S^{12} \overline{N}_1^c N_2 S + \text{h.c.} \end{aligned} \tag{5.64}$$

h^3 $\sigma^2 h$ $\sigma^2\phi^2$ $S^2\phi$ $\phi\sigma^+\sigma^-$	h^4 $h\phi S$ $\sigma^2 h^2$ hS^2 $S\sigma^+\sigma^-$	S^3 $\sigma^2\phi$ $h^2 S$ $\sigma^+\sigma^-\sigma^+\sigma^-$ $h\phi\ \sigma^+\sigma^-$	S^4 $\sigma^2 S$ $h^2\phi$ $h^2\sigma^+\sigma^-$ $S^2\sigma^+\sigma^-$	ϕ^3 $\phi^2 S^2$ $\phi^2 h$ $\phi^2\sigma^+\sigma^-$	ϕ^4 $h^2 S^2$ $\sigma^2 S^2$ $\sigma^2\sigma^+\sigma^-$	σ^4 $h^2\phi^2$ $\phi^2 S$ $h\sigma^+\sigma^-$
$Z^2 h$ $W^- A\sigma^+\phi$ $W^- A\sigma^+ h$	$W^+W^-\phi$ $W^+W^-\sigma^2$ $W^+W^- h$	$Z^2\sigma^+\sigma^-$ $W^+W^-\phi^2$ $W^+W^- h^2$	$ZA\sigma^+\sigma^-$ $ZW^-\sigma^+\sigma$ $Z^2\sigma^2$	$ZW^-\sigma^+\phi$ $W^+A\sigma^-\sigma$ $Z^2\phi$	$A^2\sigma^+\sigma^-$ $W^+W^-\sigma^+\sigma^-$ $Z^2\phi^2$	$Z^2 h^2$ $ZW^-\sigma^+ h$
$Z'^2\phi^2$ $W^+Z'\sigma^-$	$Z'^2 S^2$ $Z'^2\phi$	$W^-Z'\sigma^+\phi$ $Z'^2 S$	$ZZ'\sigma^+\sigma^-$ $Z'^2\sigma^2$	$AZ'\sigma^+\sigma^-$ $ZZ'\sigma^2$	$W^+Z'\sigma^-\sigma$ $ZZ'\phi$	$Z'^2\sigma^+\sigma^-$ $ZZ'\phi^2$
$A\sigma^+\sigma^-$ $Z'\phi\sigma$	$Z\sigma^+\sigma^-$ $Z'\sigma S$	$Z\sigma h$ $Z'\sigma^+\sigma^-$	$Z\sigma\phi$	$W^-\sigma^+\sigma$	$W^-\sigma^+ h$	$W^-\sigma^+\phi$

Table 5.2: Interaction vertices involving scalars among themselves (first row), with SM vector bosons (second row), with the Z' boson (third row), and couplings to vector bosons involving derivatives (last row).

In unitary gauge, denoting $\sin\beta$ with s_β etc., this becomes:

$$\begin{aligned}
-\mathcal{L} \supset & \sum_{\ell=e,\mu,\tau} \lambda_H^{\ell\ell}\left[\frac{v}{\sqrt{2}}\overline{\ell}_L\ell_R + \frac{1}{\sqrt{2}}\overline{\ell}_L\ell_R(h+ic_\beta\sigma) + c_\beta^-\overline{\nu}_\ell\ell_R\sigma^+\right] \\
& + \lambda_H^{e1}\left[-\frac{v}{\sqrt{2}}\overline{\nu}_e N_1 - \frac{1}{\sqrt{2}}\overline{\nu}_e N_1(h-ic_\beta\sigma) + c_\beta^-\overline{e}_L N_1\sigma^-\right] + (e1\to\mu2,\tau3) \\
& + \lambda_\phi^{e\mu}\left[\frac{d}{\sqrt{2}}\overline{e}_L\mu_R + \frac{1}{\sqrt{2}}\overline{e}_L\mu_R(\phi - is_\beta c_\theta\sigma) - s_\beta^-\overline{\nu}_e\mu_R\sigma^+\right] + (e\mu\to\tau e) \\
& + \lambda_\phi^{e3}\left[-\frac{d}{\sqrt{2}}\overline{\nu}_e N_3 - \frac{1}{\sqrt{2}}\overline{\nu}_e N_3(\phi + is_\beta c_\theta\sigma) - s_\beta^-\overline{e}_L N_3\sigma^-\right] + (e3\to\mu1) \\
& + \lambda_S^{12}\left[\frac{s}{\sqrt{2}}\overline{N}_1^c N_2 + \frac{1}{\sqrt{2}}\overline{N}_1^c N_2(S+is_\beta s_\theta\sigma)\right] + \text{h.c.}\,,
\end{aligned} \tag{5.65}$$

which can be further simplified using $\overline{\ell}_L\ell_R(h+ic_\beta\sigma)+\text{h.c.} = \overline{\ell}(h+ic_\beta\gamma_5\sigma)\ell$, emphasising the pseudoscalar nature of σ.

The coupling to quarks is of the same form as in the Standard Model (since they are singlets under $U(1)'$):

$$-\mathcal{L} \supset \sum_{i,j=1,2,3}\lambda_d^{ij}\overline{Q}_L^i H d_R^j + \sum_{i,j=1,2,3}\lambda_u^{ij}\overline{Q}_L^i\tilde{H}u_R^j + \text{h.c.} \tag{5.66}$$

Diagonalisation of the mass matrices goes through as usual, via biunitary transformations [32]. We end up with

$$-\mathcal{L} \supset \overline{\boldsymbol{d}}_L D_d \boldsymbol{d}_R H^0 + \overline{\boldsymbol{u}}_L D_u \boldsymbol{u}_R \overline{H}^0 + \overline{\boldsymbol{u}}_L V D_d \boldsymbol{d}_R H^+ - \overline{\boldsymbol{d}}_L V^\dagger D_u \boldsymbol{u}_R H^- + \text{h.c.}\,, \tag{5.67}$$

with the matrices in generation space

$$D_d \equiv \sqrt{2}/v \,\mathrm{diag}(m_d, m_s, m_b)\,, \qquad D_u \equiv \sqrt{2}/v \,\mathrm{diag}(m_u, m_c, m_t)\,, \tag{5.68}$$

and V (the usual unitary Cabibbo-Kobayashi-Maskawa matrix of the Standard Model). In the SM, the terms with $H^\pm$ vanish in unitary gauge, while in our case we have the Yukawa interactions:

$$\begin{aligned} -\mathcal{L} \supset & \sum_i \frac{m_i^d}{v}\, \overline{d}_L^i d_R^i (h + i c_\beta \sigma) + \sum_i \frac{m_i^u}{v}\, \overline{u}_L^i u_R^i (h - i c_\beta \sigma) \\ & + c_\beta^- \frac{\sqrt{2}}{v} \sum_{i,j} m_j^d V_{ij}\, \overline{u}_L^i d_R^j \sigma^+ - c_\beta^- \frac{\sqrt{2}}{v} \sum_{i,j} m_j^u V_{ji}^*\, \overline{d}_L^i u_R^j \sigma^- + \text{h.c.} \end{aligned} \tag{5.69}$$

The flavour-changing interactions are suppressed by the Yukawa couplings m_q/v and the angle $\cos\beta^- \approx d/v$, compared to those induced by $W^\pm$. The interaction of the charged scalars with the quarks is very similar to the Two-Higgs-Doublet Model of Type I (2HDM-I) [127, 128] (see App. F for a short overview over the 2HDM-Types), where the parameter $\cos\beta^-$ is denoted by $\tan\beta$. The corresponding bound $m_{\sigma^-} \gtrsim 80\,\mathrm{GeV}$ on a charged scalar with decay channels $\sigma^- \to \bar{c}s, \tau\bar{\nu}_\tau$, set by LEP [129, 130], applies. Additional contributions from $\sigma^\pm$ to charged-current decays are already well suppressed; for example, the decay $\tau \to \nu_\tau \sigma^- \to \nu_\tau \overline{\nu}_\mu \mu$ has the width

$$\Gamma(\tau \to \nu_\tau \overline{\nu}_\mu \mu) \approx \frac{1}{192} \frac{1}{(2\pi)^3} \left(\frac{c_\beta^-}{m_{\sigma^-}}\right)^4 \left(\frac{m_\tau m_\mu}{v^2}\right)^2 m_\tau^5\,, \tag{5.70}$$

resulting in an additional branching ratio of $\Delta\mathrm{BR} \approx 10^{-3}(c_\beta^-/m_{\sigma^-}[\mathrm{GeV}])^4$, which is already small enough and presents no bound on c_β^-.

There are two different kinds of Lepton Family number Violation (LFV) associated with this model, we will discuss them in the following. Since we choose the charge $Y' = -1$ for our Higgs fields ϕ and S, the $L_\mu - L_\tau$ number of a process will only changed by 1 unit in the simplest Feynman diagrams, i.e. we expect decays $\tau \to eX$ and $\mu \to eX$, but not $\tau \to \mu X$.

LFV Mediated by Z' As can be seen immediately in Eq. (5.65), the VEV d introduces non-diagonal elements in the mass matrix of the charged leptons:

$$\mathcal{M}_{\text{leptons}} = \frac{1}{\sqrt{2}} \begin{pmatrix} \lambda_H^{ee} v & \lambda_\phi^{e\mu} d & 0 \\ 0 & \lambda_H^{\mu\mu} v & 0 \\ \lambda_\phi^{\tau e} d & 0 & \lambda_H^{\tau\tau} v \end{pmatrix}. \tag{5.71}$$

The mass eigenbasis is obtained by means of a biunitary diagonalisation, i.e. $\ell_L \to U_L \ell_L$, $\ell_R \to U_R \ell_R$, with $U_L \neq U_R$. Since these matrices operate in flavour space, they do not

change the normal SM gauge interactions, but only the Z' coupling:

$$\begin{aligned} j'_\mu Z'^\mu &= \sum_{i=L,R} \bar{\ell}_i \begin{pmatrix} 0 & & \\ & 1 & \\ & & -1 \end{pmatrix} \gamma_\mu \ell_i Z'^\mu \\ &\to \sum_{i=L,R} \bar{\ell}_i U_i^\dagger \begin{pmatrix} 0 & & \\ & 1 & \\ & & -1 \end{pmatrix} U_i \gamma_\mu \ell_i Z'^\mu \,, \end{aligned} \tag{5.72}$$

Since $U_i^\dagger \,\mathrm{diag}(0,1,-1) U_i$ is not diagonal, Z' introduces decays like $\tau \to e Z'^* \to e\mu\bar{\mu}$. This also generates a coupling of Z' to electrons, suppressed by $\sin^2\theta_{L,R}$, and furthermore all the couplings become chiral, i.e. the Z' couples differently to left- and right-handed fermions. The same reasoning applies to LFV mediated by neutral scalars, since they couple in a generation-dependent way as well. Setting for simplicity $\lambda_\phi^{e\mu} = 0$, and using the approximations $m_e, m_\mu \ll m_\tau \ll M_{Z'}$, we obtain the LFV decay ratio

$$\begin{aligned} \frac{\Gamma(\tau \to e\mu\bar{\mu})}{\Gamma(\tau \to \mu\nu_\tau\bar{\nu}_\mu)} &\approx \frac{1}{4G_F^2} \left(\frac{g'}{M_{Z'}}\right)^4 \left(s_L^2 + s_R^2\right) \\ &\approx \left(\frac{200\,\mathrm{GeV}}{M_{Z'}/g'}\right)^4 \left(s_L^2 + s_R^2\right) \,, \end{aligned} \tag{5.73}$$

which is constrained to be $< 3.7 \times 10^{-8}/0.1736 = 2.1 \times 10^{-7}$ [22]. The angles $\theta_{L,R}$ can be approximated via

$$s_L^2 + s_R^2 \approx s_R^2 \approx \theta_R^2 \approx \frac{1}{2}\left(\frac{\lambda_\phi^{\tau e} d}{m_\tau}\right)^2 \,, \tag{5.74}$$

so for $d \sim m_\tau$ and $M_{Z'}/g' \sim 200\,\mathrm{GeV}$ we find the constraint $\lambda_\phi^{\tau e} < 10^{-3} - 10^{-4}$ for the coupling. There are, of course, additional channels mediated by neutral scalars, which should give similar limits, depending on the scalar masses. Since nothing in the motivation for our model depends on $\lambda_\phi^{e\mu}$ and $\lambda_\phi^{\tau e}$, we can make them arbitrarily small. On the other hand, any observation of LFV can be used to distinguish this model from other BSM effects, since it features a unique pattern, to be discussed now.

To discuss the general case $\lambda_\phi^{e\mu}, \lambda_\phi^{\tau e} \neq 0$, we approximate the rotation matrices for the left- and right-handed fields as

$$U_{L,R} \approx \begin{pmatrix} 1 & \theta_{12}^{L,R} & \theta_{13}^{L,R} \\ -\theta_{12}^{L,R} & 1 & \theta_{23}^{L,R} \\ -\theta_{13}^{L,R} & -\theta_{23}^{L,R} & 1 \end{pmatrix} \,, \tag{5.75}$$

where a proper calculation gives the rough scaling $\theta_{23} \ll \theta_{13} \sim \theta_{12}$. Setting $\theta_{23} = 0$

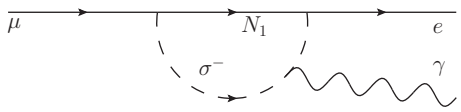

Figure 5.3: Charged-scalar mediated lepton-flavour-changing radiative decay.

yields the Z'-coupling matrix

$$U^\dagger \,\mathrm{diag}(0,1,-1)\, U \approx \begin{pmatrix} 0 & -\theta_{12} & \theta_{13} \\ \cdot & 1 & \theta_{13}\theta_{12} \\ \cdot & \cdot & -1 \end{pmatrix} . \tag{5.76}$$

As expected, our model basically only allows the LFV $\tau \to e$ and $\mu \to e$, with $\tau \to \mu$ being highly suppressed.

LFV via Loops The second source of LFV stems from the charged scalars, inducing the decays $\mu \to e\gamma$ and $\tau \to e\gamma$ via diagrams like Fig. 5.3, with a heavy right-handed neutrino in the loop. Since these decays involve the same Yukawa coupling $\lambda^{\ell i}$ that generate the $U(1)'$-breaking elements in the neutrino mass matrix, they better not be zero in our model. Calculating the branching ratio of the decay $\mu \to e\gamma$ in the approximation $m_N \gg m_{\sigma^+}, m_\mu, m_e$, we find [131]

$$\mathrm{BR}(\mu \to e\gamma) \approx \frac{3}{128\pi^2}\,\frac{d^2}{v^2}\left(\frac{\lambda_H^{e1}\lambda_\phi^{\mu 1}}{m_\mu G_F m_N}\right)^2 \overset{!}{<} 1.2\times 10^{-11}\,, \tag{5.77}$$

which is highly suppressed by the neutrino masses. Expressing the $\lambda^{\ell i}$ via the entries of the Dirac mass matrix m_D for the neutrinos, we can translate this into a bound on the matrix element of the low-energy neutrino matrix $\mathcal{M}_\nu$ (see the discussion in Sec. 5.1.5):

$$(\mathcal{M}_\nu)_{e\mu} \approx \frac{m_{\nu_e 1} m_{\nu_\mu 1}}{X} \overset{!}{\lesssim} 1\,\mathrm{keV}\,, \tag{5.78}$$

easily satisfied since we choose $X \sim m_N$ high enough to scale $\mathcal{M}_\nu \sim 0.1\,\mathrm{eV}$.

Contribution to Δa_μ The physical scalars contribute to the anomalous magnetic moment of the muon via loop diagrams similar to Fig. 3.5. Setting the LFV Yukawa couplings $\lambda_\phi^{e\mu} = \lambda_\phi^{\tau e} = 0$, only h, σ and σ^- couple directly to the muon. The one-loop contributions from the pseudoscalar σ and the charged σ^- are [132]

$$\delta a_\mu^{1-\mathrm{loop}} = \frac{-m_\mu^4}{8\pi^2 v^2}\int_0^1 \mathrm{d}x\,\left[\left(\frac{c_\beta^-}{m_{\sigma^-}}\right)^2 \frac{x(1-x)}{1+(x-1)m_\mu^2/m_{\sigma^-}^2} + \left(\frac{c_\beta}{m_\sigma}\right)^2 \frac{x^3}{1-x+x^2 m_\mu^2/m_\sigma^2}\right], \tag{5.79}$$

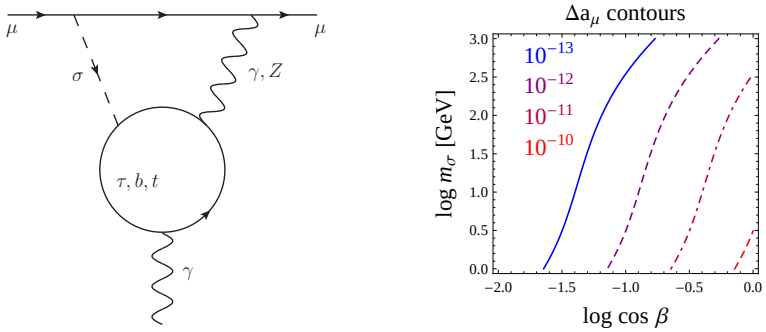

Figure 5.4: Dominating two-loop Barr-Zee-type diagram contributing to Δa_μ (left), actual values for Δa_μ in the approximation $\cos\beta^- \approx \cos\beta$, $m_\sigma \approx m_{\sigma^-}$ (right).

which are orders of magnitude below the current limit, even for $c_\beta \sim 1$. The two-loop contribution of σ however is also important [133] due to a larger coupling of σ to heavy fermions in the loop, which compensates the additional loop suppression (see Fig. 5.4). The dominant effect gives

$$\delta a_\mu^{2-\text{loop}} = \frac{\alpha}{8\pi^3}\frac{m_\mu^2}{v^2}c_\beta^2 \sum_{f=t,b,\tau} N_{\text{colour}}^f Q_f^2 \frac{m_f^2}{m_\sigma^2}\int_0^1 \mathrm{d}x \frac{\ln\left(\frac{m_f^2/m_\sigma^2}{x(1-x)}\right)}{m_f^2/m_\sigma^2 - x(1-x)}\,, \tag{5.80}$$

the combined one and two loop contributions are shown in Fig. 5.4 (right) for the case $\cos\beta^- \approx \cos\beta$, $m_\sigma \approx m_{\sigma^-}$, corresponding to the $d \ll v$ limit we are interested in. As can be seen the effects are about two orders of magnitude too small to have any effect.

5.5.3 Signatures at the LHC

The effects of additional scalars in collider experiments, especially concerning the disentanglement of different nHDM, has been reviewed in Ref. [134]; since our model is similar to the 2HDM-I in the decoupling limit, we expect similar signatures. The best candidate for observation will be the scalar h, with couplings reduced by mass mixing, which we did not discuss before, and smaller branching ratios due to the additional decay modes via the other scalars ($h \to \sigma\sigma$, $\sigma^+\sigma^-$, $\phi\phi$, ϕS, SS) and in association with gauge bosons ($h \to ZW^-\sigma^+$, $AW^-\sigma^+$, $W^-\sigma^+$, $Z\sigma$), most important for a heavy h. An analysis of the branching ratios of h will therefore not suffice to distinguish our model from the 2HDM-I. Since the interactions of $\sigma, \sigma^\pm, \phi$ and S with the leptons are suppressed not only by $\cos\beta$, but also by their small Yukawa couplings, whereas the gauge boson couplings scale with $\cos\beta$, this sector will be the most interesting. For example the decay channel $h \to Z\sigma$ (discussed in Ref. [135]) scales with $\cos\beta$; the decay $h \to Z'\sigma$ is induced by mass mixing of the scalars and thus goes roughly with μ/v, of the same order as $\cos\beta$. This could lead to interesting signatures, since the invariant mass of the subsequently created leptons gives information about the virtual particles, their angular distribution about the spin of the bosons and the rates of electrons, muons and tauons about the admixture of Z' over Z. Such an analysis would however require a lot of luminosity. In general, the most dominant effect of the scalars and Z' will be

the difference in the e, μ, τ rates due to Z' decays.

5.6 Conclusion

In this chapter, we presented several models to spontaneously break the $U(1)_{L_\mu - L_\tau}$ symmetry. We already concluded from the neutrino mass matrix (Sec. 5.1), that a viable tree-level seesaw mechanism is only possible by adding at least two complex scalar fields to the theory. Here we showed that the minimal scenario (two SM singlets charged under $U(1)'$) works, but is hard to detect experimentally. The other model with two scalar fields (combined to an $SU(2)_L$ doublet) is basically excluded by NSI measurements, although there are regions in parameter space where some of our approximations are not valid ($M_{Z'} \lesssim 1\,\text{GeV}$) and the one-doublet model could still be allowed, but this is not particularly interesting. To cure the one-doublet model of its problems, we introduced an additional scalar that pushes the Z' mass high enough to forbid dangerous decays, without increasing the Z–Z'-mixing angle. This model provides a rich phenomenology, similar to conventional two-Higgs-doublet models, such as charged scalars, mixing of the neutral scalars, in principle additional CP violation and LFV. The distinction to other 2HDM can, in principle, be done via its LFV, but will ultimately demand a combined measurement with Z', to extract the necessary quantum numbers.

Chapter 6

Conclusion and Outlook

Motivated by the $\mu-\tau$-symmetric structure of the neutrino mass matrix and the absence of quantum anomalies in the global $U(1)_{L_\mu - L_\tau}$ symmetry of the Standard Model, we have considered the gauged abelian $U(1)_{L_\mu - L_\tau}$ flavour symmetry. Only small perturbations to the $U(1)_{L_\mu - L_\tau}$-symmetric neutrino mass matrix are necessary to generate the observed mixing angles. We showed that we can generate a valid neutrino mass matrix at tree-level (using the seesaw mechanism) by extending the scalar sector by at least two complex fields that acquire a vacuum expectation value. We discussed the implications of said fields for the neutral gauge boson Z' associated with the local $U(1)_{L_\mu - L_\tau}$ and its mixing with the Standard Model Z boson. The mixing effects generate interesting additional neutrino interactions, not discussed previously.

Specifically, we first examined the limiting case of an ultralight Z', giving rise to a new long-range force between muonic and tauonic leptons. The generally present Z–Z' mixing exposes first-generation particles to this force, resulting in a potential for the muon- and tauon-neutrinos generated by the large number of neutrons inside the Earth and/or the Sun. This affects neutrino oscillations (mainly those in atmospheric and long-baseline experiments) in an intricate way, different from the usually considered contact interactions (non-standard neutrino interactions). Our model describes in general a different oscillatory behaviour for $\nu_{\mu,\tau}$ and $\overline{\nu}_{\mu,\tau}$ (CP violation), an effect that has recently been measured at MINOS, albeit with low precision. By performing a simulation with the GLoBES software, we showed how the constraints can be improved in various long-baseline experiments.

Aside from the ultralight limit, we also examined the more mainstream Z' around the electroweak scale. Once again the Z–Z' mixing affects neutrino interactions, this time as a concrete realisation of the NSI parameters $\varepsilon_{\mu\mu} = -\varepsilon_{\tau\tau}$. We discuss the current constraints, from the anomalous magnetic moment (that our model seeks to explain) to direct detection at colliders. Performing an involved global fit to a vast amount of electroweak precision data, we find a preferred region in $(M_{Z'}, g', \sin\xi_{\text{mix}})$ space that improves the Standard Model fit and can lead to small NSI:

$$\begin{aligned} 160\,\text{GeV} \lesssim M_{Z'}/g' \lesssim 560\,\text{GeV}\,, \\ -0.0008 < g' \sin\xi_{\text{mix}} < +0.0003\,. \end{aligned}$$

To complete the model, we discussed several simple models of spontaneous symmetry breaking. We exclude the simplest possible models (one singlet/doublet/triplet) but find the two-singlet and one-singlet-one-doublet models to be viable. Further analysing the

implications of the scalar sector, we deem the two-singlet model very difficult to observe, while the one-singlet-one-doublet model provides an interesting phenomenology and is in principle testable at the LHC. It is however challenging to distinguish this sector from conventional models with two Higgs doublets; measurements together with the Z' are needed to analyse the $U(1)_{L_\mu - L_\tau}$ quantum numbers of the scalars.

The most promising way to test the model would be a pure muonic system, such as a low-energy bound state (muonium) or $\mu\mu$ scattering (muon collider). Both experiments are challenging due to the finite lifetime of the muon, but have been under serious consideration for many years. This could not only probe the unmixed $U(1)_{L_\mu - L_\tau}$ vector boson but more generally lepton universality, shedding light on whether the three families of the Standard Model are really just copies with different masses or if there is more to it.

A worthwhile expansion of the work presented here would be an analysis of higher-order effects, i.e. the running and stability of our parameters under the renormalisation group. This would of course be most interesting in the fifth-force case, since there we are working with highly fine-tuned parameters that might change significantly. Especially loop-generated mixing effects are of interest, since they are in a sense naturally small. Radiatively generated neutrino masses, e.g. in the vein of the Zee-Babu model [136, 137], could give interesting signatures as well. In the framework of unification, the question arises if $G_{\mathrm{SM}} \times U(1)_{L_\mu - L_\tau}$ can be embedded in a larger GUT, for example in family-unifying models with all generations in one irreducible representation, as proposed by Georgi [138] (typically needs gauge groups of high dimension like $SU(9)$ or $SU(11)$).

An analogous discussion of models based on gauged $U(1)_{L_e}$ or $U(1)_{L_e - L_\mu - L_\tau}$ symmetries (killing the anomalies by additional charged fermions) will be interesting mainly in the symmetry-breaking sector, i.e. the generation of viable neutrino matrices. Otherwise, the models will be much more constrained than $U(1)_{L_\mu - L_\tau}$, not only by the additional charged fermions, but also by the precision experiments with electrons. Neutrino oscillations will be barely influenced, since the flavour structure of the potentials (be they long-range or contact interactions) is of the form $\mathrm{diag}(1,0,0)$ and $\mathrm{diag}(1,-1,-1) = \mathrm{diag}(2,0,0) - \mathrm{diag}(1,1,1)$, respectively, so this merely changes to the usual MSW potential (only the NSI parameter ε_{ee} will be generated).

Appendix

A Notation, Conventions and Constants

Units Throughout this thesis, we make use of natural units, i.e. we replace the reduced Planck constant $\hbar$, the Boltzmann constant k_B and the speed of light in vacuum c, with 1. Consequently, masses, energies, momenta and temperatures will mostly be given in units of eV, while distances and time have units eV^{-1}. The conversion back into the SI unit system follows from the identities

$$\begin{aligned} (1\,\mathrm{GeV})/c^2 &= 1.783 \times 10^{-24}\,\mathrm{g}\,, \\ (1\,\mathrm{GeV})^{-1}(\hbar c) &= 0.1973 \times 10^{-13}\,\mathrm{cm}\,, \\ (1\,\mathrm{GeV})/k_B &= 1.1605 \times 10^{13}\,\mathrm{K}\,. \end{aligned} \tag{A.1}$$

Cross sections will be given in units of barn, where $1\,\mathrm{barn} = 10^{-24}\,\mathrm{cm}^2$. Unless otherwise indicated, we take all numerical values for masses and coupling constants from the Particle Data Group (PDG) [22], we list a selection in Tab. A.1.

Metric We adopt the West coast convention for the Minkowski metric, i.e. $\eta_{\mu\nu} = \mathrm{diag}(+1,-1,-1,-1)$, resulting in the on-shell condition for massive particles $p^2 = \eta_{\mu\nu}p^\mu p^\nu = +M^2$. In unitary gauge (the limit $\xi \to \infty$ of the more general R_ξ gauges), the propagator of a massive gauge boson becomes

$$iD^{\mu\nu}(q) = i\left[\frac{-\eta^{\mu\nu} + \frac{q^\mu q^\nu}{M^2}}{q^2 - M^2 + i\varepsilon}\right], \tag{A.2}$$

while the useful relation for calculations with an unpolarised external vector boson reads

$$\sum_{\lambda=0,\pm1} \varepsilon^\mu_\lambda \bar{\varepsilon}^\nu_\lambda = -\eta^{\mu\nu} + \frac{q^\mu q^\nu}{M^2}\,. \tag{A.3}$$

The corresponding relations for unpolarised external fermions and antifermions are

$$\sum_{s=\pm} u^s(p)\bar{u}^s(p) = \not{p} + m\,, \qquad \sum_{s=\pm} v^s(p)\bar{v}^s(p) = \not{p} - m\,. \tag{A.4}$$

Hypercharge and $SU(2)$ Invariants We use the electric charge convention $Q = T_3 + \frac{Y}{2}$, yielding the $SU(3)_C \times SU(2)_L \times U(1)_Y$ representations of Tab. 1.1, for convenience

α	$1/137.036$
$\alpha(M_Z)$	$1/128.91$
G_F	$1.16637 \times 10^{-5}\,\mathrm{GeV}^{-2}$
M_Z	$91.1876\,\mathrm{GeV}$
M_W	$80.399\,\mathrm{GeV}$
$\sin^2(\theta_W)(M_Z)$	0.23108
$\alpha_s(M_Z)$	0.118
m_e	$0.511\,\mathrm{MeV}$
m_μ	$105.658\,\mathrm{MeV}$
m_τ	$1776.82\,\mathrm{MeV}$

Table A.1: Numerical values for masses and couplings in the Standard Model [22]. The Weinberg angle is defined in the NOV-scheme, i.e. via $s_W^2 c_W^2 \equiv \frac{\pi\alpha(M_Z)}{\sqrt{2}G_F M_Z^2}$.

repeated here for the first generation and the SM Higgs:

$$L_e = \begin{pmatrix}\nu\\ e\end{pmatrix}_L \sim (1,2,-1)\,, \qquad \overline{e_R} \sim (1,1,+2)\,, \qquad H_{\mathrm{SM}} = \begin{pmatrix}h_+\\ h_0\end{pmatrix} \sim (1,2,+1)\,, \tag{A.5}$$

$$Q_L^u = \begin{pmatrix}u\\ d\end{pmatrix}_L \sim (3,2,+1/3)\,, \quad \overline{u_R} \sim (\overline{3},1,-4/3)\,, \qquad \overline{d_R} \sim (\overline{3},1,+2/3)\,. \tag{A.6}$$

To construct $SU(2)$-invariant expressions of fields in the fundamental representation, one can use the invariant symbols δ_{ij} (Kronecker delta) and $\varepsilon_{ij} \sim i\sigma_2$ (Levi-Civita tensor). To simplify notation, we do not use the latter explicitly, but rather define a field that transforms again like a doublet, but with opposite hypercharge:

$$\tilde{H}_{\mathrm{SM}} \equiv -i\sigma_2 H_{\mathrm{SM}}^* = \begin{pmatrix}-\overline{h}_0\\ \overline{h}_+\end{pmatrix} \equiv \begin{pmatrix}-\overline{h}_0\\ h_-\end{pmatrix} \sim (1,2,-1)\,. \tag{A.7}$$

This allowes gauge invariant Yukawa couplings like $\overline{Q}_L H d_R$ and $\overline{Q}_L \tilde{H} u_R$, where the scalar product $\overline{Q}_L \tilde{H}$ has the metric δ_{ij}, i.e. $\overline{Q}_L \tilde{H} \equiv \overline{u}_L(-\overline{h}_0) + \overline{d}_L h_-$.

Low Energy Kinetic Mixing In the literature, different conventions are used to describe kinetic mixing, namely the choice of the abelian part of the SM ($U(1)_{\mathrm{EM}}$ or $U(1)_Y$). We use the hypercharge, since this ensures gauge invariance even above the electroweak scale; other authors use kinetic mixing in the low-energy regime, i.e.

$$\mathcal{L} \supset \sin\chi F_{\mathrm{EM}}^{\mu\nu} F'_{\mu\nu}\,. \tag{A.8}$$

Since we can write $F_Y^{\mu\nu} = c_W F_{\mathrm{EM}}^{\mu\nu} - s_W Z^{\mu\nu}$, this effectively drops the contribution of the Z boson. While this may be appropriate for low energies, we will try to keep our model as general as possible, especially since the mixing with the Z (albeit actually from mass mixing) induces the main effect under study in Ch. 3. We just mention that the constraints on the kinetic mixing angle basically differ by a factor c_W, depending on which model is used.

B Statistics

In this appendix, we will give a brief introduction to the statistical tools used in this thesis, namely the chi-square test, confidence intervals, as well as sensitivity. Most of this section is based on the "Statistics" chapter of the PDG review [22], albeit in a radically simplified manner.

Chi-Square Test When trying to compare a set of N independent measurements y_i (with variance σ_i^2) at points x_i to the expected mean $F(x_i;\boldsymbol{\theta})$, a quantity is needed to describe the compatibility as a function of the unknown parameters $\boldsymbol{\theta}$. The method of least squares uses the function

$$\chi^2(\boldsymbol{\theta}) \equiv \sum_{i=1}^{N} \frac{(y_i - F(x_i;\boldsymbol{\theta}))^2}{\sigma_i^2}\,, \tag{B.1}$$

to describe how far off the expected value $F(x_i)$ is from the measured y_i, compared to the variance σ_i. As such, a perfect agreement would mean $\chi^2(\boldsymbol{\theta}) = 0$, which is however extremely unlikely due to the statistical nature of any measurement process. More reasonable is an agreement within the variance, yielding $\chi^2 \sim N$.

The process of fitting a physical model to data describes, how to find the n parameters $\boldsymbol{\theta}$ of our model that maximise the level of agreement with the data, i.e. that minimise $\chi^2(\boldsymbol{\theta})$:

$$\frac{\partial}{\partial\theta_i}\chi^2(\boldsymbol{\theta})\bigg|_{\boldsymbol{\theta}=\hat{\boldsymbol{\theta}}} = 0\,, \qquad i = 1\ldots n\,. \tag{B.2}$$

These n equations reduce the number of degrees of freedom from N to $n_d \equiv N - n$ (for Poisson-distributed data), and we expect (B.1) to be distributed according to the chi-squared distribution for n_d degrees of freedom, i.e. following the probability density function (p.d.f.)

$$f(x;n_d) = \frac{1}{2^{n_d/2}\Gamma(n_d/2)} x^{n_d/2-1} e^{-x/2}\,, \tag{B.3}$$

with a mean $\mu = n_d$. This can be used, to properly define how probable the datapoints (x_i, y_i) are under the assumption of the model parameters $\hat{\boldsymbol{\theta}}$ ("goodness-of-fit"). To that effect we define the p-value

$$p = \int_{\chi^2(\hat{\boldsymbol{\theta}})}^{\infty} \mathrm{d}x\; f(x;n_d)\,, \tag{B.4}$$

which gives the probability to find a χ^2 larger than $\chi^2(\hat{\boldsymbol{\theta}})$. For example, for $n_d = 1$, the probability to find a $\chi^2 > 2.71$ is 10%. To summarise, we found a way to determine the best-fit values $\hat{\boldsymbol{\theta}}$ (minimising $\chi^2(\boldsymbol{\theta})$ (B.1)), and to quantify how good these values describe the data (the value $\chi^2(\hat{\boldsymbol{\theta}})$ compared to $n_d = \#\text{d.o.f.}$).

Now we want to define an estimate for the statistical precision of the obtained $\hat{\boldsymbol{\theta}}$ (a

$(1-\alpha)$ (%)	$m=1$	$m=2$
68.27	1.00	2.30
90.	2.71	4.61
95.	3.84	5.99
95.45	4.00	6.18
99.	6.63	9.21
99.73	9.00	11.83

Table B.1: $\Delta\chi^2$ corresponding to a coverage probability $1-\alpha$ in the large data sample limit, for joint estimation of m parameters [22].

"confidence interval"); assuming for a large number of experiments we obtain values for $\hat{\theta}^i$ in the interval $[\theta_1^i, \theta_2^i]$ with a probability $(1-\alpha)$ (confidence level), then the corresponding $\chi^2(\hat{\theta}^i)$ (following the χ^2 p.d.f. with one degree of freedom, if we vary only θ^i) changes in the interval $[\chi^2_{\min}(\hat{\theta}^i), \chi^2_{\min}(\hat{\theta}^i) + \Delta\chi^2]$ which covers the same probability:

$$(1-\alpha) = \int_{\chi^2_{\min}(\hat{\theta}^i)}^{\chi^2_{\min}(\hat{\theta}^i)+\Delta\chi^2} \mathrm{d}x \; f(x;1)\,. \tag{B.5}$$

So, if we want values for θ^i that cover the real value with a probability of, say 99%, we have to find the interval around $\chi^2_{\min}$ in which $\chi^2(\theta^i)$ changes by 6.63 units (see Tab. B.1). In general, the θ^i are not independent, and one needs to take this into account by specifying the confidence interval by all $\boldsymbol{\theta}$ satisfying

$$\chi^2(\boldsymbol{\theta}) = \chi^2(\hat{\boldsymbol{\theta}}) + \Delta\chi^2(\alpha, m)\,, \tag{B.6}$$

where $\Delta\chi^2$ not only depends on the confidence level $(1-\alpha)$, but also on the number of parameters $m \leq n$ estimated together. Due to the form of χ^2 (B.1), the contours of constant $\Delta\chi^2$ are typically ellipses in the θ^i-space, the angles between the major axes of which and the θ^i-axes give information about the correlation of the parameters (e.g. the covariance matrix). In practice, this just means that it is not enough to state the best-fit value $\hat{\theta}^i$ with its error-estimate $\delta\theta^i$ (e.g. its 1σ standard deviation corresponding to $(1-\alpha) = 68.27\%$); one should rather include information about the correlations to the other parameters θ^j, be it in form of a covariance matrix, a correlation coefficient or by simply projecting the χ^2 onto different (θ^i, θ^j)-planes to illustrate the dependence.

Let this suffice as an introduction to the used statistical tools for fitting a model to real-life data. In the next paragraph we will describe the interpretation of such fits for simulated data.

Analysis of Simulated Data While the above χ^2 analysis can be performed in exactly the same way with simulated data (as used in Sec. 3.5 for the simulation of future LBL experiments with GLoBES), the interpretation of the $\Delta\chi^2$ contours obviously has to change. There are essentially two different ways to analyse a simulated experiment. One

can either simulate data with a *true value* $\hat{\theta}^i$ and then perform a χ^2-analysis, this gives the "sensitivity" of said experiment to the parameter θ^i, i.e. one can predict how the statistical error will improve (e.g. the standard deviation of that parameter), and how it depends on the values and errors of the other parameters (in case the parameters are not independent).

The other way is to vary the true value and each time perform a χ^2-analysis. This way one obtains a confidence interval $[\theta_1, \theta_2]$ as a function of the true value $\hat{\theta}$, which can be used to find the value $\hat{\theta}$ at which some other value $\hat{\theta}'$ is excluded at a given confidence level. This is referred to as the "discovery" potential of that experiment. As an example, one can try to find out which real value the mixing angle θ_{13} has to have to exclude the $\theta_{13} = 0$ hypothesis at a given experiment.

C Stückelberg Mechanism

For a gauged abelian symmetry (it does not extend to non-abelian symmetries) there exists an interesting mechanism to generate a massive gauge boson, while retaining renormalisability [139] (see Ref. [140] for a recent review of Stückelberg extensions of the Standard Model). It can be understood as a Higgs mechanism with a scalar field σ in an affine representation of the $U(1)'$ (which is isomorph to $\mathbb{R}$). A gauge transformation of a matter field ψ and the gauge boson Z' takes the form

$$\begin{aligned} \psi &\to e^{-ig'Y'\theta(x)}\psi\,, \\ Z'_\mu &\to Z'_\mu - \partial_\mu\theta(x)\,. \end{aligned} \tag{C.1}$$

Defining the gauge transformation of σ as

$$\sigma \to \sigma + M_{Z'}\theta(x)\,, \tag{C.2}$$

it is easy to see that the Lagrangian

$$\mathcal{L} = -\frac{1}{4}Z'^{\mu\nu}Z'_{\mu\nu} + \frac{1}{2}(M_{Z'}Z'_\mu + \partial_\mu\sigma)(M_{Z'}Z'^\mu + \partial^\mu\sigma) \tag{C.3}$$

is gauge invariant. Fixing the gauge $\sigma(x) \equiv 0$ reduces the above Lagrangian to the usual Proca-Lagrangian for a massive vector boson. Interestingly, this formalism does not "leave" any scalar particles, like the usual Higgs mechanism, it is the most economic way to introduce a massive vector boson, concerning degrees of freedom.

The most general Lagrangian for the gauge group $G_{\mathrm{SM}} \times U(1)'$ takes the form

$$\mathcal{L} \supset -\frac{1}{4}\hat{Z}'^{\mu\nu}\hat{Z}'_{\mu\nu} - \frac{1}{4}\hat{B}^{\mu\nu}\hat{B}_{\mu\nu} - \frac{\sin\chi}{2}\hat{B}^{\mu\nu}\hat{Z}'_{\mu\nu} + \frac{1}{2}\left(\partial_\mu\sigma + \hat{M}_{Z'}\hat{Z}'_\mu + \hat{M}_B\hat{B}_\mu\right)^2\,, \tag{C.4}$$

where σ is charged under both $U(1)'$ and $U(1)_Y$, i.e. transforms like

$$\sigma \to \sigma + \hat{M}_{Z'}\theta_{Z'}(x) + \hat{M}_B\theta_B(x)\,. \tag{C.5}$$

Fixing the gauge $\sigma \equiv 0$ via $\theta_{Z'}$, we obtain

$$\mathcal{L} \supset -\frac{1}{4}\hat{Z}'^{\mu\nu}\hat{Z}'_{\mu\nu} - \frac{1}{4}\hat{B}^{\mu\nu}\hat{B}_{\mu\nu} - \frac{\sin\chi}{2}\hat{B}^{\mu\nu}\hat{Z}'_{\mu\nu} + \frac{1}{2}\hat{M}^2_{Z'}\hat{Z}'^2 + \frac{1}{2}\hat{M}^2_B\hat{B}^2 + \hat{M}_{Z'}\hat{M}_B\hat{Z}'_\mu\hat{B}^\mu\,, \tag{C.6}$$

in addition to the mass terms from the Standard Model Higgs:

$$\mathcal{L} \supset +\frac{1}{2}\hat{M}^2_Z\hat{Z}^2 = +\frac{1}{2}\hat{M}^2_Z\left(\hat{c}^2_W\hat{W}^2_3 - 2\hat{c}_W\hat{s}_W\hat{W}^\mu_3\hat{B}_\mu + \hat{s}^2_W\hat{B}^2\right). \tag{C.7}$$

We diagonalise the kinetic terms by performing a non-unitary transformation

$$\begin{pmatrix}\hat{B}\\ \hat{W}_3\\ \hat{Z}'\end{pmatrix} = \begin{pmatrix}1 & 0 & -\tan\chi\\ 0 & 1 & 0\\ 0 & 0 & \frac{1}{\cos\chi}\end{pmatrix}\begin{pmatrix}\tilde{B}\\ \tilde{W}_3\\ \tilde{Z}'\end{pmatrix} \equiv R\begin{pmatrix}\tilde{B}\\ \tilde{W}_3\\ \tilde{Z}'\end{pmatrix}, \tag{C.8}$$

leading to the mass matrix in $(\tilde{B}, \tilde{W}_3, \tilde{Z}')$ basis

$$\frac{1}{2}R^\dagger\begin{pmatrix}\hat{s}^2_W\hat{M}^2_Z + \hat{M}^2_B & -\hat{c}_W\hat{s}_W\hat{M}^2_Z & \hat{M}_{Z'}\hat{M}_B\\ -\hat{c}_W\hat{s}_W\hat{M}^2_Z & \hat{c}^2_W\hat{M}^2_Z & 0\\ \hat{M}_{Z'}\hat{M}_B & 0 & \hat{M}^2_{Z'}\end{pmatrix}R\,. \tag{C.9}$$

This can be diagonalised analogously to the mass mixing case discussed in Sec. 2.2, basically with similar phenomenology as discussed before. Since the determinant of the mass matrix vanishes, one of the bosons will be massless. While this may be interesting in its own right, there is a huge drawback in the neutrino sector. Although the Z' in this scenario is massive, we did not "break" the $L_\mu - L_\tau$ symmetry, i.e. the σ does not acquire a VEV which could lead to additional Yukawa terms. The σ actually does not couple to anything but the Z', because of its unusual transformation properties. To get a neutrino mass matrix without the $L_\mu - L_\tau$ symmetry, we must break it with additional fields. This can lead to interesting models, for simplicity we only consider one additional scalar, charged with $Y' = 1$ under $U(1)'$:

$$\begin{aligned}\mathcal{L} = &-\frac{1}{4}Z'^{\mu\nu}Z'_{\mu\nu} + \frac{1}{2}(MZ'_\mu + \partial_\mu\sigma)(MZ'^\mu + \partial^\mu\sigma)\\ &+ |(\partial_\mu - ig'Z'_\mu)S|^2 + \mu^2|S|^2 - \lambda|S|^4\,.\end{aligned} \tag{C.10}$$

After S acquires the VEV $v = \sqrt{\mu/\lambda}$ and we fix the unitary gauge, this leads to

$$\begin{aligned}\mathcal{L} = &-\frac{1}{4}Z'^{\mu\nu}Z'_{\mu\nu} + \frac{1}{2}M^2_{Z'}Z'^2 + \frac{1}{2}(\partial_\mu\phi)^2 - \frac{1}{2}m^2_\phi\phi^2 + \frac{1}{2}(\partial_\mu H)^2\\ &+ g'\frac{M}{M_{Z'}}Z'_\mu\left(H\partial^\mu\phi - \phi\partial^\mu H\right) + \frac{g'^2}{2}Z'^2\left(\phi^2 + 2v\phi + \frac{M^2}{M^2_{Z'}}H^2\right)\\ &- \frac{\lambda}{4}\phi^4 - \lambda v\phi^3 - \frac{\lambda}{2}\frac{M^2}{M^2_{Z'}}\phi^2H^2 - \lambda v\frac{M^2}{M^2_{Z'}}\phi H^2 - \frac{\lambda}{4}\frac{M^4}{M^4_{Z'}}H^4\,,\end{aligned} \tag{C.11}$$

where $M^2_{Z'} = M^2 + g'^2v^2$, $m^2_\phi = 2\lambda v^2$ and we introduced the real fields $\phi = \mathrm{Re}\,(S)$ and

$H = \frac{g'v}{M_{Z'}}\sigma - \frac{M}{M_{Z'}}\mathrm{Im}\,(S)$, the latter being massless.

D Perturbative Formulae for Oscillation Probabilities

To show the effect of α on the oscillation probabilities in the full three-flavour framework, we perform a perturbation expansion. We use the second-order formulae (in the constant matter density approximation) given in Ref. [141], where an expansion in the parameters $\Delta m^2_{21}/\Delta m^2_{31}$, s_{13} and $\varepsilon_{\alpha\beta}$ is made, assuming them to be of the same order ε. Here, $\varepsilon_{\alpha\beta}$ are the usual NSI parameters (introduced in Sec. 1.3), which in our case are all zero except for

$$\varepsilon \equiv \varepsilon_{\mu\mu} = -\varepsilon_{\tau\tau} = 2EV/A \approx 0.96 \left(\frac{\rho}{\mathrm{g/cm^3}}\right)^{-1} \frac{\alpha}{10^{-50}}\,. \tag{D.1}$$

Since the average matter density in long-baseline experiments is $\rho \approx 3\,\mathrm{g/cm^3}$, we need $\alpha \lesssim 10^{-50}$ for an accurate expansion.

The expressions were obtained rewriting the Hamiltonian as $H = H_0 + H_1(\varepsilon)$ and using the usual time-dependent perturbation theory for the S-matrix. It proves convenient to work in the flavour basis but without the 23-rotation, i.e. $\tilde{H} = U_{23}^\dagger H_{\mathrm{flavour}} U_{23}$. With this, the S-matrix (in flavour basis) can be written as

$$S(L) = U_{23} e^{-i\tilde{H}_0 L} \Omega(L) U_{23}^\dagger\,,$$

where $\Omega(x)$ follows from the expansion

$$\begin{aligned}\Omega(x) = 1 &+ (-i)\int_0^x \mathrm{d}x' \,\left[e^{i\tilde{H}_0 x'} \tilde{H}_1(x') e^{-i\tilde{H}_0 x'}\right] \\ &+ (-i)^2 \int_0^x \mathrm{d}x' \,\left[e^{i\tilde{H}_0 x'} \tilde{H}_1(x') e^{-i\tilde{H}_0 x'}\right] \int_0^{x'} \mathrm{d}x'' \,\left[e^{i\tilde{H}_0 x''} \tilde{H}_1(x'') e^{-i\tilde{H}_0 x''}\right] + \mathcal{O}(\varepsilon^3)\,.\end{aligned}$$

In the presence of NSI, it is useful to also omit the 13-rotation, i.e. work in the basis $\tilde{\tilde{H}} = U_{13}^\dagger U_{23}^\dagger H_{\mathrm{flavour}} U_{23} U_{13}$ in an analogous way. The oscillation probabilities follow from the S-matrix in the usual way, via $P(\nu_\beta \to \nu_\alpha, L) = |S_{\alpha\beta}|^2$.

With $P(\nu_\alpha \to \nu_\beta) \equiv P_{\alpha\beta}$ one obtains

$$P_{ee} = 1 - 4c_{12}^2 s_{12}^2 \left(\frac{\Delta m^2_{21}}{A}\right)^2 \sin^2\left(\frac{AL}{4E}\right) - \left(\frac{2s_{13}\Delta m^2_{31}}{\Delta m^2_{31} - A}\right)^2 \sin^2\left(\frac{\Delta m^2_{31} - A}{4E} L\right) \tag{D.2}$$

and

$$
\begin{aligned}
P_{e\mu} = {} & 4c_{23}^2 c_{12}^2 s_{12}^2 \left(\frac{\Delta m_{21}^2}{A}\right)^2 \sin^2\left(\frac{AL}{4E}\right) + \left(\frac{2s_{23}s_{13}\Delta m_{31}^2}{\Delta m_{31}^2 - A}\right)^2 \sin^2\left(\frac{\Delta m_{31}^2 - A}{4E}L\right) \\
& + 8c_{23}s_{23}c_{12}s_{12}s_{13}\left(\frac{\Delta m_{31}^2 \Delta m_{21}^2}{A^2}\right)\frac{A(\cos\delta + \sin\delta)}{\Delta m_{31}^2 - A} \\
& \times \sin\left(\frac{AL}{4E}\right)\cos\left(\frac{\Delta m_{31}^2 L}{4E}\right)\sin\left(\frac{\Delta m_{31}^2 - A}{4E}L\right),
\end{aligned}
\tag{D.3}
$$

so α has no effect on the electron oscillation to this order, but it appears in third order. The same holds for $P_{e\tau}$, which can be obtained from $P_{e\mu}$ by the transformation $s_{23} \to c_{23}$, $c_{23} \to -s_{23}$. The muon survival probability consists of two lengthy parts, one without α:

$$
\begin{aligned}
P_{\mu\mu} = {} & 1 - 4c_{23}^2 s_{23}^2 \sin^2\left(\frac{\Delta m_{31}^2 L}{4E}\right) \\
& - 4c_{23}^2 c_{12}^2 s_{12}^2 \left(\frac{\Delta m_{21}^2}{A}\right)^2 \sin^2\left(\frac{AL}{4E}\right) \\
& - 2c_{23}^2 s_{23}^2 c_{12}^2 s_{12}^2 \left(\frac{\Delta m_{21}^2}{A}\right)^2 \left(\frac{AL}{2E}\right)\sin\left(\frac{\Delta m_{31}^2 L}{2E}\right) \\
& + 8c_{23}^2 s_{23}^2 c_{12}^2 s_{12}^2 \left(\frac{\Delta m_{21}^2}{A}\right)^2 \sin\left(\frac{AL}{4E}\right)\sin\left(\frac{\Delta m_{31}^2 L}{4E}\right)\cos\left(\frac{\Delta m_{31}^2 - A}{4E}L\right) \\
& - \left(\frac{2s_{23}s_{13}\Delta m_{31}^2}{\Delta m_{31}^2 - A}\right)^2 \sin^2\left(\frac{\Delta m_{31}^2 - A}{4E}L\right) \\
& - 2\left(\frac{\left(c_{23}s_{23}s_{13}\Delta m_{31}^2\right)^2}{\Delta m_{31}^2 - A}\frac{L}{2E}\right)\sin\left(\frac{\Delta m_{31}^2 L}{2E}\right) \\
& + 8\left(\frac{c_{23}s_{23}s_{13}\Delta m_{31}^2}{\Delta m_{31}^2 - A}\right)^2 \cos\left(\frac{AL}{4E}\right)\sin\left(\frac{\Delta m_{31}^2 L}{4E}\right)\sin\left(\frac{\Delta m_{31}^2 - A}{4E}L\right) \\
& + 8c_{23}s_{23}c_{12}s_{12}s_{13}\left(\frac{\Delta m_{31}^2}{\Delta m_{31}^2 - A}\frac{\Delta m_{21}^2}{A}\right)\cos\delta\left[s_{23}^2\sin^2\left(\frac{\Delta m_{31}^2 - A}{4E}L\right)\right. \\
& \left. + c_{23}^2\sin^2\left(\frac{AL}{4E}\right) - s_{23}^2\sin^2\left(\frac{\Delta m_{31}^2 L}{4E}\right) - (c_{23}^2 - s_{23}^2)\frac{A}{\Delta m_{31}^2}\sin^2\left(\frac{\Delta m_{31}^2 L}{4E}\right)\right],
\end{aligned}
\tag{D.4}
$$

and finally with the α-dependent part:

$$
\begin{aligned}
P_{\mu\mu}(\alpha) = P_{\mu\mu} & \\
& + 2c_{23}^2 s_{23}^2 \left(s_{13}^2 \Delta m_{31}^2 + c_{12}^2 \Delta m_{21}^2 - 4EV(s_{23}^2 - c_{23}^2)\right) \left(\frac{L}{2E}\right) \sin\left(\frac{\Delta m_{31}^2 L}{2E}\right) \\
& - c_{23}^2 s_{23}^2 \left(4EV(s_{23}^2 - c_{23}^2) - c_{12}^2 \Delta m_{21}^2\right)^2 \left(\frac{L}{2E}\right)^2 \cos\left(\frac{\Delta m_{31}^2 L}{2E}\right) \\
& + 8c_{23}s_{23}(c_{23}^2 - s_{23}^2)\left[c_{12}s_{12}s_{13}\cos\delta\Delta m_{21}^2 - 4EV\ c_{23}s_{23}\right] \left(\frac{\sin^2\left(\frac{\Delta m_{31}^2 L}{4E}\right)}{\Delta m_{31}^2}\right) \\
& - 16EV\ c_{23}^2 s_{23}^2 (c_{23}^2 - s_{23}^2)\left(4EV\ (s_{23}^2 - c_{23}^2) - c_{12}^2 \Delta m_{21}^2\right) \left(\frac{1}{\Delta m_{31}^2}\right) \\
& \quad \times \left[\left(\frac{L}{2E}\right) \sin\left(\frac{\Delta m_{31}^2 L}{2E}\right) - 2\left(\frac{1}{\Delta m_{31}^2}\right) \sin^2\left(\frac{\Delta m_{31}^2 L}{4E}\right)\right] \\
& - (8EV)^2\ c_{23}^4 s_{23}^4 \left(\frac{1}{\Delta m_{31}^2}\frac{L}{2E}\right) \sin\left(\frac{\Delta m_{31}^2 L}{2E}\right) \\
& - (8EV)^2\ c_{23}^2 s_{23}^2 \left((c_{23}^2 - s_{23}^2)^2 - 4c_{23}^2 s_{23}^2\right) \left(\frac{1}{\Delta m_{31}^2}\right)^2 \sin^2\left(\frac{\Delta m_{31}^2 L}{4E}\right) .
\end{aligned}
\tag{D.5}
$$

The probability for $\nu_\mu \to \nu_\tau$ follows from

$$
\begin{aligned}
P_{\mu\tau} = & \ 4c_{23}^2 s_{23}^2 \sin^2\left(\frac{\Delta m_{31}^2 L}{4E}\right) \\
& + 4c_{23}^2 s_{23}^2 c_{12}^2 s_{12}^2 \left(\frac{\Delta m_{21}^2}{A}\right)^2 \left(\frac{AL}{4E}\right) \sin\left(\frac{\Delta m_{31}^2 L}{2E}\right) \\
& - 8c_{23}^2 s_{23}^2 c_{12}^2 s_{12}^2 \left(\frac{\Delta m_{21}^2}{A}\right)^2 \sin\left(\frac{AL}{4E}\right) \sin\left(\frac{\Delta m_{31}^2 L}{4E}\right) \cos\left(\frac{\Delta m_{31}^2 - A}{4E} L\right) \\
& + 4c_{23}^2 s_{23}^2 s_{13}^2 \left(\frac{(\Delta m_{31}^2)^2}{\Delta m_{31}^2 - A}\right) \left(\frac{L}{4E}\right) \sin\left(\frac{\Delta m_{31}^2 L}{2E}\right) \\
& - 8c_{23}^2 s_{23}^2 s_{13}^2 \left(\frac{\Delta m_{31}^2}{\Delta m_{31}^2 - A}\right)^2 \cos\left(\frac{AL}{4E}\right) \sin\left(\frac{\Delta m_{31}^2 L}{4E}\right) \sin\left(\frac{\Delta m_{31}^2 - A}{4E} L\right) \\
& + 8c_{23}s_{23}(c_{23}^2 - s_{23}^2) s_{13} c_{12} s_{12} \left(\frac{\Delta m_{21}^2}{\Delta m_{31}^2 - A}\right) \cos\delta\ \sin^2\left(\frac{\Delta m_{31}^2 L}{4E}\right) \\
& + 8c_{23}s_{23}s_{13}s_{12}c_{12} \left(\frac{\Delta m_{21}^2}{\Delta m_{31}^2 - A}\frac{\Delta m_{31}^2}{A}\right) \sin\left(\frac{AL}{4E}\right) \sin\left(\frac{\Delta m_{31}^2 L}{4E}\right) \\
& \quad \times \left[s_{23}^2 \cos\left(\delta - \frac{\Delta m_{31}^2 - A}{4E} L\right) - c_{23}^2 \cos\left(\delta + \frac{\Delta m_{31}^2 - A}{4E} L\right)\right]
\end{aligned}
\tag{D.6}
$$

and

$$
P_{\mu\tau}(\alpha) = P_{\mu\tau} - (P_{\mu\mu}(\alpha) - P_{\mu\mu}) = P_{\mu\tau} + P_{\mu\mu} - P_{\mu\mu}(\alpha) . \tag{D.7}
$$

E Seesaw with Different N_R Charge Assignments

In Sec. 5.1, we discussed the $U(1)_{L_\mu - L_\tau}$ charges of the three right-handed neutrinos necessary for the seesaw mechanism. While it seems natural to assign them the same lepton numbers as ν_e, ν_μ and ν_τ, it is not strictly mandatory. Introducing three right-handed neutrinos N_i is also possible in the trivial way, i.e. taking them to be singlets under the full gauge group $G_{\mathrm{SM}} \times U(1)'$, $N_i \sim (1,1,0)(0)$, without introducing anomalies.

The Majorana mass matrix $\mathcal{M}_R$ is arbitrary and will be chosen to be diagonal ($\mathcal{M}_R = \mathrm{diag}(X,Y,Z)$) while the Dirac matrix m_D, with only the Standard Model Higgs, has the form

$$m_D = \begin{pmatrix} a & b & c \\ 0 & 0 & 0 \\ 0 & 0 & 0 \end{pmatrix} , \tag{E.1}$$

so we obtain the low-energy neutrino mass matrix $\mathcal{M}_\nu = \mathrm{diag}(a^2/X + b^2/Y + c^2/Z, 0, 0)$. Including scalar singlets with $U(1)'$ charge changes nothing, so we take doublets with charge $Y' = \pm 1$, which acquire a VEV. This changes the Dirac matrix to

$$m_D \to \begin{pmatrix} a & b & c \\ a_{-1} & b_{-1} & c_{-1} \\ a_{+1} & b_{+1} & c_{+1} \end{pmatrix} , \tag{E.2}$$

giving rise to the low-energy neutrino mass matrix

$$\mathcal{M}_\nu = -\begin{pmatrix} \frac{a^2}{X} + \frac{b^2}{Y} + \frac{c^2}{Z} & \frac{aa_{-1}}{X} + \frac{bb_{-1}}{Y} + \frac{cc_{-1}}{Z} & \frac{aa_{+1}}{X} + \frac{bb_{+1}}{Y} + \frac{cc_{+1}}{Z} \\ \cdot & \frac{a_{-1}^2}{X} + \frac{b_{-1}^2}{Y} + \frac{c_{-1}^2}{Z} & \frac{a_{-1}a_{+1}}{X} + \frac{b_{-1}b_{+1}}{Y} + \frac{c_{-1}c_{+1}}{Z} \\ \cdot & \cdot & \frac{a_{+1}^2}{X} + \frac{b_{+1}^2}{Y} + \frac{c_{+1}^2}{Z} \end{pmatrix} . \tag{E.3}$$

The discussion is now similar to the one-doublet case in Sec. 5.1.3, the main difference of this model being, that we do not break the $L_\mu - L_\tau$ symmetry to improve an otherwise almost viable model, but rather have to break it to get anything in accordance with experiment (because without the doublets, there would be only one massive neutrino).

F Conventional Two-Higgs-Doublet Models

The addition of one or more scalar fields is the simplest extension of the SM Higgs sector. While the extension with $SU(2)_L$ singlets (dubbed xSM or cxSM, if the scalar is complex [123]) is interesting, models with more than one $SU(2)_L$ doublet have been under much more consideration due to their impact on the fermion sector. One distinguishes between four kinds of Two-Higgs-Doublet Models (2HDM), depending on their allowed interactions with fermions (e.g. by imposing additional discrete symmetries).

In all models, the VEVs are constrained by the W and Z masses to fulfil $v_{\mathrm{SM}}^2 = v_1^2 + v_2^2$, so one can parameterise them via $v_1 = v_{\mathrm{SM}} \cos\beta$, $v_2 = v_{\mathrm{SM}} \sin\beta$. The most general 2HDM predicts Flavour-Changing Neutral Currents (FCNC), yielding constraints on

$\tan\beta$ and the couplings to fermions.

- The Type-I 2HDM (2HDM-I) contains the two doublets Ψ_f and Ψ_0, the latter not coupling to fermions. Hence, there are no FCNC at tree-level.
- 2HDM-II consists of Ψ_u and Ψ_d with hypercharge $Y_{u,d} = \pm 1$, coupling only to up- and down-type fermions, respectively:

$$-\mathcal{L} \supset \sum_{i,j=1,2,3} \lambda_d^{ij} \overline{Q}_L^i \Psi_d d_R^j + \sum_{i,j=1,2,3} \lambda_u^{ij} \overline{Q}_L^i \Psi_u u_R^j + \sum_{\ell=e,\mu,\tau} \lambda^\ell \overline{L}_\ell \Psi_d \ell_R + \text{h.c.}$$

  This is also the pattern of the MSSM Higgs sector (at tree-level), making it a widely researched model.
- 2HDM-III is the most general model, allowing all Yukawa interactions consistent with gauge symmetry.
- The 2HDM-IV (goes also by the names leptonic 2HDM, leptophilic 2HDM, lepton-specific 2HDM, L2HDM) consists of the two doublets Ψ_Q and Ψ_L, coupling solely to quarks and leptons, respectively (see e.g. Ref. [142]):

$$-\mathcal{L} \supset \sum_{i,j=1,2,3} \lambda_d^{ij} \overline{Q}_L^i \Psi_Q d_R^j + \sum_{i,j=1,2,3} \lambda_u^{ij} \overline{Q}_L^i \tilde{\Psi}_Q u_R^j + \sum_{\ell=e,\mu,\tau} \lambda^\ell \overline{L}_\ell \Psi_L \ell_R + \text{h.c.}$$

The 2HDM provide a rich phenomenology, e.g. the possibility of a new source of CP violation, the occurrence of charged scalars and possibly stable pseudoscalars.

G Electroweak Precision Observables

In this appendix, we list the electroweak precision data used in the fit with GAPP in Sec. 4.4. We also provide the definitions of some of the more involved observables, such as

$$\sigma_{\text{had}} \equiv \frac{12\pi}{M_Z^2} \frac{\Gamma(e^+e^-)\Gamma(Z \to \text{hadrons})}{\Gamma_Z^2}\,, \qquad R_\ell \equiv \frac{\Gamma(\text{had})}{\Gamma(\ell\bar{\ell})}\,, \tag{G.1}$$

$$R_q \equiv \frac{\Gamma(q\bar{q})}{\Gamma(\text{had})}\,,\ q = b, c\,, \qquad R_\nu \equiv \frac{\sigma_{\nu N}^{\text{NC}}}{\sigma_{\nu N}^{\text{CC}}}\,, \tag{G.2}$$

$$A^{FB} \equiv \frac{\sigma^F - \sigma^B}{\sigma^F + \sigma^B}\,, \qquad A_{LR} \equiv \frac{\sigma_L - \sigma_R}{\sigma_L + \sigma_R}\,. \tag{G.3}$$

$\kappa \equiv \frac{2s}{u_s + d_s}$ denotes the relative size of the strange sea in the nucleon and Q_W stands for the weak charge:

$$Q_W(Z,N) \equiv -2\left[C_{1u}(2Z+N) + C_{1d}(Z+2N)\right] \approx Z(1-4s_W^2) - N\,. \tag{G.4}$$

Z lineshape:
M_Z, Γ_Z
$\sigma_{\rm had}$
R_e, R_μ, R_τ
$A^{FB}(e)$
$A^{FB}(\mu)$
$A^{FB}(\tau)$
other LEP 1 measurements:
$P(\tau)$
$P^{FB}(\tau)$
$\sin^2\theta_e^{\rm eff}(Q_{FB})$
$A^{FB}(s)$ (DELPHI + OPAL)
$R_{d,s}/(R_d+R_u+R_s)$
LEP 1 and SLC heavy flavour:
R_b
R_c
$A^{FB}(b)$
$A^{FB}(c)$
$A_{LR}^{FB}(b)$
$A_{LR}^{FB}(c)$
other SLD asymmetries:
A_{LR} (hadrons)
A_{LR} (leptons)
$A_{LR}^{FB}(\mu)$
$A_{LR}^{FB}(\tau)$
$A_e(Q_{LR})$
$A_{LR}^{FB}(s)$
quark masses:
m_t (pole) lepton + jets (CDF I)
m_t (pole) dilepton (CDF I)
m_t (pole) all hadronic (CDF I)
m_t (pole) lepton + jets (D0 I)
m_t (pole) dilepton (D0 I)
m_t (pole) lepton + jets (CDF II)
m_t (pole) dilepton (CDF II)
m_t (pole) all hadronic (CDF II)
m_t (pole) l+j JES free (CDF II)
m_t (pole) lepton + jets (D0 II)
m_t (pole) dilepton (D0 II)
m_t (pole) all hadronic (D0 I)
m_t (pole) TOTAL TEVATRON average
$m_c(m_c)$
$m_b(m_b)$

W properties:
M_W (LEP)
Γ_W (LEP)
M_W (Tevatron)
Γ_W (Tevatron)
gauge couplings and related:
$\Delta\alpha^{(3)}_{\rm had}$ (1.8 GeV)
$(g_\mu-2-\alpha/\pi)/2$
τ lifetime
neutrino-nucleon DIS:
g_L^2 (NuTeV 2002)
g_R^2 (NuTeV 2002)
κ (CCFR 1997)
R_ν (CHARM 1984)
R_ν (CDHS 1984)
$R_{\overline{\nu}}$ (CHARM 1984)
$R_{\overline{\nu}}$ (CDHS 1984)
$R_{\overline{\nu}}$ (CDHS 1979)
other low energy:
$g_V^{(\nu,e)}$ (CHARM II)
$g_A^{(\nu,e)}$ (CHARM II)
$Q_W(e)$ (SLAC E-158)
$Q_W(Cs)$
$Q_W(Tl)$
$4C1d+9C1u$ (pol. e- scattering)
$9C1d-4C1d$ (pol. e- scattering)
CKM 1st row unitarity
$B(b\to s\gamma)/B(b\to ce\nu)$
other Tevatron:
$A^{FB}(e)$ (CDF II amd D0)
PVDIS
other LEP 2:
σ(hadrons)(183 GeV)
$\sigma(\mu)$(183 GeV)
$\sigma(\tau)$(183 GeV)
$A^{FB}(\mu)$(183 GeV)
$A^{FB}(\tau)$(183 GeV)
σ(hadrons)(183 GeV)
$\sigma(\mu)$(183 GeV)
$\sigma(\tau)$(183 GeV)
$A^{FB}(\mu)$(183 GeV)
$A^{FB}(\tau)$(183 GeV)

Bibliography

[1] T. Schwetz, M. A. Tortola, and J. W. F. Valle, "*Three-flavour neutrino oscillation update*," New J. Phys. **10** (2008) 113011, arXiv:0808.2016 [hep-ph].

[2] P. F. Harrison, D. H. Perkins, and W. G. Scott, "*Tri-bimaximal mixing and the neutrino oscillation data*," Phys. Lett. **B530** (2002) 167, arXiv:hep-ph/0202074.

[3] G. Altarelli and F. Feruglio, "*Discrete Flavor Symmetries and Models of Neutrino Mixing*," Rev. Mod. Phys. **82** (2010) 2701–2729, arXiv:1002.0211 [hep-ph].

[4] L. Wolfenstein, "*Neutrino oscillations in matter*," Phys. Rev. **D17** (1978) 2369–2374.

[5] C. Biggio, M. Blennow, and E. Fernandez-Martinez, "*General bounds on non-standard neutrino interactions*," JHEP **08** (2009) 090, arXiv:0907.0097 [hep-ph].

[6] E. Fernandez-Martinez, "*Bounds on neutrino non-standard interactions*," AIP Conf. Proc. **1222** (2010) 150–154.

[7] P. Langacker, "*The Physics of Heavy Z' Gauge Bosons*," Rev. Mod. Phys. **81** (2009) 1199–1228, arXiv:0801.1345 [hep-ph].

[8] A. Leike, "*The Phenomenology of extra neutral gauge bosons*," Phys. Rept. **317** (1999) 143–250, arXiv:hep-ph/9805494.

[9] H. Fritzsch and P. Minkowski, "*Unified Interactions of Leptons and Hadrons*," Ann. Phys. **93** (1975) 193–266.

[10] T. Fukuyama, A. Ilakovac, T. Kikuchi, S. Meljanac, and N. Okada, "*SO(10) group theory for the unified model building*," J. Math. Phys. **46** (2005) 033505, arXiv:hep-ph/0405300.

[11] R. W. Robinett and J. L. Rosner, "*Prospects for a Second Neutral Vector Boson at Low Mass in SO(10)*," Phys. Rev. **D25** (1982) 3036.

[12] E. Salvioni, G. Villadoro, and F. Zwirner, "*Minimal Z-prime models: Present bounds and early LHC reach*," JHEP **0911** (2009) 068, arXiv:0909.1320 [hep-ph].

[13] B. Holdom, "*Two U(1)'s and Epsilon Charge Shifts*," Phys. Lett. **B166** (1986) 196.

[14] S. Abel, M. Goodsell, J. Jaeckel, V. Khoze, and A. Ringwald, "*Kinetic Mixing of the Photon with Hidden U(1)s in String Phenomenology*," JHEP **0807** (2008) 124, arXiv:0803.1449 [hep-ph].

[15] S. Abel and B. Schofield, "*Brane anti-brane kinetic mixing, millicharged particles and SUSY breaking*," Nucl.Phys. **B685** (2004) 150–170, arXiv:hep-th/0311051 [hep-th].

[16] M. Goodsell, J. Jaeckel, J. Redondo, and A. Ringwald, "*Naturally Light Hidden Photons in LARGE Volume String Compactifications*," JHEP **0911** (2009) 027, arXiv:0909.0515 [hep-ph].

[17] D. Feldman, Z. Liu, and P. Nath, "*The Stueckelberg Z-prime Extension with Kinetic Mixing and Milli-Charged Dark Matter From the Hidden Sector*," Phys.Rev. **D75** (2007) 115001, arXiv:hep-ph/0702123 [HEP-PH].

[18] K. Cheung and T.-C. Yuan, "*Hidden fermion as milli-charged dark matter in Stueckelberg Z- prime model*," JHEP **0703** (2007) 120, arXiv:hep-ph/0701107 [hep-ph].

[19] L. B. Okun, "*Limits Of Electrodynamics: Paraphotons?*," Sov. Phys. JETP **56** (1982) 502.

[20] J. Jaeckel and A. Ringwald, "*A Cavity Experiment to Search for Hidden Sector Photons*," Phys.Lett. **B659** (2008) 509–514, arXiv:0707.2063 [hep-ph].

[21] P. Arias, J. Jaeckel, J. Redondo, and A. Ringwald, "*Improving the Discovery Potential of Future Light-Shining- through-a-Wall Experiments*," arXiv:1009.1519 [hep-ph].

[22] **Particle Data Group** Collaboration, K. Nakamura, "*Review of particle physics*," J. Phys. **G37** (2010) 075021.

[23] L. B. Okun, "*Leptonic photon and light element abundancies*," Mod. Phys. Lett. **A11** (1996) 3041–3042, arXiv:hep-ph/9611360.

[24] J. A. Grifols and E. Masso, "*Leptonic photons and nucleosynthesis*," Phys. Lett. **B396** (1997) 201–202, arXiv:astro-ph/9610205.

[25] S. N. Gninenko, "*Limit on leptonic photon interactions from SN1987a*," Phys. Lett. **B413** (1997) 365–368, arXiv:hep-ph/9708465.

[26] A. D. Dolgov, "*Long-range forces in the universe*," Phys. Rept. **320** (1999) 1–15.

[27] A. S. Joshipura and S. Mohanty, "*Constraints on flavour-dependent long-range forces from atmospheric neutrino observations at Super-Kamiokande*," Phys. Lett. **B584** (2004) 103–108, arXiv:hep-ph/0310210.

[28] A. Bandyopadhyay, A. Dighe, and A. S. Joshipura, "*Constraints on flavor-dependent long range forces from solar neutrinos and KamLAND*," Phys. Rev. **D75** (2007) 093005, arXiv:hep-ph/0610263.

[29] S. Choubey and W. Rodejohann, "*A flavor symmetry for quasi-degenerate neutrinos: $L_\mu - L_\tau$*," Eur. Phys. J. **C40** (2005) 259–268, arXiv:hep-ph/0411190.

[30] M. Srednicki, *Quantum Field Theory*. Cambridge University Press, 1 ed., 2007.

[31] S. Weinberg, *The Quantum Theory of Fields. Vol. 2: Modern Applications*. Cambridge University Press, 1996.

[32] M. E. Peskin and D. V. Schroeder, *An Introduction To Quantum Field Theory (Frontiers in Physics)*. Westview Press, 1995.

[33] D. J. Gross and R. Jackiw, "*Effect of anomalies on quasirenormalizable theories*," Phys.Rev. **D6** (1972) 477–493.

[34] L. Alvarez-Gaume and E. Witten, "*Gravitational Anomalies*," Nucl. Phys. **B234** (1984) 269.

[35] G. Dutta, A. S. Joshipura, and K. B. Vijaykumar, "*Leptonic flavor violations in the presence of an extra Z*," Phys. Rev. **D50** (1994) 2109–2115, arXiv:hep-ph/9405292.

[36] A. Samanta, "*Long range forces, oscillation parameters and mass hierarchy with atmospheric neutrinos at a magnetized muon detector*," arXiv:1001.5344 [hep-ph].

[37] E. Ma, D. P. Roy, and S. Roy, "*Gauged $L_\mu - L_\tau$ with large muon anomalous magnetic moment and the bimaximal mixing of neutrinos*," Phys. Lett. **B525** (2002) 101–106, arXiv:hep-ph/0110146.

[38] E. Ma and D. P. Roy, "*Anomalous neutrino interaction, muon $g-2$, and atomic parity nonconservation*," Phys. Rev. **D65** (2002) 075021.

[39] S. Baek, N. G. Deshpande, X. G. He, and P. Ko, "*Muon anomalous $g-2$ and gauged $L_\mu - L_\tau$ models*," Phys. Rev. **D64** (2001) 055006, arXiv:hep-ph/0104141.

[40] S. Baek and P. Ko, "*Phenomenology of $U(1)(L_\mu - L_\tau)$ charged dark matter at PAMELA and colliders*," JCAP **0910** (2009) 011, arXiv:0811.1646 [hep-ph].

[41] **NuTeV Collaboration** Collaboration, G. Zeller *et al.*, "*A Precise determination of electroweak parameters in neutrino nucleon scattering*," Phys.Rev.Lett. **88** (2002) 091802, arXiv:hep-ex/0110059 [hep-ex].

[42] **PAMELA** Collaboration, O. Adriani *et al.*, "*An anomalous positron abundance in cosmic rays with energies 1.5-100 GeV*," Nature **458** (2009) 607–609, arXiv:0810.4995 [astro-ph].

[43] E. Salvioni, A. Strumia, G. Villadoro, and F. Zwirner, "*Non-universal minimal Z' models: present bounds and early LHC reach*," JHEP **1003** (2010) 010, arXiv:0911.1450 [hep-ph].

[44] K. S. Babu, C. F. Kolda, and J. March-Russell, "*Implications of generalized $Z - Z'$ mixing*," Phys. Rev. **D57** (1998) 6788–6792, arXiv:hep-ph/9710441.

[45] B. Holdom, "*Oblique electroweak corrections and an extra gauge boson*," Phys. Lett. **B259** (1991) 329–334.

[46] V. Novikov, L. Okun, and M. Vysotsky, "*On the Electroweak one loop corrections*," Nucl.Phys. **B397** (1993) 35–83.

[47] E. A. Paschos, *Electroweak Theory*. Cambridge Univ. Press, Cambridge, MA, 2007.

[48] B. Arnett, "*The Nine Planets*,". http://www.nineplanets.org/earth.html.

[49] **MINOS** Collaboration, E. Ables *et al.*, "*P-875: A Long baseline neutrino oscillation experiment at Fermilab*,". FERMILAB-PROPOSAL-0875.

[50] **MINOS** Collaboration, D. G. Michael *et al.*, "*Observation of muon neutrino disappearance with the MINOS detectors and the NuMI neutrino beam*," Phys. Rev. Lett. **97** (2006) 191801, arXiv:hep-ex/0607088.

[51] Talk given by P. Vahle at 24th International Conference On Neutrino Physics And Astrophysics (Neutrino 2010), June 14, 2010, slides can be found at http://indico.cern.ch/getFile.py/access?contribId=201&sessionId=1&resId=0&materialId=slides&confId=73981.

[52] E. G. Adelberger, J. H. Gundlach, B. R. Heckel, S. Hoedl, and S. Schlamminger, "*Torsion balance experiments: A low-energy frontier of particle physics*," Prog. Part. Nucl. Phys. **62** (2009) 102–134.

[53] G. L. Smith, C. D. Hoyle, J. H. Gundlach, E. G. Adelberger, B. R. Heckel, and H. E. Swanson, "*Short-range tests of the equivalence principle*," Phys. Rev. D **61** (1999) no. 2, 022001.

[54] S. Schlamminger, K.-Y. Choi, T. Wagner, J. Gundlach, and E. Adelberger, "*Test of the equivalence principle using a rotating torsion balance*," Phys.Rev.Lett. **100** (2008) 041101, arXiv:0712.0607 [gr-qc].

[55] S. Hannestad, "*Neutrino physics from precision cosmology*," Prog. Part. Nucl. Phys. **65** (2010) 185–208, arXiv:1007.0658 [hep-ph].

[56] Y. I. Izotov and T. X. Thuan, "*The primordial abundance of 4He: evidence for non-standard big bang nucleosynthesis*," Astrophys. J. **710** (2010) L67–L71, arXiv:1001.4440 [astro-ph.CO].

[57] B. Malaescu, "*The Current Status of g-2*," arXiv:1006.4739 [hep-ph].

[58] K. P. Jungmann, "*Muonium Spectroscopy*," Hyperfine Interact. **127** (2000) 189–196, arXiv:physics/9910023.

[59] S. J. Brodsky and R. F. Lebed, "*Production of the Smallest QED Atom: True Muonium (mu+ mu-)*," Phys. Rev. Lett. **102** (2009) 213401, arXiv:0904.2225 [hep-ph].

[60] D. F. Bartlett and S. Loegl, "*Limits on an Electromagnetic Fifth Force*," Phys. Rev. Lett. **61** (1988) 2285–2287.

[61] H. Kloor, E. Fischbach, C. Talmadge, and G. L. Greene, "*Limits on new forces coexisting with electromagnetism*," Phys. Rev. D **49** (1994) no. 4, 2098–2113.

[62] P. Huber, M. Lindner, and W. Winter, "*Simulation of long-baseline neutrino oscillation experiments with GLoBES*," Comput. Phys. Commun. **167** (2005) 195, arXiv:hep-ph/0407333.

[63] P. Huber, J. Kopp, M. Lindner, M. Rolinec, and W. Winter, "*New features in the simulation of neutrino oscillation experiments with GLoBES 3.0*," Comput. Phys. Commun. **177** (2007) 432–438, arXiv:hep-ph/0701187.

[64] A. Dziewonski and D. Anderson, "*Preliminary reference earth model*," Phys.Earth Planet.Interiors **25** (1981) 297–356.

[65] F. D. Stacey, *Physics of the Earth*. Wiley, 2nd ed., 1977.

[66] **The T2K** Collaboration, Y. Itow *et al.*, "*The JHF-Kamioka neutrino project*," arXiv:hep-ex/0106019.

[67] **T2K** Collaboration, A. K. Ichikawa, "*Status of the T2K long baseline neutrino oscillation experiment*," J. Phys. Conf. Ser. **203** (2010) 012104.

[68] M. Fechner, *Détermination des performances attendues sur la recherche de l'oscillation $\nu_\mu \to \nu_e$ dans l'experiénce T2K depuis l'étude des données recueilles dans l'éxperience K2K*. PhD thesis, Université Paris VI, 2006.

[69] *Neutrino 2008*. 2008.

[70] J.-E. Campagne, M. Maltoni, M. Mezzetto, and T. Schwetz, "*Physics potential of the CERN-MEMPHYS neutrino oscillation project*," JHEP **04** (2007) 003, arXiv:hep-ph/0603172.

[71] M. D. Messier, "*Evidence for neutrino mass from observations of atmospheric neutrinos with Super-Kamiokande*,". UMI-99-23965.

[72] E. A. Paschos and J. Y. Yu, "*Neutrino interactions in oscillation experiments*," Phys. Rev. **D65** (2002) 033002, arXiv:hep-ph/0107261.

[73] P. Huber, M. Lindner, and W. Winter, "*Superbeams versus neutrino factories*," Nucl. Phys. **B645** (2002) 3–48, arXiv:hep-ph/0204352.

[74] M. Ishitsuka, T. Kajita, H. Minakata, and H. Nunokawa, "*Resolving Neutrino Mass Hierarchy and CP Degeneracy by Two Identical Detectors with Different Baselines*," Phys. Rev. **D72** (2005) 033003, arXiv:hep-ph/0504026.

[75] **NOvA** Collaboration, I. Ambats *et al.*, "*NOvA proposal to build a 30-kiloton off-axis detector to study neutrino oscillations in the Fermilab NuMI beamline*," hep-ex/0503053.

[76] P. Huber, M. Lindner, T. Schwetz, and W. Winter, "*First hint for CP violation in neutrino oscillations from upcoming superbeam and reactor experiments*," JHEP **11** (2009) 044, arXiv:0907.1896 [hep-ph].

[77] **NOvA** Collaboration, T. Yang and S. Woijcicki, "*Study of physics sensitivity of $\nu_m u$ disappearance in a totally active version of NOνA detector*,". Off-Axis-Note-SIM-30.

[78] J. E. Campagne and A. Cazes, "*The theta(13) and delta(CP) sensitivities of the SPL- Frejus project revisited*," Eur. Phys. J. **C45** (2006) 643–657, arXiv:hep-ex/0411062.

[79] M. Mezzetto, "*Physics potential of the SPL super beam*," J. Phys. **G29** (2003) 1781–1784, hep-ex/0302005.

[80] **ISS Physics Working Group** Collaboration, A. Bandyopadhyay *et al.*, "*Physics at a future Neutrino Factory and super-beam facility*," Rept. Prog. Phys. **72** (2009) 106201, arXiv:0710.4947 [hep-ph].

[81] P. Huber, M. Lindner, M. Rolinec, and W. Winter, "*Optimization of a neutrino factory oscillation experiment*," Phys. Rev. **D74** (2006) 073003, arXiv:hep-ph/0606119.

[82] D. Autiero *et al.*, "*The synergy of the golden and silver channels at the Neutrino Factory*," Eur. Phys. J. **C33** (2004) 243–260, hep-ph/0305185.

[83] J. Bernabeu *et al.*, "*EURONU WP6 2009 yearly report: Update of the physics potential of Nufact, superbeams and betabeams*," arXiv:1005.3146 [hep-ph].

[84] **NOvA Collaboration** Collaboration, R. Plunkett, "*Status of the NOvA experiment*," J.Phys.Conf.Ser. **120** (2008) 052044.

[85] J. Heeck and W. Rodejohann, "*Gauged $L_\mu - L_\tau$ and different Muon Neutrino and Anti-Neutrino Oscillations: MINOS and beyond*," arXiv:1007.2655 [hep-ph].

[86] G. Barenboim and J. D. Lykken, "*MINOS and CPT-violating neutrinos*," Phys.Rev. **D80** (2009) 113008, arXiv:0908.2993 [hep-ph].

[87] D. Choudhury, A. Datta, and A. Kundu, "*Mutual consistency of the MINOS and MiniBooNE Antineutrino Results and Possible CPT Violation*," arXiv:1007.2923 [hep-ph].

[88] C. M. Ho, "*Leptogenesis and CPT Violation*," arXiv:1012.1053 [hep-ph].

[89] W. A. Mann, D. Cherdack, W. Musial, and T. Kafka, "*Apparent multiple Δm^2_{32} in muon anti-neutrino and muon neutrino survival oscillations from non-standard interaction matter effect*," Phys. Rev. **D82** (2010) 113010, arXiv:1006.5720 [hep-ph].

[90] J. Kopp, P. A. N. Machado, and S. J. Parke, "*Interpretation of MINOS data in terms of non-standard neutrino interactions*," Phys. Rev. **D82** (2010) 113002, arXiv:1009.0014 [hep-ph].

[91] E. Akhmedov and T. Schwetz, "*MiniBooNE and LSND data: Non-standard neutrino interactions in a (3+1) scheme versus (3+2) oscillations*," JHEP **1010** (2010) 115, arXiv:1007.4171 [hep-ph].

[92] N. Engelhardt, A. E. Nelson, and J. R. Walsh, "*Apparent CPT Violation in Neutrino Oscillation Experiments*," Phys.Rev. **D81** (2010) 113001, arXiv:1002.4452 [hep-ph].

[93] J. Heeck and W. Rodejohann, "*Neutrino Phenomenology of gauged $L_\mu - L_\tau$: MINOS and beyond*," arXiv:1012.2298 [hep-ph].

[94] S. Davidson, C. Pena-Garay, N. Rius, and A. Santamaria, "*Present and future bounds on non-standard neutrino interactions*," JHEP **03** (2003) 011, arXiv:hep-ph/0302093.

[95] W. Magnus, "*On the exponential solution of differential equations for a linear operator*," Commun. Pure Appl. Math. **7** (1954) 649–673.

[96] C. Ishihara, *Full three flavor oscillation analysis of atmospheric neutrino data observed in Super-Kamiokande*. PhD thesis, University of Tokyo, 2010. http://www-rccn.icrr.u-tokyo.ac.jp/kajita/thesis/isihara_dthesis.pdf.

[97] M. Honda, T. Kajita, K. Kasahara, S. Midorikawa, and T. Sanuki, "*Calculation of atmospheric neutrino flux using the interaction model calibrated with atmospheric muon data*," Phys. Rev. **D75** (2007) 043006, arXiv:astro-ph/0611418.

[98] P. Lipari, M. Lusignoli, and F. Sartogo, "*The Neutrino cross-section and upward going muons*," Phys. Rev. Lett. **74** (1995) 4384–4387, arXiv:hep-ph/9411341.

[99] W. Grimus, R. Pfeiffer, and T. Schwetz, "*A 4-neutrino model with a Higgs triplet*," Eur. Phys. J. **C13** (2000) 125–132, arXiv:hep-ph/9905320.

[100] K. Fujikawa, B. W. Lee, and A. I. Sanda, "*Generalized Renormalizable Gauge Formulation of Spontaneously Broken Gauge Theories*," Phys. Rev. **D6** (1972) 2923–2943.

[101] K. R. Lynch, "*A note on one loop electroweak contributions to g-2*," arXiv:hep-ph/0108081.

[102] M. C. Gonzalez-Garcia and M. Maltoni, "*Atmospheric neutrino oscillations and new physics*," Phys. Rev. **D70** (2004) 033010, arXiv:hep-ph/0404085.

[103] G. Mitsuka, *Study of Non-Standard Neutrino Interactions with Atmospheric Neutrino Data in Super-Kamiokande*. PhD thesis, University of Tokyo, 2009. http://www-sk.icrr.u-tokyo.ac.jp/sk/pub/dthesis_feb9-mitsuka.pdf.

[104] **TASSO** Collaboration, W. Braunschweig *et al.*, "*A measurement of Muon pair production in e+ e- annihilation at center-of-mass energies 35-GeV $\leq \sqrt{s} \leq$ 46.8-GeV*," Z. Phys. **C40** (1988) 163–170.

[105] **VENUS** Collaboration, K. Abe *et al.*, "*Measurement of the reactions e+ e- $\to$ mu+ mu- and e+ e- $\to$ tau+ tau- between $\sqrt{s}$ = 50-Gev and 60.8-Gev*," Z. Phys. **C48** (1990) 13–22.

[106] **ALEPH** Collaboration, R. Barate *et al.*, "*Study of the muon pair production at center-of-mass energies from 20-GeV to 136-GeV with the ALEPH detector*," Phys. Lett. **B399** (1997) 329–341.

[107] **ALEPH** Collaboration, R. Barate *et al.*, "*Study of fermion pair production in e^+e^- collisions at 130-GeV to 183-GeV*," Eur. Phys. J. **C12** (2000) 183–207, arXiv:hep-ex/9904011.

[108] **ALEPH** Collaboration, S. Schael *et al.*, "*Fermion pair production in e^+e^- collisions at 189-209-GeV and constraints on physics beyond the standard model*," Eur. Phys. J. **C49** (2007) 411–437, arXiv:hep-ex/0609051.

[109] **ALEPH** Collaboration, D. Buskulic *et al.*, "*Study of the four fermion final state at the Z resonance*," Z. Phys. **C66** (1995) 3–18.

[110] A. Pukhov *et al.*, "*CompHEP: A package for evaluation of Feynman diagrams and integration over multi-particle phase space. User's manual for version 33*," arXiv:hep-ph/9908288. http://comphep.sinp.msu.ru/.

[111] **CompHEP** Collaboration, E. Boos *et al.*, "*CompHEP 4.4: Automatic computations from Lagrangians to events*," Nucl. Instrum. Meth. **A534** (2004) 250–259, arXiv:hep-ph/0403113.

[112] J. Bagger, V. D. Barger, K.-m. Cheung, J. F. Gunion, T. Han, *et al.*, "*The Strongly interacting W W system: Gold plated modes*," Phys.Rev. **D49** (1994) 1246–1264, arXiv:hep-ph/9306256 [hep-ph].

[113] R. J. Hooper, "*A Search for large extra spatial dimensions and Z' bosons in the dimuon final state in $\sqrt{s}$ = 1.96-TeV $p\bar{p}$ collisions at D0*,". FERMILAB-THESIS-2004-03.

[114] **D0** Collaboration, "*Search for Heavy Z Bosons in the Dimuon Channel with 250 pb^{-1} of Data with the D0 Detector (preliminary)*,". http://www-d0.fnal.gov/Run2Physics/WWW/results/prelim/NP/N20/N20.pdf.

[115] **CDF** Collaboration, T. Aaltonen *et al.*, "*A search for high-mass resonances decaying to dimuons at CDF*," Phys. Rev. Lett. **102** (2009) 091805, arXiv:0811.0053 [hep-ex].

[116] **CDF** Collaboration, D. Whiteson, K. Cranmer, E. Quinlan, A. Kotwal, C. Hays, and O. Stelzer-Chilton, "*Search for high mass resonances decaying to muon pairs (preliminary)*,". http://www-cdf.fnal.gov/physics/exotic/r2a/20100527.zprime_mumu/conference_note.pdf.

[117] J. Erler, "*Global fits to electroweak data using GAPP*," arXiv:hep-ph/0005084.

[118] J. Erler and P. Langacker, "*Constraints on extended neutral gauge structures*," Phys. Lett. **B456** (1999) 68–76, arXiv:hep-ph/9903476.

[119] V. D. Barger, M. Berger, J. Gunion, and T. Han, "*Physics of Higgs factories*," arXiv:hep-ph/0110340 [hep-ph].

[120] L. Basso, S. Moretti, and G. M. Pruna, "*Phenomenology of the minimal $B - L$ extension of the Standard Model: the Higgs sector*," arXiv:1011.2612 [hep-ph].

[121] P. H. Frampton, S. L. Glashow, and D. Marfatia, "*Zeroes of the neutrino mass matrix*," Phys. Lett. **B536** (2002) 79–82, arXiv:hep-ph/0201008.

[122] S. Goswami, S. Khan, and W. Rodejohann, "*Minimal Textures in Seesaw Mass Matrices and their low and high Energy Phenomenology*," Phys. Lett. **B680** (2009) 255–262, arXiv:0905.2739 [hep-ph].

[123] V. Barger, P. Langacker, M. McCaskey, M. Ramsey-Musolf, and G. Shaughnessy, "*Complex Singlet Extension of the Standard Model*," Phys. Rev. **D79** (2009) 015018, arXiv:0811.0393 [hep-ph].

[124] S. Dawson and W. Yan, "*Hiding the Higgs Boson with Multiple Scalars*," Phys. Rev. **D79** (2009) 095002, arXiv:0904.2005 [hep-ph].

[125] O. Bahat-Treidel, Y. Grossman, and Y. Rozen, "*Hiding the Higgs at the LHC*," JHEP **05** (2007) 022, arXiv:hep-ph/0611162.

[126] W. Grimus, L. Lavoura, O. Ogreid, and P. Osland, "*A Precision constraint on multi-Higgs-doublet models*," J.Phys.G **G35** (2008) 075001, arXiv:0711.4022 [hep-ph].

[127] H. E. Haber, G. L. Kane, and T. Sterling, "*The Fermion Mass Scale and Possible Effects of Higgs Bosons on Experimental Observables*," Nucl. Phys. **B161** (1979) 493.

[128] M. Sher, "*Electroweak Higgs Potentials and Vacuum Stability*," Phys. Rept. **179** (1989) 273–418.

[129] **LEP Higgs Working Group for Higgs boson searches** Collaboration, "*Search for charged Higgs bosons: Preliminary combined results using LEP data collected at energies up to 209- GeV*," arXiv:hep-ex/0107031.

[130] **DELPHI** Collaboration, J. Abdallah *et al.*, "*Search for charged Higgs bosons at LEP in general two Higgs doublet models*," Eur. Phys. J. **C34** (2004) 399–418, arXiv:hep-ex/0404012.

[131] L. Lavoura, "*General formulae for $f_1 \to f_2\gamma$*," Eur. Phys. J. **C29** (2003) 191–195, arXiv:hep-ph/0302221.

[132] J. P. Leveille, "*The Second Order Weak Correction to (G-2) of the Muon in Arbitrary Gauge Models*," Nucl.Phys. **B137** (1978) 63.

[133] D. Chang, W.-F. Chang, C.-H. Chou, and W.-Y. Keung, "*Large two-loop contributions to g-2 from a generic pseudoscalar boson*," Phys. Rev. **D63** (2001) 091301, arXiv:hep-ph/0009292.

[134] V. Barger, H. E. Logan, and G. Shaughnessy, "*Identifying extended Higgs models at the LHC*," Phys.Rev. **D79** (2009) 115018, arXiv:0902.0170 [hep-ph].

[135] S. de Visscher, J.-M. Gerard, M. Herquet, V. Lemaitre, and F. Maltoni, "*Unconventional phenomenology of a minimal two-Higgs- doublet model*," JHEP **08** (2009) 042, arXiv:0904.0705 [hep-ph].

[136] A. Zee, "*Quantum Numbers Of Majorana Neutrino Masses*," Nucl.Phys. **B264** (1986) 99. Revised version.

[137] K. Babu, "*Model of 'Calculable' Majorana Neutrino Masses*," Phys.Lett. **B203** (1988) 132.

[138] H. Georgi, "*Towards a Grand Unified Theory of Flavor*," Nucl.Phys. **B156** (1979) 126.

[139] E. C. G. Stueckelberg, "*Interaction forces in electrodynamics and in the field theory of nuclear forces*," Helv. Phys. Acta **11** (1938) 299–328.

[140] B. Kors and P. Nath, "*Aspects of the Stueckelberg extension*," JHEP **07** (2005) 069, arXiv:hep-ph/0503208.

[141] T. Kikuchi, H. Minakata, and S. Uchinami, "*Perturbation Theory of Neutrino Oscillation with Nonstandard Neutrino Interactions*," JHEP **03** (2009) 114, arXiv:0809.3312 [hep-ph].

[142] V. D. Barger, J. Hewett, and R. Phillips, "*New Constraints On The Charged Higgs Sector In Two Higgs Doublet Models*," Phys.Rev. **D41** (1990) 3421.

Acknowledgements

I would like to express my gratitude to those who have helped and accompanied me during the course of this work. I thank Werner Rodejohann, not only for his supervision and for introducing me to the challenging and versatile topic of this diploma thesis, but also for the interesting discussions and the countless times he provided a solution to an aggravating problem.

For including me into the multifaceted institute that is the MPIK, I thank Manfred Lindner; for interesting discussions I thank all members of the institute. Anja Berneiser is to be thanked, among other things, for all the help with the bureaucracy.

I am however most grateful for the company of my fellow diploma students. My office mates for the better part of a year, Nico Kronberg and Felix Kahlhöfer, were never too busy to discuss physics and everything else, I thank them for the supportive and stimulating atmosphere they created. The same holds for my other colleagues in room B, Alexander Dück, Michael Dürr and Daniel Schmidt, who were always accommodating. I thank Angnis Schmidt-May for enlightening conversations, in particular about group theory.

Further thanks goes out to my new office mates Kher Sham Lim and Alina Wilhelm for interesting conversations, Kher Sham Lim especially for the fruitful discourses about renormalisation.

Apart from all these physicists, I am also indebted to my parents Barbara and Christian, among other things for providing the means for me to study and for building my confidence by being easily impressed by what I do.

Finally, for proofreading parts of this work, I thank Angnis Schmidt-May, Nico Kronberg and Alexander Dück.

Erklärung:

Ich versichere, dass ich diese Arbeit selbstständig verfasst habe und keine anderen als die angegebenen Quellen und Hilfsmittel benutzt habe.

Heidelberg, den 28.02.2011 .....

(Julian Niklas Heeck)